DEVELOPMENT OF GROUP-CONTRIBUTION MODELS FOR USE IN SURFACTANT SELECTION – CASE STUDIES OF SINGLE AND MIXED SURFACTANT APPLICATIONS

Woramet Chanachichalermwong

A Thesis Submitted in Partial Fulfilment of the Requirements
for the Degree of Master of Science
The Petroleum and Petrochemical College, Chulalongkorn University
in Academic Partnership with
The University of Michigan, The University of Oklahoma,
Case Western Reserve University, and Institut Français du Pétrole
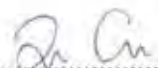2018

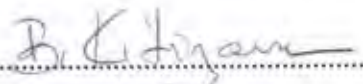|	
Thesis Title:	Development of Group-Contribution Models for Use in Surfactant Selection – Case Studies of Single and Mixed Surfactant Applications
By:	Woramet Chanachichalermwong
Program:	Petroleum Technology
Thesis Advisors:	Asst. Prof. Uthaiporn Suriyapraphadilok
	Dr. Ampira Charoensaeng

Accepted by The Petroleum and Petrochemical College, Chulalongkorn University, in partial fulfilment of the requirements for the Degree of Master of Science.

.... College Dean

(Prof. Suwabun Chirachanchai)

Thesis Committee:

....

(Asst. Prof. Uthaiporn Suriyapraphadilok)

....

(Dr. Ampira Charoensaeng)

....

(Assoc. Prof. Boonyarach Kitiyanan)

....

(Assoc. Prof. Siripon Anantawaraskul)

ABSTRACT

5973017063:   Petroleum Technology Program
                Woramet Chanachichalermwong: Development of Group-
                Contribution Models for Use in Surfactant Selection – Case Studies
                of Single and Mixed Surfactant Applications.
                Thesis Advisors: Asst. Prof. Uthaiporn Suriyapraphadilok and
                Dr. Ampira Charoensaeng 331 pp.
Keywords: Characteristic Curvature/ Group-Contribution model/ Hydrophilic-
   lipophilic deviation/ Krafft Point/ Microemulsion

        Microemulsion is the surfactant/oil/water system that is applied to many applications such as enhanced oil recovery, cleaning agents, environmental remediation and drug delivery system. To select the suitable surfactant to form an efficient microemulsion system for each specific condition and application, a systematic selection method is needed to reduce time and valuable resources that may be required in the design of an interest product. This work developed a systematic method to select suitable surfactants for a specific application based on several properties including but not limited to types of emulsion, emulsion stability, solubility and toxicology. Since not all models are available in the literature, this work developed properties models based on the molecular structure of the surfactants by using the concept of Group-Contribution (GC) based on Marrero and Gani method. One important key of surfactant properties for Hydrophilic-Lipophilic property through an Hydrophilic-Lipophilic Deviation (HLD) equation is the characterictic curvature (C_c) that indicates the hydrophobicity or hydrophilicity of a surfactant based on their molecular structure. This work developed the GC-model for prediction of characteristic curvature of anionic and nonionic surfactants to use in the HLD equation to aid in the design of surfactant formulation. Krafft point—another key property to indicate the solubility of anionic surfactant, was also modeled based on the GC concept. The application of this work was performed through case studies in the fields of enhanced oil recovery, soil remediation and detergency.

บทคัดย่อ

วรเมธ ชนะชัยเฉลิมวงศ์ : การพัฒนาแบบจำลอง Group-Contribution เพื่อนำไปใช้ใน การเลือกสารลดแรงตึงผิว - กรณีศึกษาการนำไปประยุกต์ใช้ในระบบที่มีสารลดแรงตึงผิวชนิดเดียว และระบบที่มีสารลดแรงตึงผิวผสม (Development of Group-Contribution Models for Use in Surfactant Selection – Case Studies of Single and Mixed Surfactant Applications) อ. ที่ปรึกษา : ผศ. ดร.อุทัยพร สุริยประภาดิลก และ ดร.อัมพิรา เจริญแสง 331 หน้า

ไมโครอิมัลชัน (Microemulsion) เป็นระบบที่ประกอบไปด้วยสารลดแรงตึงผิว/น้ำมัน/น้ำ ที่ถูกนำไปประยุกต์ใช้ในงานต่างๆ เช่น การผลิตน้ำมันดิบขั้นตติยภูมิ, สารทำความสะอาด และระบบ นำส่งยา เป็นต้น ในการเลือกสารลดแรงตึงผิวที่เหมาะสมเพื่อนำไปใช้สร้างไมโครอิมัลชันที่มี ประสิทธิภาพนั้น จำเป็นต้องมีวิธีการเลือกที่เหมาะสมเพื่อประหยัดเวลาและทรัพยากรที่จำเป็นต้อง ใช้ในการออกแบบผลิตภัณฑ์หรืองานที่สนใจ งานวิจัยนี้ได้ทำการพัฒนาระเบียบวิธีเพื่อเลือกสารลด แรงตึงผิวที่เหมาะสมกับงานแต่ละประเภท โดยการใช้สมบัติต่างๆ ไก้แก่ ชนิดของอิมัลชั่น เสถียรภาพของอิมัลชัน ความสามารถในการละลาย และความเป็นพิษต่อสิ่งแวดล้อม โดยสมบัติบาง ชนิดจะนำโมเดลจากงานวิจัยอื่นมาใช้ งานวิจัยนี้ได้พัฒนาแบบจำลองทำนายสมบัติของสารลดแรงตึง ผิวจากโครงสร้างโมเลกุลของสาร โดยใช้วิธีการ Group-Contribution ของ Marrero และ Gani สมบัติหนึ่งที่สำคัญของสารลดแรงตึงผิวคือคุณสมบัติ Characteristic curvature (C_c) ซึ่งเป็นส่วน หนึ่งของสมการ Hydrophilic-Lipophilic Deviation (HLD) และสามารถนำมาใช้ระบุสมบัติ ความชอบน้ำของสารลดแรงตึงผิว ในงานวิจัยนี้ได้พัฒนาแบบจำลอง Group-Contribution สำหรับ ทำนายค่า Characteristic curvature ของสารลดแรงตึงผิวชนิดประจุลบ และชนิดไม่มีประจุ เพื่อ นำไปใช้ในสมการ HLD สำหรับการเลือกสารลดแรงตึงผิว นอกจากนี้ สมบัติอื่นๆ ของสารลดแรงตึง ผิว เช่น Krafft point เป็นอีกหนึ่งสมบัติที่สำคัญในการบอกความสามารถการละลายของสารลดแรง ตึงผิวชนิดประจุลบ ได้ถูกพัฒนาแบบจำลองขึ้นตามหลักการของ Group-Contribution เช่นกัน การ ประยุกต์ใช้งานวิจัยนี้สามารถนำไปใช้ได้ในงานหลายประเภท ได้แก่ การผลิตน้ำมันดิบขั้นตติยภูมิ การฟื้นฟูสภาพดิน และสารทำความสะอาด

GRAPHICAL ABSTRACT
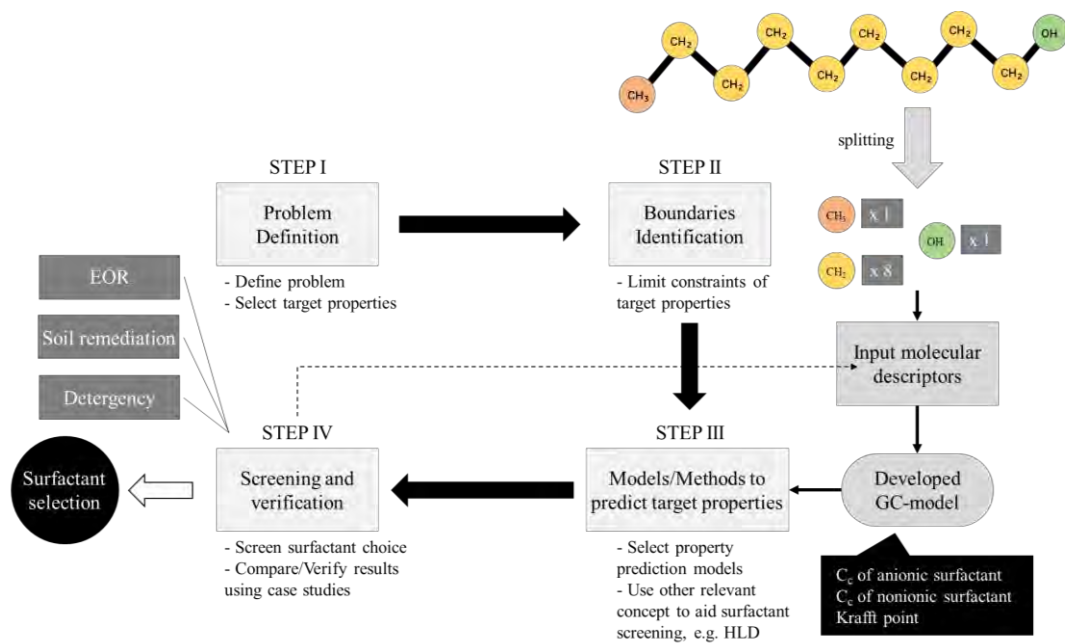
ACKNOWLEDGEMENTS

Firstly, I would like to express my sincere gratitude to my thesis advisor, Asst. Prof. Dr. Uthaiporn Suriyapraphadilok and my thesis co-advisor, Dr. Ampira Charoensaeng for the continuous support. They always listen to my troubles and give the suggestion to guide me in the right direction.

I am grateful for the full scholarship and full funding of the thesis work provided by the Petroleum and Petrochemical College, and other supports by Center of Excellence on Petrochemical and Materials Technology, Thailand, the Special task force for applied surfactant research in petroleum and environmental applications, Ratchadaphiseksomphot Endowment Fund, Chulalongkorn University, the Government Budget Fund and the 90th Anniversary of Chulalongkorn University, Ratchadapisek Sompote Fund.

Finally, I gratefully acknowledge to my parent and my friends for providing me with good support and continuous encouragement throughout the period of thesis study. This accomplishment would not have been possible without them.

TABLE OF CONTENTS

LIST OF TABLES

LIST OF TABLES

LIST OF TABLES

LIST OF TABLES

LIST OF TABLES

LIST OF TABLES

LIST OF FIGURES

LIST OF FIGURES

LIST OF FIGURES

LIST OF FIGURES

LIST OF FIGURES

LIST OF FIGURES

LIST OF FIGURES

LIST OF FIGURES

LIST OF FIGURES

LIST OF FIGURES

LIST OF FIGURES

LIST OF FIGURES

LIST OF FIGURES

LIST OF FIGURES

LIST OF FIGURES

LIST OF FIGURES

ABBREVIATIONS

Abbreviation	Description
HLD	Hydrophilic-Lipophilic Deviation
EOR	Enhanced oil recovery
OOIP	Original oil in place
IFT	Interfacial tension
O/W	oil-in-water microemulsion or Winsor type I microemulsion
W/O	water-in-oil microemulsion or Winsor type II Microemulsion
SOW	Surfactant/Oil/Water system
CMC	Critical micelle concentration
EO	Polyethylene structure
PO	Polypropylene structure
QPPRs	Quantitative Property-Property Relationships
QSPRs	Quantitative Structure-Property Relationships
GCMs	Group-Contribution Methods
%RD	Percentage of relative deviation
%ARD	Percentage of absolute relative deviation
%AARD	Percentage of average absolute deviation
CAMD	Computer Aided Molecular Design
EACN	Equivalent Alkane Carbon Number
SDHS	Sodium dihexyl sulfosuccinate
RHS	Right hand side

LIST OF SYMBOLS

Symbol	Description
N_c	Capillary number
u	Darcy valocities
μ	Displacing fluid viscosity
μ_S	Viscousity of saturated phase
μ_D	Viscosity of displacing phase
σ	Interfacial tension between water and oil
θ	contact angle between water and oil
$k_{rD}S_{or}$	Relative permeability of displacing fluid at the residual oil saturation
$k_{rDS}S_{wc}$	Relative permeability of oil at the immobile water saturation
S	Optimal salinity of surfactant/oil/water system
K	Slope of the logarithm of optimum salinity in range 0.1 to 0.2 and it is an indicator of surfactant properties (head part)
f(A) or φ(A)	The alcohol function depended on type and concentration of additional alcohol
α or c	The temperature coefficients at optimal salinity condition
ΔT	Temperature difference from reference temperature
C_c	Characteristic curvature
C_{ci}	Characteristic curvature of ionic surfactant
C_{ca}	Characteristic curvature of anionic surfactant
C_{cn}	Characteristic curvature of nonionic surfactant
b	Constant of nonionic surfactants
G_{EX}/RT	Term of excess free energy normalized by RT
T_k	Krafft point temperature of anionic surfactant in °C
CP	Cloud point temperature of nonionic surfactant in K

LIST OF SYMBOLS

Symbol	Description
f(X)	Function of the target property that depends on three terms of group contribution: first-order group, second-order group and third-order group
C_i	Contribution of the first-order group
N_i	Number of group occurrences in type-i chemicals
D_i	Contribution of the second-order group
M_i	Number of group occurrences in type-j chemicals
E_k	Contribution of the third-order group
O_k	Number of group occurrences in type-k chemicals

CHAPTER I
INTRODUCTION

Microemulsion is the surfactant/oil/water system that is applied to many applications such as enhanced oil recovery, cleaning agents, environmental remediation and drug delivery system. From the industrial development, surfactants are developed with many types and structures such as internal olefin sulfonate (IOS) or extended surfactants. There is a wide space of surfactant choices. The challenge is how we select the suitable surfactant for use in specific application. To select the suitable surfactant to form an efficient microemulsion system for each specific condition and application, a systematic selection method is needed to reduce time and valuable resources that may be required in the design of an interest product.

For the use of surfactant, the surfactant properties estimation is used for developing methodology of surfactant screening, based on group contribution concept by Marrero *et al.* (2001). This model was applied to hydrophilic-lipophilic difference (HLD) equation to predict type of emulsion along with other properties and criteria to screen and select the suitable surfactants for a specified case study.

Finally, all of results were compared with experimental results and the case studies from literatures were used to verify the selection methodology. Case studies included several applications that are related to microemulsion such as EOR, detergents and soil remediation. The accuracy of all models were identified to make the strong reliability of this work.

CHAPTER II
LITERATURE REVIEW

This part demonstrates an overview of literature related to enhanced oil recovery with focusing on surfactant flooding in chemical process including the limitation and researches for solutions, explains the fundamental correlation for predicting the hydrophilic and lipophilic quality of surfactant in enhanced oil recovery, which is hydrophilic-lipophilic difference (HLD) and mentions the use of group contribution model to estimate the chemical properties for overcoming the limitation of surfactant flooding and receiving the method to select surfactant for EOR.

2.1 Enhanced Oil Recovery

From the demand of energy consumption and the limited resource of natural crude oil, the techniques for oil production are needed to respond the continuously increasing energy demand of the world. Typically, the primary oil production, called primary oil recovery is the production of hydrocarbon by natural force owing to pressure difference between the production well and reservoir. Oil recovery can be divided into three levels: primary recovery, secondary recovery and tertiary recovery (Sultan *et al.*, 2010). Primary recovery is the first step that oil can be produced by natural force of the reservoir with recovering 5-30 percent of the original oil in place (OOIP). Then, the secondary oil recovery is usually applied after the primary recovery has ceased or no more economically gain. The secondary oil recovery can recover up to 20-35 percent of the OOIP. Tertiary recovery, or enhanced oil recovery (EOR), can produce oil up to 30-60 percent of the OOIP or more (Elmofty, 2012).

EOR techniques have long been developed by many researches. Typically, this oil recovery step covers the injection of specific substances as the fluid into the reservoir, such as chemical and microbial. The injection fluid will displace crude oil and push it through the production well. The key purpose of the EOR process are to control interfacial tension, the wettability, pressure gradient and fluid properties to mobilize the remaining crude oil. (Nagy *et al.*, 2015). From the development of the technology, there are a number of techniques for enhanced oil recovery that can be

briefly classified into 4 types: chemical flooding, thermal oil recovery, gas injection, and microbial oil recovery (Ahmadi *et al.*, 2014) as shown in the Figure 1. The significance of selecting the best recovery method is to give the largest amount of profit (Taber *et al.*, 1997). This work focused on the surfactant flooding that is one of the sub-types of chemical flooding.
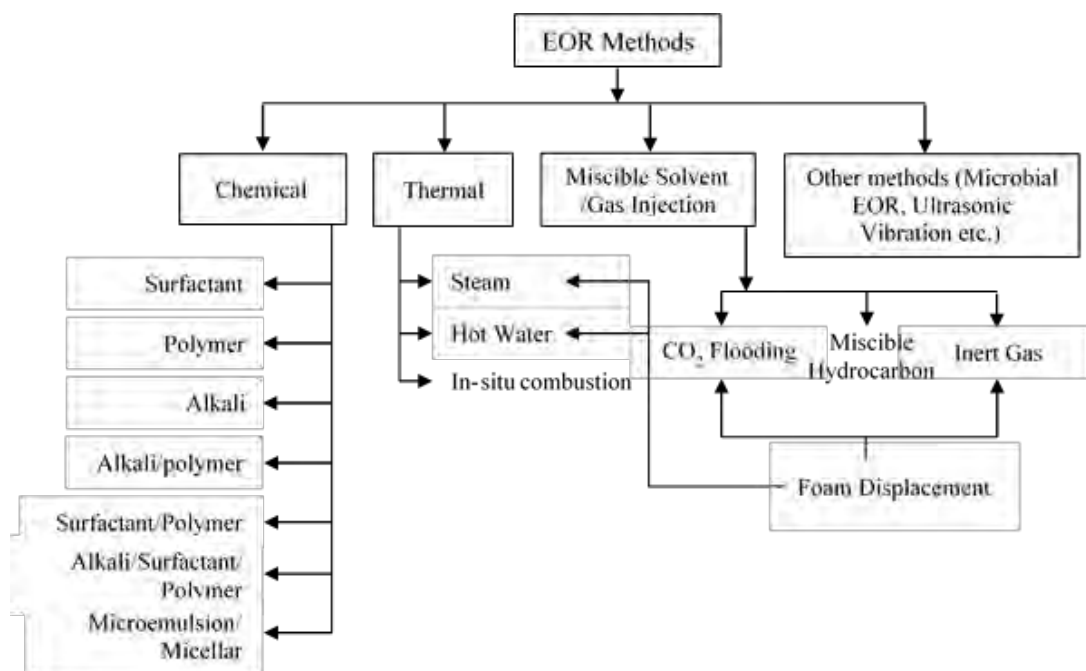
Figure 2.1 Classification of EOR methods (Bera *et al.*, 2014).

2.2 Surfactant Flooding

Surfactant flooding is the one of the effective enhanced oil recovery techniques, which is one type of chemical flooding. It has been found that chemical flooding can significantly improve oil recovery by microscopic displacement of oil remaining in the fine pores of the reservoir rock after water flooding or secondary oil recovery (Jeirani *et al.*, 2013). The injected chemicals are surfactant, alkali and/or polymer. Surfactants injection has been regarded as the potential chemicals in enhanced oil recovery since 1970s because of their capabilities to reduce interfacial tension (IFT) and altering the wettability of reservoir rocks (Ahmadi *et al.*, 2014, Kumar *et al.*, 2016). This work will mainly focus on the interfacial tension capability of the surfactant flooding technique.

First of all, there are two main variables for considering the efficiency of enhanced oil recovery techniques: capillary number and mobility ratio (Sofla *et al.*, 2016). The capillary number is defined as follows:

$$N_c = \frac{u\mu}{\sigma cos\theta}$$ Eq. 2.1

Capillary number is the variable that related to the residual oil saturation (see Equation 1) where N_c is the capillary number, u is the Darcy velocities, μ is the displacing fluid viscosity, σ is the interfacial tension between water and oil, and θ is the contact angle. The higher capillary number is preferred. From the equation, surfactant can lower the σ (or IFT) by generating microemulsion. There is the preferred condition for EOR (Sheng, 2015). Another variable is mobility ratio. The mobility ratio for EOR is the relationship of relative permeability of water to oil ratio (see Equation 2)

$$M = \frac{\mu_S k_{rD}(S_{or})}{\mu_D k_{rDS}(S_{wc})}$$ Eq. 2.2

where M is the mobility ratio, μ is the viscosity of saturated phase (subscribed S) and displacing phase (subscribed D), $k_{rD}S_{or}$ is the relative permeability of displacing fluid at the residual oil saturation, and $k_{rDS}S_{wc}$ is the relative permeability of oil at the immobile water saturation (Muggeridge *et al.*, 2014). Surfactant injection can improve the mobility ratio by removing the residual oil, also increasing the oil permeability and decreasing the water permeability. Simultaneously, the IFT becomes lower in this point and the movement of oil is more effective (Sheng, 2015).

Microemulsion, the key of successful mechanism for chemical flooding in oil recovery process, is introduced to the surfactant flooding because of capability of extraction efficiency by reducing oil–water IFT (Bera *et al.*, 2014). The fluid that is normally insoluble together can disperse in another fluid by adding surfactant. The microemulsions consist of at least three phases: polar phase, non-polar phase and surfactant phase, as shown in the Figure 2. The microemulsion can simply be divided into two types: oil-in-water microemulsion (O/W), or called micelle structure and water-in-oil microemulsion (W/O), or called reverse micelle structure (Malik *et al.*, 2012).
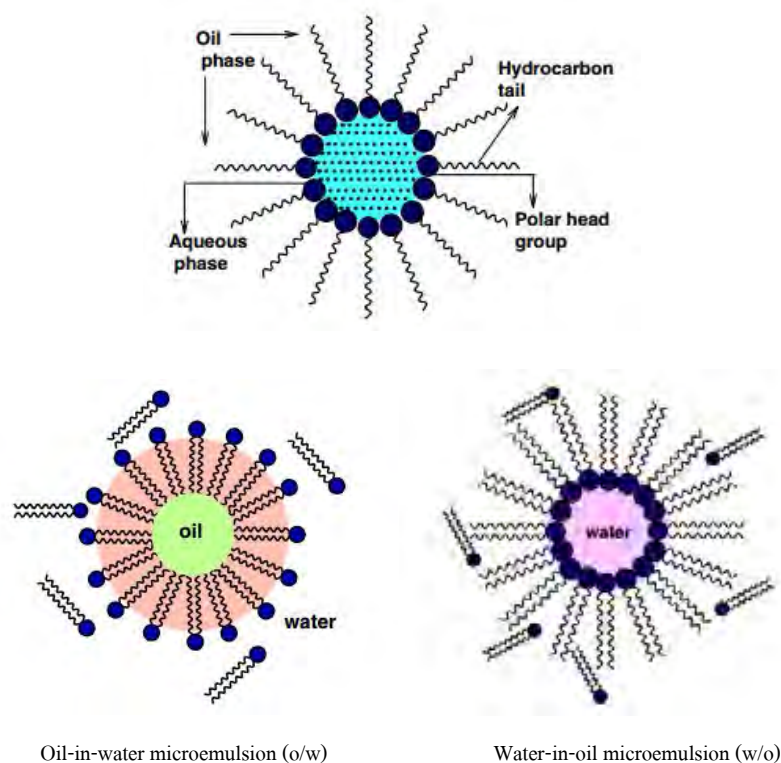
Figure 2.2 Typical structure of microemulsion: microemulsion for oil-in-water (O/W) and reverse microemulsion for water-in-oil (W/O) (Malik *et al.*, 2012).

The Winsor type system is studied for the systematic approach to select the surfactants for microemulsion formation. In Figure 3, there are three types of the Winsor microemulsion systems. First starting at low salinity, Winsor type I (oil-in-water, O/W) microemulsions are formed when oil is solubilized in water. When the salinity is increased, the solubilization of the microemulsion is increased. Until a certain point, microemulsions are changed to Winsor type III (middle-phase) system which is the lowest interfacial tension system. As the salinity increased, the system is converted from the middle-phase to Winsor type II (water-in-oil, W/O) system and at this point water is solubilized in oil. By the reasons, salts can increase the tendency of the surface active substances to collect at the interface and reduce the interfacial tension (Baran, 2001, Kumar *et al.*, 2016). In this work, Winsor type III microemulsion is considered because of the lowest interfacial tension in this point. Low interfacial tension can increase the solubility of water and oil and make the better attraction

between two phases. It is important in several applications such as detergency, cosmetics use, organic contaminated soil remediation, drug delivery system (Chen *et al.*, 2007) and EOR process (Sandersen, 2012).
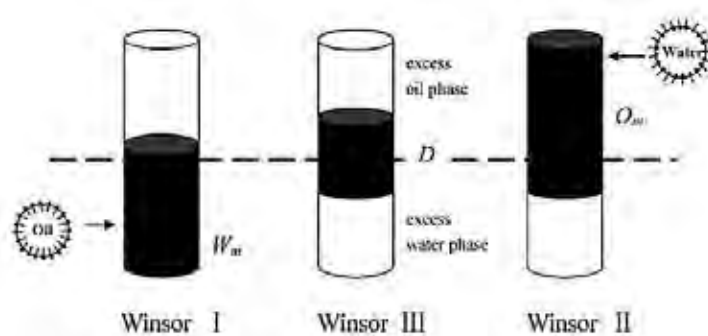
Figure 2.3 Winsor-Type microemulsion system, Winsor type I is O/W, Winsor type III is the middle phase and Winsor type II is W/O (Pan *et al.*, 2010).

However, there are some limitations of surfactant flooding. The formation of microemulsions may plug the pore, adsorb in the reservoir rock and then lose the high amount of surfactant in the reservoir rock. Consequently, high quantity of surfactant is needed. Meanwhile, the costs of synthetic surfactants are expensive. Also, this point became the major limitation in cost of surfactant and this technique has been considered uneconomical for investment (Ahmadi *et al.*, 2015, Sofla *et al.*, 2016).

To overcome the limitations, mixing surfactant with co-surfactant and co-solvent in the surfactant flooding is one of the alternative solutions to make better efficiency and reduce the investment cost (Taber *et al.*, 1997). For example, some fields solved the problems by using alcohol to improve phase behavior and controlling the quantity of brine to increase solubilization of oil and water in microemulsion or by the use of co-surfactant to adjust the mobility control (Jones *et al.*, 1976), especially mixture of anionic and nonionic surfactant (Lu *et al.*, 2012). The significance of blending surfactant with others is considered as the synergistic effect. Synergistic effect is specified as a condition that the properties of a mixture are better than those of individual component alone. As previously mentioned, the mixing of surfactant with other chemicals both surfactant and alcohol can reduce the interfacial tensions and

critical micelle concentrations (CMC) better than using single surfactant (Trawiľska *et al.*, 2016). Nevertheless, the use of alcohol has some disadvantages since alcohol decreases the solubilization of oil and water in microemulsion and slightly increases the minimum IFT achieved by the surfactant flooding (Hirasaki *et al.*, 2011). Also, the trend of using alcohol as co-solvent has decreased while there is a wide interest in using co-surfactant.

Another solution is related to numerous screening methods, for examples, the use of combined evaluation correlation for selecting nonionic surfactants for EOR applications (Nagy *et al.*, 2015), the correlation of bulk foam stability and core-flood experiment (Jones *et al.*, 2016) or the chemical property model for selecting a suitable the surfactant in any applications such the cloud point group-contribution model of nonionic surfactant (Mattei *et al.*, 2014). This solution approach is widely used until now.

Conclusion, the surfactant flooding is one of the dominant and effective EOR methods but this process is limited to the high cost of surfactant. So, the surfactant selection is needed to find the most suitable surfactant for reducing cost and improving the efficiency for EOR applications (Nagy *et al.*, 2015). There is a need to investigate the best methodology to select surfactants from the many available choices, including the combination of co-solvent or co-surfactant with the main surfactant.

2.3 Features of Surfactant

2.3.1 Definition and Structure

Surfactants are chemical compounds that consist of two parts: head and tail. The head of surfactant contains polar structure that is hydrophilic part and the tail of surfactant composes of non-polar structure that is hydrophobic part (see Figure 4). The combination of these two parts makes the surfactant soluble in both aqueous and oil phase (Najafi *et al.*, 2017). Generally, surfactant can be divided into four main types: anionic, cationic, nonionic and zwitterionic surfactant. Each type of surfactants is based on their association during dispersion in water (Sofla *et al.*, 2016). Anionic surfactant has negative charge in its head part, while the cationic surfactant contains positive charge. Nonionic surfactant has no charge in the head part and zwitterion

surfactant has both negative and positive charges in the head part. The summary table of surfactant mechanism in EOR applications in each type is shown in the Table 1 and the commonly used surfactant for EOR is shown in Table 2. The cationic surfactants are only one that can change the wettability of rock with the adsorption on the surface, but they are still in the research scale. Anionic and nonionic surfactants are usually employed in EOR such as alkyl sulfate, Tweens, Spans etc. and cationic surfactant is used in a few areas (Negin *et al.*, 2017).
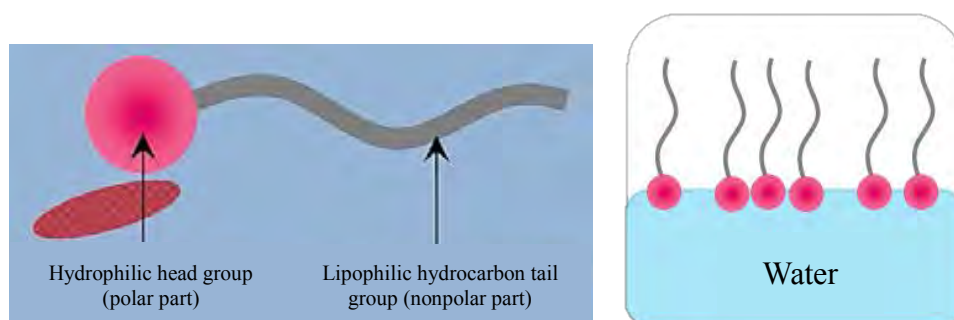
Figure 2.4 Simple structure of surfactants (Sandersen, 2012).
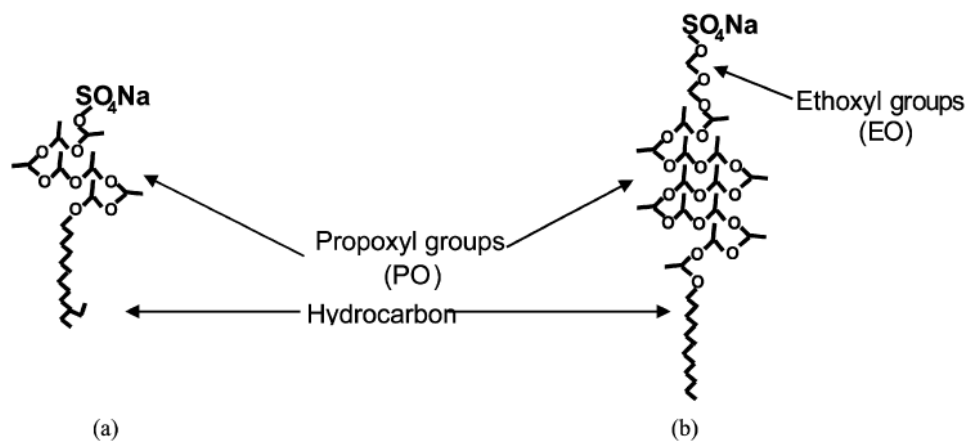
Figure 2.5 Example of extended surfactant structures (a) R-(PO)x-SO₄Na, (b) R-(PO)y-(EO₂)-SO₄Na (Witthayapanyanon *et al.*, 2008).

Table 2.1 Summary mechanism of using in each surfactant type in EOR applications (Negin *et al.*, 2017)

Types	Advantages	Mechanism
Anionic	Mostly use, effective in sandstone	Reducing IFT
Nonionic	Use as co-surfactant, not highly effective compared to other types, tolerate for hard water	Reducing IFT
Cationic	Stable solution in brine, effective in carbonate reservoir	Reducing IFT and Wettability alteration

Table 2.2 Examples of surfactants that used in EOR applications (Negin *et al.*, 2017)

Types	Common use in surfactant EOR process
Anionic surfactant	Alkyl Aryl Sulfonates, Alkyl Benzene Sulfonate, Alkyl Sulfate, N-Ethoxy Sulfonate, Sodium Dodecyl Sulfate, Alcohol Propoxy Sulfate, Alpha-Olefin Sulfonate, Alpha-Olefin Sulfate, Alkyl Ethoxy Sulfate, Sodium Petroleum Sulfonate, Gemini Anionic Surfactant
Nonionic surfactant	Alkyl Ethoxy Carboxylated, Alkyl Polyglycoside, Neodol, Tweens, Spans, Tridecyl Alcohol, Triphenylmethane
Cationic surfactant	Cetyl Trimethyl Ammonium Bromide, Dodecyl Trimethyl Ammonium Bromide, Ethoxylated Alkyl Amine

For the research and development of surfactant technology, the chemical groups are added to conventional surfactants as intermediate polarity molecules, called extended surfactant, such as polyethylene (EOs group) and/or polypropylene oxide groups (POs group) (Witthayapanyanon *et al.*, 2008). The additional groups can improve the surfactant properties to achieve ultralow interfacial tension, lower optimal salinity and higher solubility from extending the tail of surfactant (see Figure 5). So, these surfactants are currently used in many applications (Witthayapanyanon *et al.*, 2006).

2.3.2 Important Properties of Surfactants

2.3.2.1 Critical Micelle Concentration

Critical micelle concentration (CMC) is the concentration at which the surfactant molecules start to self-associate with others to form micelle or reverse micelle structure. This CMC depends on the specific surfactants (Lavkush Bhaisare *et al.*, 2015). There are some tools that are used for predicting the CMC of each surfactant. Group-contribution model is one of many tools that can predict the CMC value by considering the chemical group of surfactant structures (Mattei *et al.*, 2013). This model will be discussed in later part.

2.3.2.2 Interfacial Tension

Interfacial tension (IFT) is a property of two immiscible phases (condensed phase), considered as the free energy per unit surface area. This property is important to many fields such as enhanced oil recovery, water quality in aquifers, and stability of emulsion (Andersson *et al.*, 2014). For the EOR application, the factors that affect to the interfacial tension between polar and non-polar phase are oil composition, surfactant concentration, solvent concentration, water-oil ratio, salinity and divalent ions, and operating conditions. However, the major parameters that affect the interfacial tension are surfactant concentration and salinity of the system. Higher surfactant concentration can lead to lower interfacial tension of the system while the lowest interfacial tension occurs at certain salinity, called optimal salinity (Sheng, 2015).

2.3.2.3 Solubility

The solubility is significant for indicating the microemulsion of surfactant. The total surfactant solubility does not only depend on monomer structure, but also on the micelle solubility. Solubility of a surfactant differs in ionic and nonionic surfactants. The solubility of ionic surfactant increases with increasing temperature. In contrast, nonionic surfactants typically consist of ethoxylate groups whose solubility is lower with increasing temperature. These different mechanisms will affect other properties (Li *et al.*, 2005, Ahmadi *et al.*, 2014, Zarate-Munoz *et al.*, 2015).

2.3.2.4 Krafft Point and Cloud Point

Krafft point is one of the important properties of ionic surfactants. For ionic surfactants, the solubility increases with temperature. So, that is at a temperature below the Krafft point, the surfactant is a useless solid or in other words, when the temperature decreases below this point, the concentration is below the surfactant critical micelle concentration and the solubility is confined (Li *et al.*, 2005).

For nonionic surfactants, the characteristic property that is related to the temperature is cloud point. At this point, the surfactant separates from an aqueous phase and solution becomes opaque because of the weakening of hydrogen bonds between molecules of surfactant and water and the strengthening of attraction force among surfactant tails. So, when the temperature increases, the solubility of a nonionic surfactant will decrease and cloudy solution will occur. When using nonionic surfactant, a higher cloud point is desired to avoid phase separation (Zarate-Munoz *et al.*, 2015). Instance, the prediction model for cloud point property of nonionic surfactant is can be predicted by the group contribution model (see Eq. 2.11) in the following part.

2.4 Hydrophilic-Lipophilic Difference (HLD)

Hydrophilic-lipophilic difference (HLD) is a fundamental correlation of thermodynamically formulated equation to explain microemulsion system. This equation is first proposed by Salager *et al.* (1979). Not only the potential of transferring

surfactants from oil phase to aqueous phase, but also the balances of each parameter (temperature, oil, water and salt) for the oil-water-surfactant system are included in the correlation. In addition, HLD can determine the optimum formulation of a system involving with various alcohol and divalent ions (Salager *et al.*, 1979, Acosta *et al.*, 2012, Budhathoki *et al.*, 2016). The HLD equations for ionic and nonionic surfactants are expressed in Eq. 2.3 and Eq. 2.4, respectively (Castellino *et al.*, 2011):

For ionic surfactants,
$$HLD = \ln(S) - K*EACN - f(A) - \alpha\Delta T + C_c \qquad \text{Eq. 2.3}$$

For nonionic surfactants,
$$HLD = b(S) - K*EACN - \varphi(A) + c\Delta T + C_{cn} \qquad \text{Eq. 2.4}$$

where $\ln(S)$ and $b(S)$ are the function of salinity concentration in the aqueous phase in g/100mL; b is the constant for nonionic surfactants; K is the slope of the logarithm of optimum salinity in range 0.1 to 0.2 and it is an indicator of surfactant properties (head part); EACN is the equivalent alkane carbon number which depends on the nature of oil; the function $f(A)$ and $\varphi(A)$ are the alcohol function depended on type and concentration of additional alcohol; the variables α and c are the temperature coefficient at optimum salinity condition; ΔT is the temperature difference from a reference temperature (typically 298 K); and C_c and C_{cn} are the characteristic curvature that is explained intensively in a later part.

The HLD value is related to the Winsor type of microemulsion. The negative HLD value indicates the Winsor type I (O/W). For HLD of zero value, it is classified as the Winsor type III (middle phase microemulsion). And the positive value of HLD indicates the Winsor type II (W/O) (Jin *et al.*, 2015). The phase transition of microemulsion from Winsor type I to type III and continually to type II is occurred together with the shift of a negative HLD value to a positive value (Castellino *et al.*, 2011).

For the HLD application, sometimes, the mixtures of surfactants are employed with synergistic effect both the mixture of ionic-ionic surfactants and the mixture of ionic-nonionic surfactants. Acosta *et al.* (2008a) reviewed the HLD

equation of mixed surfactant systems. Eq. 2.5 represents the HLD calculation for ionic-ionic surfactant mixtures and Eq. 2.6 is the HLD calculation for ionic-nonionic surfactants (Acosta *et al.*, 2008a):

$$HLD_{mix} = X_1(HLD_1) + X_2(HLD_2) \qquad \text{Eq. 2.5}$$

$$HLD_{mix} = X_i \times HLD_i + X_{ni} \times HLD_{ni} + G_{EX}/RT \qquad \text{Eq. 2.6}$$

where HLD_1 and HLD_2 are the HLD value of surfactant 1 and 2; X_1 and X_2 are the molar fractions of each surfactant; subscripts i and ni represent ionic and nonionic surfactant, respectively; and G_{EX}/RT is the term of excess free energy normalized by RT.

In the application of HLD equation, the estimation of parameters in HLD equation is determined. Some of researchers proposed the use of a mathematic model to predict the value corresponded to HLD equation. However, there are still less models to predict the characteristic curvature values of surfactants. One of a few works is the C_c model developed by Acosta (2008) is explained below.

For the characteristic curvature (C_c or C_{cn}), a negative value is defined as a hydrophilic surfactant while a positive value is defined as a lipophilic surfactant. It is important to imply the characteristics of surfactants since it is related to the type of micelle forming in the oil-water-surfactant system (micelle or reverse micelle) (Hammond *et al.*, 2011).

One of the examples of simple equation for predicting C_c was developed by Acosta (2008). His work used the phase inversion temperature (PIT) to examine the C_{cn} parameter. Eq. 2.7 shows the correlation of C_c value of nonionic surfactants that followed the linear relationship with the number of carbon atoms in the surfactant head and tail (Acosta, 2008):

$$C_{cn} = 0.28 \times N_{CS} + 2.4 - N_{ES} \qquad \text{Eq. 2.7}$$

where N_{CS} is the number of carbon in hydrophobic tail of a surfactant and N_{ES} is the number of ethoxylate groups in hydrophilic head of a surfactant.

The prediction of C_c values developed by Acosta (2008) is limited to nonionic surfactants with ethoxylate groups. It is of interest to explore a more generic model to predict the C_c property of ionic and nonionic surfactants. Group contribution method is a powerful tool to predict a property of chemical substances based on their structure. One of the objectives in this work is to develop the C_c model based on Marrero *et al.* (2001) group contribution model (see topic 2.5) for extending the C_c group contribution model developed by Acosta (2008).

2.5 Group Contribution Model (GC Model or GCM)

In the screening or selecting of the suitable chemicals for any processes, the property estimation methods are needed for the fast and accurate design to match the property needed for a certain application. Typical compounds in industry or other fields are often limited to the available experimental data for a large number of organic compounds that are produced. Knowing the chemical properties of organic compounds is a preliminary step to select the most appropriate chemicals for the desired task. There are many methods for predicting properties of chemical compounds such as Quantitative property-property relationships (QPPRs), Quantitative structure-property relationships (QSPRs), and Group contribution models (GCMs) (Reinhard *et al.*, 1998). This work focuses the Group contribution method which has the higher accuracy than the others (Mattei *et al.*, 2013, Mattei *et al.*, 2014).

Group contribution method is the method that uses the effect of chemical structures or functional groups to the chemical properties. This method has the advantages of fast prediction and isomer diversity (Marrero *et al.*, 2001). The group contribution model that has been widely used by many researches was developed by Marrero and Gani. They developed a model to describe the relationship between the functional groups in a molecule to the target property as shown in Eq. 2.8.

$$f(X) = \sum_i N_i C_i + \sum_j M_j D_j + \sum_k O_k E_k \qquad \text{Eq. 2.8}$$

where $f(X)$ is a function of the target property that depends on three terms of group contribution: first-order group, second-order group and third-order group. C_i is the

contribution of the first-order group multiplied with N_i that is the number of group occurrences in type-i chemicals. D_j is the contribution of the second-order group multiplied with M_j that is the number of group occurrences in type-j chemicals. Also, E_k is the contribution of the third-order group multiplied with O_k that is the number of group occurrences in type-k chemicals. In the first-level of group contribution, the target property is predicted by the effect of basic functional groups. For the higher levels group contribution, the prediction is considered as the effect of polyfunctional groups or the combination of repeating chemical structure.
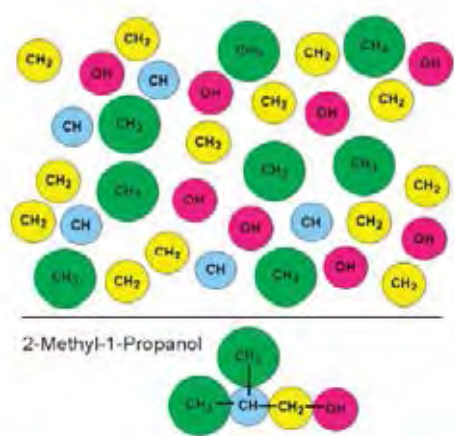
Figure 2.6 Breaking scheme of 2-methyl-1-propanol molecule into fragment to represent the concept of GC-model (van Speybroeck *et al.*, 2010).

To obtain accuracy, the objective function of this model must be set to minimize the error or deviation from comparing experimental and predicted data. The following equations show the statistical parameters for the objective function (Evangelista *et al.*, 2017):

$$\%RD = 100 \left(\frac{X^{exp} - X^{calc}}{X^{exp}} \right) \qquad \text{Eq. 2.9}$$

$$\%ARD = 100 \left| \frac{X^{exp} - X^{calc}}{X^{exp}} \right| \qquad \text{Eq. 2.10}$$

$$\%AARD = 100 \frac{1}{N_{data}} \sum_{i=1}^{N_{data}} \left| \frac{X^{exp} - X^{calc}}{X^{exp}} \right| \qquad \text{Eq. 2.11}$$

where X^{exp} is the experimental data; X^{calc} is the calculated data from model; and N_{data} is the amount of data points.

There are several works that construct the model based on Marrero and Gani such as enthalpy of formation model (Hukkerikar *et al.*, 2013), critical micelle concentration model (Mattei *et al.*, 2013), cloud point model (Mattei *et al.*, 2014), and critical properties model for organic compounds containing halogen (Mondejar *et al.*, 2017). The examples of these models that related to the criteria for surfactant screening in this work are explained below.

Example application of Marrero and Gani model that is related to surfactant properties is the cloud point model (Mattei *et al.*, 2014). This model used three-level of group contribution to predict the cloud point property of nonionic surfactants (see Eq. 2.12). The equation shows that the function of square of cloud point can predict the cloud point of nonionic surfactants with 15.83% in maximum absolute deviation that was lower than other models.

$$CP^2 = \sum_i N_i C_i + \sum_j M_j D_j + \sum_k O_k E_k \qquad \text{Eq. 2.12}$$

Another predicted property is critical micelle concentration (CMC) of nonionic surfactant (Mattei *et al.*, 2013). This model considered the function of CMC as the logarithmic function (see Eq. 2.13). The new third-order group was proposed to improve the accuracy of this model. The value of 1.5082 maximum absolute deviation was obtained, indicating the high accuracy of the CMC model from the group contribution method.

$$-\log (CMC) = \sum_i N_i C_i + \sum_j M_j D_j + \sum_k O_k E_k \qquad \text{Eq. 2.13}$$

In this work, the three-level Marrero and Gani group contribution model is used to predict the surfactant properties including Krafft point, and C_c values of anionic and nonionic surfactants. In the Cc value models, it is aimed to develop the models for mixed surfactant systems of anionic-anionic or nonionic-nonionic surfactants.

2.6 Screening Criteria

From the surfactant flooding process, sub-division of EOR, there are many surfactants in the list that can be employed for EOR application (example of surfactants shown in Table 2). The approach to screen and select the suitable chemicals are needed to reduce the cost and maintain the efficiency of operation. This approach is called chemical production design. The chemical production design is an important step in any fields. Its objectives is to screen and search a product that expresses a set of desirable behavior (Gani, 2004, Mattei *et al.*, 2012).

The simple scheme for chemical product design is shown in the Figure 7. It can conclude the principle procedure as follows: identify the needs, generate ideas to reach needs, choose among ideas, and manufacture products (Gani, 2004). The first step of chemical product design is the definition of the problem or goal of the desired product. This step is important to make a decision in the following steps. Then, the set of target properties is required and the list of chemicals which satisfy these targets is established. The method to use is consequently determined and limited in some constraints. Next, the design step that uses the selected method is considered. In the molecular problems, the popular method is Computer Aided Molecular Design (CAMD). This programming method provides the possibility of designing products by solving with mathematical optimization. The results from this step are analyzed and verified to assure the feasibility of results before final verification of candidate selection through the case studies(Acosta *et al.*, 2003) (Gani, 2004, Mattei *et al.*, 2012, Cignitti *et al.*, 2015).
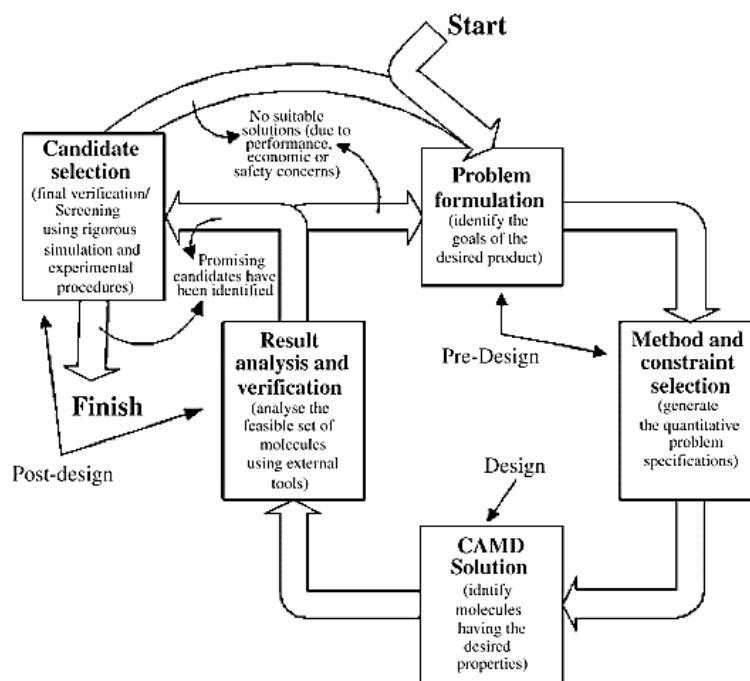
Figure 2.7 Schematic process for chemical product design (Gani, 2004).

This chemical product design procedure is considered in this work. To preliminarily screen the surfactants for EOR, several criteria and constraints are required. It is noted that CAMD is not included in this work. This work focuses only the development of the approach for surfactant screening and it is examined with other criteria and constraints to recommend the suitable surfactant (or chemical) for the specific applications.

2.7 Motivation

Nowadays, there are limited energy sources, especially petroleum sources while the energy demand are continuously increasing. The development of oil recovery techniques is needed to produce oil to meet the energy demand of the world. Enhanced oil recovery process (EOR) is applied for oil recovery. Chemical flooding is one of the EOR techniques to enhance oil by using suitable chemicals. The space of chemical substances is wide and the selection of suitable chemicals is still challenge. Surfactants

are one of the chemicals used in EOR techniques. Their structure consists of head and tail parts that can solubilize in both water (or polar substances) and oil (or non-polar substances), respectively, and reduce the interfacial tension between the two phases. This work can improve EOR process and reach a higher oil production. However, the surfactant screening method is needed to select the most suitable surfactant. The group contribution method is a powerful tool to correlate the chemical structures to their properties. This method will be applied to hydrophilic-lipophilic difference (HLD) and then is used together with other properties and criteria to screen and select the suitable surfactants for EOR process.

2.8 Objectives

    2.8.1 <u>To develop models to predict properties of single and mixed surfactant systems based on group contribution concept.</u>

    2.8.2 <u>To introduce a systematic methodology to select the most suitable surfactant for several applications such as EOR process, detergents and soil remediation via HLD value and other criteria.</u>

2.9 Scope of Research

The scope of this research will cover the following:

    2.9.1 <u>Scope for Objective 1</u>

        2.9.1.1 The Model Based on Group Contribution Concept Include Krafft Point for Anionic Surfactants, and the Characteristic Curvature Values of Anionic and Nonionic Surfactants.

        2.9.1.2 The Group Contribution Concept Proposed by Marrero et al. (2001) Will Be Used for Developing Model.

        2.9.1.3 Available Experimental Data of Krafft Point and the Characteristic Curvature Values Will Be Collected from Literature.

2.9.1.4 The Simplified Method to Measure Characteristic Curvature of Nonionic Surfactant Proposed by Zarate-Muñoz et al. (2016) Will Be Conducted to Supplement the Data for Group Contribution Model.

2.9.1.5 The Mixed Surfactant Systems of Anionic-Anionic and Nonionic-Nonionic Surfactants Will Be Included.

2.9.2 <u>Scope for Objective 2</u>

2.9.2.1 Information of Selected Reservoir Conditions, Properties and Other Case Studies that are Related to Microemulsion Systems Will Be Collected from Literatures.

2.9.2.2 The HLD Value of Single Surfactant System Will Be Determined in Surfactant Selection.

2.9.2.3 The HLD Value of Mixed Anionic-Anionic or Nonionic-Nonionic Surfactant Systems Will Be Determined in the Surfactant Selection for Selected Application.

2.9.2.4 Other Group Contribution Models Such as Cloud Point Model, and Critical Micelle Concentration Will Be Collected from Other Literatures to Use as the Criteria in Surfactant Selection.

2.9.2.5 The HLD Value or Related Parameters Will Be Determined for Surfactant Screening of Case Studies Such as Detergents and Health Care Products.

2.9.2.6 Selected Surfactant from this Work Will Be Compared with the Selected Surfactant from Literatures.

CHAPTER III
EXPERIMENTAL

3.1 Materials and Equipment

3.1.1 Equipment

3.1.1.1 Laptop Computer (Intel® Core™ i5-5200U CPU 2.20 GHz, 4 GB of RAM, Windows 10)

3.1.1.2 SVT 20 Spinning Drop Video Tensiometer

3.1.1.3 WiseCircu Water Bath with Digital Fuzzy Control System

3.1.1.4 Wisemix Vortex Mixer (VM), WVM00010

3.1.2 Glassware

3.1.2.1 Flat bottom vials 15 ml

3.1.2.2 Test tube rack

3.1.3 Software

3.1.3.1 Microsoft Excel 2013

3.1.3.2 Minitab

3.1.4 Chemicals

3.1.4.1 Surfactants

- Sodium dihexyl sulfosuccinate (SDHS)
- C12-14EO1 Dehydol LS 1 TH from Thai Ethoxylate Co., Ltd. (>99.7% active ingredients)
- C12-14EO2 Dehydol LS 2 TH from Thai Ethoxylate Co., Ltd. (>99.7% active ingredients)
- C12-14EO3 Dehydol LS 3 TH from Thai Ethoxylate Co., Ltd. (>99.7% active ingredients)
- C12-14EO3 Dehydol LS 5 TH from Thai Ethoxylate Co., Ltd. (>99.7% active ingredients)

- C12-14EO9 Dehydol LS 9 TH from Thai Ethoxylate Co., Ltd. (>99.7% active ingredients)

- C12-14EO12 Dehydol LS 12 TH from Thai Ethoxylate Co., Ltd. (>99.7% active ingredients)

- Marlox RT 42 (C16-18 with EO4-PO2) from Sasol (100% active ingredients)

- Marlox RT 64 (C16-18 with EO6-PO4) from Sasol (100% active ingredients)

3.1.4.2 Hydrocarbons

- Cyclohexane from Carlo Erba Reagent (99.8% purity)

- Decahydronaphthalene or decalin, mixture of cis and trans isomers from Merck (99% purity synthesis grade)

- Hexane from RCI Labscan Limited. (purity 95% AR grade)

- Heptane from Univar Canada Ltd. (99.5% purity)

- Dodecane from Merck (99% purity synthesis grade)

- Hexadecane from Acros Organics (99% purity)

3.1.4.3 Others

- Sodium Chloride from RCI Labscan Limited. (purity 99% AR grade)

3.2 Methodology

    3.2.1 <u>Literature Review</u>

        The concepts of enhanced oil recovery, surfactant properties, HLD equation, methodology for finding parameters in HLD equation, the application of surfactant in single and mixed system, and the group contribution model were reviewed. The necessary data for developing model were listed, including the range of parameter values that related to HLD equation, some surfactant properties and other parameters that affected to surfactant selection. In addition, the case studies for surfactant selection both EOR and others were considered.

    3.2.2 <u>Data Collection</u>

        The literatures from the literature reviews step were collected for developing the group contribution model and surfactant selection methodology. Some essential data for developing the group contribution model and surfactant selection, including the characteristic curvature of anionic and nonionic surfactants, krafft point of anionic surfactants, cloud point of nonionic surfactants, and critical micelle concentration of surfactants were collected. The methodology for conducting the experiment of characteristic curvature was determined from literatures. The case studies for verifying the results were also collected.

    3.2.3 <u>Measurement of Characteristic Curvature of Nonionic Surfactant</u>

        The experiment was conducted with the simplified methodology proposed by Zarate-Muñoz *et al.* (2016).

      3.2.3.1 EACN Consideration

        The EACN of hydrocarbons used in the experiment were investigated from the HLD equation according to Zarate-Muñoz et al. (2016). Three methods were proposed to measure optimal salinity of surfactant-oil-water systems: solubilization curve, interfacial tension measurement and emulsion stability or coalescence rate. They concluded that the emulsion stability method was the simplest and fastest way to measure optimal salinity. This method considers the optimal salinity by recording the time (coalescence time) that the middle phase of Winsor Type III is

separated from the excess phase in the stable position (or the middle phase does not change its position). The salinity that reaches the stable condition with the shortest time is identified as the optimal salinity. So, the emulsion stability is applied for this work. Sodium dihexyl sulfosuccinate (SDHS) was used as a reference surfactant because of its perfor-mance that is suitable for different oils (Acosta et al., 2003). The system was carried out at 25 °C and no alcohol was added. The EACN of each hydrocarbons was determined with adjusting the ionic HLD equation at a condition of optimal salt where type III microemulsion was achieved. At this condition the HLD was equal to zero; hence, Eq. 2.3 becomes:

$$EACN = (\ln S^* + C_c)/K \qquad \text{Eq. 3.1}$$

The K and C_c values for SDHS are 0.17 and -0.92, respectively (Zarate-Muñoz et al., 2016). The salinity scan was conducted and then, EACN value will be calculated. In addition, the EACN of hexadecane were determined by mixing with lighter hydrocarbon in 1:1 ratio and using linear mixing rule to calculate EACN.

3.2.3.2 Preparation

The surfactant/oil/water system was performed in flat-bottom vials with 2 mL of aqueous phase and 2 mL of oil. The concentration of surfactant was fixed in the same molarity for all systems and the amount of Sodium Chloride (NaCl) in the system were varied in range of 0 – 26 g to 100 mL. Single surfactant scans were conducted with selected reference surfactants and mixed surfactant scans were conducted with mixture of reference surfactant and test surfactant in varying ratio by keeping the sum of surfactant concentration at the same molarity.

3.2.3.3 Salinity Scans

This part will conduct using different oil (different EACN) in case of single surfactant and mixed surfactants. Microemulsion formulation was carried out by shaking with Vortex Mixer and was left at room temperature.

3.2.3.4 Temperature Scans

This part conducted only single surfactant. The steps were performed at a fixed salinity value and the temperature was increased at 5 °C of increment. The maximum temperature of each oil type was kept below its flash point.

The optimal salinity was verified by using coalescence time. At the optimal value, the coalescence time of each surfactant system reached fastest time.

However, the EACN consideration needed the lowest interfacial tension measurement to obtain the most accurate value. This point was discussed in the later part.

3.2.3.5 Data Analysis

The results of single surfactants were used to find parameters for HLD equation by regression analysis and the results of mixed surfactants were used to calculate the characteristic curvature of test surfactants, according to the work of Zarate-Muñoz et al. (2016) and the range of each parameter was determined with previous work (Salager et al., 2001).

3.2.4 <u>Developing the Group Contribution Model of Characteristic Curvature</u>

In this step, the developing of characteristic curvature model was based on Marrero *et al.* (2001) concept with accumulated data from literatures and experiment. The regression analysis was also performed to find the group contribution parameters corrected by minimizing deviation between predicted values and experimental values.
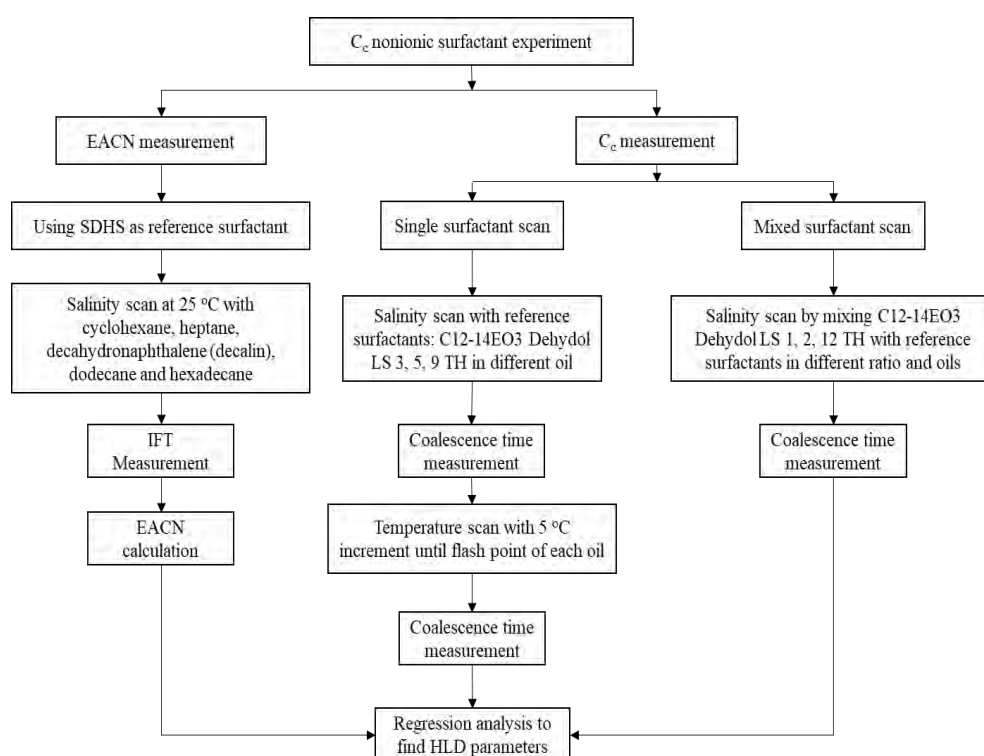
Figure 3.1 Schematic flowchart of measurement of C_{cn} nonionic surfactant.

3.2.5 Developing the Group Contribution Model of Krafft Point

The similar procedure as the developing of characteristic curvature model was applied. The database of krafft point model of anionic surfactants was obtained from literatures only. The same objective function was applied to minimize the overall deviation.

3.2.6 Product Design via HLD Values

The scope of determination HLD equation was in case of no co-solvents and/or co-surfactants, no alcohol inclusion and mixed surfactant with different type (anionic and nonionic surfactants). The HLD value was calculated via the characteristic curvature model. The determination of other properties and their models that were used to screening criteria in the case studies were included.

3.2.7 Surfactant Selection and Comparing to the Case Studies

The case studies of various applications were selected from literatures. The surfactant selection methodology employed to the selected case study to find the list of suitable surfactants. Moreover, the comparison of the selected surfactants to the surfactants in selected case study was determined to verify the result.

CHAPTER IV
KRAFFT POINT MODEL

4.1 Introduction

Surfactants are commonly used chemicals that are presented in many applications both in daily human activities and in industrial processes due to their remarkable ability to change the surface and interface properties (Schramm *et al.*, 2003). One of the important properties of surfactants is their solubility. Surfactant can be soluble in both polar (or aqueous phase) and non-polar phases (or oil phase). The solubility of surfactants can be described by their structure which consist of hydrophilic head groups and hydrophobic tails. Surfactants can be categorized into four types by the charge of their head groups: anionic, cationic, nonionic and zwitterionic surfactant (Sofla *et al.*, 2016, Najafi *et al.*, 2017). The applications of these surfactants are different. For example, anionic surfactants or a mixture of anionic-nonionic surfactants are used in enhanced oil recovery (EOR) to reduce the interfacial tension (IFT) between water and oil and to alter the rock surface properties. Anionic surfactants can lower the IFT between the two phases more than other amphoteric surfactants (Kamal *et al.*, 2015). Other applications such as the removal of organic compounds or heavy metals from soil also utilize both anionic and nonionic surfactants (Liang *et al.*, 2017). Cationic surfactants can be used to change the wettability of solid surface such as rock or polytetrafluoroethylene (PTFE) that are hydrophobic (Thakkar *et al.*, 2017). Other applications include the room-temperature radical polymerization where the presence of surfactant helped enhance the decomposition of free-radical inhibitor (Zhang *et al.*, 2017). Although most surfactants are hydrocarbon compounds, some fluorocarbon surfactants are employed in some applications (Li *et al.*, 2005) because of their higher chemical stability in acidic, oxidative and reducing agents (Kunieda *et al.*, 1976).

The solubility of surfactants plays an important role in performing their normal function at a given condition. The solubility of surfactants both their monomer and the micelles depends on temperature (Myers, 2006). Krafft point (or Krafft temperature) is used to identify the solubility of ionic surfactants or, in other word

Krafft point is also known as the surfactant melting temperature. When the temperature is below this point, surfactant will separate from the aqueous phase and become the ineffective solid (Chu *et al.*, 2012). This point is presented as a sharp break in the plot between solubility and temperature. For nonionic surfactants, different mechanism occurs when describing the solubility and temperature relationship. As the temperature increases, the solubility of nonionic surfactant decreases until reaching a point where surfactant separates from the aqueous phase and makes the solution cloudy. This point is called a Cloud point (Zarate-Munoz *et al.*, 2015). Both Krafft point and Cloud point are the simple indication for surfactant solubility and they are a characteristic property of each surfactant. A correlation between the Krafft point or cloud point properties and the surfactant structure is of importance to select proper surfactants that can perform in a specific condition. A model that is based on the surfactant structure and can reliably predict the surfactant property seems to give the best answer to this propose.

There are various methods proposed to predict chemical properties. Quantitative structure-property relationships (QSPR) and Group-Contribution (GC) Method are widely used for the property prediction. The QSPR approach is based on structure and quantum chemistry of substances where the descriptors were obtained from advanced statistical analyses based on the relationship between structural information and the characteristics of substances including their topology, geometry, electrostatics, and molecular-orbital characteristics (Acosta *et al.*, 2003). The QSPR method has been widely used to predict surfactant-related properties such as solubility parameter (Wang *et al.*, 2006), critical micelle concentration (Huibers *et al.*, 1996, PDT *et al.*, 1997, Yuan *et al.*, 2002), surface tension (Stanton *et al.*, 1990), cloud point (Ren *et al.*, 2011) and Krafft temperature (Li *et al.*, 2005). Although the QSPR is versatile and can be used as a property prediction model, it is heavily relied on extensive regression analysis which involves a software specifically developed for this purpose. The group contribution method is well-known for its simplicity and provides quick estimates of property based on the component structure. The property of a compound is calculated by the summation of frequency of each molecular fragment (group) occurrence multiplying by the contribution of that group (Marrero *et al.*, 2001). The GC method has been widely used to predict the pure organic compound properties, for instance, normal boiling point, normal melting point, critical properties,

standard enthalpy of formation, standard enthalpy of vaporization, standard Gibbs energy, and standard enthalpy of fusion (Marrero *et al.*, 2001). Some surfactant-related properties have been predicted by the GC method, including critical micelle concentration (Mattei *et al.*, 2013), hydrophilic-lipophilic balance (Guo *et al.*, 2006), relative solubility number (Wu *et al.*, 2004) and cloud point (Mattei *et al.*, 2014). To the authors knowledge no studies have been done to develop the GC method to predict the Krafft temperature of surfactants.

The group contribution based on Marrero and Gani GC-model (Marrero *et al.*, 2001) can be performed at three levels as described by its generic form as follows:

$$F(X) = \sum_i N_i C_i + \sum_j M_j D_j + \sum_k O_k E_k \qquad \text{Eq. 4.1}$$

where $F(X)$ is a function of the target property that depends on three terms: first-order group, second-order group and third-order group. C_i, D_j, E_k are the contribution of the first-order, second-order, and third-order group, respectively. These variables are multiplied with the number of group occurrences in each level, as N_i, M_j, O_k in Eq. 4.1, respectively (Marrero *et al.*, 2001). It is noted that the main assumption of Marrero and Gani GC-model is based on the linear relationship of the main representative molecular fragment and $F(X)$. For instance, the number of ethoxylate groups (CH_2CH_2O) of hydrophilic chain in anionic surfactant owes a linear relationship with the square of the cloud point (CP); hence, $F(X) = CP^2$ (Mattei *et al.*, 2014). This assumption must be verified in applying the GC concept to the property prediction models (Reinhard *et al.*, 1998, Li *et al.*, 2005, Mattei *et al.*, 2013).

This study is focused on the development of a model to estimate the Krafft temperature of anionic surfactants based on Marrero and Gani GC-model. A comparison of the GC-model and the QSPR model for Krafft temperature is presented. The application of the model is highlighted through example.

4.2 Methodology

4.2.1 Data Collection

The experimental data set for Krafft point of anionic surfactants that used in this work consists of 53 anionic surfactants. The various classes of anionic surfactants are collected: alkyl sulfonate; alkyl sulfate; alkyl benzene sulfonate; branched alkyl sulfonate; branched alkyl sulfate; branched alkyl benzene sulfonate; alkyl ethoxy sulfate; alkyl ester sulfonate; alkyl ester sulfate; alkyl (di)sulfate; Alkyldiphenylether(di)sulfonates; Alkyl (di)estersulfonate; alkyl naphthalene sulfonate; and fluorohydrocarbon surfactants. Their Krafft points and structures are shown in Table 1. Sources of these data set come from many works (Raisen, 1957, Weil *et al.*, 1963, J.K. *et al.*, 1966, Smith *et al.*, 1966, Götte, 1969, Takeshi *et al.*, 1970, Shinoda *et al.*, 1972, Ueno *et al.*, 1974, Valint *et al.*, 1987, Os *et al.*, 1993, Ohbu *et al.*, 1998, Vautier-Giongo *et al.*, 2003).

Before using all of data set, the relationship of Krafft point property in each class will be investigated. The linear relation of data set is needed to verify before applying Group-Contribution Method. As shown in Figure. 4.1, the relation between carbon atoms in alkyl chain and Krafft point is determined. There are linear relationship in each class with increasing number of carbon atoms, the temperature will be increased. In addition, the effect of ethoxylate group is also investigated. There are also linear relationship shown in Figure. 4.2. When the number of ethoxylate group are increased, the temperature will be decreased. The results have same trend as the previous work about the effect of surfactant structure on Krafft point (Gu *et al.*, 1992). Therefore, these relations are agreeable for Group-Contribution Method. In addition, it can be noticed from these trends that surfactant structures or number of fragment molecules affect the Krafft point of the surfactant.

Table 4.1 The experimental Krafft points of anionic surfactants and their structures
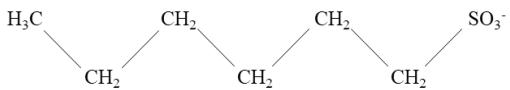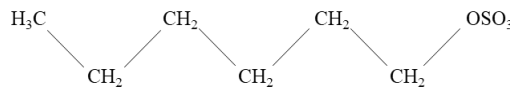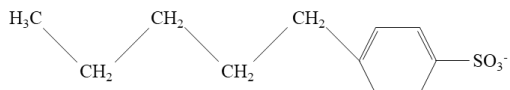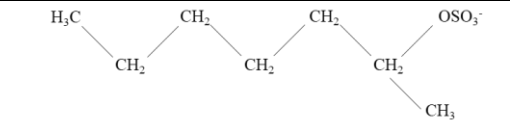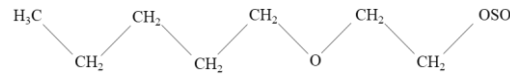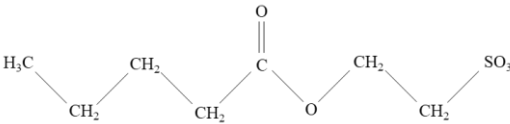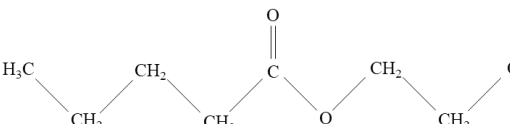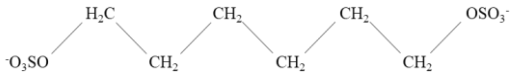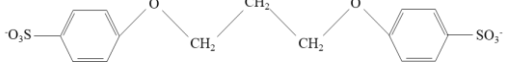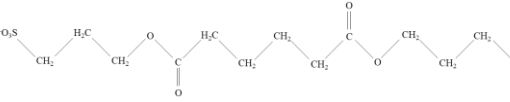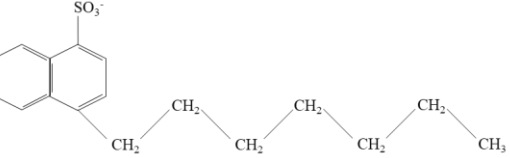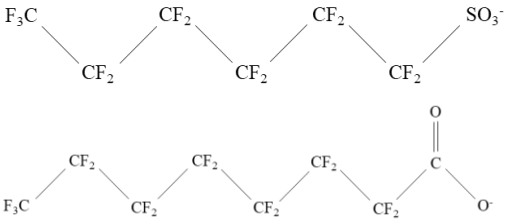
Anionic surfactants	Representative structures	Exp. Krafft point (°C)
Alkyl Sulfonate (Negin *et al.*, 2017)		
C10SO3	H₃C, CH₂, CH₂, SO₃⁻, CH₂, CH₂, CH₂	22.5
C12SO3		38.0
C14SO3		48.0
C17SO3		62.0
C18SO3		70.0
Alkyl Sulfate (Negin *et al.*, 2017)		
C10OSO3	H₃C, CH₂, CH₂, OSO₃⁻, CH₂, CH₂, CH₂	8.0
C12OSO3		19.0
C13OSO3		20.8
C14OSO3		30.0
C15OSO3		31.5
C16OSO3		45.0
C18OSO3		56.0
Alkyl Benzene Sulfonate (Negin *et al.*, 2017)		
C7PhSO3	H₃C, CH₂, CH₂, CH₂, CH₂, SO₃⁻	9.0
C8PhSO3		18.5
Branched Alkyl Benzene Sulfonate (Negin *et al.*, 2017)		
2C10PhSO3	CH₃, H₃C, CH₂, CH, CH₂, CH₂, SO₃⁻	22.0
2C12PhSO3		31.5
2C16PhSO3		54.2
2C18PhSO3		60.8
Branched Alkyl Sulfate (Negin *et al.*, 2017)		
2C13COSO3	H₃C, CH₂, CH₂, OSO₃⁻, CH₂, CH₂, CH₂, CH₃	11.0
2C15COSO3		25.0
2C17COSO3		30.0
Alkyl Ethoxy Sulfate (Negin *et al.*, 2017)		
C16E1OSO3	H₃C, CH₂, CH₂, CH₂, OSO₃⁻, CH₂, CH₂, O, CH₂	36.0
C16E2OSO3		24.0
C16E3OSO3		19.0
C18E3OSO3		32.0
C18E4OSO3		18.0
Alkyl Ester Sulfonate (Xu *et al.*, 2018)		
C10AESO3	O, H₃C, CH₂, C, CH₂, SO₃⁻, CH₂, CH₂, O, CH₂	8.1
C12AESO3		24.2
C14AESO3		36.2
Alkyl Ester Sulfate (Xu *et al.*, 2018)		
C10AEOSO3	O, H₃C, CH₂, C, CH₂, OSO₃⁻, CH₂, CH₂, O, CH₂	12.5
C12AEOSO3		26.5
C14AEOSO3		39.0

Table 4.1 The experimental Krafft points of anionic surfactants and their structures (continued)

Anionic surfactants	Representative structures	Exp. Krafft point (°C)
Alkyl (di)sulfate (Schmitt, 2001)		
O3SOC12OSO3		12.0
O3SOC14OSO3		24.8
O3SOC16OSO3		39.1
O3SOC18OSO3		44.9
Alkyldiphenylether(di)sulfonates (Rosen, 1989)		
O3SPhOC6OPhSO3		20.0
O3SPhOC8OPhSO3		28.0
O3SPhOC10OPhSO3		59.0
O3SPhOC12OPhSO3		70.0
Alkyl (di)estersulfonate (Schmitt, 2001)		
O3SCEAC12AECSO3		23.5
O3SCEAC14AECSO3		31.0
O3SCEAC16AECSO3		38.5
Alkyl Naphthalene Sulfonate (Valint *et al.*, 1987)		
1,4 NS-8		9.0
1,4 NS-10		21.0
1,4 NS-14		50.0
1,4 NS-16		64.0
Fluorocarbon Surfactants (Li *et al.*, 2005)		
C7F15COONa		8.6
C8F17COONa		24.6
C10F21COONa		58.3
C12F25COONa		89.0
C7F15SO3Na		56.5
C8F17SO3Na		75.0

Where Ph represents a phenyl group; E represents an ethoxylate group; A represents a ketone group;

NS represents a Naphthalene sulfonate group
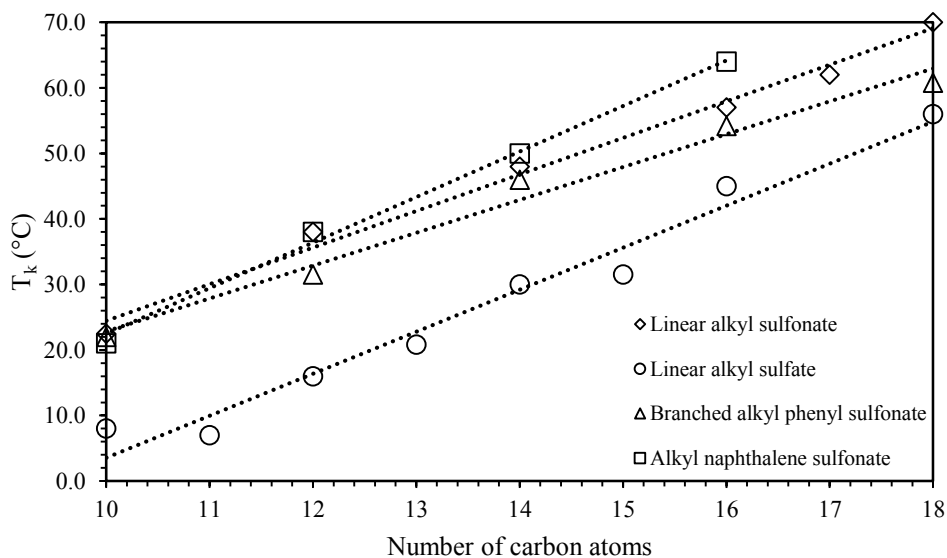
Figure 4.1 The relationship between Krafft point and the number of carbon atoms in alkyl chain for anionic surfactants: linear alkyl sulfonate; linear alkyl sulfate; branched alkyl phenyl sulfonate; and alkyl naphthalene sulfonate.
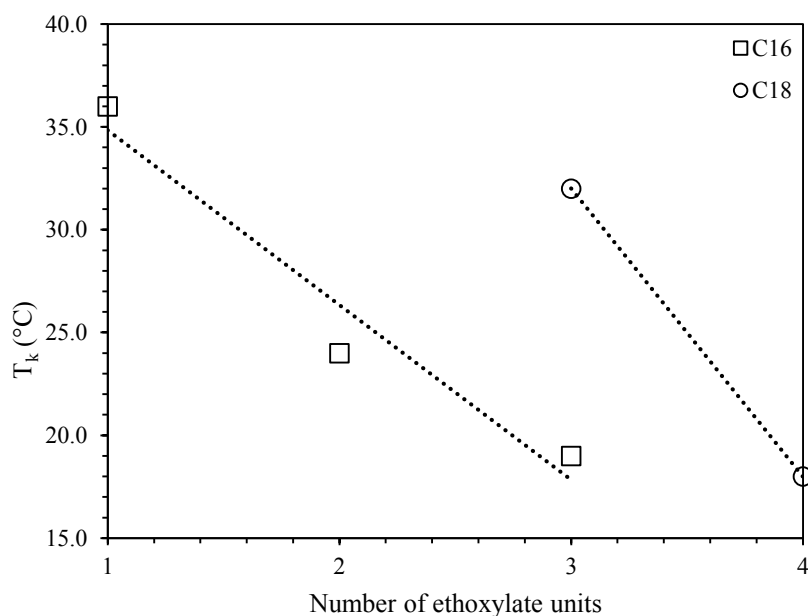
Figure 4.2 The relationship between Krafft point and number of ethoxylate units in alkyl chain for anionic surfactants: C16 and C18 alkyl chain length.

This work also includes the fluorocarbon surfactants in the Group-Contribution Model. There are 6 fluorohydrocarbon surfactants: only carboxylate and sulfonate classes that contain sodium ion as the counterion. According to the work from Lucassen-Reynders (1981) and Gu *et al.* (1992), it was evidenced that the types of counterion ion influence to Krafft point in both hydrocarbon and fluorohydrocarbon surfactants. However, the data for developing model is more available with sodium counterion ion (Na^+) and less in other counterion ions such as potassium (K^+) and ammonium (NH_4^+) ions, especially there is a lack of other counterion data set in conventional hydrocarbon surfactant. So, this work focused on the model development that includes only anionic surfactants with sodium counterion ion.

4.2.2 Development of GC-Model

In the development of Group-Contribution Model according to Marrero and Gani method (Marrero *et al.*, 2001), the first step is to define a suitable function (f(X)) in Eq. 4.1. To develop a characteristic of Group-Contribution Model Figure 4.1 and Table 4.1 show a linear relationship between the molecular structure and the predicted property, i.e. Krafft point. Therefore, F(X) in Eq. 4.1 can be substituted with Krafft point temperature (T_k) directly. Then Eq. 4.1 becomes:

$$T_k \; (°C) = \Sigma_i N_i C_i + \Sigma_j M_j D_j + \Sigma_k O_k E_k \qquad \text{Eq. 4.2}$$

The next step is defining the molecular structure of data set and classifying these structure into three level groups: first-order and higher-order levels. For the first-order, the molecular structure in each chemical is considered in a simple functional group such as $–CH_3$, $CH=CH$, CH_2COO, SO_3, and OSO_3^-. For the higher order, there are second-order and third-order groups. These higher level groups aim to obtain more accuracy of the Group-Contribution Model. The second-order groups are multiple functional groups that can describe the molecular effects for some chemicals, which cannot describe obviously by the first-order groups such as $OH-CH_n-COO$, alicyclic substituents and aromatic rings. For the third-order groups, these are the complex structures that contain fused cyclic molecule and/or large multiple functional groups such as fused ring aromatic (naphthalene) and polyfunctional group with long

alkyl chain or cyclic structure. If the available higher order groups from Marrero *et al.* (2001) are not enough to develop the accurate model, the new third-order group may be needed.

4.2.3 Correlation Analysis

The multiple linear regression is carried out between number of molecular groups or fragments and experimental Krafft point. Minitab is used in this step by setting experimental Krafft point as the response (Y) and number of molecular groups as the predictors (X). To obtain high accuracy, the Goal seek function in Excel Tool is used by minimizing the deviation by comparing the experimental and the calculated data. The equation for calculating deviation in this work is shown in Eq. 4.3:

$$\%\text{Deviation} = 100 \, \frac{1}{\text{Ndata}} \sum_{i=1}^{\text{Ndata}} \left| \frac{Tk^{exp} - Tk^{calc}}{Tk^{exp}} \right| \qquad \text{Eq. 4.3}$$

where T_k^{exp}, T_k^{calc} are the Krafft point from experiment and developed model, respectively, and N_{data} is the total data point.

4.2.4 Benchmark

To benchmark the GC model developed in this work for Krafft point temperature of anionic surfactants, the QSPR model proposed by Li *et al.* (2005) is used to compare the results.

4.3 Results and Discussion

To develop a GC-model for Krafft point temperature of anionic surfactants, a linear relationship between F(X) in Eq. 4.1 and the group contribution terms on the RHS of Eq. 4.1 must be established as the assumption of the Group-Contribution Method. This work investigated the imperative of a constant (or intercept in linear function) to obtain higher accuracy predicted by the GC-model (Roughton *et al.*, 2012, Kulajanpeng *et al.*, 2016). By adding a constant Eq. 4.2 becomes:

$$T_k \ (°C) = \Sigma_i N_i C_i + \Sigma_j M_j D_j + \Sigma_k O_k E_k + \text{constant} \qquad \text{Eq. 4.4}$$

The results from the regression analysis to minimize deviation between the experimental data and the regressed values are shown in Table 4.2 and 4.3. Table 4.2 tabulated the group definition and their coefficients for the first-order groups and Table 4.3 shows the group definition and their coefficients for the second- and third-order groups. An example of the decomposition of alkyl naphthalene sulfonate and its associated fractional groups is given in Table 4.4. The higher the group contribution level, the larger the group of molecular structures are combined. The comparison of results is presented in a parity plot, or a relative error plot with the percentage of absolute deviation.

The development of the GC-model for Krafft point temperature is divided into three parts: the development of the first-order GC-model, improvement of the GC-model by using a higher-order group and the introduction of a new third-order group.
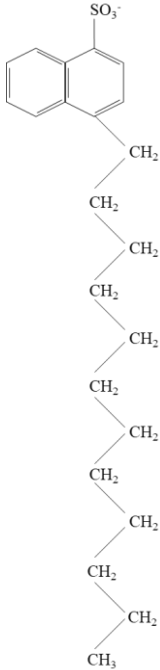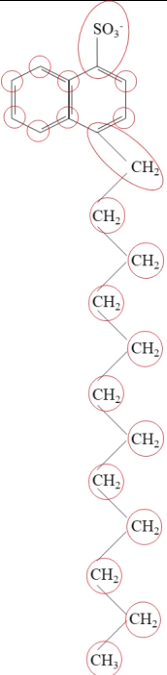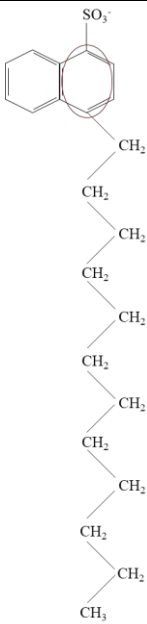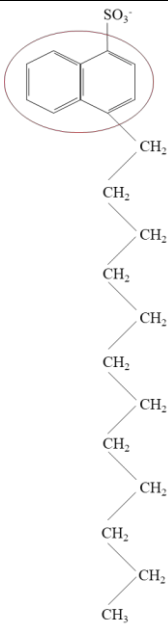
Table 4.2 Group definition and their coefficients for the first-order GC-model of Krafft point of anionic surfactants

First order group	Coefficient, C_i (°C)
CH_3	45.9329
CH_2	6.1141
CH	-54.1220
CH_2-O	-15.5808
CH_2COO	1.2907
SO_3^-	26.5247
OSO_3^-	32.6928
aC-O	65.8270
aCH	-2.7166
aC-CH_2	69.9810
aC-CH	22.0837
aC-SO_3^-	0.0060
aC fused aromatic ring	-0.2730
CF_3	38.7274
CF_2	16.0812
COO^-	0.0137
Constant	-126.6285

Table 4.3 Group definition and their coefficients for the higher-order GC-model (both second- and third-order groups) of Krafft point of anionic surfactants

Higher order group	Coefficient (°C)
Second order, D_j	
AROMRINGs^{1}s^4	0.0060
$^-O_3$S-aromatic-O	-0.0005
Third order, E_k	
OOC-(CH$_2$)$_n$-COO	-7.6915
^-O_xS-(CH$_2$)$_n$-OCO	-0.1607
aC-O-(CH$_2$)$_n$-O-aC	-0.0003
AROFUSEDs^{1}s^4	-0.1365
$^-O_3$S-alkyl tail	21.6530

Table 4.4 Example of the decomposition of 1,4 NS-12 (Alkyl Naphthalene Sulfonate) in First-order, Second-order and Third-order groups for calculating in the Krafft point GC-model

Molecular structure	First-Order groups	Second-Order groups	Third-Order groups
	1-CH$_3$ 10-CH$_2$ 6-aCH 1-aC-CH$_2$ 1-aC-SO$_3^-$ 2-aC fused aromatic	AROMRINGs^{1}s^4	AROFUSEDs^{1}s^2

4.3.1 Development of the First-Order GC-Model

To develop the first-order group, the molecular structure of each surfactant is analyzed to decompose into several fractional groups. 16 first-order groups in the Krafft point temperature model are proposed as shown in Table 4.2. The coefficient of each fractional group is obtained by a regression analysis. To assure the validity of the GC-model, the coefficient of each group must be analyzed. First, the coefficients of -CH_3 and -CH_2 are positive. There are some works indicated that an increase in alkyl chain length decreases the solubility of anionic surfactants (Gu *et al.*, 1992, Chu *et al.*, 2012). It means that the more number of -CH_3 and -CH_2 group presence in the surfactant structure, the lower the solubility of that surfactant is performed. Hence, it is reasonable for a Krafft point to increase with adding more contribution of –CH_3 and –CH_2 groups to Eq. 4.4. Likewise, -CF_3 and -CF_2 for fluorocarbon surfactants give a similar effect as –CH_3 and CH_2 and their regressed positive coefficients are justified. Huibers *et al.* (1996) justified obviously the molecular structure into hydrophobic part and hydrophilic part. They showed that –CH_3, –CH_2, -CF_3 and -CF_2 were included in the hydrophobic part of surfactant. Their contributions are relatively positive to make the higher Krafft point temperature.

The presence of -CH group is an indicator of a branching structure in a surfactant. O'Lenick (2007) reported a lower wetting behavior in surfactants with branching structure. For the wetting, this value indicates the ability to alter hydrophobicity. If the lower wetting value, the lower hydrophobicity is observed. Hence, the branching structure of hydrophobic part of surfactant can lead to high solubility in aqueous phase. Alexander *et al.* (2014) also successfully synthesized branched anionic surfactants and obtained remarkably low surface tension. As the branching factor increased, the lower surface tension and higher aqueous solubility were observed. These points come to explain the reason why the branched anionic surfactant gave the lower krafft point temperature and negative contribution. For example, the Krafft point temperature of linear C13OSO3 is 20.8 °C while branched C13OSO3 gives the lower value with 11.0 °C. Some works also supported that the branching structure of a surfactant gave easier micelle formation and better interfacial properties (Zhang *et al.*, 2017). Therefore, -CH fraction can increase the surfactant solubility and decrease the Krafft point temperature as presented in the negative

contribution in Table 4.2. Next, the ethoxylate group ($-CH_2O$) gave negative coefficient value to the Krafft point temperature. According to the study by Acosta *et al.* (2008a), the more number of ethoxylate groups, the lower the Krafft point was observed. Hence, its negative coefficient is justified.

The aromatic structure is also investigated as fractional groups in the GC-model. As illustrated in Table 4.4, the first-order level decomposes aromatic ring into fraction of aromatic carbon (aCH), aromatic carbon that fused with other rings (aC fused) and aromatic carbon that linked with substituted groups, i.e. $aC-CH_2$, AC-CH, and $aC-SO_3^-$. Typically, molecules with aromatic structure are relatively more soluble in water than those containing aliphatic structure. The π electrons of aromatic carbon can be delocalized and transferred among carbon atoms in an aromatic ring, resulting in a stronger electrostatic field as compared to a molecule with aliphatic structure when comparing two molecules with the same number of carbon atoms. So, an aromatic structure is stable and more soluble in water than an aliphatic structure molecule (Hanke *et al.*, 2003). However, the polarity of aromatic compounds is not high enough to be soluble in water as other polar groups. Hence, aromatic structure is categorized in the non-polar structure and is considered a part of hydrophobic tails of the surfactants (Huibers *et al.*, 1996). Therefore, the contributions of aromatic fractions are mostly positive; however, there are small magnitude of negative values from the regression that may come from the decomposition of aromatic structure into small fractions. For more complete representation of aromatic compounds, higher-order groups are required.

For functional group in the head part of anionic surfactants, Sulfonate ($-SO_3^-$) and Sulfate (OSO_3^-) are among the most common head groups of anionic surfactants. The head part of the surfactant should give negative contribution to indicate the more soluble structure in water but the results are not as expected. The contributions of sulfonate and sulfate are positive with high value. However, there is a constant added to the equation (Eq. (4.4)) to help the accuracy of model. Hence, the expected negative contribution from the sulfonate and sulfate groups might have been included in the constant in Eq. 4.4 during the regression. This work concludes that the contributions of sulfonate and sulfate mathematically correspond to the constant in the linear equation that is very low with a value of -126.6285.

The results from prediction by the first-order level are plotted in the parity plot with the experimental value as shown in Figure 4.3. It appears that some data points are deviated from the linear line, so the higher-order is necessary to be applied to improve the GC-model.
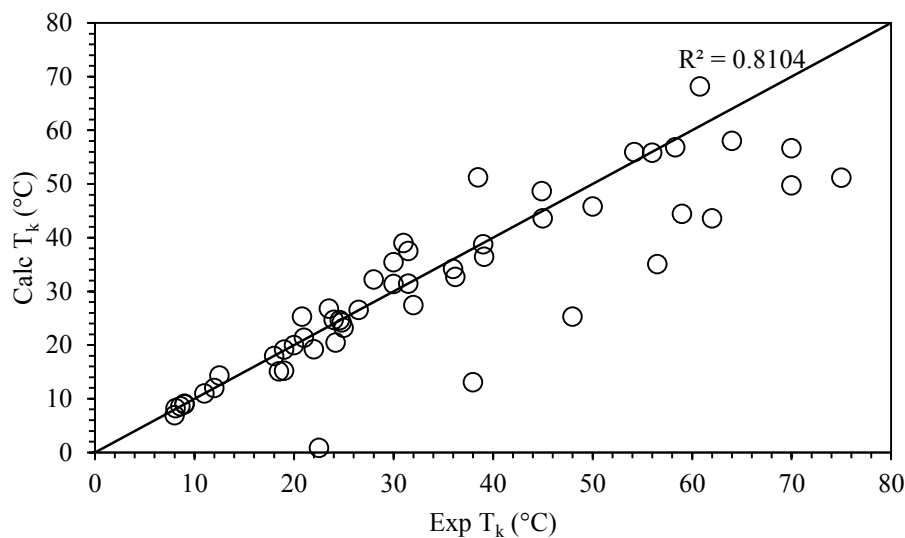
Figure 4.3 Parity plot between experimental Krafft point of anionic surfactants and calculated value from the first-order Group-Contribution Model.

An attempt was done to include fluorohydrocarbon surfactants in the GC-model developed in this work. Referred to the QSPR model developed by Li *et al.* (2005) a separated dataset of fluorohydrocarbon surfactants with a different set of descriptors were used for 19 fluorohydrocarbon surfactants consisting of Li^+, Na^+, K^+, H^+, and NH_4^+ as the counterion. This work investigated the effect of carbon chain length in fluorohydrocarbon surfactant and a linear relationship between number of carbon atoms and Krafft point of fluorohydrocarbon surfactants $C_nF_mCOO^-Na^+$ series was observed (see Figure 4.4.). The results shows the same trend as the conventional surfactants in Fig. 4.1. It seems that these dataset can be used in the development of the GC-model; however, there was insufficient data for regression analysis. Therefore, the effect of counterion of fluorohydrocarbon surfactant was neglected. Hence, in this

work only the dataset of fluorohydrocarbon surfactants with Na^+ counterion was only included in the GC-model developed in this study.
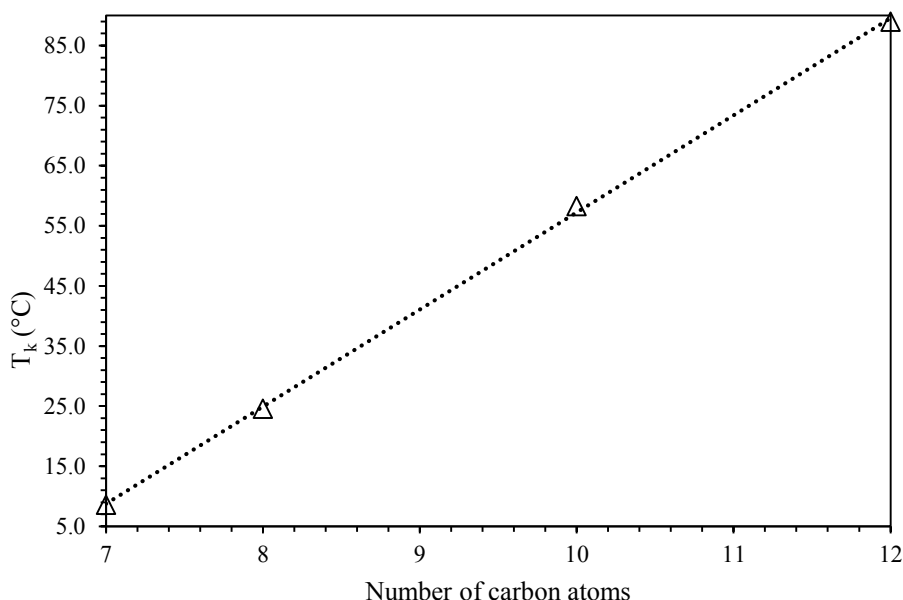
Figure 4.4 The relationship between Krafft point and number of carbon atoms in alkyl chain for carboxylate series of fluorohydrocarbon anionic surfactants.

4.3.2 Improvement of GC-Model by Using Higher-Order Group

The higher order groups are applied to the GC-model after achieving the first-order level. The advantage of adding the second-order groups was the consideration of polyfunctional groups and, hence, this could give the model with higher accuracy to predict the chemical properties than the first-order level. Based on Marrero *et al.* (2001), the second-order groups was proposed such as aromatic ring, cyclic carbon linked with substituted group and the linkage between two or more function groups. In this work, there are only two polyfunctional groups included as the second-order groups: AROMRINGs[1]s[4] represents the complete aromatic ring occupied with two substituents in the opposite ends of the ring (position 1 and 4) and ^-O_3S-aromatic-O represents the aromatics ring containing substituents of SO_3^- and O with a valence electron movement from substituted group. After regression analysis to

obtain the contribution of these second-order groups, there was no significant improvement in the prediction of the Krafft point temperature because of their very low contribution (see Table 4.3). The obvious reason for this problem is the lack of various dataset to arrange the second-order groups. Hence, the third order level is determined in the GC-model. Based on the criteria given by Marrero *et al.* (2001), the third-order groups from this work include OOC-$(CH_2)_n$-COO, -O_xS-$(CH_2)_n$-CO, aC-O-$(CH_2)_n$-O-aC and AROMFUSEDs[1]s[4]. The subscript n represents the length of hydrocarbon chain, which should be two or more. The subscript x represents the oxygen atoms in the sulfate compound that should be three or four. The addition of the third-order groups can improve the accuracy of those surfactants with aromatic rings and two-headed structure. However, some error still exists. As shown in parity plot (Figure 4.3), there are data points that are not in linear line but they are seem linear relationship. It is of interest those data point to analyze and change the relationship to the same linear line. A new third-order group should be proposed to improve the GC-model. Hukkerikar *et al.* (2013) suggested the procedure to establish the new third-order group to obtain the GC-model with high accuracy. Their recommendation is as follows:

- Finding and adding the supplement dataset to extend the available molecular structure in the GC-model and then, inspecting the validity and uncertainty of the dataset;

- Analyzing the dataset and searching chemicals that make the high deviation to the GC-model;

- Determining those previous chemicals to find the suitable group descriptors;

- Proposing new group descriptors that can improve the accuracy of the GC-model; and,

- Carrying the regression analysis to find the contribution values.

Hence, in this work new third-order groups were proposed to improve the accuracy of the GC-model.

4.3.3 Introduction of the new third-order groups

The introduction of the new third-order group initially considers based on the high deviation in the same molecular structure. From Figure 4.4, it seems that there are some data points that are deviated from the linear line with a relative constant deviation. These deviated data points are mostly from alkyl sulfonate groups (Alkyl tail-SO_3^-). The trend of deviated data is linear. Hence, the group of alkyl sulfonate surfactants, including hydrocarbon and fluorocarbon chain is of interest to be assigned by the new third-order group.

First, the solubility of alkyl sulfonate surfactants (CH_3-$(CH_2)_n$-SO_3^-) were compared with that of the alkyl sulfate surfactants (CH_3-$(CH_2)_n$-OSO_3^-). Chen et $al.$ (2004) concluded that alkyl sulfonate surfactants are less soluble than alkyl sulfate surfactants, consequently, the Krafft point temperature of alkyl sulfonate surfactants is higher. This is obviously revealed by the molecular structure of the head groups of these two surfactants. For alkyl sulfonate, the surfactant head consists of SO_3^-, while the head of alkyl sulfate consists of OSO_3^-. There is only difference in bridging between the head and the tail structure, -CH_n-SO_3^- bonding and CH_n-O-SO_3^- bonding for alkyl sulfonate and alkyl sulfate, respectively. The -CH_n-O-SO_3^- bridge extends the head of surfactant with an additional oxygen atom, providing one more available oxygen with its lone pair electrons to make hydrogen bonds with water molecules; consequently, the alkyl sulfate head is more soluble in water than the alkyl sulfonate (Del Re et $al.$, 2010). Hence, the Krafft point temperature of alkyl sulfate surfactants is lower than that of alkyl sulfonate surfactants with the same tail.

Huibers (1999) investigated the grouped atomic partial charges for each part of surfactant. The results showed that the charge of the head group of a surfactant greatly affects the other parts and partially distributes to the rest. The partial charge of each segment of a surfactant was measured including the head group, alpha methylene (α-CH_2), combining the head group and α-CH_2 (HG + α-CH_2) and the alkyl tail. The author used many methods to measure the charge distribution and the results showed the charge on α-CH_2 of alkyl sulfonate surfactant is more negative than the charge on α-CH_2 of alkyl sulfate surfactant. Due to the high polarity of CH_n-SO_3^- bond in alkyl sulfonate structure, the head group is highly negative and significantly distributes to the α-CH_2 and consequently to the alkyl tail. Huibers (1999) used NMR data to suggest

that the charge distribution on α-CH2 group lead to make this group included in the hydrophilic part of surfactant and gave the high repulsive force between head group of surfactant monomer, while the surfactant with a sulfate head group is prone to attract with other molecule due to the lower polarity of CH_n-OSO_3^- bond. Additionally, it seems that the critical micelle concentration (CMC) value of alkyl sulfonate is higher than alkyl sulfate, for example, the CMC value of $C_{12}H_{25}SO_3^-$ was equal to 0.0120 M while the CMC value of $C_{12}H_{25}OSO_3^-$ was equal to 0.0082 M, both of them was measured at 25 °C (Rosen, 2004). These results also justify the high polarity of sulfonate head group with C-S bond, leading to high repulsive force between surfactant monomer and decreasing the solubility in aqueous phase. Therefore, these two suggestions make the sulfonate head significantly interact with the α-CH2 and alkyl chain. This makes the sulfonate group and the attached alkyl chain, i.e. ^-O_3S-$(CH_2)_n$-CH_3, dissolve differently in an aqueous phase and support the establishment of the new third-order group to represent its behavior.
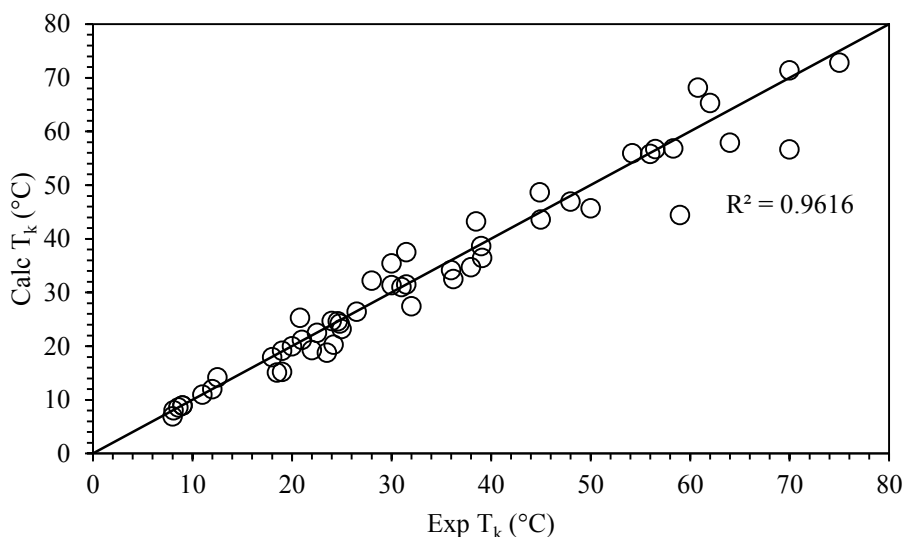
Figure 4.5 Parity plot between experimental Krafft point of anionic surfactants and calculated value from the higher-order Group-Contribution Model (both second-order and third-order groups).

The performance of the GC-model after applying the new third-order group is improved and the higher the accuracy is observed. Figure 4.5 presents the parity p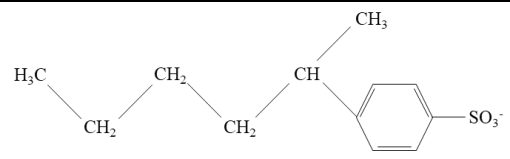lot between experimental Krafft point of anionic surfactants and the calculated values after applying the higher-order Group-Contribution Model with the new third-order groups. To compare the previous parity plot in Figure 4.3, the results show that most of deviated data points are shifted toward the diagnol line when the new third-order groups have been proposed. The accuracy is much improved and will be discussed in details later. Example calculations for using the proposed GC-model are represents in Tables 4.5 to 4.7. In Table 4.5, Krafft point of 2C14PhSO3 is calculated. There is no difference in Krafft point that is predicted by both the GC-model without any higher-order groups and the GC-model with higher-order groups. Only the second-order group namely AROMRINGs[1]s[4] appear in the 2C14PhSO3 structure and there is no third-order group in the structure. Since AROMRINGs[1]s[4] gives very low contribution; hence, no improvement was obtained after adding the second-order level. However, the propsed GC-model gave higher accuracy in predicting the Krafft point temperature than the predicted value obtained from the QSPR model (Li *et al.*, 2005). Tables 4.6 and 4.7 show the significant effect of applying the third-order groups to improve the accuracy of the proposed GC-model. Table 4.6 represents the calculation of Krafft point of C10AEOSO3. The addition of ($-O_xS-(CH_2)_n-OCO$) as a third-order group significantly improve the Krafft point. The %absolute deviation is reduced from 14.93% in the first-order level GC-model to 13.64% when predicted from the higher-order level. Likewise, the GC-model both first-order and higher-order groups gave higher accuracy than the predicted Krafft temperature obtained from the QSPR model for this particular surfactant (as compared in Table 4.8). Another remarkable example of applying the new third-order group is the introduction of the alkyl sulfonate, $^-O_3S-(CH_2)_n-CH_3$, as the new third-order group. C16SO3 is one of the alkyl sulfonate surfactants that face a problem with high deviation when only first-order level is applied. After adding of the third-order level, the %absolute deviation of the Krafft point prediction has improved from 37.54% in the first-order level to 3.85%. The accuracy from GC-model is comparable to that predicted by the QSPR model.

Table 4.5 Calculation of Krafft point of 2C14PhSO3 (Branched-Alkyl Phenyl Sulfonate group) with Group-Contribution Method compared with the QSPR method

2C14PhSO3		
Molecular structure:		
First-order group:		
Groups	Occurrences	Coefficients (°C)
CH$_3$	2	45.9329
CH$_2$	11	6.1141
aCH	4	-2.7166
aC-CH	1	22.0837
aC-SO$_3^-$	1	0.0060
Second-order group:		
Groups	Occurrences	Coefficients (°C)
AROMRINGs^{1}s^4	1	0.0060
Third-order group:		
Groups	Occurrences	Coefficients (°C)
No Third-order group		
T$_k$ calculation		
GC model without higher-order group; T$_k$ (°C) = $\Sigma_i N_i C_i$ + Constant = 43.71 °C		
GC model with higher-order group; T$_k$ (°C) = $\Sigma_i N_i C_i$ + $\Sigma_j M_j D_j$ + $\Sigma_k O_k E_k$ + Constant = 43.72 °C		
QSPR model; T$_{k,calc}$ = 42.20 °C		
%Absolute deviation from experimental value (T$_{k,exp}$ = 46.0 °C)		
GC-model without higher-order group; 4.98%		
GC model with higher-order group; 4.96%		
QSPR model; 8.26%		

Table 4.6 Calculation of Krafft point of C10AEOSO3 (Linear-Acyl ethoxylate Sulfate) with Group-Contribution Method compared with the QSPR method
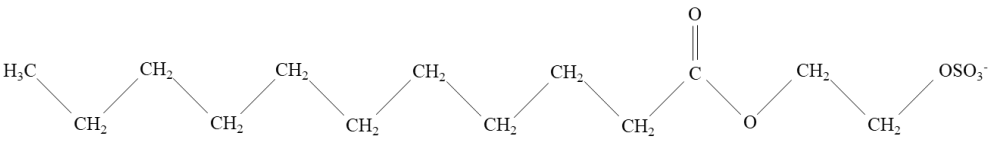
<table>
<tr><td colspan="3" align="center">C10AEOSO3</td></tr>
<tr><td colspan="3">Molecular structure:</td></tr>
<tr><td colspan="3">

</td></tr>
<tr><td colspan="3">First-order group:</td></tr>
<tr><td align="center">Groups</td><td align="center">Occurrences</td><td align="center">Coefficients (°C)</td></tr>
<tr><td align="center">CH_3</td><td align="center">1</td><td align="center">45.9329</td></tr>
<tr><td align="center">CH_2</td><td align="center">10</td><td align="center">6.1141</td></tr>
<tr><td align="center">CH_2COO</td><td align="center">1</td><td align="center">1.2907</td></tr>
<tr><td align="center">OSO_3^-</td><td align="center">1</td><td align="center">32.6298</td></tr>
<tr><td colspan="3">Second-order group:</td></tr>
<tr><td align="center">Groups</td><td align="center">Occurrences</td><td align="center">Coefficients (°C)</td></tr>
<tr><td colspan="3" align="center">No Second-order group</td></tr>
<tr><td colspan="3">Third-order group:</td></tr>
<tr><td align="center">Groups</td><td align="center">Occurrences</td><td align="center">Coefficients (°C)</td></tr>
<tr><td align="center">$-O_xS-(CH_2)_n-OCO$</td><td align="center">1</td><td align="center">-0.1607</td></tr>
<tr><td colspan="3">T_k calculation</td></tr>
<tr><td colspan="3">

GC model without higher-order group; T_k (°C) = $\Sigma_i N_i C_i$ + Constant = 14.37 °C

GC model with higher-order group; T_k (°C) = $\Sigma_i N_i C_i + \Sigma_j M_j D_j + \Sigma_k O_k E_k$ +

Constant = 14.20 °C

QSPR model; $T_{k,calc}$ = 9.30 °C

</td></tr>
<tr><td colspan="3">

%Absolute deviation from experimental value ($T_{k,exp}$ = 12.5 °C)

GC-model without higher-order group; 14.93%

GC model with higher-order group; 13.64%

QSPR model; 25.60%

</td></tr>
</table>

Table 4.7 Example calculation of Krafft point of C16SO3 (Hexadecyl sulfonate) with Group-Contribution Method compared with the QSPR method
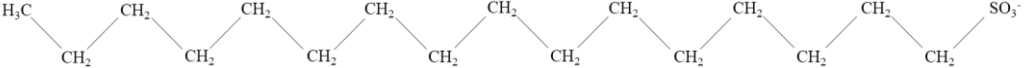
<table>
<tr><td colspan="3" align="center">C16SO3</td></tr>
<tr><td colspan="3">Molecular structure:</td></tr>
<tr><td colspan="3"></td></tr>
<tr><td colspan="3">First-order group:</td></tr>
<tr><td align="center">Groups</td><td align="center">Occurrences</td><td align="center">Coefficients (°C)</td></tr>
<tr><td align="center">CH_3</td><td align="center">1</td><td align="center">45.9329</td></tr>
<tr><td align="center">CH_2</td><td align="center">15</td><td align="center">6.1141</td></tr>
<tr><td align="center">SO_3^-</td><td align="center">1</td><td align="center">26.5247</td></tr>
<tr><td colspan="3">Second-order group:</td></tr>
<tr><td align="center">Groups</td><td align="center">Occurrences</td><td align="center">Coefficients (°C)</td></tr>
<tr><td colspan="3" align="center">No Second-order group</td></tr>
<tr><td colspan="3">Third-order group:</td></tr>
<tr><td align="center">Groups</td><td align="center">Occurrences</td><td align="center">Coefficients (°C)</td></tr>
<tr><td align="center">^-O_3S-alkyl tail</td><td align="center">1</td><td align="center">21.6530</td></tr>
<tr><td colspan="3">T_k calculation</td></tr>
<tr><td colspan="3">GC model without higher-order group; T_k (°C) = $\Sigma_i N_i C_i$ + Constant = 37.54 °C</td></tr>
<tr><td colspan="3">GC model with higher-order group; T_k (°C) = $\Sigma_i N_i C_i + \Sigma_j M_j D_j + \Sigma_k O_k E_k$ + Constant = 59.19 °C</td></tr>
<tr><td colspan="3">QSPR model; $T_{k,calc}$ = 58.90 °C</td></tr>
</table>

Table 4.8 The predicted values of the Krafft point temperature from the proposed GC-model and the QSPR model

Surfactants	$T_{k,exp}$ (°C)	The proposed GC-model in this work		The QSPR model (Li *et al.*, 2005)	
		$T_{k,calc}$ (°C)	% error	$T_{k,calc}$ (°C)	% error
C10SO3	22.50	22.51	0.00	22.40	0.44
C12SO3	38.00	34.74	8.59	35.50	6.58
C14SO3	48.00	46.96	2.16	47.60	0.83
C17SO3	62.00	65.31	5.33	64.20	3.55
C18SO3	70.00	71.42	2.03	69.40	0.86
C10OSO3	8.00	6.96	12.99	5.00	37.50
C12OSO3	19.00	19.189	1.00	17.60	7.37
C13OSO3	20.80	25.30	21.65	23.50	12.98
C14OSO3	30.00	31.42	4.72	29.30	2.33
C15OSO3	31.50	37.53	19.15	34.80	10.48
C16OSO3	45.00	43.64	3.01	40.20	10.67
C18OSO3	56.00	55.87	0.23	50.40	10.00
C7PhSO3	9.00	9.00	0.01	11.40	26.67
C8PhSO3	18.50	15.11	18.29	18.20	1.62
2C10PhSO3	22.00	19.26	12.43	14.80	32.73
2C12PhSO3	31.50	31.49	0.02	28.70	8.89
2C16PhSO3	54.20	55.95	3.23	55.30	2.03
2C18PhSO3	60.80	68.18	12.13	67.80	11.51
2C13COSO3	11.00	11.00	0.00	13.10	19.09
2C15COSO3	25.00	23.23	7.09	25.90	3.60
2C17COSO3	30.00	35.46	18.19	37.90	26.33
C16E1OSO3	36.00	34.18	5.06	38.60	7.22
C16E2OSO3	24.00	24.71	2.97	28.90	20.42

Table 4.8 The predicted values of the Krafft point temperature from the proposed GC-model and the QSPR model (Continued)

Surfactants	$T_{k,exp}$ (°C)	The proposed GC-model in this work		The QSPR model (Li *et al.*, 2005)	
		$T_{k,calc}$ (°C)	% error	$T_{k,calc}$ (°C)	% error
C16E3OSO3	19.00	15.25	19.76	18.40	3.16
C18E3OSO3	32.00	27.47	14.15	27.00	15.63
C18E4OSO3	18.00	18.01	0.04	19.30	7.22
C10AESO3	8.10	8.10	0.00	11.60	43.21
C12AESO3	24.20	20.33	16.00	24.30	0.41
C14AESO3	36.20	32.56	10.07	36.40	0.55
C10RSO3	12.50	14.21	13.64	9.30	25.60
C12RSO3	26.50	26.43	0.25	22.00	16.98
C14RSO3	39.00	38.66	0.87	34.10	12.56
O3SOC12OSO3	12.00	12.00	0.00	12.60	5.00
O3SOC14OSO3	24.80	24.23	2.31	23.50	5.24
O3SOC16OSO3	39.10	36.46	6.76	33.90	13.30
O3SOC18OSO3	44.90	48.68	8.43	43.90	2.23
O3SPhOC6OPhSO3	20.00	20.00	0.00	27.00	35.00
O3SPhOC8OPhSO3	28.00	32.23	15.10	39.10	39.64
O3SPhOC10OPhSO3	59.00	44.46	24.65	51.10	13.39
O3SPhOC12OPhSO3	70.00	56.68	19.02	63.00	10.00
O3SCRC12RCSO3	23.50	18.81	19.94	21.50	8.51
O3SCRC14RCSO3	31.00	31.04	0.14	32.60	5.16
O3SCRC16RCSO3	38.50	43.27	12.39	42.30	9.87
1,4 NS-8	9.00	9.00	0.00	No data	
1,4 NS-10	21.00	21.23	1.09	No data	
1,4 NS-14	50.00	45.68	8.63	No data	
1,4 NS-16	64.00	57.91	9.51	No data	
C7F15COONa	8.60	8.60	0.00	No data	
C8F17COONa	24.60	24.68	0.33	No data	
C7F15SO3Na	56.50	56.76	0.47	No data	
C10F21COONa	58.30	56.84	2.50	No data	
C12F25COONa	89.00	89.01	0.01	No data	
C8F17SO3Na	75.00	72.85	2.87	No data	

The comparison of first-order group, higher-order group and higher-order group with a new proposed group is concluded in Table 4.9. It is clearly seen that the addition of the higher-order groups give a significantly lower deviation, especially after including the new proposed third-order group. The lowest average absolute deviation of the proposed GC-model is 6.97% with the R-square error of the parity plot of 0.96, giving the proposed GC-model higher accuracy than the QSPR model (see the comparison in Table 4.9)

Table 4.9 Comparison the deviation of Group-Contribution Model: only first-order model; model including higher-order group (no proposed group); model including higher-order group and proposed group; and QSPR model of Krafft point of anionic surfactants

Model	Data points for regression	Average absolute deviation (%)	Maximum absolute deviation (%)	R-square error
GC-model without higher-order group (first-order only)	53	14.02	96.20	0.81
GC-model with higher-order groups (no proposed group)	53	13.05	53.91	0.87
GC-model with higher-order groups and a new proposed group	53	6.97	24.65	0.96
QSPR model	46	12.47	43.21	0.9368

Figure 4.6 shows the relative error plot of Krafft points from the proposed GC-model (Figure4.6a for the GC-model without higher-order levels and Figure 4.6b for the GC-model with higher-order levels) and the QSPR model (Figure 4.6c from Li *et al.* (2005)). It is clearly seen that the proposed GC-model with higher-order levels for Krafft temperature from this work is relatively more accurate than the more complex QSPR model.
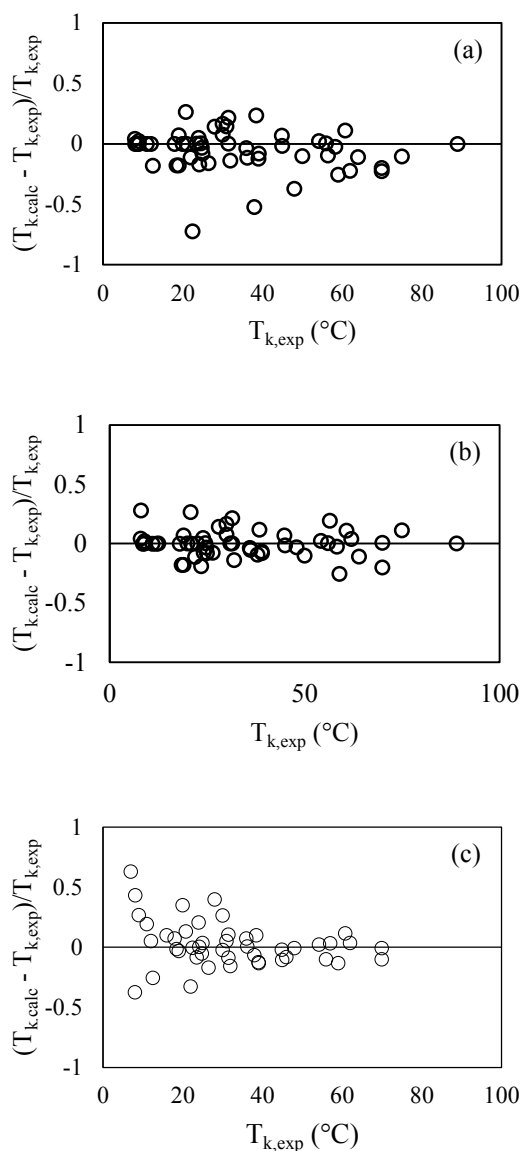
Figure 4.6 Relative error plot of Krafft point model (a) predicted Krafft point from the GC-model without higher-order (b) predicted Krafft point from the GC-model with higher-order groups (c) predicted Krafft point from the QSPR model.

It should be noted that the developed GC-model in this work is able to precisely estimate the Krafft point temperature of anionic surfactants that contain the available 16 first-order groups depicted in Table 4.2. The proposed GC-model cannot give a good predicted Krafft point of those surfactants containing the fractional groups

other than those appear in Table 4.2. For example, this model cannot predict the Krafft point temperature of Internal Olefin Sulfonate (IOS) surfactants (see structure depicted in Figures 4.7a and 4.7b) because certain contributors including alkene (CH=CH) and hydroxyl (-OH) groups are not available in the proposed GC-model. In addition, the newly developed surfactant structure, namely Gemini surfactants, contain two heads and tails linked together (see Figure 4.7c). This gemini structure gives a better performance such as stability (Negin *et al.*, 2017) as compared to any conventional surfactants. The effect of the interaction between the two tails are also not included in the high order groups proposed in this work; hence, the Krafft point prediction from the model could be inaccurate. However, the proposed GC-model can be extended to cover the surfactants with other functional groups if there are enough experimental data available.

4.4 Examples Application

In the application of anionic surfactants, it is well-known that the working temperature of the system should be higher than the Krafft point of a specified anionic surfactant to prevent surfactant crystallization (Summerton *et al.*, 2017) except a few applications that do not concern the micelle formation in the system such as the gas hydrate technology for gas storage (Kumar *et al.*, 2015). The GC-model for Krafft point prediction is useful for the preliminary criteria to select available surfactants from many choices and hence, it helps reduce cost and time for experiment. Vautier-Giongo *et al.* (2003) studied the effect of counterion ion dissociated with ionic micelle by considering the degree of ionization calculated from Krafft point of selected surfactants. They used sodium dodecyl sulfate (SDS) to represented the ionization of anionic and cetyltrimethylammonium bromide (CTAB) as their cationic surfactant. Krafft point experiment was conducted and found that SDS gave the Krafft point of around 19.00 °C. If the GC-model is applied to predict Krafft point of SDS instead of experiment. The calculated Krafft point is equal to 20.18 °C, which is close to the experimental value. It seems that the GC-model is rather practical for use to avoid the waste of time and cost for experiment.

$$CH_3\text{-}(CH_2)_6\text{-}\underset{\underset{\displaystyle OH}{|}}{CH}\text{-}(CH_2)_n\text{-}\underset{\underset{\displaystyle SO_3Na}{|}}{CH}\text{-}(CH_2)_6\text{-}CH_3$$

(a)

$$CH_3\text{-}(CH_2)_5\text{-}CH{=}CH\text{-}(CH_2)_m\text{-}\underset{\underset{\displaystyle SO_3Na}{|}}{CH}\text{-}(CH_2)_6\text{-}CH_3$$

(b)

(c)
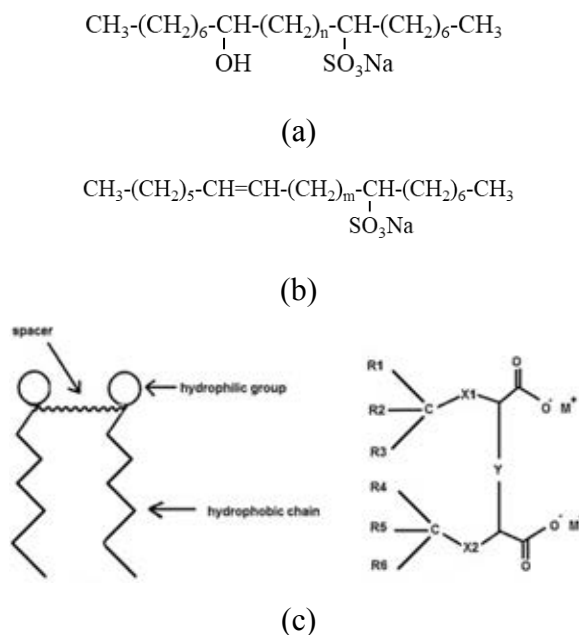
Figure 4.7 Example anionic surfactant that GC-model may not predict accurately: (a) Internal Olefin Sulfonate (IOS) that including hydroxyl, (b) Internal Olefin Sulfonate (IOS) that including alkene and (c) gemini surfactant (Negin *et al.*, 2017).

4.5 Conclusions

Krafft point model based on the concept of Group-Contribution method by Marrero *et al.* (2001) has been developed for predicting the limitation of solubility of anionic surfactants. The first-order, higher-order (second and third) and new third-order groups are applied to this model to achieve high accuracy. With the high-order groups, the accuracy of the model could achieved 7.80%average absolute deviation with high R-square of 0.9511 when comparing to the experimental data. Most of contributions of the fractional groups in each level follow the effect of molecular structure. If the polar or hydrophilic structures occur in the surfactant molecule, the contribution is negative and Krafft point is lower. This model can improve the previous Krafft point model based on QSPR (Li *et al.*, 2005) by extending data set and succeeding the higher efficiency. In addition, the fluorocarbon surfactants are included in the model. Therefore, this GC-model is easier to use with requirement of structure of anionic surfactants and apply in a wide range type of anionic surfactants.

4.6 Recommendations

In this work, some limitations of Krafft point GC-model include the availability of the type of anionic surfactants that are covered by the model. To extend the model to be used with various surfactants with various fractional groups, more experimental data must be collected; however, these data are limited in this field. Apart from the conventional surfactants, the effect of counterion ion of anionic surfactant is of interest for including in the GC-model. Surfactants have been developed with various counterion ions. Many works already showed the effect of counterion ions to surfactant properties (Benrraou *et al.*, 2003, Naskar *et al.*, 2013). To cover these surfactants with various counterion ions such as Li^+ and K^+ as those proposed by Rosen *et al.* (2012) and the fluorocarbon surfactants proposed by Li *et al.* (2005), more experimental data are needed to be collected to develop the new group structures.

CHAPTER V
MEASUREMENT OF CHARACTERISTIC CURVATURE
FOR NONIONIC SURFACTANT

5.1 Introduction

Microemulsion formulation has been applied to the oil-water system for reducing the interfacial tension between oil-water interfaces in many applications such as enhanced oil recovery, additives for fuels, detergency, cosmetics and agrochemicals (Paul et al., 2001). As its thermodynamic stability, microemulsion can stabilize two immiscible phases in a single transparent homogeneous phase (Santos et al., 2017). Surfactants are the chemical groups that can reach to microemulsion formulation. According to their structures, surfactants are the combination of hydrophilic and lipophilic parts that make the surfactant soluble in both aqueous and oil phases (Shafiee Najafi et al., 2017). Surfactants can be divided into four types: anionic, cationic, nonionic and zwitterionic surfactants, depending on charge of the hydrophilic part (Burguera et al., 2012).

Microemulsion is typically divided into three types, named Winsor Type system. Winsor Type I microemulsion is formed via oil solubilization as micelle in the water phase (oil-in-water, O/W) whereas Winsor Type II microemulsion is formed via water solubilization as reverse micelle in the oil phase (water-in-oil, W/O). The transition between Type I and Type II is called Winsor Type III microemulsion. This type of microemulsion can be observed as a separated phase in the middle between water and oil phases (middle phase) (Baran, 2001) and divides the water and oil phases into equal volume. For this type, the affinity of surfactant-oil matches to the affinity of surfactant-water and the lowest interfacial tension between water and oil phases is achieved. This situation is referred as the optimum formulation (Salager et al., 2005).

A tool for estimation of the optimum formulation of microemulsion is Hydrophilic-Lipophilic Deviation (HLD) concept. Hydrophilic-lipophilic difference (HLD) is a fundamental correlation to explain microemulsion system. This equation was firstly proposed by Salager et al. (1979). Not only the potential of transferring surfactants from the oil phase to the aqueous phase, but also the balances of each

parameter (temperature, oil, water and salt) for the oil-water-surfactant system are included in the correlation. In addition, HLD can determine the optimum formulation of a system involving with various alcohols and divalent ions (Salager et al., 1979, Acosta et al., 2012, Budhathoki et al., 2016). The HLD equations for ionic and nonionic surfactants are expressed in Eq. 5.1 and Eq. 5.2, respectively (Castellino et al., 2011):

For ionic surfactants,

$$HLD = \ln(S) - K*EACN - f(A) - \alpha\Delta T + C_{ci} \qquad \text{Eq. 5.1}$$

For nonionic surfactants,

$$HLD = b(S) - K*EACN - \varphi(A) + c\Delta T + C_{cn} \qquad \text{Eq. 5.2}$$

where $\ln(S)$ and $b(S)$ are the function of salinity concentration in the aqueous phase in g/100mL; b is the constant for nonionic surfactants; K is the slope of the logarithm of optimum salinity in the ranges of 0.1 to 0.2 and it is an indicator of surfactant properties (head part); EACN is the equivalent alkane carbon number which depends on the nature of oil; the function $f(A)$ and $\varphi(A)$ are the alcohol function depending on type and concentration of additional alcohol; the variables α and c are the temperature coefficient at optimum salinity condition; ΔT is the temperature difference from a reference temperature (typically 298 K); and C_{ci} and C_{cn} are the characteristic curvature that is focused in this work and explained intensively in a later part.

The HLD value is related to the Winsor type of microemulsion. The negative HLD value indicates the Winsor type I (O/W). For HLD of zero value, it is classified as the Winsor type III (middle phase microemulsion). And the positive value of HLD indicates the Winsor type II (W/O) (Jin et al., 2015). The phase transition of microemulsion from Winsor type I to type III and continually to type II is occurred together with the shift of a negative HLD value to a positive value (Castellino *et al.*, 2011).

For the characteristic curvature (C_c or C_{cn}), a negative value is defined as a hydrophilic surfactant while a positive value is defined as a lipophilic surfactant. It is important to imply the characteristics of surfactants since it is related to the type of micelle forming in the oil-water-surfactant system (micelle or reverse micelle) (Hammond et al., 2011). In many application, the microemulsion is needed to form the ultra-low interfacial tension between the oil phase and water phase such as cleaning

application (Acosta *et al.*, 2007) and environmental remediation (Mao *et al.*, 2015). The HLD equation is one of the important tools that can be used to determine the microemulsion system to achieve the ultra-low interfacial tension in specific conditions. The Cc value is specific for each surfactant depending on the surfactant structure and can be obtained experimentally. This work focused on the measurement of C_{cn} for nonionic surfactant to correlate the HLD equation and achieve the HLD value of zero.

C_{cn} can be measured from a phase scan measurement and calculated by the HLD equation. A simplified method proposed by Zarate-Muñoz *et al.* (2016) to measure C_{cn} of nonionic surfactants, specifically for commercial alkyl ethoxylate nonionic surfactants. This method involve a temperature scan for reference surfactants and then mixed the reference surfactant with other alkyl ethoxylate nonionic surfactants to find C_{cn} value with the aid of an HLD equation. The linear mixing rule was applied as an assumption of calculation. This method is simple and requires less time for measurement.

5.2 Materials and Experimental

5.2.1 Materials

Sodium dihexyl sulfosuccinate (SDHS) with 80% active ingredients from Sigma-Aldrich was used to determine EACN of alkane oils. Alkyl ethoxylate surfactants were kindly supplied from Thai Ethoxylate Co. (C12-14EO1 Dehydol LS 1 TH, >99.7% active ingredients, C12-14EO2 Dehydol LS 2 TH, >99.7% active ingredients, C12-14EO3 Dehydol LS 3 TH, >99.7% active ingredients, C12-14EO3 Dehydol LS 5 TH, >99.7% active ingredients, C12-14EO9 Dehydol LS 9 TH, >99.7% active ingredients, C12-14EO12 Dehydol LS 12 TH, >99.7% active ingredients). Marlox RT 42 (C16-18 with EO4-PO2), 100% active ingredients, Marlox RT 64 (C16-18 with EO6-PO4), 100% active ingredients were kindly donated from Sasol Chemical North America LLC. Cyclohexane (99.8% purity) was purchased from Carlo Erba Reagent. Synthesis grade decahydronaphthalene or decalin (99% purity of a mixture of cis and trans isomers) and dodecane (99% purity) were purchased from Merck. AR grade Hexane (95% purity) was purchased from RCI Labscan Limited. Heptane

(99.5% purity) was purchased from Univar Canada Ltd. Hexadecane (99% purity) from Acros Organics. AR grade sodium chloride (purity 99%) purchased from RCI Labscan Limited was used to prepare different salinity from deionized water.

5.2.2 Optimal Salinity Measurement by Salinity and Temperature Scans

To identify the optimum formulation of surfactant/oil/water system (SOW), the optimal salinity was determined in each condition to measure the phase inversion point by salinity and temperature scans. The experimental procedure followed the simplified method proposed by Zarate-Muñoz *et al.* (2016). As mentioned in Chapter 3, Figure 3.1 shows the schematic flowchart for C_{cn} measurement. All of experiments were conducted with 15 mL-flat bottom vials. To prepare microemulsion formulation, 2 mL oil phase and 2 mL aqueous phase were mixed thoroughly using a vortex mixer. The aqueous phase contains a fixed 0.1 M concentration of surfactant, whereas the salinity of the aqueous phase is in the ranges from 0 to 26 %wt/vol, where NaCl salt was added to ionized water to adjust the salinity. It is noted that some SOW systems were hard to prepare the stock solution for aqueous phase, especially the systems of dehydol LS 9 TH and dehydol LS 12 TH due to the effect of polyethylene oxide to CMC of surfactant system (Barry *et al.*, 1976); hence, these system were prepared from the pure solution.
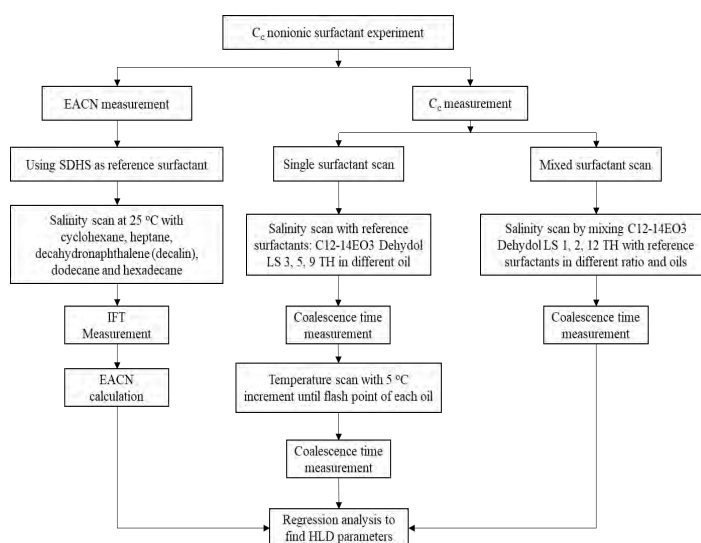
Figure 3.1 Schematic flowchart of measurement of C_{cn} nonionic surfactant.

5.2.3 EACN and C_c Measurement

In this work the EACN measurement method adopted from Zarate-Muñoz *et al.* (2016) was used to measure optimal salinity of surfactant-oil-water systems. EACN of each oil was calculated directly from the HLD equation using K and Cc values from the reference anionic surfactant SDHS (Acosta *et al.*, 2003). This calculation needs a precise optimal salinity to calculate the accurate EACN value. The optimal salinity obtained from measuring a coalescence rate was not sufficiently sensitive to distinguish the sample with the quickest time to reach a stable position (see Figure 5.1) since all of them quickly reached a stable position. Therefore, the measurement of IFT was necessary to find the optimal salinity for EACN measurement. The IFT measurement was conducted by a dynamic measurement with SVT 20 Spinning drop video tensiometer manufactured by Dataphysics. Briefly the aqueous phase was injected into the fast exchange capillary as phase 1 and the oil phase was injected as phase 2. The measurement was determined at 5000 rpm until the length of the oil droplet is four times of its width and a stable condition was reached. The optimal salinity is the salinity of a system with the lowest interfacial tension.
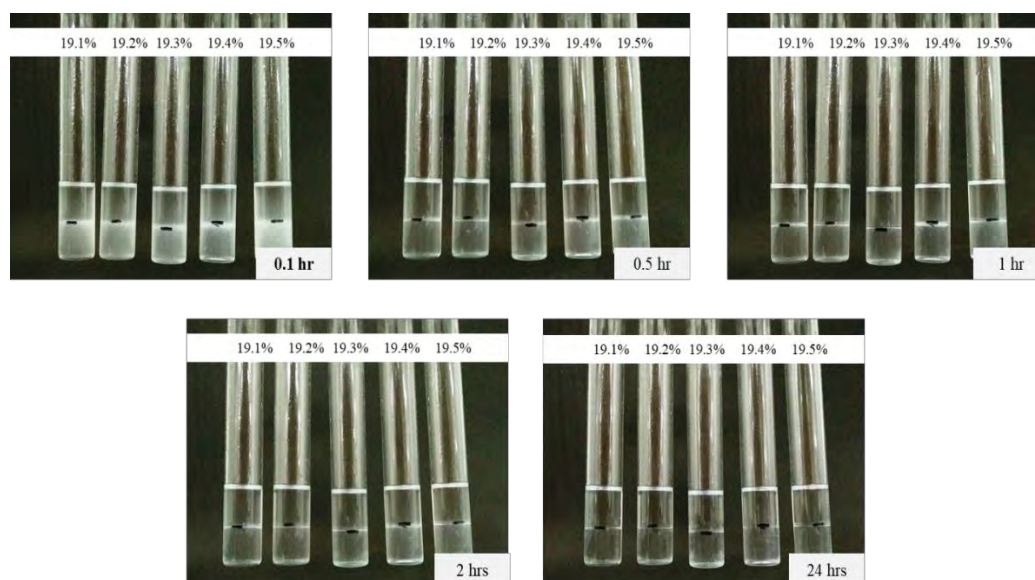
Figure 5.1 The change of phase behavior in the system of SDHS/Dodecane/Water at room temperature.

In addition, the emulsion stability using coalescence rate measurement was still suitable for the determination of C_{cn} as shown in Figure 5.2. At 9%wt/vol salt, the size of the middle phase still changed up to 60 minutes, while the size of the middle phase at 10%wt/vol salt was stable since early 20 minutes. It seems that the emulsion stability is more suitable to determine the optimal salinity of nonionic surfactant systems.
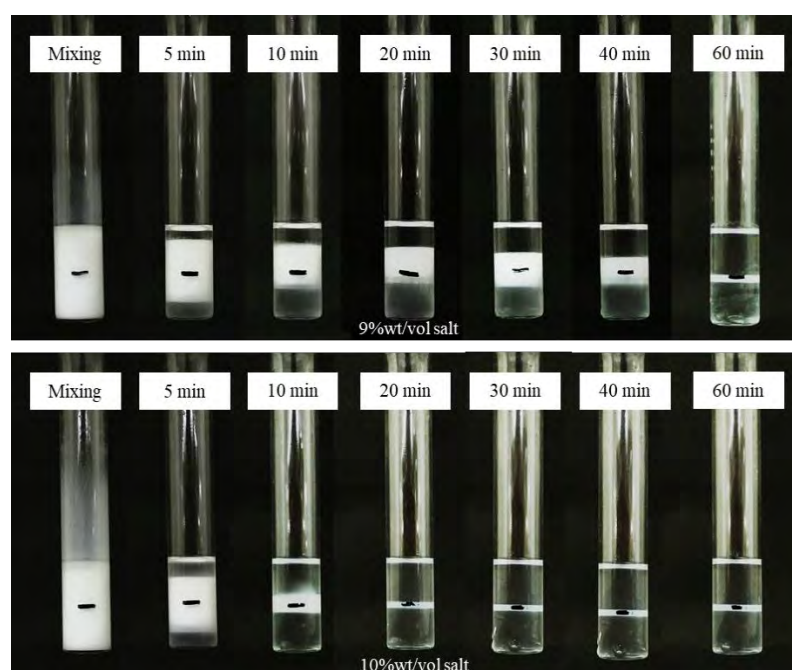
Figure 5.2 Comparison between 9%wt/vol (upper) and 10%wt/vol (lower) salinity of Dehydol LS 5 TH surfactant in dodecane oil system at different time.

5.2.4 Single surfactant system: salinity and temperature scan

For the single surfactant system, the salinity and temperature scans were applied on the reference surfactants: Dehydol LS 3 TH, Dehydol LS 5 TH and Dehydol LS 9 TH to find the optimal salinity. Oils with various EACN ranging from 3 to 16 were employed in the study. The temperature scans were conducted with 5 °C temperature increment at each salinity. The maximum temperature of each oil was kept below its flash point. The results were used to find the HLD parameters by regression analysis.

5.2.5 Mixed surfactant system: salinity scan

For the mixed surfactant system, only the salinity scan was applied. The mole ratio of the reference surfactant to the test surfactant was varied from 0.1 to 0.9. Oils with EACN ranging from 3 to 16 were also applied. The results were used to find HLD parameters by using a linear mixing rule with known parameters from reference surfactants (BaranJr. *et al.*, 1994, Witthayapanyanon *et al.*, 2008, Acosta *et al.*, 2008a, Zarate-Muñoz *et al.*, 2016).

5.3 Results and Discussion

5.3.1 Reference Oils for C_{cn} Measurement

To determine the EACN of each oil that related to the measurement of characteristic curvature, the oil was mixed with SDHS to determine the EACN values. The IFT measurement was applied to indicate the optimal salinity for the SOW system. The results of IFT are shown in the Figure 5.3. The relationship between interfacial tension and salinity is shown and the result was similar to the work of Salager *et al.* (2013a). The minimum point in the graph indicates the optimal salinity due to the suitable interaction of SOW system and leading to Winsor type III microemulsion with the lowest interfacial tension of the SOW system (see Figure 5.4). However, the values of IFT in mN/m reported in this work was not as low as the values observed in the work of Zarate-Muñoz *et al.* (2016) because this work used the dynamic interfacial tension measurement where a separate preparation of aqueous and oil phases were injected to the spinning drop tensiometer whereas the work of Zarate-Muñoz *et al.* (2016) used the excess aqueous phase and excess oil phase extracted from an equilibrated bicontinuous microemulsion vial.
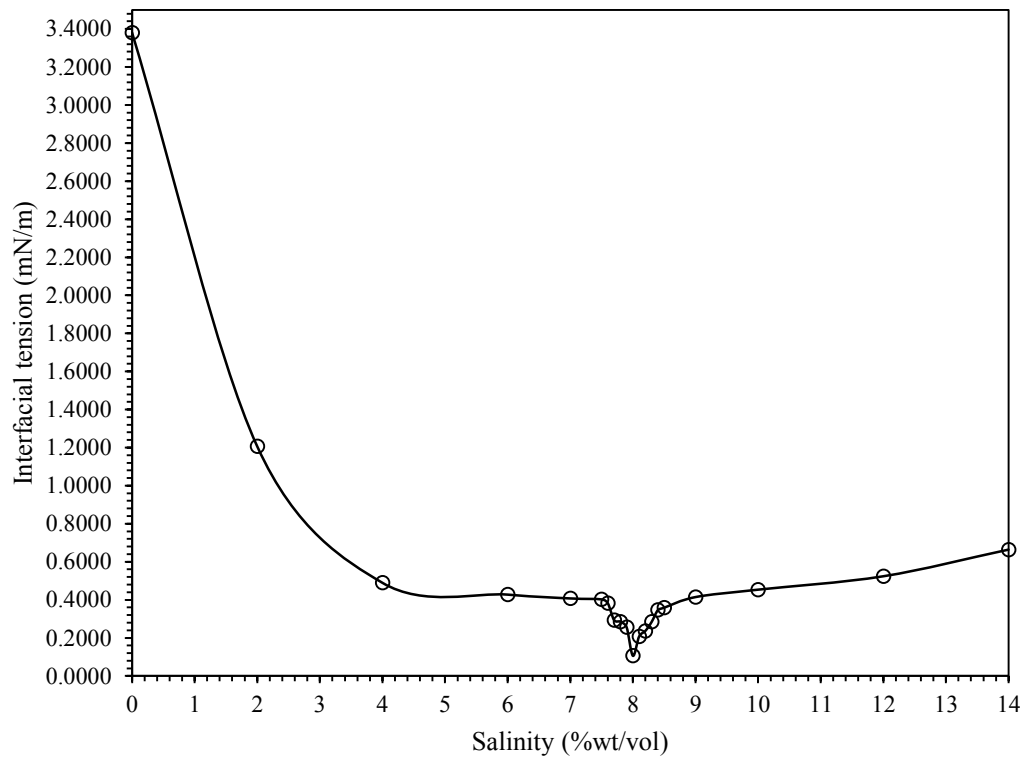
Figure 5.3 IFT results (20 data points) plotted with salinity in %wt/vol for SDHS/Heptane/Water system.
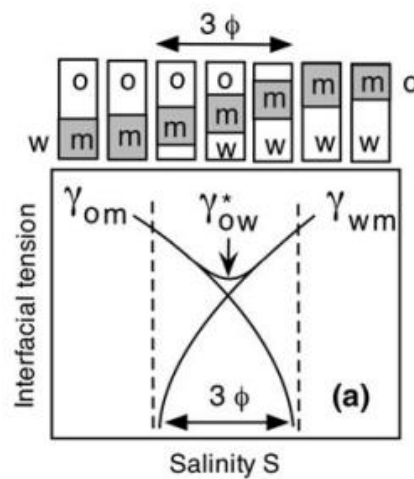
Figure 5.4 The relationship of interfacial tension when increasing the salinity (Salager *et al.*, 2013a)

After finding the IFT and indicating the optimal salinity, the EACN of oil was calculated. For the calculation, Eq. 3.1 was used with the K and C_c values of 0.17 and -0.92, respectively, for SDHS (Zarate-Muñoz *et al.*, 2016). The EACN value is reported in the Table 1. Considering the EACN of heptane, the EACN from the experiment with heptane oil is equal to 6.8. This value is in agreement with the work of Zarate-Muñoz *et al.* (2016).

Table 5.1 Summary of optimal salinity and EACN value and literature value

Oil	Optimal Salinity (%wt/vol)	Calculated EACN	Literature EACN (Zarate-Muñoz *et al.*)
Cyclohexane	4.4	3.3	3.3
Hexane	7.0	6.0	6.0
Heptane	8.0	6.8	6.8
Decalin	7.3	6.3	6.3
Decane	13.6	9.9	10.0
Dodecane	19.3	12.0	12.0
Hexadecane	17.4*	16.0	16.0

*This system was mixed with heptane in ratio 1 : 1 and used linear mixing rule for calculation the EACN of hexadecane.

To choose the reference oils for measurement the characteristic curvature of nonionic surfactants, the wide range of EACN value is needed to accurately obtain the HLD parameters. All temperature scans were conducted below the flash point of each oil (flash point of each oil is reported in Appendix A). It seems that cyclohexane and hexadecane are suitable for the phase scan with the wide range of EACN value (3.3-16). However, cyclohexane is not suitable at temperature above room temperature. So, decalin was used to replace cyclohexane scan at high temperature. Dodecane was also used to give higher accuracy to obtain the HLD parameters at high temperature.

For mixed surfactant systems, cyclohexane, heptane and decalin were used to find the optimal salinity at room temperature because of their lower optimal salinity as compared to other oils. The rest of the oils in the Table 5.1 (hexane and decane) was used to discuss in the later part of this work.

5.3.2 Single surfactant systems

To determine the optimal salinity of SOW system, the coalescence time was recorded to identify the optimal condition with the fastest phase inversion. The aspects of SOW phase were also captured in each salinity. The coalescence time measurement and phase behavior study of 0.1 M C12-14EO5 with Dodecane at 35 °C are shown in the Figures 5.5 and 5.6, respectively. The coalescence time at the optimal salinity was clearly observed and corresponded to the phase occurrence with Winsor type III (middle phase). It is noted that the reported coalescence time of 1,000 minutes shown in Figure 5.5 was for those systems with a coalescence time greater than 1,000 minutes. Typically, the fastest coalescence rate of optimal point of each system were in ranges of 10 to 200 minutes that was enough to reach the equilibrium within 3 – 5 minutes.

Temp (°C)	Salinity (%wt/vol)	time (min)
35	0.0	1000.00
	15.0	1000.00
	16.0	1000.00
	17.0	1000.00
	18.0	73.33
	19.0	72.53
	19.5	47.38
	20.0	143.57
	21.0	1000.00
	22.5	1000.00
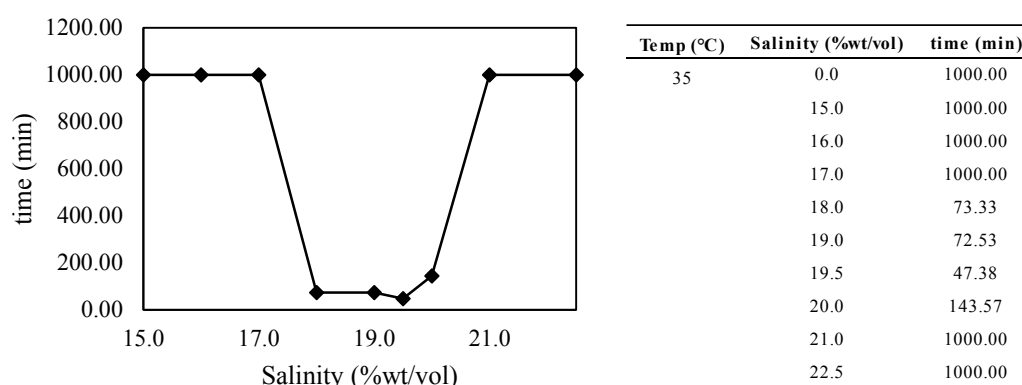
Figure 5.5 Example of coalescence time results for 0.1 M C12-14EO5 with Dodecane at 35 °C.
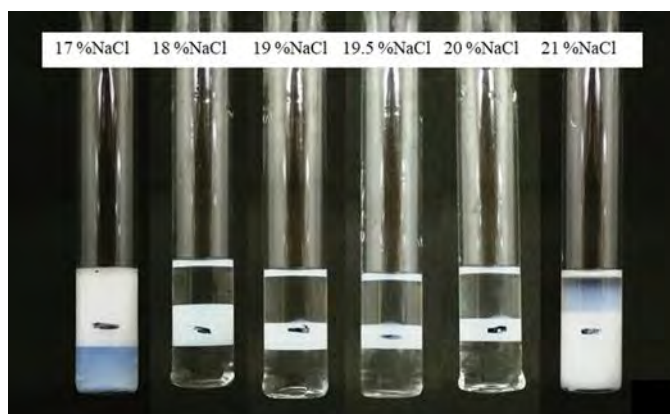
Figure 5.6 Example of phase scan for 0.1 M C12-14EO5 with Dodecane at 35 °C.

It is of interest to note that the middle phase of the linear alkyl oil and the cyclic oil is different. Figures 5.7a and 5.7b show the phase scan of 0.1 M Dehydol LS 5 TH systems with cyclohexane and hexane as an oil phase, respectively while Figures 5.8a and 5.8b show the systems of the same surfactant with decalin and decane as an oil phase, respectively. The cyclic oil gave a more turbid and cloudy middle phase while the straight-chain alkane gave a clear and light blue middle phase. To compare a cyclic oil with a straight-chain alkane with similar EACN, Figures 5.9a and 5.9b show the phase behavior of 0.1 M Dehydol LS 5 TH systems with decalin (EACN of 6.3) and heptane (EACN of 6.8), respectively. The phase scan also supports the previous result of unclear middle phase of bicyclic oil. The decalin structure may have some effects to this phenomena. Some works also reported the effect of oil structure to middle phase (Jenkins *et al.*, 2002, Sripriya *et al.*, 2007). The causes may be from the bulky structure of polycyclic alkane to form the different micelle.

Kabalnov *et al.* (1995) proposed that the unsaturated hydrocarbons have a lower IFT as compared to the saturated hydrocarbon; for example, the IFT of SDHS/cyclohexane/water system was 0.1948 mN/m while the SDHS/hexane/water system was 0.5799 mN/m at the same salinity with 4 %NaClwt/vol. So, the amount of salt for converting the type of microemulsion is lower in case of unsaturated hydrocarbon system. That point is corresponding to phase scan in Figure 5.7 and 5.8, the optimal salinity of cyclohexane is lower than hexane and optimal salinity of decalin is lower than decane. It is noticed that the effect of unsaturated hydrocarbon is similar

to the effect of EACN; for example, the EACN of decalin is 6.3 while the EACN of decane is 10 with the same amount of carbon atoms.
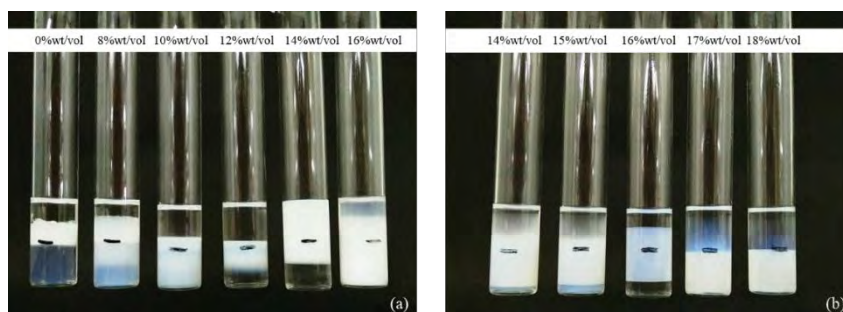
Figure 5.7 The phase scan of 0.1 M Dehydol LS 5 TH with (a) cyclohexane (b) hexane at 25 °C.
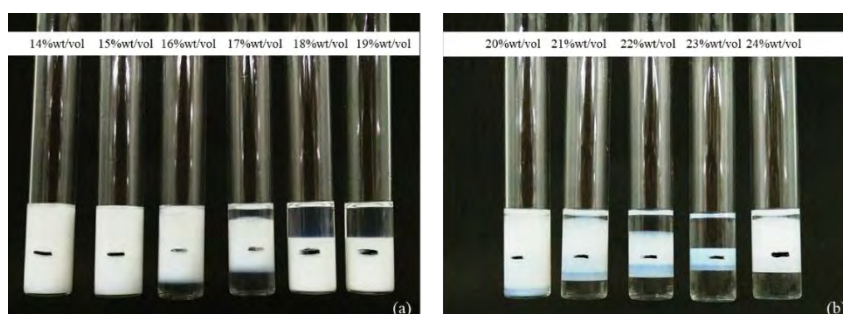
Figure 5.8 The phase scan of 0.1 M Dehydol LS 5 TH with (a) decalin (b) decane at 25 °C.
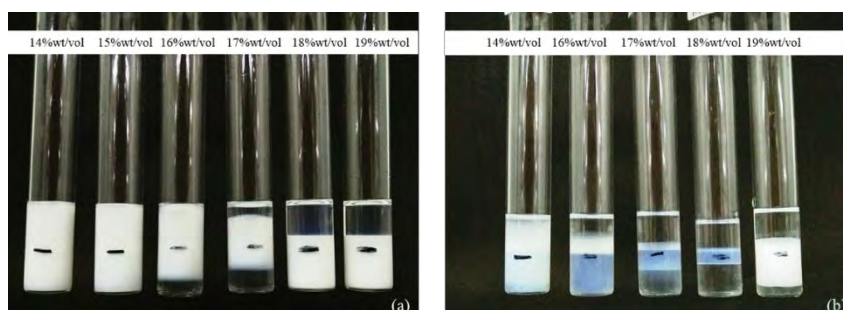
Figure 5.9 The phase scan of 0.1 M Dehydol LS 5 TH with (a) decalin (b) heptane at 25 °C.

After carrying the temperature scan for reference surfactants, the effect of temperature to the optimal salinity, which indicates the phase inversion was observed using three different EACN oils: decalin, dodecane and hexadecane. Figure 5.10 shows the relationship of temperature and optimal salinity in each surfactant: (a) Dehydol LS 3 TH (b) Dehydol LS 5 TH (c) Dehydol LS 9 TH. The results show that when the temperature increased, the lower optimal salinity was observed similar to the work of Zarate-Muñoz *et al.* (2016). The optimal solubilization of oil and water in the middle phase is the function of temperature. The optimal salinity decreased as the temperature increased (Schramm, 2009). Arachchilage *et al.* (2018) also clarified this results from their work. They found that the solubility of the SOW system containing the mixed anionic surfactant increased with the temperature. In contrast, the SOW solubility of the systems with nonionic surfactant decreases with increasing temperature, leading to the decrease in optimal salinity. Similar trend was observed in literatures that nonionic surfactants are strongly sensitive with temperature. In some cases these nonionic surfactants are limited for use in a number of applications such as cleaning and dispersion due to their temperature-sensitive property (Lindman *et al.*, 2016).

Figure 5.11 also shows the increasing in optimal salinity with increasing EACN of the reference oils (cyclohexane, decalin, hexane, dodecane and hexadecane) at room temperature as higher EACN required higher electrolyte concentrations to convert microemulsion from O/W to W/O shifting through Winsor type III (Zarate-Muñoz *et al.*, 2016).

Another interesting issue is the effect of EO group to the observed optimal salinity. Figure 5.12 shows that the optimal salinity increased in a linear function with increasing number of EO groups for all reference oils and temperature scans. The addition of NaCl makes water a more polar phase and Winsor type III microemulsion becomes oil-rich (Kabalnov *et al.*, 1995). So, if the nonionic surfactant containing shorter EO chain in structure is already more soluble in oil, the amount of needed salt to make Winsor type III microemulsion becomes oil-rich is lower than the surfactant containing longer EO chain. In addition, the addition of polyoxyethylene structure increased the repulsive force in the surfactant head group along their chain;

hence, it requires higher salinity to achieve the optimal condition (Kunieda *et al.*, 2001).
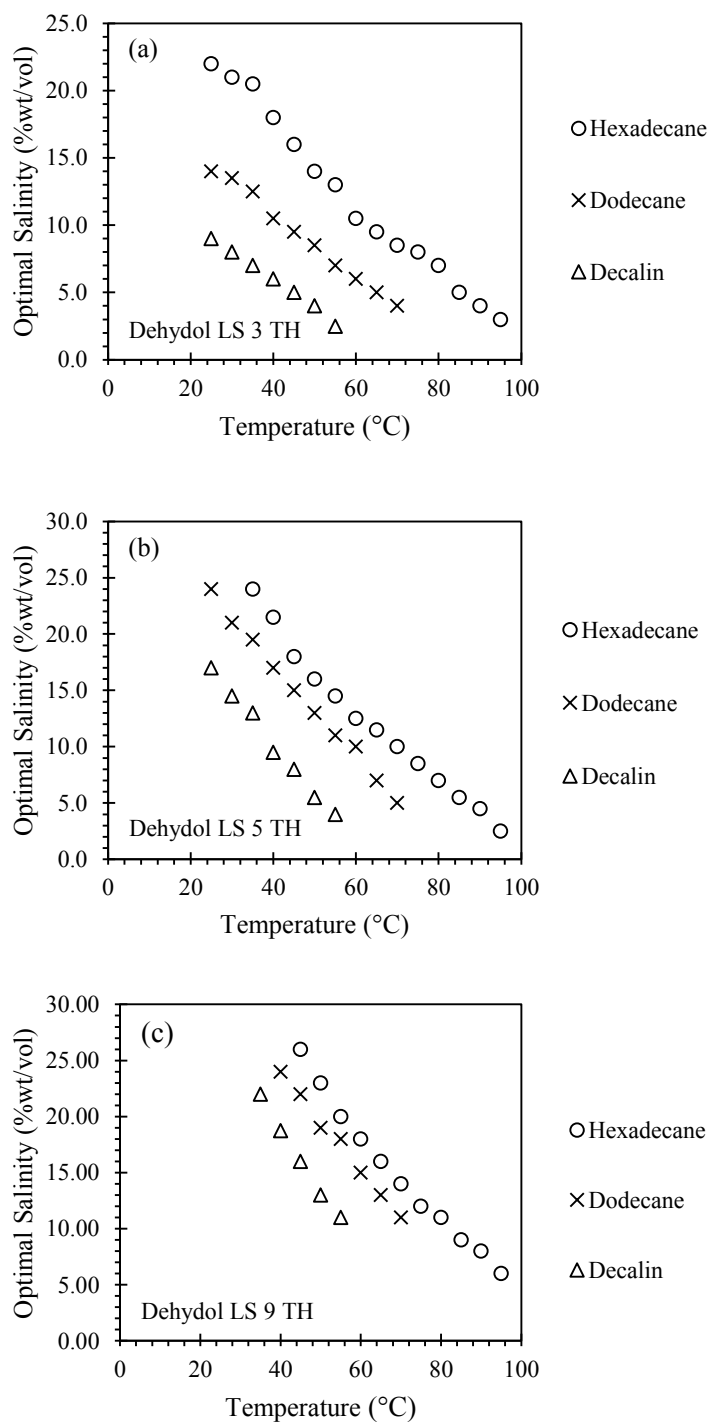
Figure 5.10 Effect of Temperature to optimal salinity in each surfactant (a) Dehydol LS 3 TH (b) Dehydol LS 5 TH (c) Dehydol LS 9 TH.
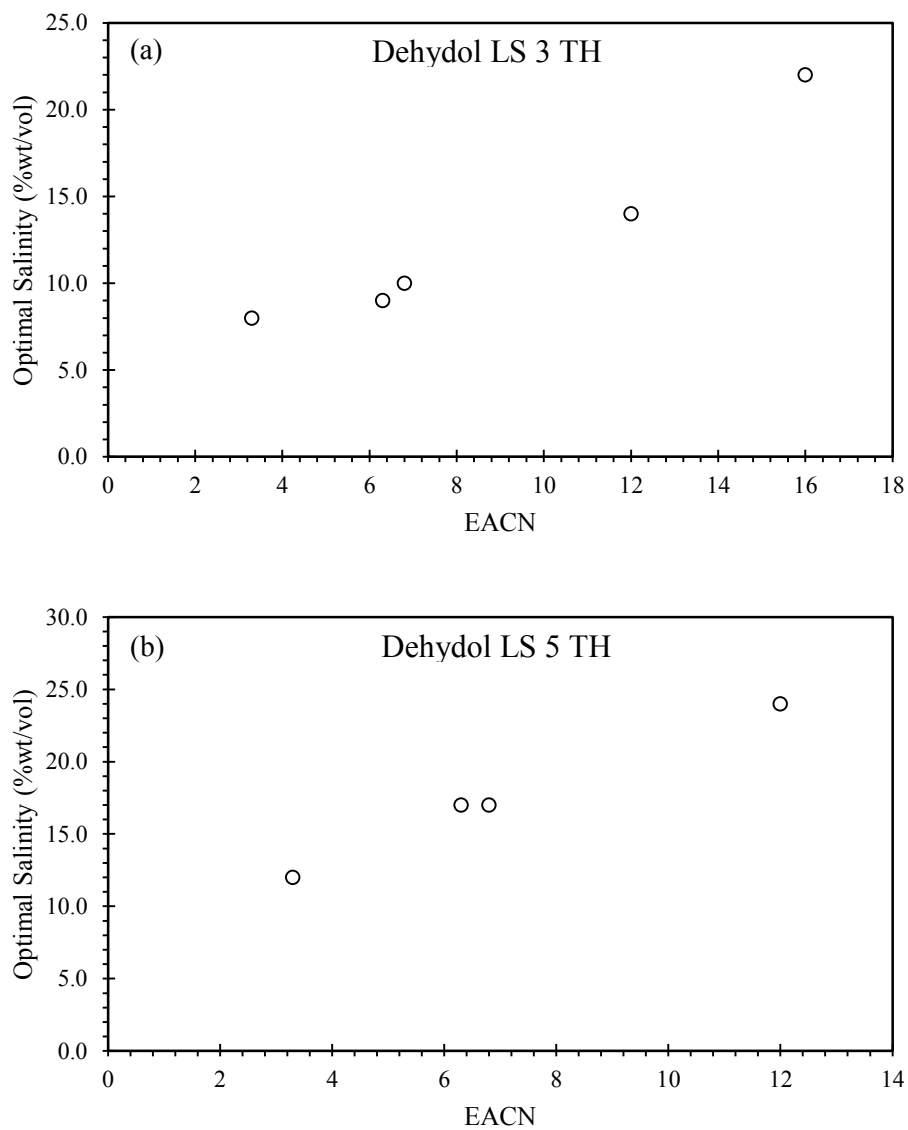
Figure 5.11 Effect of EACN to optimal salinity in each surfactant (a) Dehydol LS 3 TH (b) Dehydol LS 5 TH.
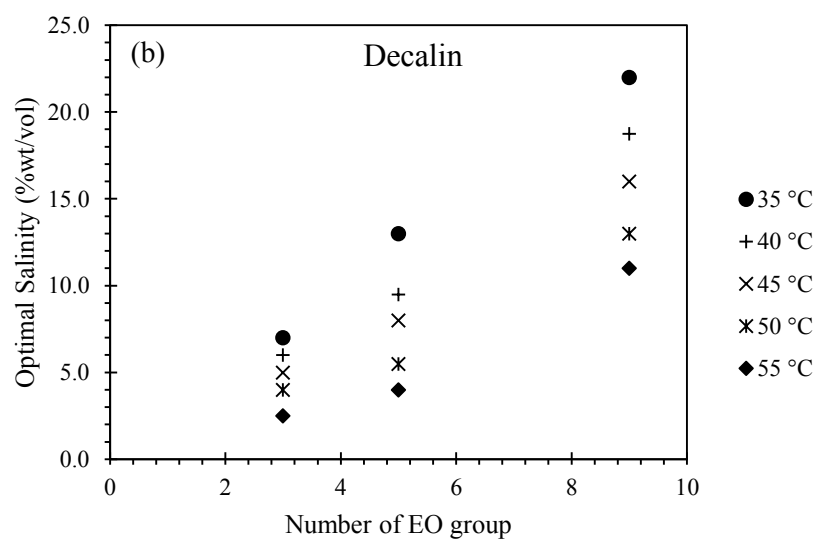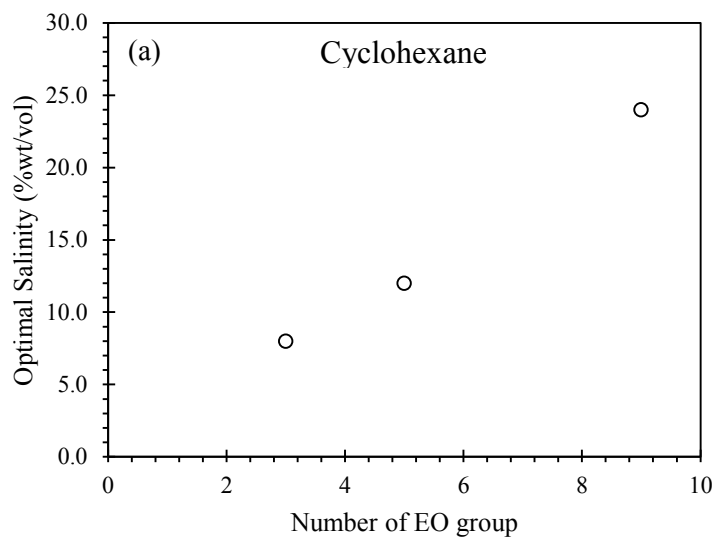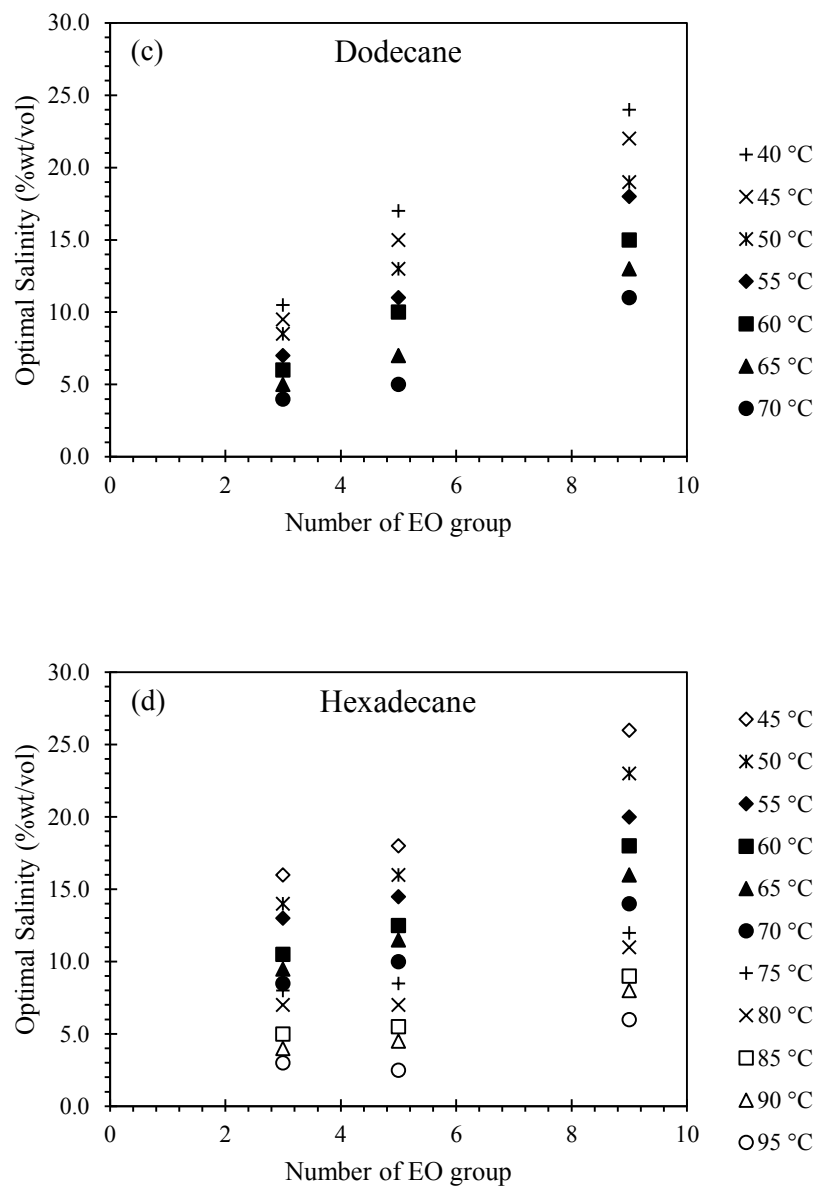
Figure 5.12 Effect of number of EO to optimal salinity in each oil (a) cyclohexane (b) decalin (c) dodecane and (d) hexadecane.

To obtain HLD parameters of all reference surfactants, the results of the salinity and temperature scans of reference surfactants with different EACN oils ranging from 3 to 16 were used. A regression analysis was performed by minimizing the summation of relative deviation between the experimental optimum salinity and the regressed values to obtained K, C_c, C_T, and b. The regressed values of HLD parameters are shown in the Table 5.2. Since NaCl was used to adjust salinity of the system, it is reasonable to assume the parameter b as a constant with a value of 0.13 for alcohol nonionic surfactants (Salager *et al.*, 2001).

The C_c value of Dehydol LS 9 TH was the highest negative value while Dehydol LS 3 TH was the lowest negative value. The results are justified as the higher solubility in the aqueous phase was observed with higher number of EO groups contained in the structure; hence, a more negative value of C_c was also achieved.

The K parameter is the property of the head group of the surfactants with values ranging from 0.1 to 0.2. The regressed K from this study corresponded to the theory even though there was no obvious trend of the three surfactants in this study. The c_T parameter is the temperature coefficient at optimal condition and the regressed c_T from this study was 0.03-0.05 for all three surfactants. The c_T parameter corresponded to the previous work (Zarate-Muñoz *et al.*, 2016).

The reliability and accuracy of the regression results are shown in the Figures 5.13, 5.14 and 5.15 for Dehydol LS 3 TH, Dehydol LS 5 TH and Dehydol LS 9 TH, respectively, where the experimental optimal salinity was plotted with the regressed value. The R-square of these plots are higher than 0.95 for all systems, indicating of a very good fit and high accuracy of the results.

Table 5.2 HLD parameter of 3 reference surfactants

Nonionic surfactants	b (g/100 mL)$^{-1}$ (Salager *et al.*, 2001)	K	C_c	c_T (°C)$^{-1}$
Dehydol LS 3 TH	0.13	0.13	-0.41	0.03
Dehydol LS 5 TH	0.13	0.16	-0.91	0.05
Dehydol LS 9 TH	0.13	0.13	-2.21	0.05
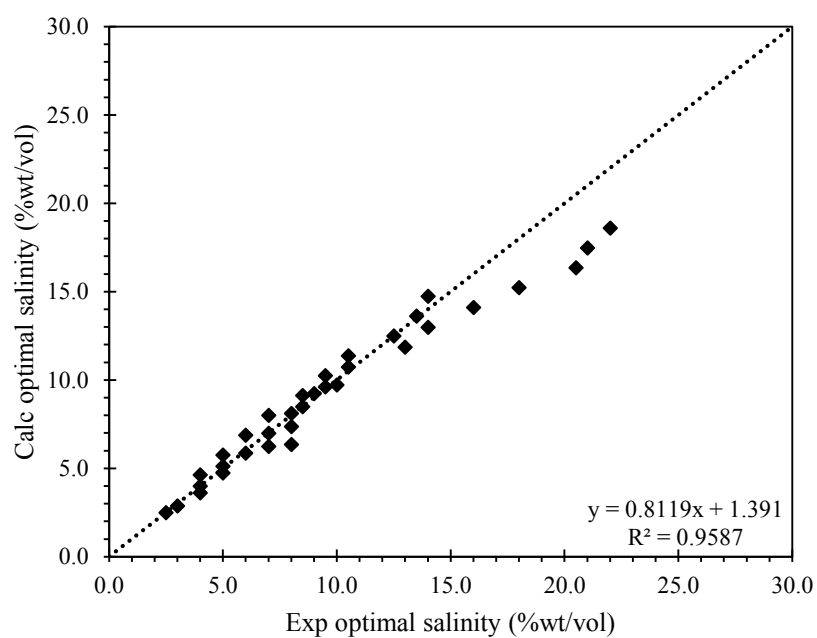
Figure 5.13 Parity plot of the experiment optimal salinity and the regressed value of Dehydol LS 3 TH system.
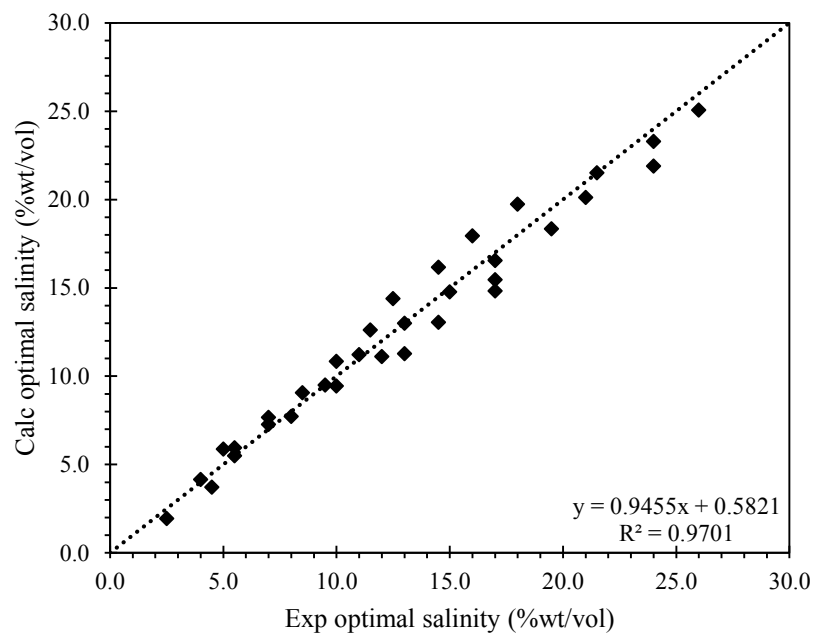
Figure 5.14 Parity plot of the experiment optimal salinity and the regressed value of Dehydol LS 5 TH system.
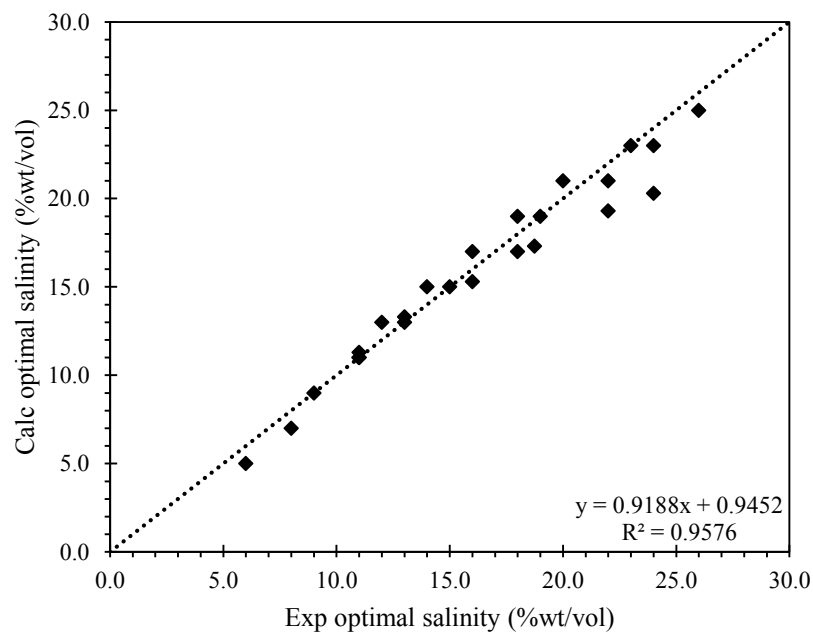
Figure 5.15 Parity plot of the experiment optimal salinity and the regressed value of Dehydol LS 9 TH system.

For other extended nonionic surfactants, there are Marlox® RT42 and Marlox® RT64 that contain both EO and PO groups in their structure with the alkyl chain length of C16-18. The salinity and temperature scans were also applied to these surfactants. The results show that the type of microemulsion of Marlox® RT42 was W/O microemulsion (Winsor type II) at low salinity, in contrast with the previous results from EO surfactants. When the salinity of the system increased, the O/W microemulsion (Winsor type I) was observed (around 7-9%wt/vol of salinity). Further increase in salinity of the system, the phase of SOW system changed back to the W/O microemulsion. From the salinity scan, the middle phase (Winsor type III) was not obviously observed. The first remark was the W/O microemulsion from the system. From the structure of Marlox® RT42 as shown in Figure 5.16, the polar part that contains oxygen atoms, excluding PO group (Salager *et al.*, 2013b) is too short as compared to the long length of alkyl chain or non-polar part. The feature of their structure is more oil soluble; hence, W/O microemulsion was observed.

For more observation, the temperature scan was applied to the system. However, the results show that there was no difference between phase scan at 40 and 90 °C (see Figure 5.17). Marlox® surfactant was still oil-liked surfactant and the optimal salinity was not found. Therefore, the salinity and temperature scans were not appropriate to find the C_c of Marlox® surfactants. Therefore, Marlox® surfactants were considered in the experiment of mixed surfactant systems in the next section.
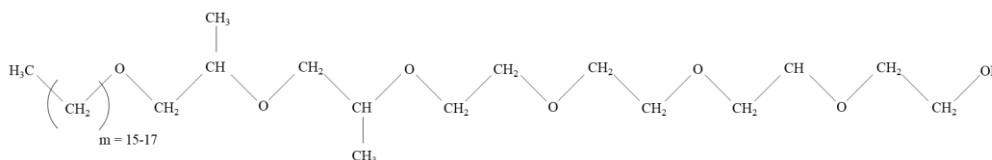
Figure 5.16 The brief molecular structure of Marlox® RT42.
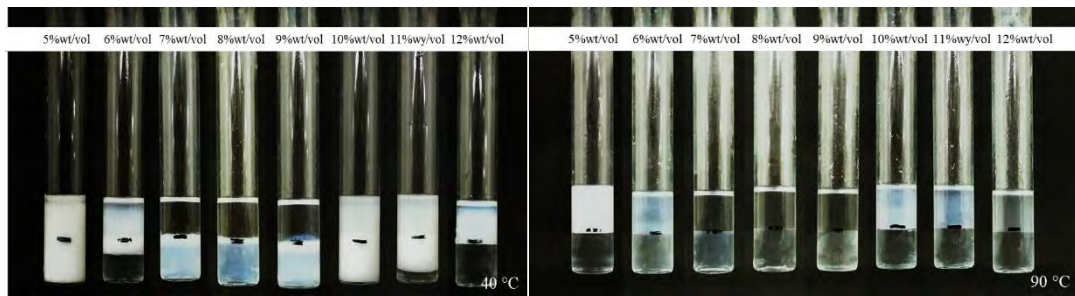
Figure 5.17 The phase scan for 0.1 M Marlox® RT42 with hexadecane at 40 °C and 90 °C.

5.3.3 Mixed Surfactant Systems

According to, The calibrated HLD parameters from the single surfactant experiment were used to determine the C_c value of other alkyl ethoxylate nonionic surfactants (Zarate-Muñoz *et al.*, 2016). In the mixed surfactant system, three different oils including cyclohexane, heptane and decalin with ranges of EACN values from 3.3 to 6.8 were carried on with 0.1 to 0.9 ratios of a reference surfactant to the test surfactant. To determine the C_c value of the test surfactant, Eq. 5.2 was considered at the optimal condition in the mixed surfactant systems:

$$HLD = b(S_{mix}^*) - K_{mix} \times EACN + C_{cn,mix} + c_{T,mix}(T - T_{ref}) \qquad \text{Eq. 5.3}$$

A linear mixing was applied to obtain the K_{mix} value for the mixed system (Acosta *et al.*, 2008a, Budhathoki *et al.*, 2016). Since the test surfactants are in the same series of ethoxylate nonionic surfactants as the reference surfactants, i.e. same head group, it is reasonable to assume an equal K value of the test surfactants and the reference surfactants. The salt parameter b was assumed to be equal since NaCl was used in both experiments. In addition, the experiments were conducted at room temperature (25 °C); hence, the temperature term in Eq. 5.3 is equal to zero and no need to determine the value of c_T. Equating Eq. 5.2 and Eq. 5.3, the HLD equation at optimal salinity and room temperature becomes:

$$S_{mix}^* = S_{ref}^* + (\frac{C_{c,ref} - C_{c,mix}}{b})$$ Eq. 5.4

To obtain the high accuracy of C_c values of the test surfactants, the linear mixing rule was applied to the $C_{c,mix}$:

$$C_{c,mix} = Y_{test}C_{c,test} + (1 - Y_{test})C_{c,ref}$$ Eq. 5.5

Combining and rearranging Eq. 5.4 and 5.5, Eq. 5.4 becomes

$$S_{mix}^* = S_{ref}^* + (\frac{C_{c,ref} - C_{c,test}}{b})Y_{test}$$ Eq. 5.6

The optimal salinity of each mixed surfactant system was plotted versus the ratio of test surfactant and reference surfactant. C_c value of the test surfactant was determined from the slope of this plot, given a constant b value of 0.13 according to Salager *et al.* (2001) for ethoxylate nonionic surfactant. Figures 5.18, 5.19 and 5.20 show the plot of optimal salinity in mixed surfactant systems with different reference surfactants: dehydol LS 3 TH, dehydol LS 5 TH and dehydol LS 9 TH, respectively.
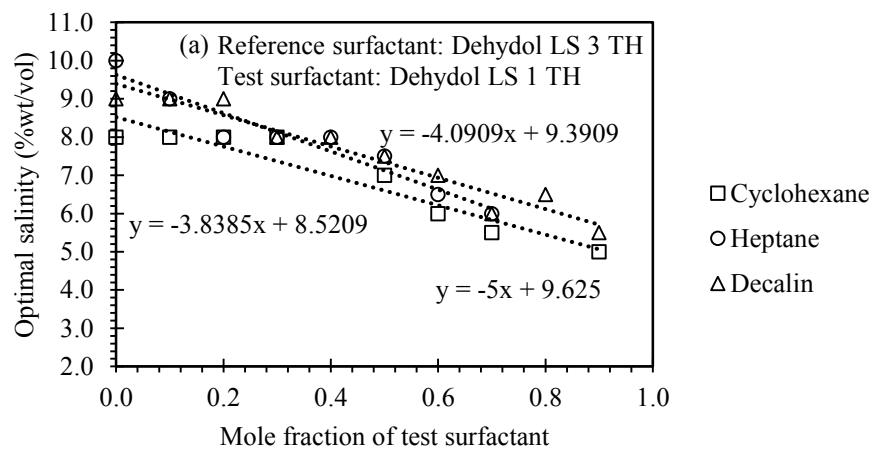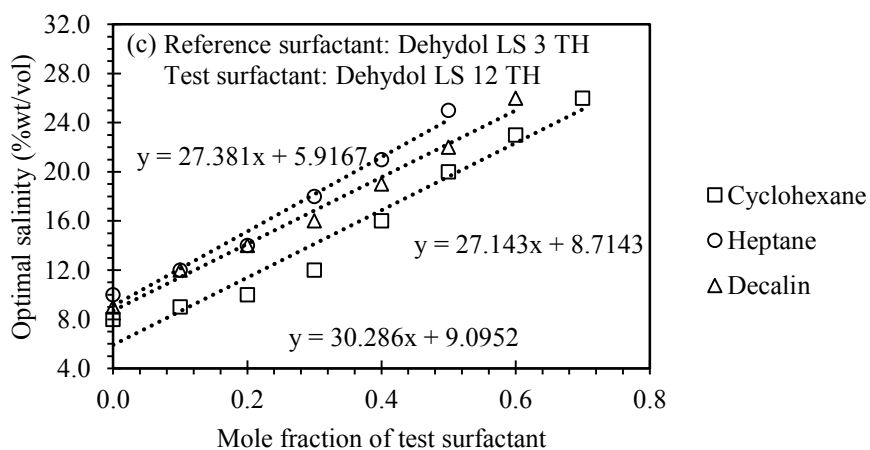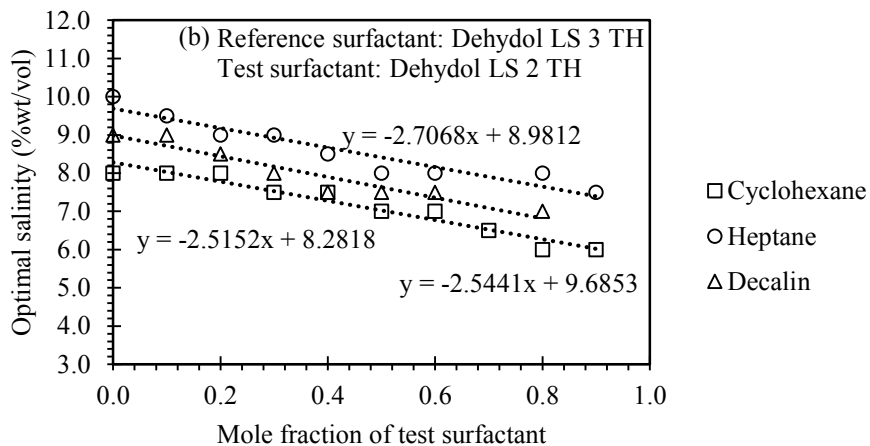
Figure 5.18 The plot between optimal salinity versus mole fraction of test surfactant with 3 oils using dehydol LS 3 TH as reference surfactant at room temperature (25 °C) with different test surfactants (a) dehydol LS 1 TH (b) dehydol LS 2 TH and (c) dehydol LS 12 TH.

(a) Reference surfactant: Dehydol LS 5 TH
Test surfactant: Dehydol LS 1 TH

y = -8.3333x + 17

y = -9.4583x + 17.654

y = -11.083x + 12.156

□ Cyclohexane
○ Heptane
△ Decalin

(b) Reference surfactant: Dehydol LS 5 TH
Test surfactant: Dehydol LS 2 TH

y = -5.5152x + 16.982

y = -5.0606x + 17.027

y = -6.2424x + 12.009

□ Cyclohexane
○ Heptane
△ Decalin
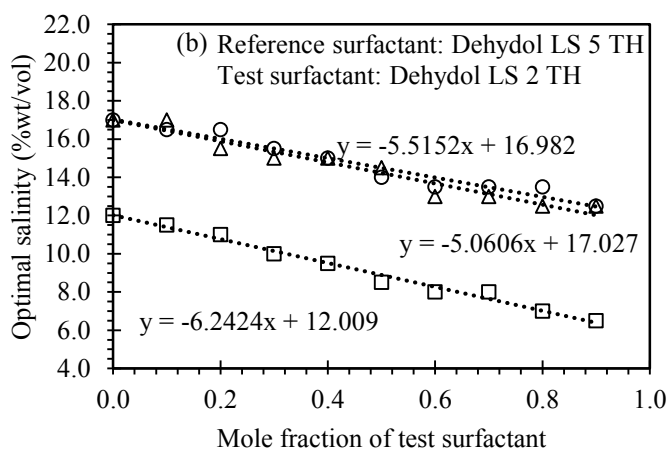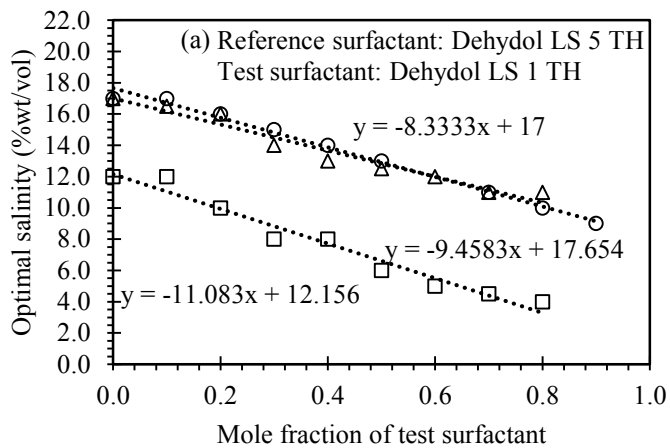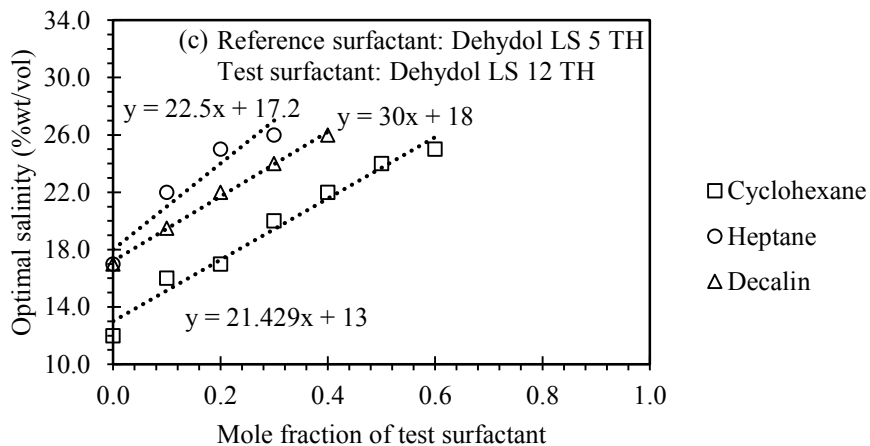
Figure 5.19 The plot between optimal salinity versus mole fraction of test surfactant with 3 oils using dehydol LS 5 TH as reference surfactant at room temperature (25 °C) with different test surfactants (a) dehydol LS 1 TH (b) dehydol LS 2 TH and (c) dehydol LS 12 TH.
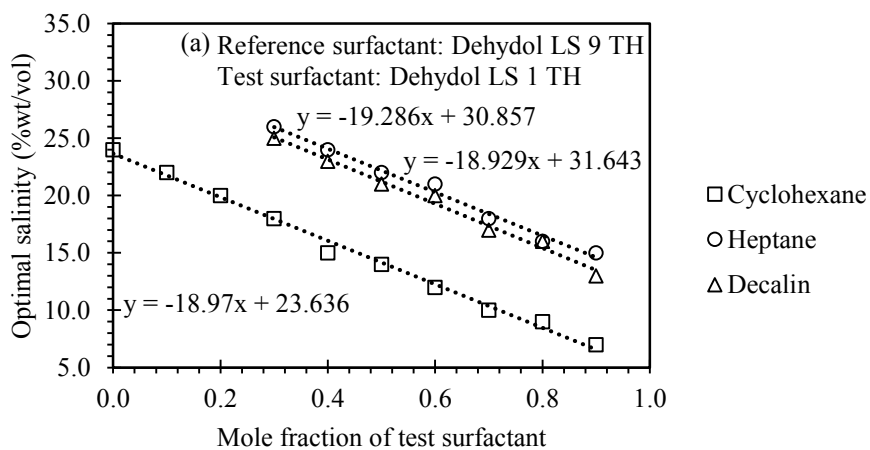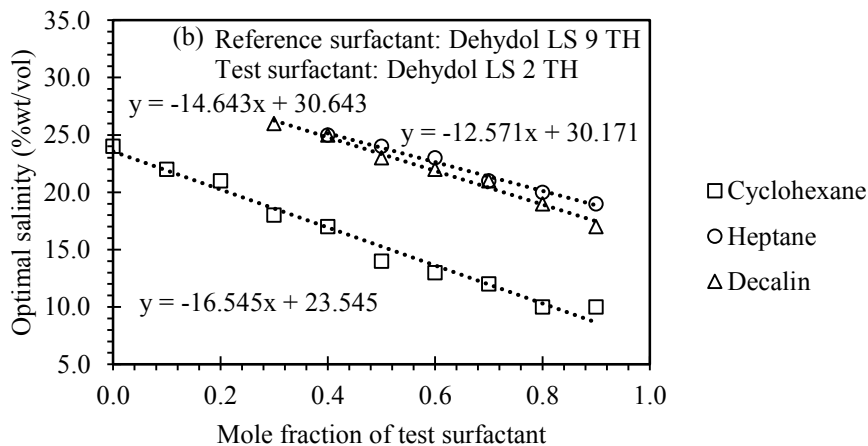
Figure 5.20 The plot between optimal salinity versus mole fraction of test surfactant with 3 oils using dehydol LS 9 TH as reference surfactant at room temperature (25 °C) with different test surfactants (a) dehydol LS 1 TH (b) dehydol LS 2 TH.

A linear relationship between the optimal salinity and the increasing ratio of the test surfactant to the reference surfactant was observed in all surfactant systems as illustrated in Figures 5.18-5.20 as a result of a reduction in the repulsive force between hydrophilic parts in the mixed nonionic surfactant system (Kunieda *et al.*, 2001). Hence, the optimal salinity was decreased in the mixed surfactant system with dehydol LS 1 TH and dehydol LS 2 TH as a reference surfactant. For the mixed systems with dehydol LS 12 TH, the optimal salinity increased due to the long length of polyethoxylate chain of the hydrophilic part as compared to the reference surfactant. As the ratio of dehydol LS 12 TH was higher, a higher optimal salinity was observed; however, the experiment was limited by the maximum optimal salinity of 26%wt/vol NaCl that could be prepared in this study for the phase inversion scans. Therefore, there are some missing data at high concentration of dehydol LS 12 TH (see Figures 5.18c and 5.19c).

For the mixed surfactant systems of dehydol LS 12 TH as the test surfactant and the dehydol LS 9 TH as the reference surfactant, no optimal salinity was observed. Although the single surfactant system of dehydol LS 9 TH can promote the

Winsor type III microemulsion with cyclohexane as an oil phase at room temperature, the mixed systems of dehydol LS 9 TH and the longer chain hydrophilic ethoxylates such as dehydol LS 12 TH would require salinity higher than the maximum limit of 26%wt/vol NaCl in this study to formulate the Winsor type III microemulsion.

From these results, the slope from each trend line of the mixed system was used to calculate the C_c value of the test surfactants using Eq. 5.6. The C_c value of the test surfactant was the value that gave the smallest absolute average deviation between the experimental and calculated optimal salinity among the three alkane oils. The results of C_c values in each mixed surfactant system are shown in Table 5.3.

Table 5.3 The C_c value of test surfactants with different reference surfactant

Test surfactants	Reference surfactants	C_c	%Absolute average deviation
Dehydol LS 1 TH	Dehydol LS 3 TH	0.02 ± 0.08	7.10
	Dehydol LS 5 TH	0.39 ± 0.18	6.72
	Dehydol LS 9 TH	0.32 ± 0.03	2.43
Dehydol LS 2 TH	Dehydol LS 3 TH	-0.09 ± 0.01	3.33
	Dehydol LS 5 TH	-0.17 ± 0.08	2.71
	Dehydol LS 9 TH	-0.22 ± 0.26	6.11
Dehydol LS 12 TH	Dehydol LS 3 TH	-3.66 ± 0.23	6.61
	Dehydol LS 5 TH	-4.03 ± 0.61	9.37
	Dehydol LS 9 TH	-	-

However, there was still a variation among the C_c values of the test surfactant obtained from each reference surfactant as seen in Table 5.3. According to Zarate-Muñoz *et al.* (2016), the selected C_c value of the test surfactant was obtained from the test and reference surfactant pair that give high R-square value of the plot between optimal salinity and mole fraction of test surfactant. If the R-square values were close or above 95%, that reference surfactant is suitable for specified test surfactants while if R-square values were close to zero, the reference surfactant was not promoting the phase transition of the test surfactant, meaning that the C_c of reference surfactant was close to the test surfactant. However, all of the R-square values of each test and reference pair in this study were higher than 95%; hence, all reference surfactant was suitable and could promote the phase transition (see Figure 5.21).
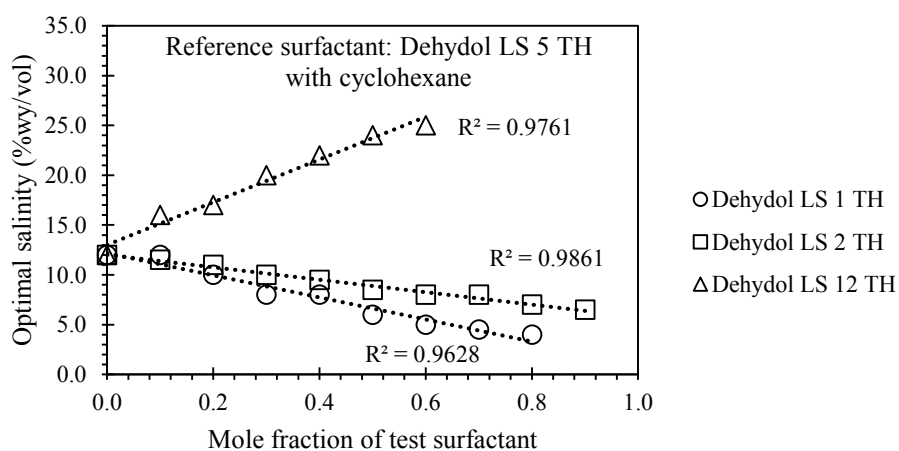
Figure 5.21 Optimal salinity for the test surfactant using Dehydol LS 5 TH as a reference surfactant and cyclohexane as oil in SOW system at 25 °C.

This study decided to select by considering other factors. The absolute average deviation should be considered. When the absolute average deviation of test surfactant were compared among the different reference surfactants, it seems that the system with the lower absolute average deviation should be selected, for example, the C_c values of dehydol LS 1 TH from dehydol LS 9 as reference surfactant showed the

lowest absolute average deviation (in Table 5.3). Therefore, the C_c value of 0.32 was selected for dehydol LS 1 TH. For dehydol LS 2 TH, the lowest absolute average deviation was from the mixed system with dehydol LS 5 TH as a reference surfactant; however, the standard deviation of this C_c value is around 50% (with -0.17 $\pm$ 0.08 in Table 5.3). Therefore, the C_c value from dehydol LS 3 as a reference surfactant is more suitable with low absolute average deviation and standard deviation (with -0.09 $\pm$ 0.01). It shows that both absolute average deviation and standard deviation of all systems are needed to determine before making a selection. The summary of selected C_c is shown in Table 5.4.

Table 5.4 The selected C_{cn} of test surfactants

Test surfactants	Reference surfactants	Selected C_c
Dehydol LS 1 TH	Dehydol LS 9 TH	0.32
Dehydol LS 2 TH	Dehydol LS 3 TH	-0.09
Dehydol LS 12 TH	Dehydol LS 3 TH	-3.66

Figure 5.22 shows a linear relationship between the C_c values with the number of ethoxylate groups with a high R-square of 99%. It is noted that the C_c value of dehydol LS 1 TH is positive in contrast with other surfactants with longer EO groups, meaning that dehydol LS 1 TH presents lipophilic property; hence, the selected C_c values were reasonable and could represent the physical property of the studied surfactants.
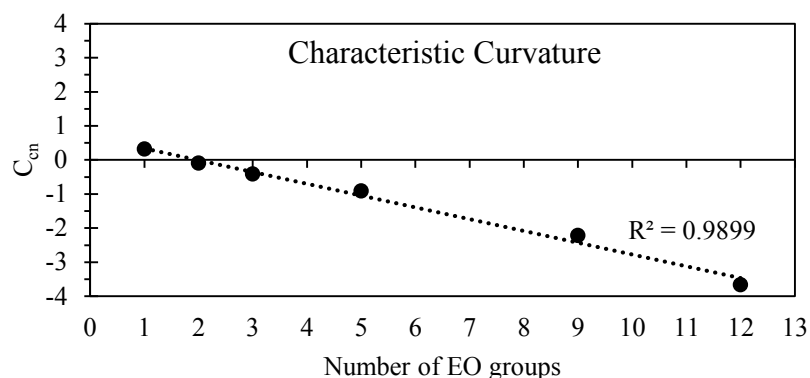
Figure 5.22 The relationship of number of EO group and C_{cn} of reference and test surfactants.

To evaluate the C_c values compared to their structure, Figure 5.23 shows the simple apprehensive. As the number of ethoxylate groups is higher, the more negative C_c value was observed due to the increasing of their solubility in the aqueous phase. It also confirmed that the presence of ethoxylate structure gave the surfactant more soluble in the aqueous phase; however, dehydol LS 1 TH is still lipophilic surfactant because the additional ethoxylate group is not enough to give hydrophilic property to the whole surfactant as the hydrophilic part was too short as compared to hydrophobic alkyl chain.
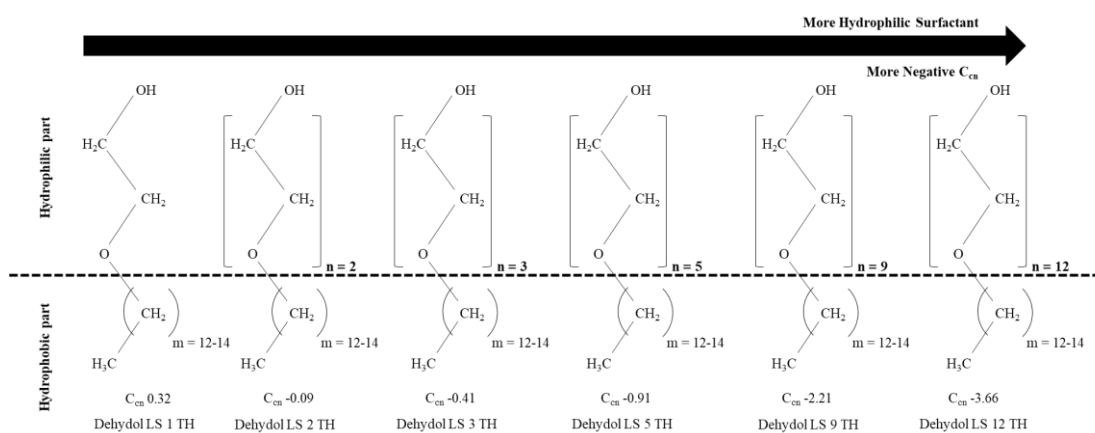
Figure 5.23 The C_{cn} relationship of a ethoxylate nonionic surfactant series.

5.3.4 Mixed Marlox® Surfactant Systems

From single surfactant systems, this work observed that the temperature scan cannot be used to identify the obvious phase inversion point (see Figure 5.17); hence, the mixed surfactant system was applied. The results was analyzed from varying the mole fraction of test surfactant with three different oils: cyclohexane, heptane and decalin and observed at room temperature (25 °C). The observed optimal salinity gave the decreasing trend; likewise, the trend of optimal salinity in mixed surfactant system of C12-14EO1 and C12-14EO2 (see Figures 5.24 and 5.25).
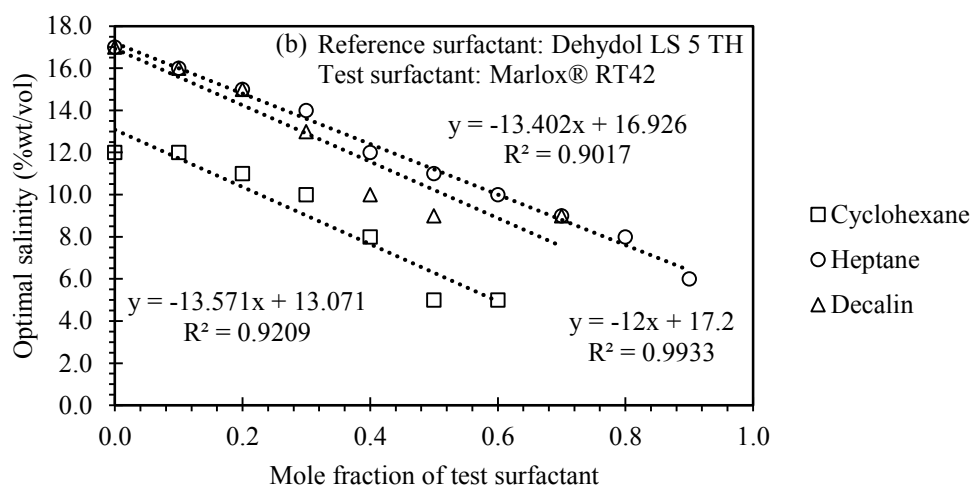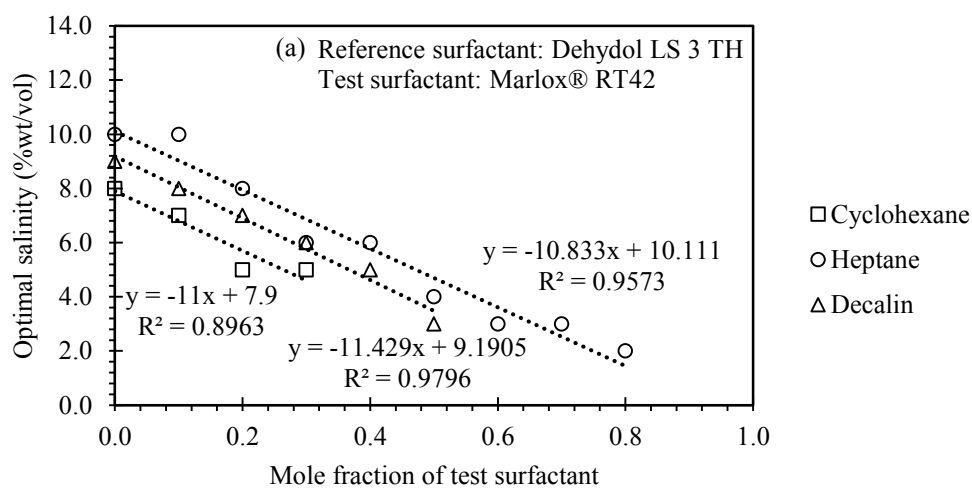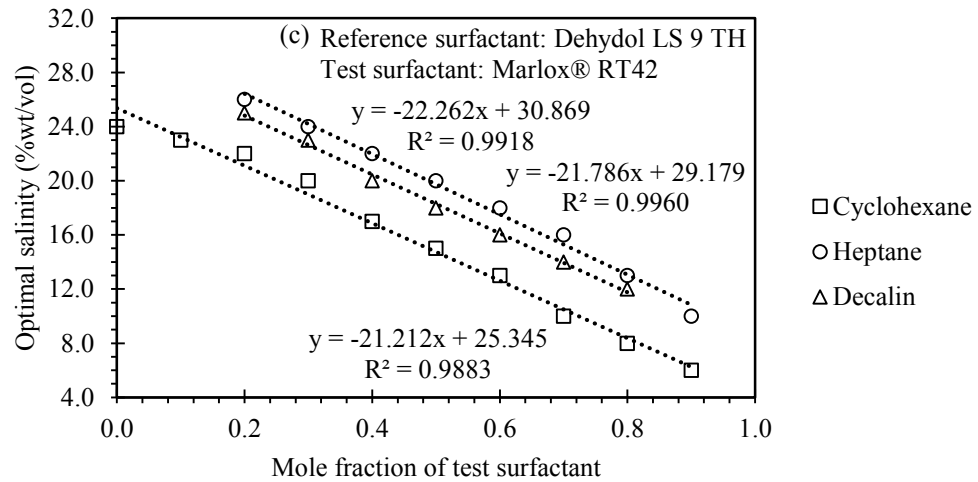
Figure 5.24 The plot between optimal salinity versus mole fraction of test surfactant with 3 oils using Marlox® RT42 as test surfactant at room temperature (25 °C) with different reference surfactants (a) dehydol LS 3 TH (b) dehydol LS 5 TH and (c) dehydol LS 9 TH.
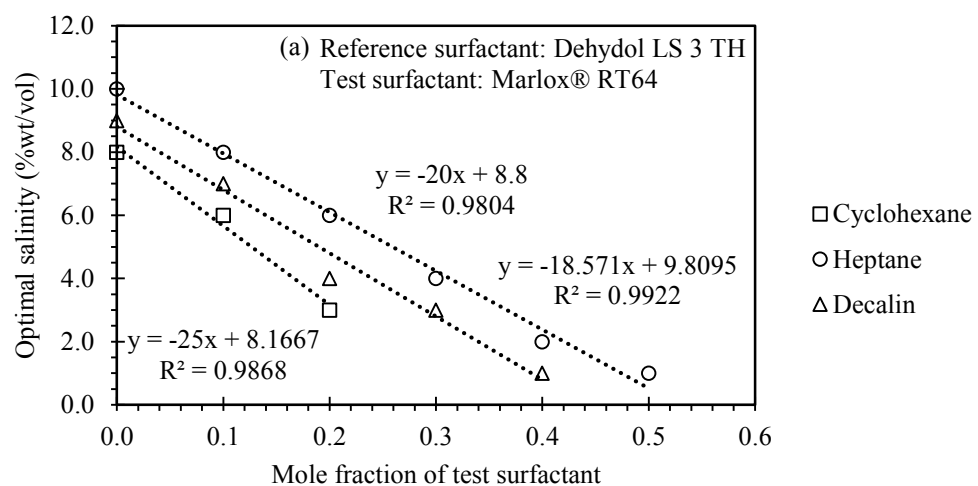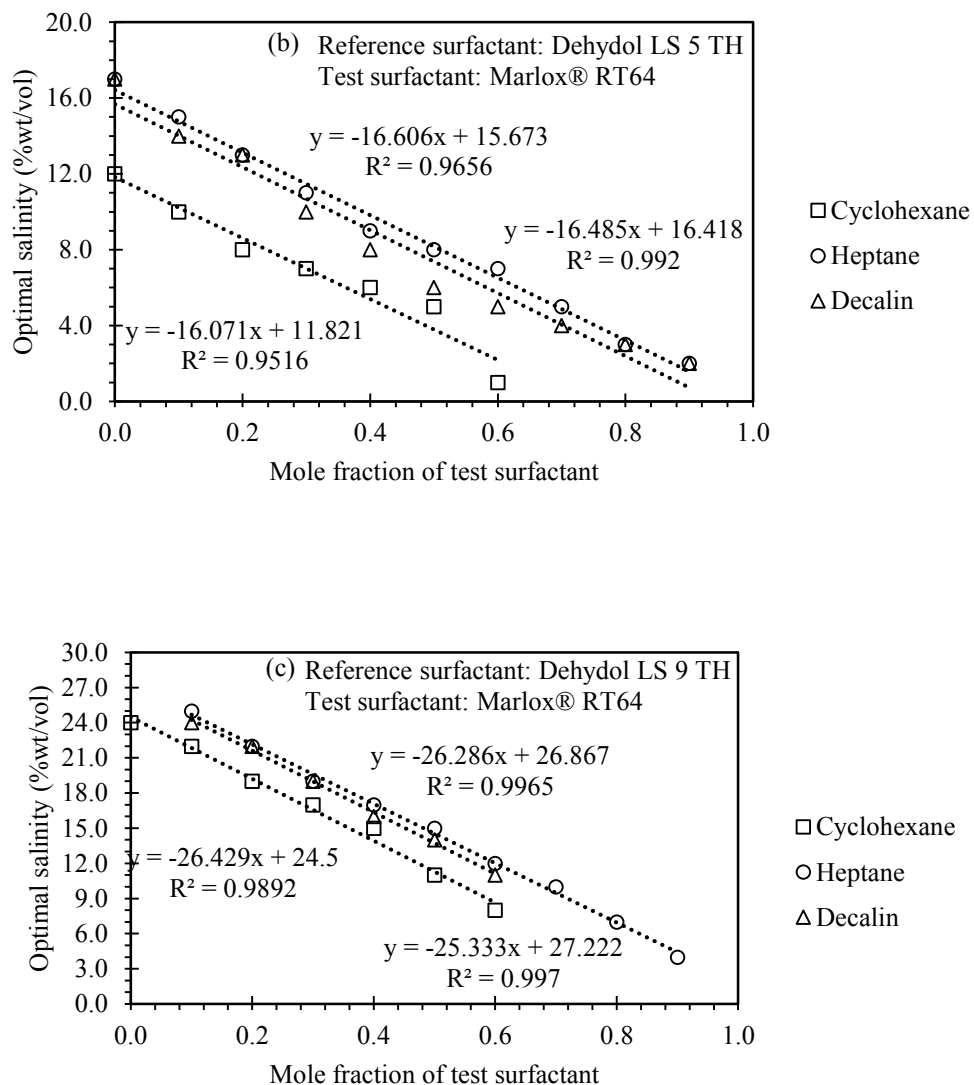
Figure 5.25 The plot between optimal salinity versus mole fraction of test surfactant with 3 oils using Marlox® RT64 as test surfactant at room temperature (25 °C) with different reference surfactants (a) dehydol LS 3 TH (b) dehydol LS 5 TH and (c) dehydol LS 9 TH.

Similar to the mixed systems in the previous section, a decreasing trend was observed when Marlox® was used as the test surfactants due to the reduction of repulsive force between the hydrophilic heads (Kunieda *et al.*, 2001). However, the mixed system with Marlox® gave higher decline of slope (i.e. higher negative slope) in the plot between the mole fraction of test surfactant and the optimal salinity. This behavior came from the more oil-like structure of Marlox® surfactant as compared to polyethoxylate surfactant. The Marlox® RT42 and Marlox® RT46 contain longer hydrophobic chain of alkyl chain with 16-18 carbon atoms and another hydrophobic part is propoxylate structure that is less soluble in water as observed in Salager's work (Salager *et al.*, 2013b). Moreover, these surfactants contain highly hydrophilic part with only ethoxylate groups, 4 groups for Marlox® RT42 and 6 groups for Marlox® RT64. It seem that the hydrophilic part is too small as compared to hydrophobic part; hence, when Marlox® surfactant was mixed with more hydrophilic surfactant, especially dehydol LS 9 TH that contains 9 groups of ethoxylate structure, the results gave the high value of decline. Furthermore, the phase inversion point was not observed at high mole fraction of test surfactant (around 0.8-0.9). The observed phase was Type II microemulsion (W/O microemulsion) even if the phase scan was carried out at low salinity content as shown in Figure 5.26. The oil-like structure of Marlox® surfactants also clarify this observation.
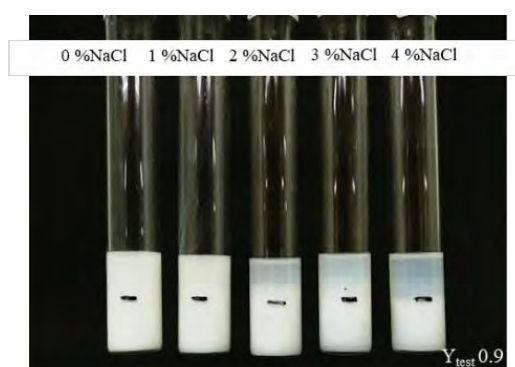
Figure 5.26 The phase scan of mixed surfactant system between C12-C14EO9 and Marlox® RT64 in cyclohexane with 0.9 mole fraction of test surfactant at room temperature.

Therefore, the characteristic curvature that were calculated from these slope in the plot are corresponding with oil-like structure of Marlox® surfactants with the positive characteristic curvature as shown in Table 5.5.

Table 5.5 The C_c value of Marlox® surfactants with different reference surfactant

Test surfactants	Reference surfactants	C_c	%Absolute average deviation
Marlox® RT42 (C16-18PO2EO4)	Dehydol LS 3 TH	0.89 ± 0.04	7.28
	Dehydol LS 5 TH	0.60 ± 0.11	6.26
	Dehydol LS 9 TH	0.55 ± 0.07	5.85
Marlox® RT64 (C16-18PO4EO6)	Dehydol LS 3 TH	2.19 ± 0.44	11.31
	Dehydol LS 5 TH	1.36 ± 0.04	13.67
	Dehydol LS 9 TH	1.14 ± 0.08	2.74

The criteria of selecting the suitable C_c value from different reference surfactants was similar to the mixed surfactant systems in the previous section. The standard deviation was calculated from average value of three different oils and percentage of absolute average deviation was considered between the observed optimal salinities and the calculated values using HLD equation. This study considered the standard deviation of value and percentage of absolute average deviation. For Marlox® RT42, the value of 0.55 in system that used dehydol LS 9 TH as the reference surfactant was selected due to the lowest %AAD and low standard deviation. For Marlox® RT64, the C_c also was selected from the system that used dehydol LS 9 TH as reference surfactant with the C_c value of 1.14. The summary of selected C_c for Marlox® is shown in Table 5.6.

Table 5.6 The selected C_{cn} of Marlox® surfactants

Test surfactants	Reference surfactants	Selected C_c
Marlox® RT42	Dehydol LS 9 TH	0.55
Marlox® RT64	Dehydol LS 9 TH	1.14

In discussion of two selected values, Marlox® RT64 gave the more oil-like surfactant than Marlox® RT42. Considering the ratio of ethoxylate and propoxylate group (EO/PO), the higher EO/PO ratio identifies the higher amount of water-like structure containing in the Marlox® surfactant. From the experimental results and molecular structure of Marlox® surfactant, the EO/PO ratios are 2 and 1.5 for Marlox® RT42 and for Malox® RT64, respectively. The higher EO/PO ratio, the lower C_c value was observed. The lower C_c or more negative C_c value indicates the more water-soluble surfactant (Acosta *et al.*, 2008b). Therefore, Marlox® RT42 is more water-like surfactant than Marlox RT64 that is more oil-like surfactant as illustrated in the schematic of molecular structure in Figure 5.27.
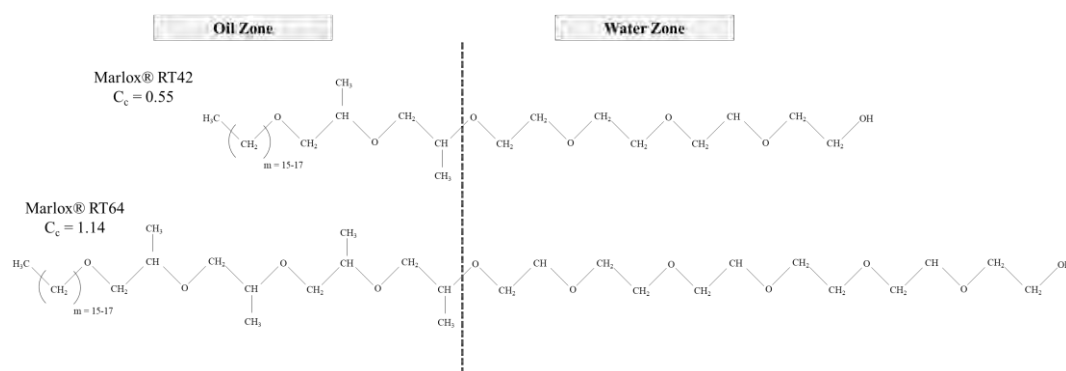
Figure 5.27 The molecular structure of Marlox® RT42 and Marlox® RT64.

5.4 Conclusions

The measurement of the characteristic curvature of nonionic surfactant by using the simplified method from Zarate-Muñoz *et al.* (2016) gave the reasonable results. The polyethylene oxide nonionic surfactants showed the linear relationship between molecular structure and characteristic curvature. The trend of characteristic curvature values were determined with their structures in different ethylene oxide group (EO group). If the nonionic surfactant contained more EO group, the more negative value of characteristic curvature was observed. For Marlox® surfactants that contain both polyethylene oxide (EO group) and polypropylene oxide (PO group) groups, the characteristic curvature value were more positive to represent the oil-like surfactant as compared to the series of alcohol polyethylene oxide surfactants. Additional observation is the ratio of EO and PO groups in the Marlox® surfactants. If the ratio of EO/PO is lower, the more positive value of characteristic curvature is observed when considering the same alkyl chain length.

CHAPTER VI
CHARACTERISTIC CURVATURE MODEL

6.1 Introduction

Surfactants are general chemicals that are used for many emulsifying systems, especially surfactant/oil/water system (SOW), for example, enhanced oil recovery process, solid dispersion manufacturing process and pharmaceutical industry (Chaudhari *et al.*, 2017). The key property for selection of surfactants for a certain application is their solubility. Surfactant structure is composed of the hydrophilic (head part) and hydrophobic parts (tail part). The hydrophilic part can dissolve in aqueous phase and the hydrophobic part can dissolve in oil phase or non-polar phase. This structure makes the surfactant soluble in two immiscible phase. Surfactants can be categorized into four types, depending on their hydrophilic head. The hydrophilic head that contains negative charge is known as anionic surfactant while the surfactants with positively charged head is known as cationic surfactant. The surfactants that contain both negative and positive charges are called zwitterionic surfactants. If there is no charge on the head part, the group of surfactants are called nonionic surfactant. The use of each type of surfactants depends on a specific system and other related chemicals.

One of the key property for surfactant selection for any application is its characteristic curvature. Characteristic curvature (C_c) presents the hydrophobicity of the surfactant when the surfactant is applied to the water-oil system (Hammond *et al.*, 2011). The value of C_c indicates the trend of a surfactant to be soluble in aqueous and oil phase. If the C_c shows a positive value, the surfactant tends to form reverse micelle and likes to dissolve in an oil phase while a positive C_c value indicates that the surfactant tends to form normal micelle and likes to dissolve in an aqueous phase (Acosta *et al.*, 2008b). The C_c property is one of the parameters in a hydrophilic-lipophilic difference (HLD) equation that is used to estimate type of microemulsion of an SOW system (Acosta *et al.*, 2008a). The HLD equations for ionic and nonionic surfactants are expressed in Eq. 6.1 and Eq. 6.2, respectively (Castellino *et al.*, 2011):

For ionic surfactants,

$$HLD = \ln(S) - K*EACN - f(A) - \alpha\Delta T + C_c \qquad \text{Eq. 6.1}$$

For nonionic surfactants,

$$HLD = b(S) - K*EACN - \varphi(A) + c_T\Delta T + C_{cn} \qquad \text{Eq. 6.2}$$

where $\ln(S)$ and $b(S)$ are the function of salinity content in the aqueous phase (g/100mL); b, K, α and c_T are the constants depending on type of surfactants; EACN is the equivalent alkane carbon number of oil; the function $f(A)$ and $\varphi(A)$ are the alcohol function; ΔT is the temperature difference from a 25 °C; and C_c and C_{cn} are the characteristic curvature.

For the characteristic curvature, there are some works that developed the model for prediction C_c value of anionic (Hammond *et al.*, 2011) and nonionic surfactants (Zarate-Muñoz *et al.*, 2016), shown in Eq. 6.3 and 6.4). These model showed the relationship that C_c value is the function of molecular structure; however, the available models cannot be used for various surfactant structures and are limited for some groups of surfactant such as polyoxyethylene surfactant. Therefore, the prediction method to estimate the characteristic curvature of surfactant is needed.

For ionic surfactants proposed by Hammond *et al.* (2011),

$$C_c = C1 \text{ x } C_L + C2 \text{ x } C_{MB} + C3 \text{ x } C_\beta + C4 \qquad \text{Eq. 6.3}$$

For nonionic surfactants proposed by Zarate-Muñoz *et al.* (2016),

$$C_{cn} = 0.28 \text{ x } N_{CS} + 2.4 - N_{ES} \qquad \text{Eq. 6.4}$$

Group-Contribution method is the method based on a concept of summation of structural dependent parameter multiplied by the frequency of occurrence of that molecular fragment in a molecule to obtain the chemical property with an assumption of no interaction between the molecular fragments (Joback *et al.*, 1987). This method has the advantages of fast prediction with simple computational tool but lack of accuracy in the prediction of isomers (Marrero *et al.*, 2001). Marrero *et al.* (2001) has overcome this over-simplification of the original group contribution model by performing this method in three levels. The first level covers variety of simple molecular fragments but still cannot differentiate among isomers. The second level

includes groups that can describe proximity effects such as polyfunctional groups and isomers. The size of molecular groups in this second level is the fragmented groups with carbon number from 3 to 6 including aromatic one ring or cycloalkane. The third level adds more complex structural groups such as polyfunctional cyclic and acyclic structures. The carbon number of molecule fragments of the third level ranges from 7 to 60. By the concept of multilevel approach, the contributions of the higher-order levels are used to correct the over-simplification of the lower levels (Mattei *et al.*, 2013). A generic relationship of the fractional groups in all three levels to the target property is shown in Eq. 6.5.

$$f(X) = \sum_i N_i C_i + \sum_j M_j D_j + \sum_k O_k E_k \qquad \text{Eq. 6.5}$$

Where f(X) is a function of the target property that depends on three terms of group contribution: first-order group, second-order group and third-order group. C_i is the contribution of the first-order group multiplied with N_i that is the number of group occurrences in type-i chemicals. D_j is the contribution of the second-order group multiplied with M_j that is the number of group occurrences in type-j chemicals. Also, E_k is the contribution of the third-order group multiplied with O_k that is the number of group occurrences in type-k chemicals.

The group contribution concept has been widely used to estimate various properties including specific properties of chemical substances such as boiling and freezing points, critical properties, heat capacity, viscosity (Joback *et al.*, 1987); enthalpy of formation (van Speybroeck *et al.*, 2010, Hukkerikar *et al.*, 2013); Gibbs free energy (van Speybroeck *et al.*, 2010); Hildebrand solubility parameter (Roughton *et al.*, 2012, Kulajanpeng *et al.*, 2016). Some specific properties of surfactants such as cloud point (Mattei *et al.*, 2014), CMC (Mattei *et al.*, 2013) have been estimated by the group contribution concept.

This work focused on the development of characteristic curvature prediction for anionic and nonionic surfactants. The group contribution model based on Marrero *et al.* (2001) was applied for developing of the C_c models.

6.2 Methodology

6.2.1 Data Collection

The database of characteristic curvature was collected from many literatures. The various surfactant structures are needed to make the GC model more accurate and practical for variety of surfactants. For anionic surfactants, 33 anionic surfactants were collected, including sodium alkyl carboxylate (Abbott, 2015), sodium alkyl-propoxylate sulfate (Witthayapanyanon *et al.*, 2008, Abbott, 2015, Budhathoki *et al.*, 2016), sodium branched alkyl-propoxylate sulfate (Hammond *et al.*, 2011, Abbott, 2015) and some anionic surfactants containing cyclic and aromatic structures (Acosta *et al.*, 2008b, Hammond *et al.*, 2011, Abbott, 2015). For nonionic surfactants, 25 nonionic surfactants were collected and combined with additional data from experiment in Chapter 5. The surfactant structures covered for characteristic curvature model of nonionic surfactants, including alkyl ethoylate (Abbott, 2015, Zarate-Muñoz *et al.*, 2016), alkyl phenyl ethoxylate, alkyl glucoside and polysorbate structures (Abbott, 2015) .

Table 6.1 Database of characteristic curvature of 33 anionic surfactants

Anionic Surfactants	C_c	References
SDHS Na Dihexylsulfosuccinate	-0.920	Abbott (2015)
SDBS Na Dodecyl Benzene sulfonate	-0.900	Abbott (2015)
SDS/SLS Na Dodecyl Sulfate	-2.500	Hammond *et al.* (2011)
Sodium Octanoate	-3.000	Abbott (2015)
Sodium Decanoate	-2.550	Abbott (2015)
Sodium Dodecanoate	-2.100	Abbott (2015)
Sodium stearate	-0.750	Abbott (2015)
Sodium Oleate	-1.700	Abbott (2015)

Table 6.1 Database of characteristic curvature of 33 anionic surfactants (Continued)

Anionic Surfactants	C_c	References
Sodium Dimethylnaphthalene sulfonate	-3.500	Abbott (2015)
Sodium Strearoyl glutamate	-5.000	Abbott (2015)
Lecithin	4.000	Abbott (2015)
NaC12PO4Sulfate	-1.900	Abbott (2015)
NaC12PO6Sulfate	-1.600	Abbott (2015)
NaC12PO10sulfate	-1.000	Abbott (2015)
NaBrancedC12PO4Sulfate	-1.400	Abbott (2015)
NaBrancedC12PO6Sulfate	-1.100	Abbott (2015)
NaBrancedC12PO8Sulfate	-0.800	Abbott (2015)
NaBrancedC12PO10Sulfate	-0.500	Abbott (2015)
NaBrancedC14PO8Sulfate	-0.600	Abbott (2015)
NaC12PO14EO2sulfate	0.740	Abbott (2015)
NaC10PO18EO2Sulfate	1.990	Abbott (2015)
NaC8PO4Sulfate	-2.480	Budhathoki *et al.* (2016)
NaC8PO4EOSulfate	-2.470	Budhathoki *et al.* (2016)
NaC10PO4EOSulfate	-2.220	Budhathoki *et al.* (2016)
NaC10PO4Sulfate	-2.150	Budhathoki *et al.* (2016)
NaC12EO3Sulfate	-2.890	Budhathoki *et al.* (2016)
Sodium naphthenate	-2.400	Acosta *et al.* (2008b)
NaC12-15EO2Sulfate	-2.970	Witthayapanyanon *et al.* (2008)
NaC12-13PO8Sulfate	-0.784	Witthayapanyanon *et al.* (2008)
NaC12-13PO3Sulfate	-1.770	Witthayapanyanon *et al.* (2008)
Br-Oxo 123	-1.550	Hammond *et al.* (2011)
TDA	-1.610	Hammond *et al.* (2011)
L-Oxol123	-1.950	Hammond *et al.* (2011)

Table 6.2 Database of characteristic curvature of 33 nonionic surfactants

Nonionic surfactants	C_c	References
C6EO3	0.100	Abbott (2015)
C6EO4	-1.600	Abbott (2015)
C8EO4	0.300	Abbott (2015)
C8EO5	-1.000	Abbott (2015)
C9EO4.5	0.420	Zarate-Muñoz *et al.* (2016)
C9EO5	-0.080	Zarate-Muñoz *et al.* (2016)
C10EO4	1.300	Abbott (2015)
C10EO6	-0.900	Abbott (2015)
C11.5EO5	0.620	Zarate-Muñoz *et al.* (2016)
iC13EO8	-1.960	Zarate-Muñoz *et al.* (2016)
C14EO7	-0.700	Abbott (2015)
C9PhEO2	1.000	Abbott (2015)
C9PhEO5	0.120	Abbott (2015)
C9PhEO9	-1.600	Abbott (2015)
$C_{18}H_{34}O_6$	3.500	Abbott (2015)
$C_{28}H_{52}O_{12}$	-0.800	Abbott (2015)
$C_{48}H_{90}O_{13}$	4.000	Abbott (2015)
C16EO14	-2.900	Abbott (2015)
C10Glucoside	-1.700	Abbott (2015)
C12Glucoside	-1.000	Abbott (2015)
C9GEO6	-1.080	Zarate-Muñoz *et al.* (2016)
iC13EO6	0.040	Zarate-Muñoz *et al.* (2016)
C12EO6.5	-1.200	Abbott (2015)
C58H114O26	-7.900	Zarate-Muñoz *et al.* (2016)
C64H124O26	-3.700	Zarate-Muñoz *et al.* (2016)

Table 6.2 Database of characteristic curvature of 33 nonionic surfactants (Continued)

Nonionic surfactants	C_c	References
C12-14EO1	0.32	Experiment in this work
C12-14EO2	-0.09	Experiment in this work
C12-14EO3	-0.41	Experiment in this work
C12-14EO5	-0.91	Experiment in this work
C12-14EO9	-2.21	Experiment in this work
C12-14EO12	-3.66	Experiment in this work
C16-18PO2EO4	0.55	Experiment in this work
C16-18PO4EO6	1.14	Experiment in this work

6.2.2 Development of Group Contribution Model

In the development of GC model, the collected database from the previous step were analyzed. A few surfactants of each anionic and nonionic were kept aside and not used in the development of the model for later used in the model verification. The C_c data used to develop the model must be able to represent various structures of surfactants with enough data points for each repeating structure such as NaC12PO4sulfate, NaC12PO6sulfate and NaC12PO10sulfate that were used to represent the polypropylene oxide series of anionic surfactants.

To develop a model for characteristic curvature (C_c) an appropriate form of the property function f(X) is needed to be analyzed. Figures 6.1 and 6.2 show the effect molecular structures to the characteristic curvature of anionic and nonionic surfactants, respectively. The polypropylene oxide (-PO-) tends to have a linear relationship with the characteristic curvature of anionic surfactants while polyethylene structure (-EO-) is a linear function with the characteristic curvature of nonionic surfactants. Although some slight deviation from linearity was observed in dodecyl alcohol ethylene oxide surfactant (see Figure 6.2) and the surfactants with polypropylene oxide (-PO-) groups (see Figure 6.1b), an approximated linear

relationship between molecular fractions and C_c was still acceptable; hence, a linear relationship between the property function f(X) and the contribution of molecular fractions was justified. Eq. 6.5 then becomes:

$$C_{ca} = \sum_i N_i C_i + \sum_j M_j D_j + \sum_k O_k E_k + \text{constant} \qquad \text{Eq. 6.6}$$

$$C_{cn} = \sum_i N_i C_i + \sum_j M_j D_j + \sum_k O_k E_k + \text{constant} \qquad \text{Eq. 6.7}$$

where C_{ca} and C_{cn} represent the characteristic curvature of anionic and nonionic surfactants, respectively. The coefficients in the equation were determined as explained in the next step.
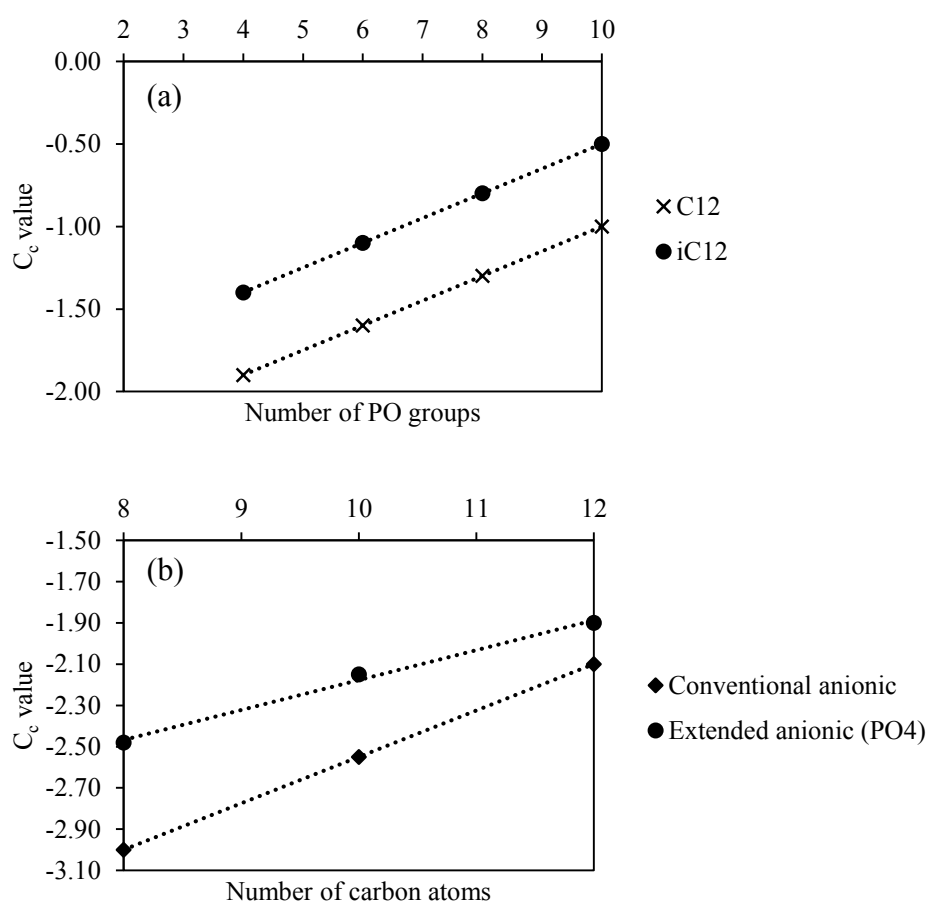
Figure 6.1 A linear relationship between (a) polypropylene oxide (-PO-) group, (b) length of carbon chain and characteristic curvature of anionic surfactants.
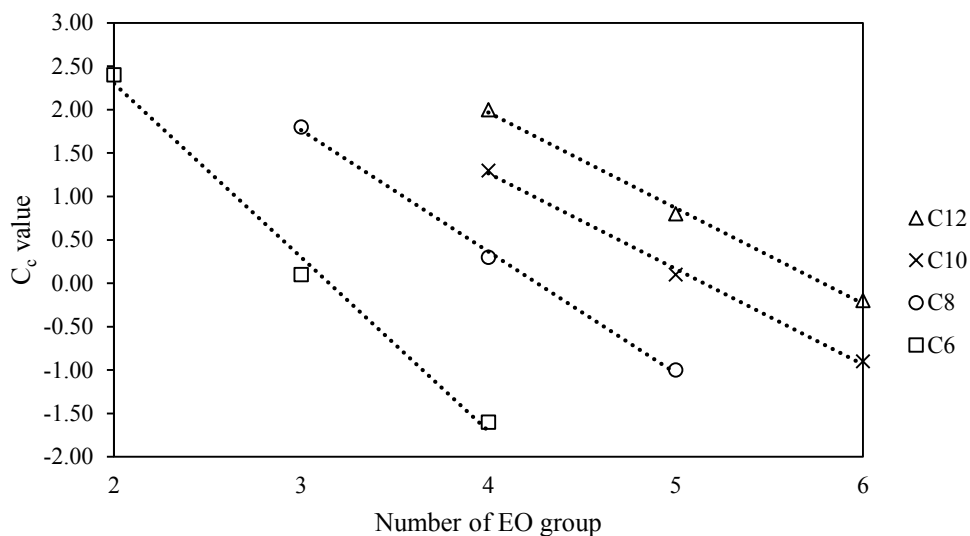
Figure 6.2 A linear relationship between the polyethylene oxide (-EO-) group and the characteristic curvature of nonionic surfactants.

6.2.3 Correlation Analysis

In this step, the regression analysis was applied to determine the contribution values of each molecular fractions as proposed by Marrero et al. (2001). The values of contribution of each molecular fragment was fitted through a regression analysis by minimizing the deviation between experiment and predicted C_c data.

6.3 Results and Discussion

6.3.1 Characteristic Curvature GC-Model of Anionic Surfactants

As previously mentioned, the GC-model for characteristic curvature of anionic surfactant is shown in the Eq. 6.6. In this work a constant was added in the group contribution model both first-order and higher-order levels for higher accuracy of the model. Adding of a constant in the group contribution function was performed in the work of Roughton et al. (2012) and Kulajanpeng *et al.* (2016). Thus, it becomes to Eq. 6.6.

Table 6.3 Group definition and their coefficients for first-order, and higher-order Group-Contribution Model of characteristic curvature of anionic surfactants

Molecular Fragment	Coefficient
First-order, C_i	
CH_3	0.6325
CH_2	0.2088
CH	-0.2082
$CH=CH$	-0.5123
CH_2-O	-0.1555
CH_2COO	-1.0115
$CHCOO$	0.2491
$CONH$	-4.8786
SO_3^-	0.0297
OSO_3^-	-2.1970
PO_4^-	1.5828
aC fused aromatic	0.0444
aCH	-0.0335
$aC-CH_3$	0.0300
$aC-CH_2$	0.0047
$aC-SO_3^-$	0.0197
CH_3N^+	-0.0551
$CH_{2,cyc}$	0.3260
CH_{cyc}	-0.0212
Constant	-3.5236

Table 6.3 Group definition and their coefficients for first-order, and higher-order Group-Contribution Model of characteristic curvature of anionic surfactants (continued)

Molecular Fragment	Coefficient
Second-order, D_j	
AROMRINGs^{1}s^4	0.0122
-EO-	0.0475
-PO-	-0.0310
CH$_{cyc}$-CH$_2$	0.0747
Third-order, E_k	
OOC-(CH$_n$)$_m$-COO	-0.0170
COO-(CH$_n$)$_m$-OOC	-0.0551
AROMFUSED[2]s^{1}s^2	0.0225

After multiple regression analyses had been performed, the coefficient of each group in the first-order, second-order and third-order groups was obtained. The coefficients of all molecular fragments are shown in Table 6.3 for the first-order and higher-order groups. The coefficient values reflect the tendency of surfactant to dissolve in the aqueous phase or oil phase. The positive value of C_{ca} coefficient indicates the more hydrophobicity of surfactant to dissolve in oil phase, as the definition of C_c while the negative value indicates the more hydrophilicity of surfactant to dissolve in aqueous phase. For example, coefficient of CH$_3$ is equal to 0.6325 or coefficient of CH$_2$ is equal to 0.2088. The CH$_3$ and CH$_2$ molecules are part of hydrocarbon chain that are hydrophobic. So, it is reasonable that the coefficients for these two molecular fractions are positive. In contrast with the coefficients with negative value, the surfactant is more soluble in the aqueous phase such as ethylene oxide structure (CH$_2$O) and sulfate structure (OSO$_3^-$) which contain polar structures.

The model for prediction of characteristic curvature of anionic surfactants was reported in literature. Hammond et $al.$ (2011) developed a simple GC-model for the prediction of the characteristic curvature of alkyl propylene oxide sulfate groups as shown in the Eq. 6.8:

$$C_{ci} = C1 \times C_L + C2 \times C_{MB} + C3 \times C_\beta + C4 \qquad \text{Eq. 6.8}$$

where C1, C2, C3 are the contributions of GC-model. C4 is the contribution that represents the occurrence of $4PO-SO_4Na$ group in the anionic surfactant that equals to -3.181. C_L represents the number of carbons in the linear chain that its contribution (C1) equals to 0.100. C_{MB} represents the mid-chain carbons that its contribution (C2) equals to 0.071. C_β represents the carbon attached to the β position that its contribution (C3) equals to 0.690. In addition, some contributions are not included in the Eq. 6.8. There are contribution of polypropylene structure (-PO-) and sulfate structure with 0.158 and -3.813, respectively. The GC-model by Hammond et $al.$ (2011) only available for alkyl propylene oxide sulfate surfactants and other anionic surfactants were covered. There are many missing groups that this model cannot predict. Nevertheless, the GC-model by Hammond et $al.$ (2011) did propose a linear relationship between property C_c and the number of PO group that was in agreement with the function f(X) defined in this work.

Table 6.4 Example calculation of characteristic curvature of Sodium Dimethylnaphthalene sulfonate with Group-Contribution Method compared to the work of Hammond *et al.* (2011)
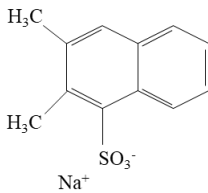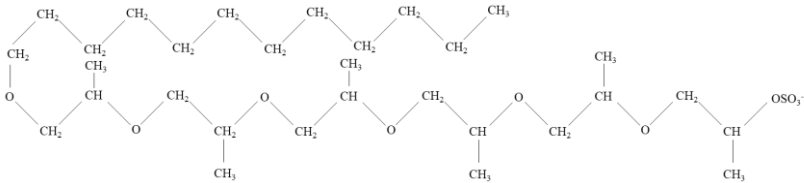
Sodium Dimethylnaphthalene sulfonate		
Molecular structure: First-order group:		

Groups	Occurrences	Coefficients
aC fused aromatic	2	0.0444
aCH	5	-0.0335
aC-CH$_2$	2	0.0047
aC-SO$_3^-$	1	0.0197

Second-order group:

Groups	Occurrences	Coefficients
No Second-order group		

Third-order group:

Groups	Occurrences	Coefficients
AROMFUSED[2]s^{1}s^2	1	0.0225

C_c calculation

GC model without higher-order group; $C_c = \Sigma_i N_i C_i + \text{Constant} = -3.5225$

GC model with higher-order group; $C_c = \Sigma_i N_i C_i + \Sigma_j M_j D_j + \Sigma_k O_k E_k + \text{Constant} = -3.5000$

Previous model (Hammond *et al.*, 2011) cannot be used to predict this surfactant

%Absolute deviation from experimental value $C_{c,exp} = -3.5000$

GC-model without higher-order group; 0.64 %

GC model with higher-order group; 0.00%

Previous model (Hammond *et al.*, 2011) cannot be used to predict this surfactant

Table 6.5 Example calculation of characteristic curvature of NaC12PO6Sulfate with Group-Contribution Method compared to the work of Hammond *et al.* (2011)

NaC12PO6Sulfate		
Molecular structure:		
First-order group:		
Groups	Occurrences	Coefficients
CH_3	7	0.6325
CH_2	11	0.2088
CH	6	-0.2082
CH_2-O	6	-0.1555
OSO_3^-	1	-2.1970
Second-order group:		
Groups	Occurrences	Coefficients
-PO-	6	-0.0310
Third-order group:		
Groups	Occurrences	Coefficients
No Third-order group		
C_c calculation		
GC model with higher-order group; $C_c = \Sigma_i N_i C_i + \Sigma_j M_j D_j + \Sigma_k O_k E_k + Constant = -1.3640$		
Previous model (Hammond *et al.*, 2011) $C_{c,calc} = -0.6200$		
%Absolute deviation from experimental value $C_{c,exp} = -1.6000$		
GC-model with higher-order group; 14.75%		
Previous model (Hammond *et al.*, 2011); 61.25%		

Examples of calculation of this GC-model are presented in Tables 6.4 and 6.5. As the equation of GC-model, the number of occurrence of each molecular fraction in each level group are counted and multiplied with its contribution from regression analysis. The characteristic curvature of the surfactant was calculated and compared to the experimental value. Table 6.4 illustrates the calculation to obtain a C_c value of Sodium Dimethylnaphthalene sulfonate. The results gave 0.64% and 0.00% deviation between calculated and experimental C_c for first-order and higher-order level GC-models, respectively. This example obviously showed the higher-level GC-model can slightly improve the accuracy with the addition of fused aromatic group to the calculation. It is noted that this type of surfactant cannot be predicted by the work proposed by Hammond *et al.* (2011) since aromatic group was not included in their model. Table 6.5 shows the calculation of C_c value of NaC12PO6Sulfate. There is the surfactant that all molecular fragments contained in NaC12PO6Sulfate were included in our GC-model as well as in the model proposed by Hammond *et al.* (2011). The calculation showed that our GC-model included more available groups than the previous work and gave higher accuracy with lower deviation.

To compare the accuracy of model, the calculated value from GC-model and experimental values are shown in Figures 6.3, 6.4 and 6.5 for first-order, second-order and third-order levels, respectively.
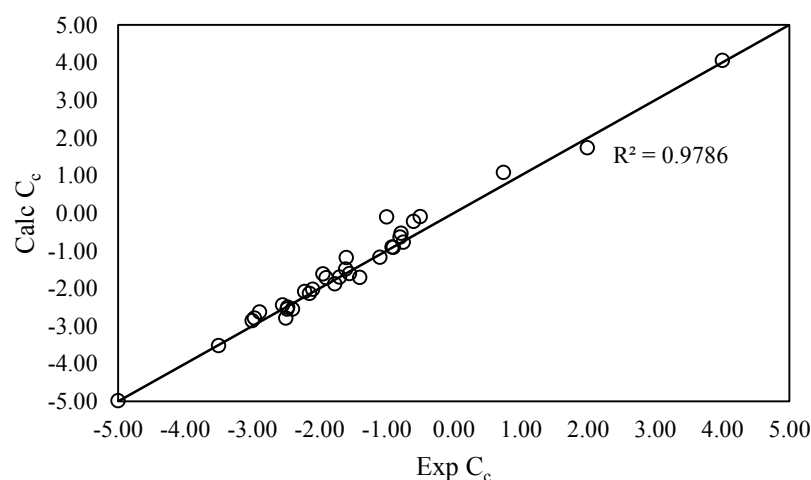
Figure 6.3 Parity plot between experimental characteristic curvature of anionic surfactants and calculated value from first order Group-Contribution Model.
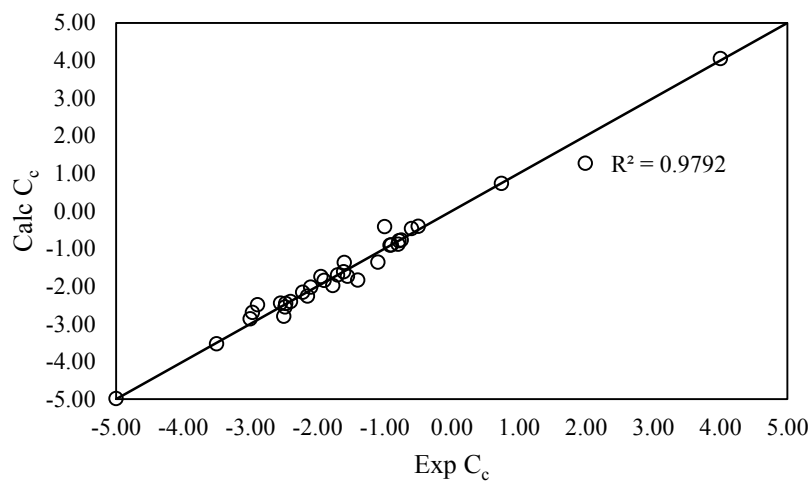
Figure 6.4 Parity plot between experimental characteristic curvature of anionic surfactants and calculated value from second-order Group-Contribution Model.
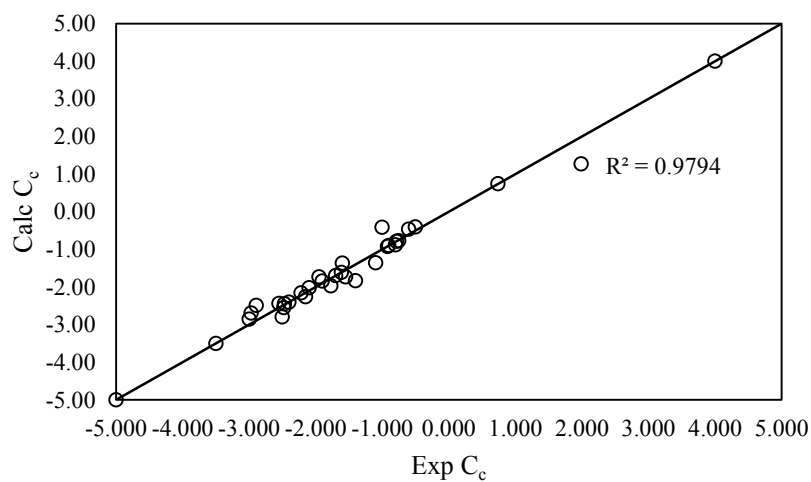
Figure 6.5 Parity plot between experimental characteristic curvature of anionic surfactants and calculated value from third-order Group-Contribution Model.

Most of database for development of anionic C_c model are extended surfactant, including polyethylene oxide (EO group) and polypropylene oxide (PO group). Many works claimed that both of them are the linker structure, hydrophilic linker (EO group) and lipophilic linker (PO group). The hydrophilic linker (EO group) and lipophilic linker (PO group) can be able to extend the molecular structure of surfactant into water phase and oil phase, respectively (Klaus *et al.*, 2010). Moreover, these structures tend to form the microemulsion system with the lower interfacial tension (Witthayapanyanon *et al.*, 2008). Such as the work from Phan *et al.* (2011), they found that the higher number of PO groups, the lower dynamic interfacial tension is observed. Hence, it is of interest to propose the new arranging group of extended surfactant for development of GC-model. That are polyethylene oxide (-CH$_2$CH$_2$O-) and polypropylene oxide (-CH$_2$CH(CH$_3$)O-). The results show that the second-order groups can improve the accuracy of model significantly. As shown in the parity plot (Figure 6.4) and the model accuracy in Table 6.6, the accuracy of the GC-model is increased when adding the second-order groups.

In contrast with the addition of third-order level, although the R-square of these plots is very high, the improvement between second-order and third-order GC-model was non-noticeable, indicating the insignificance of the third-order levels as observed in the low contributions of third-order levels from Table 6.3 for contributions of third-order levels. The highest deviation that will be observation was the lack of database for regression analysis. Some molecular structures that included in the database came from one compound and made the results from regression become insignificant, especially for higher-order groups. For example, the contribution of COO-(CH$_n$)$_m$-OOC (third-order group with contribution -0.0551) that was only available for lecithin surfactant, the contribution of cyclic group that was available only in sodium napthenate surfactant (see Figure 6.6). Therefore, the various structure and series of the same structure, such as sodium alkanoate groups, were needed for accuracy improvement of the GC-model.
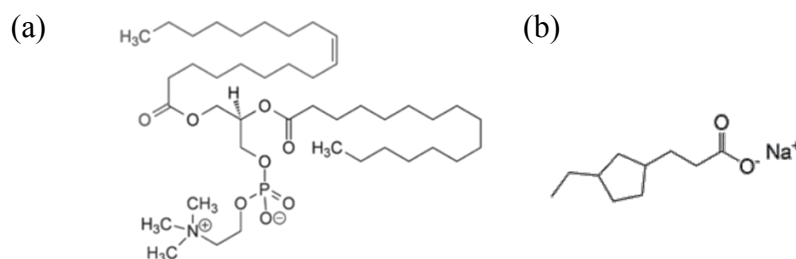
Figure 6.6 Example structures that make the uncertainty for use the GC-model (a) lecithin (b) Sodium naphthenate.

Finally, the results of GC-model in this work are summarized in Table 6.6, as compared to the previous work proposed by Hammond *et al.* (2011). No data were available in the work of Hammond *et al.* (2011) regarding the deviation and R-square. The results obtained from the GC model with higher-order levels are only slightly better that the GC-model with only first-order level. As seen in Table 6.6, the R-square value only very slightly improved from 0.9792 to 0.9794. There is additional evidence to support that the higher-order group from the database is insufficient for improving the GC-model.

Table 6.6 Comparison the deviation of Group-Contribution Model: only first order model; model including second and third-order groups and previous model of characteristic curvature of anionic surfactants

Model	Data points for regression	Average absolute deviation (%)	Maximum absolute deviation (%)	R-square
GC-model with only first-order group	33	15.46	89.76	0.9786
GC-model with second-order group	33	9.65	58.72	0.9792
GC-model with third-order group	33	9.53	58.72	0.9794
Previous model	No data	No data	No data	No data

6.3.2 Characteristic Curvature GC-Model of Nonionic Surfactants

To develop the GC-model for characteristic curvature of nonionic surfactant, the literature database of Cc value is not enough (with 25 data points); hence, some experiment was carried out to collect more database, as explained and shown in Chapter 5. However, the total database of 33 data points used in this work after including our experimental data is still not enough as compared to the other GC-model (Cordes *et al.*, 2002, Mattei *et al.*, 2013, Mattei *et al.*, 2014, Mondejar *et al.*, 2017), resulting in high error of the predicted property. This work attempt to initially provide the extended GC-model with several molecular descriptors for more practical use in property prediction of characteristic curvature.

The regression analysis was applied to obtain the coefficients of molecular descriptors. The results are shown in Table 6.7 with molecular fragment of first-, second- and third-order levels. Some third-order groups obtained from previous works (Marrero *et al.*, 2001, Mattei *et al.*, 2014): $(CH_2)_n$-C_6H_4-$(OCH_2CH_2)_m$, $(CH_2)_n$-$(OCH_2CH_2)_m$ ($m = 3$, $n < 8$ and $m > 3$, $n \geq 8$), and $(CH_2)_n$-$(OCH_2CH_2)_m$ ($n = 5$). The $(CH_2)_n$-C_6H_4-$(OCH_2CH_2)_m$ and $(CH_2)_n$-C_6H_4-$(OCH_2CH_2)_m$ ($n = 5$) groups were used as the same third-order groups while the $(CH_2)_n$-$(OCH_2CH_2)_m$ ($m = 3$, $n < 8$ and $m > 3$, $n \geq 8$) was arranged from the work of Mattei *et al.* (2014), which is $(CH_2)_n$-$(OCH_2CH_2)_m$ ($m = 3$, $n < 8$ and $m = 4,5$, $n > 8$). This work decided to adjust this group for widely used in database. Most of database are alcohol polyethylene oxide surfactants and their unique structures that can enhance the solubility in two miscible phase have been known (Witthayapanyanon *et al.*, 2008); hence, this work decided to apply the interaction of polyethylene oxide and alkyl chain to all linear alcohol polyethylene oxide. The branching structure was excluded due to some different effects of branching position (Acosta, 2008, Hammond *et al.*, 2011, Phan *et al.*, 2011). The $(CH_2)_n$-$(OCH_2CH_2)_m$ ($m = 3$, $n < 8$ and $m > 3$, $n \geq 8$) was introduced.

Moreover, the new group to represent the interaction of polyethylene oxide and long alkyl chain was introduced, i.e. $(CH_2)_n$-$(OCH_2CH_2)_m$ ($n \geq 12$) group. This group is needed to improve the high deviation of predicted value of long alkyl chain such as C14EO7 and C16EO14. It is anticipated that the long alkyl chain group will give the micelle formation differently from the shorter alkyl chain as previously

mentioned in the work of Eini *et al.* (1976); hence, it is of interest to propose the new third-order group.

Table 6.7 Group definition and their coefficients for first-order, and higher-order Group-Contribution Model of characteristic curvature of nonionic surfactants

Molecular Fragment	Coefficients
First-order, C_i	
CH_3	3.8748
CH_2	-0.1414
CH	-2.4252
$-C-$	4.0524
$CH=CH$	1.6764
CH_2O	-0.1672
$HOCH_2CH_2O$	-2.9765
$aC-CH_2$	1.2456
aCH	0.0282
$aC-O$	0.0071
OH	-3.0494
O_{cyc}	16.1778
CH_{cyc}	-1.5918
$CH_{2,cyc}$	0.0789
CH_2COO	0.2786
$-O-$	-0.3101
Constant	0.0402

The $(CH_2)_n$-$(OCH_2CH_2)_m$ $(n \geq 12)$ group was applied to C14EO7 and C16EO14 because they contained long-length alkyl chain as compared to other nonionic surfactants and their C_c values highly deviated from the linear relationship. When adding the new third-order group to these two nonionic surfactants, the relative error of them decreased from 2.93 to 0.00 and 0.79 to 0.08 for C14EO7 and C16EO14, respectively.

Table 6.7 Group definition and their coefficients for first-order, and higher-order Group-Contribution Model of characteristic curvature of nonionic surfactants (continued)

Molecular Fragment	Coefficients
Second-order, D_j	
AROMRINGs^{1}s^4	0.0071
CH_{cyc}-OH	0.3676
CH_{cyc}-CH_2	-0.0833
CH_{cyc}-CH	0.0789
CH_{cyc}-O	-0.2332
C_{cyc}-CH_2	-0.3101
$(CH_3)_2$CH	0.6385
Third-order, E_k	
$(CH_2)_n$-C_6H_4-$(OCH_2CH_2)_m$	0.0071
$(CH_2)_n$-$(OCH_2CH_2)_m$, m = 3, n < 8 and m > 3, n ≥ 8	0.9765
$(CH_2)_n$-$(OCH_2CH_2)_m$, n ≥ 12	2.0510
$(CH_2)_n$-$(OCH_2CH_2)_m$, n = 5	-0.4909

The parity plot of all database when applied both first- and higher-order groups is shown in Figure 6.7, given the R-square with 0.9118.
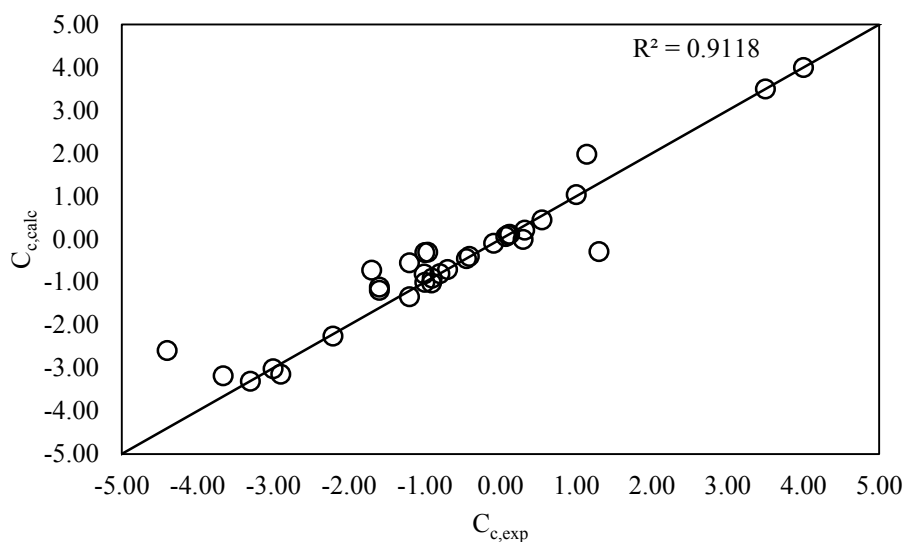
Figure 6.7 Parity plot between experimental C_c and predicted C_c including first-order and higher-order groups.

Tables 6.8 and 6.9 illustrate examples of C_c value calculation of sorbitan monolaurate ($C_{18}H_{34}O_6$) and dehydol LS 3 TH (C12-14EO3), respectively. The predicted values from both surfactants gave a very low deviation from experimental value. For sorbitan monolaurate ($C_{18}H_{34}O_6$), it is not categorized in a series of alcohol polyethylene oxide surfactants, the results showed the high accuracy of the prediction. This point also clarifies that the developed GC-model for C_c of nonionic surfactant is not only used to predict a series of alcohol polyethylene oxide surfactants, but also applied to other structures such as cyclic structure or alcohol containing aromatic ring. These results can extend the use of previous GC-model from Acosta (2008). Another example is dehydol LS 3 TH (C12-14EO3) that also gave the high prediction accuracy. This surfactant was used in the experimental part and the developed GC-model can calculate the C_c value closed to the experiment value. It is noted that there is not sufficient data for verifying the accuracy of model with dividing into training and test sets as other works (Cordes *et al.*, 2002, Mondejar *et al.*, 2017).

Table 6.8 Example calculation of characteristic curvature of C18H34O6 using the developed GC-model
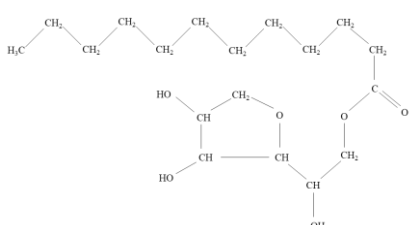
C18H34O6		
Molecular structure:		
First-order group:		
Groups	Occurrences	Coefficients
CH_3	1	3.8748
CH_2	10	-0.1414
CH	1	-2.4252
OH	3	-3.0494
O_{cyc}	1	16.1778
CH_{cyc}	3	-1.5918
$CH_{2,cyc}$	1	0.0789
CH_2COO	1	0.2786
Second-order group:		
Groups	Occurrences	Coefficients
CHcyc-OH	2	0.3676
CHcyc-CH	1	0.0789
Third-order group:		
Groups	Occurrences	Coefficients
No Third-order group		
C_c calculation		
GC model with higher-order group; $C_c = \Sigma_i N_i C_i + \Sigma_j M_j D_j + \Sigma_k O_k E_k + Constant = 3.50$		
%Absolute deviation from experimental value $C_{c,exp} = 3.50$		
%ARD = 0.00%		

Table 6.9 Example calculation of characteristic curvature of C12-14EO3 using the developed GC-model

C12-14EO3		
Molecular structure: First-order group:		
Groups	**Occurrences**	**Coefficients**
CH_3	1	3.8748
CH_2	14	-0.1414
CH_2O	2	-0.1672
$HOCH_2CH_2O$	1	-2.9765
Second-order group:		
Groups	**Occurrences**	**Coefficients**
No Second-order group		
Third-order group:		
Groups	**Occurrences**	**Coefficients**
$(CH_2)_n$-$(OCH_2CH_2)_m$, m = 3, n < 8 and m > 3, n ≥ 8	1	0.9765
C_c calculation		
GC model with higher-order group; $C_c = \Sigma_i N_i C_i + \Sigma_j M_j D_j + \Sigma_k O_k E_k + Constant = -0.40$		
%Absolute deviation from experimental value $C_{c,exp}$ = -0.41 %ARD = 0.03%		

The calculation of C_c values for dehydol and Marlox® surfactants. The results showed that the errors from the calculated value from model and the experimental value are in the ranges of 0%-32% for surfactants with EO group and 17%-74% for surfactants with both EO and PO groups or Marlox®. The error of Marlox® surfactants (C16-18PO2EO4 and C16-18PO4EO6) are very high due to the lack of database of nonionic surfactant containing polypropylene oxide group (-PO-).

A comparison is performed to compare the accuracy of the developed GC-model in this workwith the available C_c model in literature, i.e. $C_{cn} = 0.28 \times N_{CS} + 2.4 - N_{ES}$ (Acosta, 2008) as shown in Table 6.11. The GC-model proposed by Acosta (2008) is limited for the prediction of a series of alcohol polyethylene oxide surfactant. The polypropylene and branching structure is impractical to use (Acosta, 2008). The results of deviation (%ARD) in Table 6.11 show that the developed GC-model in this work is competitive. Although the form of equation for calculation is more complex than previous model, the lower deviation is of interest for C_c prediction. In addition, the developed GC-model in this work provided the various molecular descriptors for prediction of more variety surfactants.

Table 6.10 Calculated C_c of nonionic surfactant as compared to the experimental data in this work

Nonionic surfactant	$C_{c,exp}$	$C_{c,calc}$	%error
C16-18PO2EO4	0.55	0.46	16.92
C16-18PO4EO6	1.14	1.98	73.71
C12-14EO1	0.32	0.22	31.67
C12-14EO2	-0.09	-0.09	0.08
C12-14EO3	-0.41	-0.40	2.80
C12-14EO5	-0.91	-1.02	11.62
C12-14EO9	-2.21	-2.25	1.81
C12-14EO12	-3.66	-3.18	13.23

Table 6.11 Comparison the $C_{c,calc}$ of polyethylene oxide alcohol from this work GC-model and GC-model from Acosta (2008)

Nonionic surfactant		Acosta model (Acosta, 2008)		This work	
Name	$C_{c,exp}$	$C_{c,calc}$	%ARD	$C_{c,calc}$	%ARD
C6EO3	0.10	1.08	980.00	0.10	0.06
C6EO4	-1.60	0.08	105.00	-1.19	25.93
C8EO5	-1.00	-0.36	64.00	-0.31	69.11
C9EO4.5	-0.96	0.42	143.75	-0.30	69.17
C9EO5	-0.45	-0.08	82.22	-0.45	0.06
C10EO6	-0.90	-0.80	11.11	-0.90	0.03
C11.5EO5	-1.01	0.62	161.69	-0.80	20.03
C16EO14	-2.90	-7.12	145.52	-3.14	8.37
C9GEO6	-3.30	-1.08	67.27	-3.30	0.04
C12EO6.5	-1.20	-0.74	38.33	-1.34	11.44
C12-14EO1	0.32	5.04	1,475.00	0.23	28.66
C12-14EO2	-0.09	4.04	4,588.89	-0.09	0.18
C12-14EO3	-0.41	3.04	841.46	-0.41	0.49
C12-14EO5	-0.91	1.04	214.29	-1.04	14.75
C12-14EO9	-2.21	-2.96	33.94	-2.32	4.83
C12-14EO12	-3.66	-5.96	62.84	-3.27	10.62

The summary of the performance of the developed GC-model in this work is shown in Table 6.12. The R-square is equal to 0.9118 with percentage of average absolute deviation of 23.24%. It is noted that the error of the developed GC model is quite high as compared to the other GC-models due to limited experimental data available in literature.

Table 6.12 The summary of accuracy of the developed GC-model

Details	Value
Data point, points	33
R-square	0.9118
%AARD, %	23.24
The highest %ARD, %	121.77

It is noted that the high deviation of this model was affected from the lack of branching structure data and unknown branching position. Hammond *et al.* (2011) already showed the significant effect of branching position on characteristic curvature of surfactant; hence, it can make the deviation from this point.

6.4 Conclusions

The Group-Contribution model is an efficient tool for prediction of chemical properties. The characteristic curvature model for anionic and nonionic were developed in this work and gave the competitive accuracy as compared to the previous model (Acosta, 2008, Hammond *et al.*, 2011). The experimental value from simplified method of Zarate-Muñoz *et al.* (2016) work is practical and useful for developing model, which gave the more reliability of the GC-model; however, the database for development GC-model for characteristic curvature is not enough to give a model with high accuracy when compare with the database of other GC-models. So, this point is still challenging. In the future, if there are any experiment data of C_c values, the GC-model will be extended and widely used for various surfactant structures.

CHAPTER VII
THE SYSTEMATIC METHOD FOR SURFACTANT SELECTION

7.1 Introduction

The world is limited in resources while there is a continued increasing in worldwide demand of products. It is very challenging how to develop a method to design and select the optimum desired product (Gani, 2004). Surfactants are one of the usual chemicals for formulation-based emulsion system. There are wide properties that needed to be determined when some applications desire to select from the wide space (Tiddy *et al.*, 1999). Therefore, the product design and selection is needed for surfactant application.

Gani *et al.* (2007) proposed a systematic framework based on a product design concept. There are 4 main steps: problem definition, identification of any constraints for the target properties, the method or model that used to find the target properties and, lastly, the screening step to select the suitable candidate for the specified problem. The principles of procedure are as follows: identify the needs, generate ideas to reach needs, choose among ideas, and manufacture products. The first step of chemical product design is the definition of the problem or goal of the desired product. This step is important to make a decision in the following steps. Then, the set of target properties is required and the list of chemicals which satisfy these targets is established. The method to use is consequently determined and limited in some constraints. Next, the design step that uses the selected method is considered. The results from this step are analyzed and verified to assure the feasibility of results before final verification of candidate selection through case studies (Gani, 2004, Gani *et al.*, 2007, Cignitti *et al.*, 2015).

In this work, the case studies related to formulation-based emulsion system are collected to define the problem (step 1), set the target properties (step 2) and verify the screening results of the selected models (step 4). Three group contribution models have been developed in this work including Krafft point model for anionic surfactants, C_c model for anionic surfactants and C_c model for nonionic surfactants. Combining with other models developed by others in literature such as cloud point of nonionic

surfactant (Mattei et al, 2014) and critical micelle concentration (Mattei et al, 2013), a screening of suitable surfactant candidates appropriate for a certain application can be performed. The overview procedure for surfactant selection in this work is shown in Figure 7.1, which is adjusted from other works (Gani *et al.*, 2007, Mondejar *et al.*, 2017).
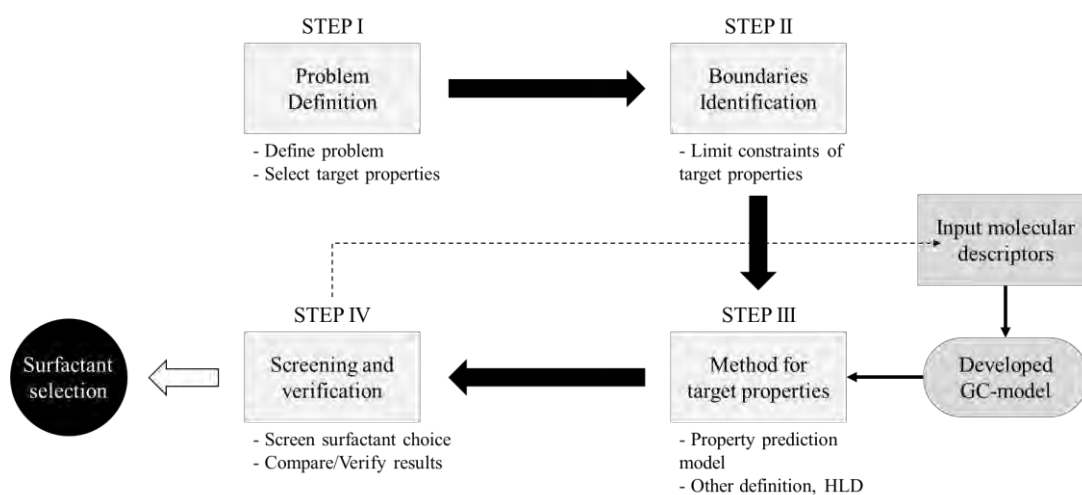
Figure 7.1 The procedure diagram for surfactant selection.

The related properties of surfactant are shown in Table 7.1 for pure surfactant properties. In case of mixed surfactant systems, this work considers their properties only same type of surfactant such as anionic-anionic mixture or nonionic-nonionic mixture by using linear mixing rule. The systems of anionic-nonionic mixture are not included in this work due to their non-ideal mixing (Acosta *et al.*, 2008a).

Table 7.1 The general surfactant properties that can be applied to work based on emulsion system

Surfactant property	Method for prediction
Hydrophilic-Lipophilic Deviation (HLD) - Characteristic curvature for anionic surfactant - Characteristic curvature for nonionic surfactant	Group-Contribution method (this work) Group-Contribution method (this work)
Hydrophilic-Lipophilic Balance (HLB)	Method from Griffin (1949)
Critical Micelle Concentration (CMC) - Anionic surfactant - Nonionic surfactant	 Reference data (Rosen *et al.*, 2012) Group-Contribution method (Mattei *et al.*, 2013)
Krafft point	Group-Contribution method (this work)
Cloud point	Group-Contribution method (Mattei *et al.*, 2014)
Boiling point	Group-Contribution method (Marrero *et al.*, 2001)
Solubility parameter	Group-Contribution method (Modarresi *et al.*, 2008)
Toxicity parameter	Group-Contribution method (Hukkerikar *et al.*, 2012)

7.2 Case Study I : Surfactant Selection for Enhanced Oil Recovery

It is well-known that petroleum is one of the major energy resources that is recovered from underground reservoirs. There are three steps of recovery processes: primary, secondary and tertiary (or enhanced) oil recovery (EOR). The tertiary step can lead to enhance more oil recovery as compared to other steps. It has long been challenging to develop the EOR method for increasing oil recovery (Hirasaki *et al.*, 2011, Ratnakar *et al.*, 2017). Surfactant EOR is of interest in the recovery process. The amphiphilic structure of surfactant can reduce the interfacial tension between oil and water, leading to an increase in oil-water solubility; hence entrapped oil can be mobilized and recovered.
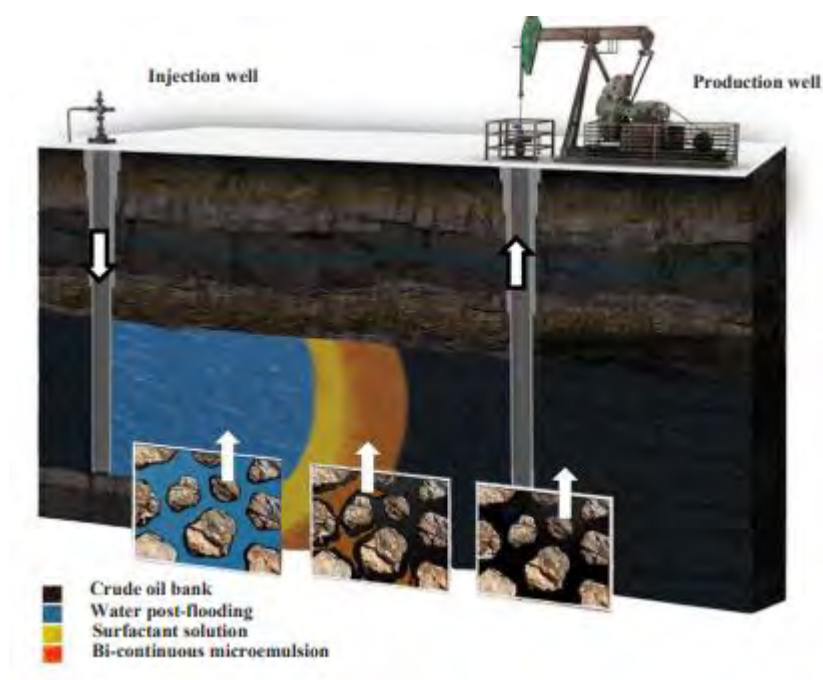
Figure 7.2 Schematic of surfactant flooding (Nourafkan *et al.*, 2018)

The case studies for EOR are collected to verify the systematic method in case of anionic surfactant, nonionic surfactant and mixed anionic-anionic surfactant.

7.2.1 EOR Experiment for Ankleswar Oil Field, India

Kumar *et al.* (2016) investigated the effect of salt on interfacial tension with different type of surfactant: SDS, CTAB and Tween 80. All of their experiment was conducted at 27 °C with Ankleswar crude oil, EACN = 9.3 (Pithapurwala *et al.*, 1986) and NaCl was used as brine in the system. This study focused on SDS and Tween 80 systems to verify the use of the developed GC-model. The procedure for consideration is based on the systematic framework (Gani *et al.*, 2007).

Table 7.2 The procedure for surfactant selection for Ankleswar oil field case with SDS as candidate

Steps	Descriptions
Step I : Problem definition	Objective : desire the lowest IFT for use in EOR Target properties : Emulsion stability, Thermal stability
Step II : Boundaries identification	Constraints of target properties : Emulsion stability – HLD close to zero Thermal stability – Krafft point < 27.00 °C
Step III : Method for target properties	Emulsion stability – HLD Predicted C_c of SDS = -2.79 Optimal salinity from case studies = 4%wt Calculated HLD = -2.31 Thermal stability Predicted Krafft point of SDS = 19.19 °C
Step IV : Screening and verification	Select the suitable HLD value that is close to zero

Table 7.3 The procedure for surfactant selection for Ankleswar oil field case with Tween 80 as candidate

Steps	Descriptions
Step I : Problem definition	Objective : desire the lowest IFT for use in EOR Target properties : Emulsion stability, Thermal stability
Step II : Boundaries identification	Constraints of target properties : Emulsion stability – HLD close to zero Thermal stability – Cloud point > 27.00 °C Micelle formation – CMC < 0.0136 mM/l
Step III : Method for target properties	Emulsion stability – HLD Predicted C_c of Tween 80 = -3.00 Optimal salinity from case studies = 6%wt Calculated HLD = -3.49 Thermal stability Predicted Cloud point of Tween 80 = 108.81 °C Micelle formation Predicted CMC of Tween 80 = 0.0021 mM/l
Step IV : Screening and verification	Select the suitable HLD value that is close to zero

From the table, the target properties are emulsion stability or HLD value and thermal stability, which are Krafft point and cloud point of anionic and nonionic surfactant, respectively. The HLD value was calculated from the following equations (Castellino *et al.*, 2011):

For ionic surfactants,

$$HLD = \ln(S) - K*EACN - f(A) - \alpha\Delta T + C_{ci} \qquad \text{Eq. 7.1}$$

For nonionic surfactants,

$$HLD = b(S) - K*EACN - \varphi(A) + c\Delta T + C_{cn} \qquad \text{Eq. 7.2}$$

In case of SDS system, C_c value was from the GC-model in this work by using EACN and S* from case study. Other HLD parameters from Acosta *et al.* (2008b) and Salager *et al.* (1979) while the HLD parameters of Tween 80 system was from Salager *et al.* (2001). The HLD value of Tween 80 was lower than SDS; hence the SDS can reach the lower IFT of SOW system than Tween 80 as corresponding as the results from the case study, IFT of SDS system was 13×10^{-3} mN/m while IFT of Tween 80 system was 99×10^{-3} mN/m.

The thermal property is also considered with the temperature that surfactant can achieve the homogeneous phase. Krafft point was calculated by the GC-model in this work while cloud point was calculated from the GC-model proposed by (Mattei *et al.*, 2014). In addition, critical micelle concentration of Tween 80 was calculated from Mattei *et al.* (2013) (at 25 °C) with the lower value that case study used. The results showed that both of SDS and Tween 80 can be used in this system as they are solubilized in the experimental condition.

However, both of them do not match for this crude oil as the lowest interfacial condition could not be attained, i.e. the calculated HLD value of both systems were -2.35 and -3.76 for SDS and Tween 80, respectively. This work recommends the other candidates of anionic surfactants for use from database. NabranchedC12PO10sulfate, NabranchedC14PO8sulfate and sodium stearate are suitable for this case with the predicted HLD values: 0.07, 0.01 and -0.29, respectively. That are close to zero more than HLD value of SDS system. Moreover, the other candidates of nonionic surfactants are C12-14EO1 and Marlox® RT42 with HLD values of -0.27 and 0.02, respectively.

The results from surfactant selection method is corresponding to the experiment from case study and this method can screen other surfactants which could give suitable candidates in for a given condition. This illustration indicates that the developed GC-model and the previous GC-model as the efficient tool for use in surfactant selection.

7.2.2 EOR Experiment for War Party Site, Oklahoma

Budhathoki *et al.* (2016) investigated the optimal middle phase microemulsion (Winsor type III) in the reservoir condition: high brine system with 28.7 gNaCl/100mL (this value is without hardness compounds), crude with EACN of 9.8 and a temperature of 52 °C. The mixture of extended surfactants was applied in the SOW system with primary surfactants: C_8-$(PO)_4$-$(EO)_1$-SO_4Na, C_8-$(PO)_4$-SO_4Na, C_{10}-$(PO)_4$-$(EO)_1$-SO_4Na and C_{10}-$(PO)_4$-SO_4Na; and Steol Cc460 (C_{12}-$(EO)_3$-SO_4Na) as the co-surfactant for all mixed systems. They found that the molar ratio as shown in Table 7.4 gave the lowest IFT in each system.

Table 7.4 The IFT measurement in each portion of mixed system with Steol Cs460 at optimal condition

Mixed System with Steol Cs460	Optimal IFT, mN/m	Mole fraction of primary surfactant	Mole fraction of Steol Cs460
C_8-$(PO)_4$-$(EO)_1$-SO_4Na	0.0087	0.31	0.69
C_8-$(PO)_4$-SO_4Na	0.0061	0.32	0.68
C_{10}-$(PO)_4$-$(EO)_1$-SO_4Na	0.0041	0.19	0.81
C_{10}-$(PO)_4$-SO_4Na	0.0049	0.17	0.83

To calculate the HLD value, a linear mixing rule was applied to the characteristic curvature of mixture ($C_{c,mix}$) as follows:

$$C_{c,mix} = \Sigma\, x_i C_{c,i} \qquad\qquad \text{Eq. 7.3}$$

Where x_i is the mole fraction of surfactant i and $C_{c,i}$ is the characteristic curvature of surfactant i.

The GC-model developed in this work was used to predict the C_c of pure anionic surfactant. The HLD_{mix} was considered from Eq. 7.1 at reservoir condition and HLD parameters from other works (Hammond *et al.*, 2011, Budhathoki *et al.*, 2016). The results are shown in Table 7.5.

The HLD value were closed to zero in the system that were corresponding to the ultra-low IFT value at optimal molar ratio from work of Budhathoki *et al.* (2016).

It is noted that Krafft point of mixed system cannot be calculated with a linear mixing rule. There is no literature proposed at this point. However, this work used the GC-model to calculate Krafft point of pure compound and the Steol Cs460 gave the highest Krafft point in this system with approximately -9.21 °C; hence, Krafft point of the surfactant mixture should not exceed this value. Another evidence for Krafft point of extended surfactant is from Falbe (1987). He proposed Krafft point of C_{12}-$(EO)_2$-SO_4Na with -1.00 °C. This value make the reasonable Krafft point of Steol Cs460 with a similar structure (C_{12}-$(EO)_3$-SO_4Na).

This work recommends the other candidates of anionic surfactants for this system with single surfactant system. The candidates are sodium dodecanoate and sodium naphthenate with HLD values 0.06 and 0.10, respectively. Two of these candidates can perform the ultralow interfacial tension and are applied to this system.

Table 7.5 The predicted HLD from the C_c model and T_k model in this work

Mixed System with Steol Cs460	Target properties	Constraints	Predicted values
C$_8$-(PO)$_4$-EO-SO$_4$Na	Emulsion Stability from HLD equation (C_c model from this work)	$HLD_{mix} \sim 0$	$C_{c,mix} = -2.48$ $HLD_{mix} = 0.23$
	Thermal stability (Krafft point model from this work)	$T_{k,mix} < 52\ °C$	$T_{k,pure} = -109.81°C$
C$_8$-(PO)$_4$-SO$_4$Na	Emulsion Stability from HLD equation (C_c model from this work)	$HLD_{mix} \sim 0$	$C_{c,mix} = -2.51$ $HLD_{mix} = 0.20$
	Thermal stability (Krafft point model from this work)	$T_{k,mix} < 52\ °C$	$T_{k,pure} = -100.35°C$
C$_{10}$-(PO)$_4$-EO-SO$_4$Na	Emulsion Stability from HLD equation (C_c model from this work)	$HLD_{mix} \sim 0$	$C_{c,mix} = -2.43$ $HLD_{mix} = 0.07$
	Thermal stability (Krafft point model from this work)	$T_{k,mix} < 52\ °C$	$T_{k,pure} = -97.58\ °C$
C$_{10}$-(PO)$_4$-SO$_4$Na	Emulsion Stability from HLD equation (C_c model from this work)	$HLD_{mix} \sim 0$	$C_{c,mix} = -2.45$ $HLD_{mix} = 0.05$
	Thermal stability (Krafft point model from this work)	$T_{k,mix} < 52\ °C$	$T_{k,pure} = -88.12\ °C$

7.3 Case Study II : Surfactant Selection for Environmental Remediation

Chemical contamination is the concerned problem such as a contaminated soil or industrial wastewater disposal that can break the balance of ecosystem. The common contaminants are mostly organic compounds or hydrocarbon. Surfactants are introduced to form the microemulsion system to dissolve these organic compounds by forming micelles of hydrocarbon entrapped in soil or wastewater to reduce the environmental contaminants (Mao *et al.*, 2015, Duan *et al.*, 2016). The brief schematic is shown in Figure 7.3.
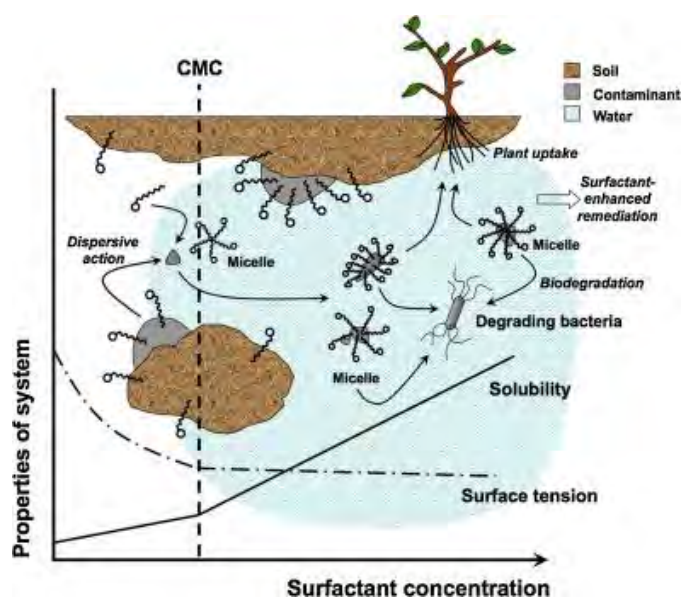
Figure 7.3 Diagram of soil remediation using surfactants (Mao *et al.*, 2015).

7.3.1 Experiment for Soil Washing

Ahn *et al.* (2008) studied the effect of various nonionic surfactants to soil remediation. The contaminant in their work was phenanthrene, which was used to represent polycyclic aromatic hydrocarbon contaminants. Four different nonionic surfactants including tween 40, tween 80, brij 30 and brij 35 were employed in the experiment due to their low CMC and low tendency of flocculate clay particles as compared to ionic surfactants. They conducted the solubilization test, surfactant adsorption and soil washing efficiency with 0.002 mol/l of each surfactant system (no

containing salt) at 23 °C. They found that the brij 30 gave the highest solubilization of phenanthrene and considered as the best candidate for soil washing in their work due to the highest washing efficiency.

This work carried out the surfactant selection for soil remediation case (Ahn *et al.*, 2008) with four steps as shown in Figure 7.1. First, the set of target properties was considered. There were four main properties: emulsion stability, micelle formation, temperature stability and toxicity. All of constraints for these target properties are shown in Table 7.6. The HLD value should be close to zero to obtain the lowest interfacial tension that make the highest solubilization of water and contaminated oil in the system. CMC was considered to ensure the presence of microemulsion formation in the system, whereas the cloud point was used to check the stability of the surfactants at the working condition. In addition, as it is required for environmental application, the Lethal concentration (LC_{50}) was determined for the toxicity disposal with a constraint value obtained from Mattei *et al.* (2012).

For the predicted value, all of target properties were predicted from the specified model in Table 7.1. The characteristic curvature value were calculated from the GC-model in this work. The C_c value for tween 40, tween 80, brij 30 and brij 35 were -2.56, -3.00, -0.57 and -6.50, respectively. Other HLD parameters were from literatures (Salager *et al.*, 2001) except the EACN value. There is no evidence to assure the EACN of phenanthrene. This work found other references for assumption and determination (Bouton *et al.*, 2009, Bouton *et al.*, 2010, Abbott, 2015). The approximate EACN value of 1 for phenanthrene was used in this work based on the ranges EACN value of benzene, naphthalene and asphaltene (EACN ranges of 0-1). The HLD parameter can be achieved from Eq. 7.2.

The results showed that all of candidate nonionic surfactants are suitable for use in the soil remediation within the given constraints of CMC, cloud point and toxicity. Brij 30 gave the HLD value that is closed to zero; hence, this result is also corresponding to the conclusion from Ahn *et al.* (2008).

Other candidates of nonionic surfactants that recommended from database in this work are C12-14EO1, C9PhEO5, C6EO3 and Marlox® RT42 with HLD values: -0.05, -0.15, -0.17 and 0.24, respectively, that are closed to zero value more than the surfactant choices in this case.

Table 7.6 The predicted target properties for work from Ahn *et al.* (2008)

Candidates	Target properties	Constraints	Predicted values
Tween 40 ($C_{58}H_{114}O_{26}$)	Emulsion stability	HLD ~ 0	HLD = -2.83
	Micelle formation	CMC < 2.00E-03 mol/l	CMC = 4.22E-05 mol/l
	Thermal stability	T_c > 23 °C	T_c = 163.03 °C
	Non-toxicity	$-\log(LC_{50})$ > 3.16 mol/m^3	$-\log(LC_{50})$ = 5.74 mol/m^3
Tween 80 ($C_{64}H_{124}O_{26}$)	Emulsion stability	HLD ~ 0	HLD = -3.27
	Micelle formation	CMC < 2.00E-03 mol/l	CMC = 2.10E-06 mol/l
	Thermal stability	T_c > 23 °C	T_c = 155.35 °C
	Non-toxicity	$-\log(LC_{50})$ > 3.16 mol/m^3	$-\log(LC_{50})$ = 5.53 mol/m^3
Brij 30 (C12E4)	Emulsion stability	HLD ~ 0	HLD = -0.84
	Micelle formation	CMC < 2.00E-03 mol/l	CMC = 1.02E-04 mol/l
	Thermal stability	T_c > 23 °C	T_c = 32.91 °C
	Non-toxicity	$-\log(LC_{50})$ > 3.16 mol/m^3	$-\log(LC_{50})$ = 3.67 mol/m^3
Brij 35 (C12E23)	Emulsion stability	HLD ~ 0	HLD = -6.79
	Micelle formation	CMC < 2.00E-03 mol/l	CMC = 8.99E-04 mol/l
	Thermal stability	T_c > 23 °C	T_c = 184.77 °C
	Non-toxicity	$-\log(LC_{50})$ > 3.16 mol/m^3	$-\log(LC_{50})$ = 9.52 mol/m^3

7.4 Case Study III : Surfactant Selection as A Surface Cleaning Agents

From the SOW system, microemulsion has capability of extraction efficiency by reducing oil–water IFT (Bera *et al.*, 2014); hence, this system is also introduced to many applications that related with the two miscible phase such as water-oil system. In the cleaning process, surfactant plays an important role to form the microemulsion systems and achieve the low interfacial tension, especially Winsor type III microemulsion. If the microemulsion system is introduced and gave very low IFT at the cleaning condition, the higher cleaning efficiency is observed (Quintero *et al.*, 2013). Microemulsion Winsor Type I system (o/w system) is introduced to hard surface cleaning while Microemulsion Winsor Type II system (w/o system) and Winsor type III system (bicontinuous phase system) are introduced to application of water-soluble contaminants, metal cleaning and improving corrosion resistance due to a faster dissolution of oil as compared to Winsor type I (Acosta *et al.*, 2007).
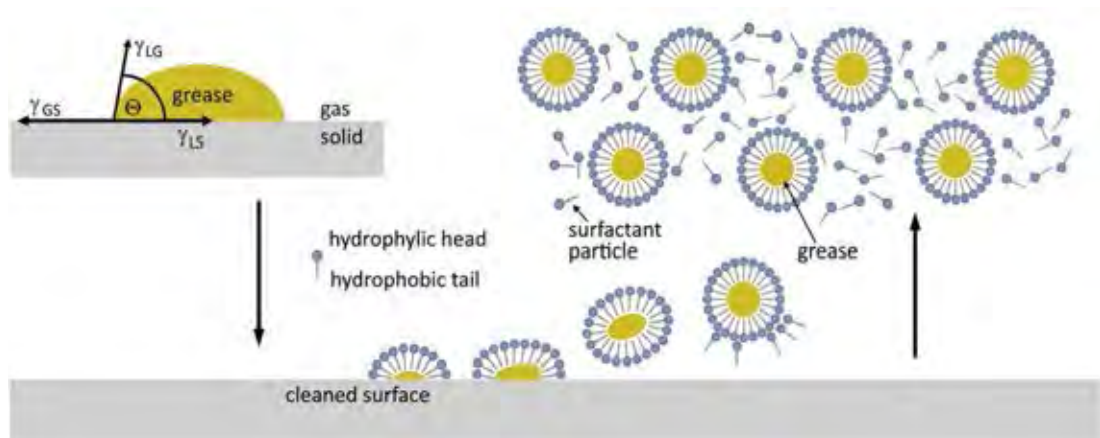
Figure 7.4 Overview mechanism of surfactant in solid surface cleaning (Rakowska *et al.*, 2017).
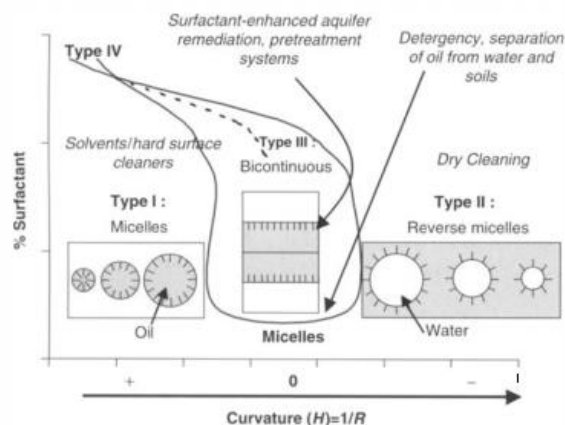
Figure 7.5 Microemulsion diagram for cleaning application (Acosta *et al.*, 2007).

7.4.1 Synthesis of Nonionic Surfactant for Detergent Application

Lee *et al.* (2016) synthesized the environmental friendly nonionic surfactants: SA08-07, SA08-15 and SA08-40 based on sugar for use in detergency applications. The characterization properties for these synthesized surfactant were interfacial tension, CMC, and detergency efficiency. The SOW system was conducted with n-decane oil (EACN = 10 from Bouton *et al.* (2010)) and no salt additive at 25 °C. Surfactant structures is shown in the Figure 7.6.
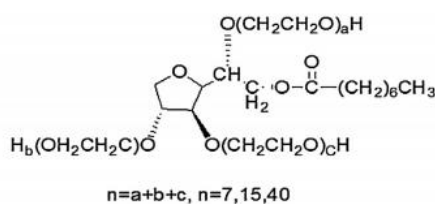
Figure 7.6 Surfactant structures of SA08-n series (Lee *et al.*, 2016).

From the experimental results, Lee *et al.* (2016) concluded that SA08-07 gave the lowest interfacial tension with 0.0112 mN/m and achieved the highest detergency efficiency. All of synthesized nonionic surfactants gave the good performance of detergency as compared to LAS anionic surfactant that is generally included in detergency applications.

The target properties in this case were calculated and shown in Table 7.7. For the very long chain of polyethylene oxide sugar base, some properties could not be calculated by using the available models in literature due to the lack of cyclic groups such as CH_{cyc} or CH_{cyc}-O. For example, the CMC model from Mattei *et al.* (2013) gave the very low calculated value due to uncertainty of very large molecular structure and prediction from model did not correspond with the experiment results. However, this study used the HLD value of SA08-07 that is not too long chain structure, for comparison the LAS surfactant as mentioned in the case study. The result still presented that SA08-07 should be the better candidate for detergency application than normal conventional anionic surfactant in term of efficiency. The HLD value of SA08-07 is close to zero more than HLD value of LAS. The results of predicted value of this case study gave the uncertainty of use model in property prediction in case of very large and complex molecular structure. The uncertainty occur in most of the GC-model (Hukkerikar *et al.*, 2012, Mattei *et al.*, 2013, Mattei *et al.*, 2014).

Another interesting point is the environmental synthesized nonionic surfactant. The LC_{50} were calculated and considered with the criteria from Mattei *et al.* (2014). The results showed that the synthesized surfactant in the work of Lee *et al.* (2016) were non-toxicity surfactant.

This work recommended the anionic surfactant and nonionic surfactant as the candidates. The candidates of anionic surfactants are NaC12PO14EO2sulfate and NaC10PO18EO2sulfate with HLD values -0.26 and 0.27, respectively and the candidates of nonionic surfactants are C9PhEO2 and Marlox® RT42 with HLD values -0.44 and -0.99 that are offered the value closed to zero value.

Table 7.7 The predicted target properties for work from (Lee *et al.*, 2016)

Candidates	Target properties	Constraints	Predicted values
SA08-07 ($C_{56}H_{110}O_{27}$)	Emulsion stability	HLD ~ 0	HLD = -1.55
	Micelle formation	CMC < 8.24E-03 mol/l	CMC = 3.3E-04 mol/l
	Thermal stability	T_c > 25 °C	T_c cannot be predicted
	Non-toxicity	$-\log(LC_{50})$ > 3.16 mol/m^3	$-\log(LC_{50})$ = 3.27 mol/m^3
SA08-15 ($C_{104}H_{206}O_{51}$)	Emulsion stability	HLD ~ 0	HLD cannot be predicted
	Micelle formation	CMC < 4.41E-03 mol/l	CMC = 3.1E-04 mol/l
	Thermal stability	T_c > 25 °C	T_c cannot be predicted
	Non-toxicity	$-\log(LC_{50})$ > 3.16 mol/m^3	$-\log(LC_{50})$ = 4.72 mol/m^3
SA08-40 ($C_{254}H_{506}O_{126}$)	Emulsion stability	HLD ~ 0	HLD cannot be predicted
	Micelle formation	CMC < 1.79E-03 mol/l	CMC = 2.6E-04 mol/l
	Thermal stability	T_c > 25 °C	T_c cannot be predicted
	Non-toxicity	$-\log(LC_{50})$ > 3.16 mol/m^3	$-\log(LC_{50})$ = 13.05 mol/m^3
LAS	Emulsion stability	HLD ~ 0	HLD = -2.50
	Micelle formation	CMC < 0.03 mol/l	CMC = 0.0012 mol/l
	Thermal stability	T_k < 25 °C	T_k = -8.32 °C
	Non-toxicity	$-\log(LC_{50})$ > 3.16 mol/m^3	$-\log(LC_{50})$ = 3.93 mol/m^3

CHAPTER VIII
CONCLUSIONS AND RECOMMENDATIONS

8.1 Conclusions

The systematic methodology was introduced by using chemical product design concept from Gani *et al.* (2007) to screen and select the suitable surfactants for a specific application. In this work, the Group-Contribution models based on the Marrero *et al.* (2001) concept were developed to predict the Krafft point of anionic surfactants, characteristic curvature of anionic surfactants and characteristic curvature of nonionic surfactants. The first-order, higher-order (second and third) and new third-order groups were applied to these models to achieve higher accuracy. Some experimental measurement of characteristic curvature of nonionic surfactant were conducted to obtain more database for model development. The results presented that the developed GC-model gave the high accuracy with R-square > 0.95 except the C_c model for nonionic surfactant with R-square around 0.91 due to lack of experimental values. Moreover, the case studies of surfactant applications: enhanced oil recovery, environmental remediation and detergency application were used to verify the reliability of the developed GC-models. The results from this study were in agreement with the selected surfactants in the case studies. In addition, other surfactant candidates were introduced from the database in this work.

8.2 Recommendations

In this work, some limitations of developed GC-model include the availability of the types of surfactant structure that are covered by the model. To extend the model for use with various surfactants with various fractional groups, more experimental data must be collected; however, these data are limited in this field. For example, the effect of counterions of anionic surfactant properties is of interest for including in the GC-model. Several surfactants have been developed using various counterion ions and these counterion ions in turn affect the surfactant properties (Benrraou *et al.*, 2003, Naskar *et al.*, 2013). To cover these surfactants with various counterions such as Li^+ and K^+ as those proposed by Rosen *et al.* (2012) and the fluorocarbon surfactants proposed by Li *et al.* (2005), more experimental data are needed to be collected to develop the new group structures. However, the understanding of commercial surfactant structure is not clear. The molecular structure of commercial surfactants is the mixture of different carbon numbers of surfactant tail or different isomer. The position of functional group also affects to surfactant properties as discussed in the work of Hammond *et al.* (2011). These variations of surfactant structure gave the deviation to the developed model.

Another recommendation is the model development for mixed surfactant systems of anionic-nonionic surfactants. An ideal mixing cannot be assumed in these systems. The challenge is the way to design a systematic methodology for applying the property prediction in these systems. An additional term like Gibb's free energy introduced in the work of Acosta *et al.* (2008a) is required to add the effect of non-ideality mixing of anionic-nonionic surfactant systems. The effect of non-ideality mixing is still under study in the field of surfactants.

REFERENCES

Abbott, P.S. (2015) Surfactant Science: Principles and Practice. Ipswich, UK: Creative Commons BY-ND, Attribution and no-Derivatives license.

Acosta, E., Mai, P.D., Harwell, J.H. and Sabatini, D.A. (2003) Linker-Modified Mocroemulsions for a variety of oils and surfactants. Journal of Surfactants and Detergents, 6(4), 353-363.

Acosta, E.J. (2008) The HLD–NAC equation of state for microemulsions formulated with nonionic alcohol ethoxylate and alkylphenol ethoxylate surfactants. Colloids and Surfaces A: Physicochemical and Engineering Aspects, 320(1-3), 193-204.

Acosta, E.J. and Bhakta, A.S. (2008a) The HLD-NAC Model for Mixtures of Ionic and Nonionic Surfactants. Journal of Surfactants and Detergents, 12, 7-19.

Acosta, E.J., Harwell, J.H., Scamehorn, J.E. and Sabatini, D.A. (2007) Application of Microemulsions in Cleaning Technologies and Environmental Remediation. Handbook for Cleaning/Decontamination of Surfaces, Somasundaran, I.J.a.P., Elsevier: 831-884.

Acosta, E.J., Kiran, S.K. and Hammond, C.E. (2012) The HLD-NAC Model for Extended Surfactant Microemulsions. Journal of Surfactants and Detergents, 15(4), 495-504.

Acosta, E.J., Yuan, J.S. and Bhakta, A.S. (2008b) The Characteristic Curvature of Ionic Surfactants. Journal of Surfactants and Detergents, 11(2), 145-158.

Ahmadi, M.A., Galedarzadeh, M. and Shadizadeh, S.R. (2014) Wettability Alteration in Carbonate Rocks by Implementing New Derived Natural Surfactant: Enhanced Oil Recovery Applications. Transport in Porous Media, 106(3), 645-667.

Ahmadi, M.A. and Shadizadeh, S.R. (2015) Experimental investigation of a natural surfactant adsorption on shale-sandstone reservoir rocks: Static and dynamic conditions. Fuel, 159, 15-26.

Ahn, C.K., Kim, Y.M., Woo, S.H. and Park, J.M. (2008) Soil washing using various nonionic surfactants and their recovery by selective adsorption with activated carbon. J Hazard Mater, 154(1-3), 153-160.

Alexander, S., Smith, G.N., James, C., Rogers, S.E., Guittard, F., Sagisaka, M. and Eastoe, J. (2014) Low-surface energy surfactants with branched hydrocarbon architectures. Langmuir, 30(12), 3413-3421.

Andersson, M.P., Bennetzen, M.V., Klamt, A. and Stipp, S.L. (2014) First-Principles Prediction of Liquid/Liquid Interfacial Tension. J Chem Theory Comput, 10(8), 3401-3408.

Arachchilage, G.W.P.P., Spilker, K.K., Tao, E.B., Alexis, D., Linnemeyer, H., Kim, D.H., Malik, T. and Dwarakanath, V. (2018) Evaluating the Effect of Temperature on Surfactant Phase Behavior and Aqueous Stability to Forecast Optimum Salinity at High Temperature. Society of Petroleum Engineers, 1-15.

Baran, J.R., Jr. (2001) Winsor I<-->;III<-->II Microemulsion Phase Behavior of Hydrofluoroethers and Fluorocarbon/Hydrocarbon Catanionic Surfactants. J Colloid Interface Sci, 234(1), 117-121.

BaranJr., J.R., Pope, G.A., Wade, W.H., Weerasooriya, V. and Yapa, A. (1994) Microemulsion Formation with Mixed Chlorinated Hydrocarbon Liquids. Journal of Colloid and Interface Science, 168(1), 67-72.

Barry, B.W. and Eini, D.I.D. (1976) Surface properties and micelle formation of long-chain polyoxyethylene nonionic surfactants. J. Coll. Interf. Sci, 54(3), 339-347.

Benrraou, M., Bales, B.L. and Zana, R. (2003) Effect of the Nature of the Counterion on the Properties of Anionic Surfactants. 1. Cmc, Ionization Degree at the Cmc and Aggregation Number of Micelles of Sodium, Cesium, Tetramethylammonium, Tetraethylammonium, Tetrapropylammonium, and Tetrabutylammonium Dodecyl Sulfates. J. Phys. Chem. B, 107, 13432-40.

Bera, A. and Mandal, A. (2014) Microemulsions: a novel approach to enhanced oil recovery: a review. Journal of Petroleum Exploration and Production Technology, 5(3), 255-268.

Bouton, F., Durand, M., Nardello-Rataj, V., Borosy, A.P., Quellet, C. and Aubry, J.M. (2010) A QSPR model for the prediction of the "fish-tail" temperature of C(i)E4/water/polar hydrocarbon oil systems. Langmuir, 26(11), 7962-70.

Bouton, F., Durand, M., Nardello-Rataj, V., Serry, M. and Aubry, J.-M. (2009) Classification of terpene oils using the fish diagrams and the Equivalent Alkane Carbon (EACN) scale. Colloids and Surfaces A: Physicochemical and Engineering Aspects, 338(1-3), 142-147.

Budhathoki, M., Hsu, T.-P., Lohateeraparp, P., Roberts, B.L., Shiau, B.-J. and Harwell, J.H. (2016) Design of an optimal middle phase microemulsion for ultra high saline brine using HLD method. Colloids and Surfaces A: Physicochemical and Engineering Aspects, 488, 36-45.

Castellino, V., Cheng, Y.-L. and Acosta, E. (2011) The hydrophobicity of silicone-based oils and surfactants and their use in reactive microemulsions. Journal of Colloid and Interface Science, 353(1), 196-205.

Chaudhari, S.P. and Dugar, R.P. (2017) Application of surfactants in solid dispersion technology for improving solubility of poorly water soluble drugs. Journal of Drug Delivery Science and Technology, 41, 68-77.

Chen, L., Shang, Y., Liu, H. and Hu, Y. (2007) Middle-phase microemulsion induced by brine in region of low cationic gemini surfactant content. Colloids and Surfaces A: Physicochemical and Engineering Aspects, 305(1-3), 29-35.

Chen, L., Xiao, J.-X. and Ma, J. (2004) Striking differences between alkyl sulfate and alkyl sulfonate when mixed with cationic surfactants. Colloid & Polymer Science, 282(5), 524-529.

Chu, Z. and Feng, Y. (2012) Empirical correlations between Krafft temperature and tail length for amidosulfobetaine surfactants in the presence of inorganic salt. Langmuir, 28(2), 1175-1181.

Cignitti, S., Zhang, L. and Gani, R. (2015) Computer-aided Framework for Design of Pure, Mixed and Blended Products. Computer - Aided Chemical Engineering, 37, 2093-2098.

Cordes, W. and Rarey, J. (2002) A new method for the estimation of the normal boiling point of non-electrolyte organic compounds. Fluid Phase Equilibria, 201(2), 409-433.

Del Re, G., D'Errico, G., Ortona, O. and Vitagliano, V. (2010) Evaluation of alkyl sulfate and sulfonate micellar structure at the water-surfactant interphase with simple geometrical calculations. J. Coll. Interf. Sci, 349(1), 230-235.

Duan, M., Wang, C., Song, X., Fang, S., Ma, Y. and Tao, T. (2016) A block polyether designed quantitatively by HLD concept for recovering oil from wastewater. Chemical Engineering Journal, 302, 44-49.

Eini, D.I.D.E., Barry, B.W. and Rhodes, C.T. (1976) Micellar size, shape, and hydration of long-chain polyoxyethylene nonionic surfactants. Journal of Colloid and Interface Science, 54(3), 348-351.

Elmofty, O. (2012) Surfactant enhanced oil recovery by wettability alteration in sandstone reservoirs. Geosciences and Geological and Petroleum Engineering, Missouri University of Science and Technology. **Master:** 64.

Evangelista, N.S., do Carmo, F.R. and de Sant'Ana, H.B. (2017) Estimation of Vapor Pressures and Enthalpies of Vaporization of Biodiesel-Related Fatty Acid Alkyl Esters. Part 1. Evaluation of Group Contribution and Corresponding States Methods. Industrial & Engineering Chemistry Research, 56(8), 2298-2309.

Falbe, P.D.J. (1987) Surfactants in Consumer Products: Theory, Technology and Application,: Springer-Verlag Heidelberg.

Gani, R. (2004) Chemical product design: challenges and opportunities. Computers & Chemical Engineering, 28(12), 2441-2457.

Gani, R., Dam-Johansen, K. and Ng, K.M. (2007) Chapter 1 Chemical product design — A brief overview. Computer Aided Chemical Engineering, Elsevier. 23.

Götte, D.E. (1969) Konstitution und Eigenschaften von Tensiden. Fette, Seifen, Anstrichmittel, 71(3), 219-223.

Griffin, W.C. (1949) Classification of Surface-Active Agents by "HLB". Journal of Cosmetic Science, 1, 311-326.

Gu, T. and Sjöblom, J. (1992) Surfactant structure and its relation to the Krafft point, cloud point and micellization: Some empirical relationships. Colloids and Surfaces, 64(1), 39-46.

Guo, X., Rong, Z. and Ying, X. (2006) Calculation of hydrophile-lipophile balance for polyethoxylated surfactants by group contribution method. Journal of Colloid and Interface Science, 298(1), 441-450.

Hammond, C.E. and Acosta, E.J. (2011) On the Characteristic Curvature of Alkyl-Polypropylene Oxide Sulfate Extended Surfactants. Journal of Surfactants and Detergents, 15(2), 157-165.

Hanke, C.G., Johansson, A., Harper, J.B. and Lynden-Bell, R.M. (2003) Why are aromatic compounds more soluble than aliphatic compounds in dimethylimidazolium ionic liquids? A simulation study. Chemical Physics Letters, 374(1-2), 85-90.

Hirasaki, G., Miller, C.A. and Puerto, M. (2011) Recent advances in surfactant EOR. SPE Journal, 16(04).

Huibers, P.D.T. (1999) Quantum-Chemical Calculations of the Charge Distribution in Ionic Surfactants. Langmuir, 15(22), 7546–7550.

Huibers, P.D.T., Lobanov, V.S., Katritzky, A.R., Shah, D.O. and Karelson, M. (1996) Prediction of Critical Micelle Concentration Using a Quantitative Structure−Property Relationship Approach. 1. Nonionic Surfactants. Langmuir, 12(6), 1462-1470.

Hukkerikar, A.S., Kalakul, S., Sarup, B., Young, D.M., Sin, G. and Gani, R. (2012) Estimation of environment-related properties of chemicals for design of sustainable processes: development of group-contribution+ (GC+) property models and uncertainty analysis. J Chem Inf Model, 52(11), 2823-2839.

Hukkerikar, A.S., Meier, R.J., Sin, G. and Gani, R. (2013) A method to estimate the enthalpy of formation of organic compounds with chemical accuracy. Fluid Phase Equilibria, 348, 23-32.

J.K., W., A.J., S. and M.V., N.-P. (1966) Ether alcohol sulfates. The effect of oxypropylation and oxybutylation on surface active properties. Journal of the American Oil Chemists' Society, 43(11), 603-606.

Jeirani, Z., Mohamed Jan, B., Si Ali, B., Noor, I.M., See, C.H. and Saphanuchart, W. (2013) Formulation, optimization and application of triglyceride microemulsion in enhanced oil recovery. Industrial Crops and Products, 43, 6-14.

Jenkins, K.M., Wettig, S.D. and Verrall, R.E. (2002) Studies of the aggregation behavior of cyclic gemini surfactants. J. Coll. Interf. Sci, 247(2), 456-462.

Jin, L., Jamili, A., Li, Z., Lu, J., Luo, H., Ben Shiau, B.J., Delshad, M. and Harwell, J.H. (2015) Physics based HLD–NAC phase behavior model for surfactant/crude oil/brine systems. Journal of Petroleum Science and Engineering, 136, 68-77.

Joback, K.G. and Reid, R.C. (1987) Estimation of Pure-Component Properties from Group-Contributions. Chemical Engineering Communications, 57(1-6), 233-243.

Jones, S.A., van der Bent, V., Farajzadeh, R., Rossen, W.R. and Vincent-Bonnieu, S. (2016) Surfactant screening for foam EOR: Correlation between bulk and core-flood experiments. Colloids and Surfaces A: Physicochemical and Engineering Aspects, 500, 166-176.

Jones, S.C. and Dreher, K.D. (1976) Cosurfactants in Micellar Systems Used for Tertiary Oil Recovery. SPE Journal, 16(3), 161-167.

Kabalnov, A., Olsson, U. and Wennerstrom, H. (1995) Salt effects on Nonionic Microemulsions are driven by Adsorption/Depletion at the surfactant monolayer. J. Phys. Chem. , 99, 6220-6230.

Kamal, M.S., Sultan, A.S. and Hussein, I.A. (2015) Screening of amphoteric and anionic surfactants for cEOR applications using a novel approach. Colloids and Surfaces A: Physicochemical and Engineering Aspects, 476, 17-23.

Klaus, A., Tiddy, G.J., Touraud, D., Schramm, A., Stuhler, G. and Kunz, W. (2010) Phase behavior of an extended surfactant in water and a detailed characterization of the concentrated phases. Langmuir, 26(22), 16871-83.

Kulajanpeng, K., Suriyapraphadilok, U. and Gani, R. (2016) Systematic screening methodology and energy efficient design of ionic liquid-based separation processes. Journal of Cleaner Production, 111, 93-107.

Kumar, A., Bhattacharjee, G., Kulkarni, B.D. and Kumar, R. (2015) Role of Surfactants in Promoting Gas Hydrate Formation. Industrial & Engineering Chemistry Research, 54(49), 12217-12232.

Kumar, S. and Mandal, A. (2016) Studies on interfacial behavior and wettability change phenomena by ionic and nonionic surfactants in presence of alkalis and salt for enhanced oil recovery. Applied Surface Science, 372, 42-51.

Kunieda, H., Kabir, H., Aramaki, K. and Shigeta, K. (2001) Phase behavior of mixed polyoxyethylene-type nonionic surfactants in water. Journal of Molecular Liquids, 90, 157-166.

Kunieda, H. and Shinoda, K. (1976) Krafft points, Critical Micelle Concentrations, Surface Tension, and Solubilizing Power of Aqueous Solutions of Fluorinated Surfactants. J. Phys. Chem., 80(22), 2468-2470.

Lavkush Bhaisare, M., Pandey, S., Shahnawaz Khan, M., Talib, A. and Wu, H.-F. (2015) Fluorophotometric determination of critical micelle concentration (CMC) of ionic and non-ionic surfactants with carbon dots via Stokes shift. Talanta, 132, 572-578.

Lee, S., Lee, J., Yu, H. and Lim, J. (2016) Synthesis of environment friendly nonionic surfactants from sugar base and characterization of interfacial properties for detergent application. Journal of Industrial and Engineering Chemistry, 38, 157-166.

Li, Y., Xu, G., Luan, Y., Yuan, S. and Xin, X. (2005) Property Prediction on Surfactant by Quantitative Structure-Property Relationship: Krafft Point and Cloud Point. Journal of Dispersion Science and Technology, 26(6), 799-808.

Liang, C. and Peng, X. (2017) Mobilization of arsenic from contaminated sediment by anionic and nonionic surfactants. Journal of Environmental Sciences (China), 56, 281-289.

Lindman, B., Medronho, B. and Karlström, G. (2016) Clouding of nonionic surfactants. Current Opinion in Colloid & Interface Science, 22, 23-29.

Lu, S., Wu, J. and Somasundaran, P. (2012) Micellar evolution in mixed nonionic/anionic surfactant systems. J Coll Interf Sci, 367(1), 272-279.

Lucassen-Reynders, E.H. (1981) Anionic Surfactants: Physical Chemistry of Surfactant Action, New York: Marcel Dekker, Inc.

Malik, M.A., Wani, M.Y. and Hashim, M.A. (2012) Microemulsion method: A novel route to synthesize organic and inorganic nanomaterials. Arabian Journal of Chemistry, 5(4), 397-417.

Mao, X., Jiang, R., Xiao, W. and Yu, J. (2015) Use of surfactants for the remediation of contaminated soils: a review. J Hazard Mater, 285, 419-435.

Marrero, J. and Gani, R. (2001) Group-contribution based estimation of pure component properties. Fluid Phase Equilibria, 183-184, 183-208.

Mattei, M., Kontogeorgis, G.M. and Gani, R. (2012) A Systematic Methodology for Design of Emulsion Based Chemical Products. Computer - Aided Chemical Engineering, 31, 220-224.

Mattei, M., Kontogeorgis, G.M. and Gani, R. (2013) Modeling of the Critical Micelle Concentration (CMC) of Nonionic Surfactants with an Extended Group-Contribution Method. Industrial & Engineering Chemistry Research, 52(34), 12236-12246.

Mattei, M., Kontogeorgis, G.M. and Gani, R. (2014) A comprehensive framework for surfactant selection and design for emulsion based chemical product design. Fluid Phase Equilibria, 362, 288-299.

Modarresi, H., Conte, E., Abildskov, J., Gani, R. and Crafts, P. (2008) Model-Based Calculation of Solid Solubility for Solvent Selection—A Review. Ind. Eng. Chem. Res., 47(15), 5234–5242.

Mondejar, M.E., Cignitti, S., Abildskov, J., Woodley, J.M. and Haglind, F. (2017) Prediction of properties of new halogenated olefins using two group contribution approaches. Fluid Phase Equilibria, 433, 79-96.

Muggeridge, A., Cockin, A., Webb, K., Frampton, H., Collins, I., Moulds, T. and Salino, P. (2014) Recovery rates, enhanced oil recovery and technological limits. Philos Trans A Math Phys Eng Sci, 372(2006), 20120320.

Myers, D. (2006) Surfactant Science and Technology, Canada: John Wiley & Sons, Inc.

Nagy, R., Sallai, R., Bartha, L. and Vágó, Á. (2015) Selection Method of Surfactants for Chemical Enhanced Oil Recovery. Advances in Chemical Engineering and Science, 05(02), 121-128.

Najafi, S.A.S., Kamranfar, P., Madani, M., Shadadeh, M. and Jamialahmadi, M. (2017) Experimental and theoretical investigation of CTAB microemulsion viscosity in the chemical enhanced oil recovery process. Journal of Molecular Liquids, 232, 382-389.

Naskar, B., Dey, A. and Moulik, S.P. (2013) Counter-ion Effect on Micellization of Ionic Surfactants: A Comprehensive Understanding with Two Representatives, Sodium Dodecyl Sulfate (SDS) and Dodecyltrimethylammonium Bromide (DTAB) Journal of Surfactants and Detergents, 16(5), 785-794.

Negin, C., Ali, S. and Xie, Q. (2017) Most common surfactants employed in chemical enhanced oil recovery. Petroleum, 3(2), 197-211.

Nourafkan, E., Hu, Z. and Wen, D. (2018) Controlled delivery and release of surfactant for enhanced oil recovery by nanodroplets. Fuel, 218, 396-405.

O'Lenick, A. (2007) Effect of Branching on Surfactant Properties of Sulfosuccinates. Cosmetics & Toiletries Science Applied, 122, 81.

Ohbu, K., Fujiwara, M. and Abe, Y. (1998) Physicochemical properties of α-sulfonated fatty acid esters. Progress in Colloid & Polymer Sci, 109, 85-92.

Os, N.M.v., Haak, J.R. and Rupert, L.A.M. (1993) Physico-Chemical Properties of Selected Anionic, Cationic and Nonionic Surfactants, Elsevier Science.

Pan, T., Wang, Z., Xu, J.-H., Wu, Z. and Qi, H. (2010) Stripping of nonionic surfactants from the coacervate phase of cloud point system for lipase separation by Winsor II microemulsion extraction with the direct addition of alcohols. Process Biochemistry, 45(5), 771-776.

PDT, H., VS, L., AR, K., DO, S. and M., K. (1997) Prediction of Critical Micelle Concentration Using a Quantitative Structure-Property Relationship Approach 2. Anionic Surfactants. J Coll Interf Sci, 187(1), 113-120.

Phan, T.T., Attaphong, C. and Sabatini, D.A. (2011) Effect of Extended Surfactant Structure on Interfacial Tension and Microemulsion Formation with Triglycerides. Journal of the American Oil Chemists' Society, 88(8), 1223-1228.

Pithapurwala, Y.K., Sharma, A.K. and Shah, D.O. (1986) Effect of salinity and alcohol partitioning on phase behavior and oil displacement efficiency in surfactant-polymer flooding. Journal of the American Oil Chemists' Society, 63(6), 804-813.

Quintero, L. and Carnahan, N.F. (2013) Microemulsions for Cleaning Applications. Developments in Surface Contamination and Cleaning, 6, 65-106.

Raisen, M. (1957) Proceedings of the Second International Congress of Surface Activity, London, London, Butterworths Scientific Publications.

Rakowska, J., Radwan, K., Porycka, B. and Prochaska, K. (2017) Experimental study on surface activity of surfactants on their ability to cleaning oil contaminations. Journal of Cleaner Production, 144, 437-447.

Ratnakar, R.R., Dindoruk, B. and Wilson, L.C. (2017) Phase behavior experiments and PVT modeling of DME-brine-crude oil mixtures based on Huron-Vidal mixing rules for EOR applications. Fluid Phase Equilibria, 434, 49-62.

Reinhard, M. and Drefahl, A. (1998) Handbook for Estimating Physicochemical Properties of Organic Compounds. United States: John Wiley & Sons, Inc.

Ren, Y., Zhao, B., Chang, Q. and Yao, X. (2011) QSPR modeling of nonionic surfactant cloud points: an update. Journal of Colloid and Interface Science, 358(1), 202-207.

Rosen, M.J. (1989) Surfactants and Interfacial Phenomena. New York: A JOHN WILEY & SONS, INC., PUBLICATION.

Rosen, M.J. (2004) Surfactants and Interfacial Phenomena. United States: John Wiley & Sons, Inc.

Rosen, M.J. and Kunjappu, J.T. (2012) Surfactants and Interfacial Phenomena. Canada: John Wiley & Sons, Inc.

Roughton, B.C., Christian, B., White, J., Camarda, K.V. and Gani, R. (2012) Simultaneous design of ionic liquid entrainers and energy efficient azeotropic separation processes. Computers & Chemical Engineering, 42, 248-262.

Salager, J.-L., Anton, R., Anderez, J.M. and Aubry, J.-M. (2001) Formulation des microémulsions par la me´thode HLD. Techniques de l'Ingénieur, Génie des Procédés J2(157), 1-20.

Salager, J.-L., Forgiarini, A.M. and Bullón, J. (2013a) How to Attain Ultralow Interfacial Tension and Three-Phase Behavior with Surfactant Formulation for Enhanced Oil Recovery: A Review. Part 1. Optimum Formulation for Simple Surfactant–Oil–Water Ternary Systems. Journal of Surfactants and Detergents, 16(4), 449-472.

Salager, J.L., Forgiarini, A.M., Marquez, L., Manchego, L. and Bullon, J. (2013b) How to Attain an Ultralow Interfacial Tension and a Three-Phase Behavior

with a Surfactant Formulation for Enhanced Oil Recovery: A Review. Part 2. Performance Improvement Trends from Winsor's Premise to Currently Proposed Inter- and Intra-Molecular Mixtures. J Surfactants Deterg, 16, 631-663.

Salager, J.L., Morgan, J.C., Schechter, R.S., Wade, W.H. and Vasquez, E. (1979) Optimum Formulation of Surfactant/Water/Oil Systems for Minimum Interfacial Tension or Phase Behavior. Society of Petroleum Engineers, 19(02), 107-115.

Sandersen, S.B. (2012) Enhanced oil recovery with surfactant flooding. Ph.D. Thesis, Technical University of Denmark, Lyngby, Denmark.

Schmitt, T.M. (2001) Analysis of Surfactants, Second Edition (Surfactant Science). United States: Marcel Dekker, Inc.

Schramm, L.L. (2009) Surfactants: Fundamentals and Applications in the Petroleum Industry. United Kingdom: Cambridge University Press.

Schramm, L.L., Stasiuk, E.N. and Marangoni, D.G. (2003) 2 Surfactants and their applications. Annu. Rep. Prog. Chem., Sect. C: Phys. Chem., 99, 3-48.

Sheng, J.J. (2015) Status of surfactant EOR technology. Petroleum, 1(2), 97-105.

Shinoda, K., Hatö, M. and Hayashi, T. (1972) The physicochemical properties of aqueous solutions of fluorinated surfactants. The Journal of Physical Chemistry, 76(6), 909-914.

Smith, F.D., Stirton, A.J. and Nunez-Ponzoa, M.V. (1966) Isomeric linear phenylalkanes and sodium alkylbenzenesulfonates. Journal of the American Oil Chemists Society, 43(8), 501-504.

Sofla, S.J.D., Sharifi, M. and Hemmati Sarapardeh, A. (2016) Toward mechanistic understanding of natural surfactant flooding in enhanced oil recovery processes: The role of salinity, surfactant concentration and rock type. Journal of Molecular Liquids, 222, 632-639.

Sripriya, R., Muthu Raja, K., Santhosh, G., Chandrasekaran, M. and Noel, M. (2007) The effect of structure of oil phase, surfactant and co-surfactant on the physicochemical and electrochemical properties of bicontinuous microemulsion. J Colloid Interface Sci, 314(2), 712-717.

Stanton, D.T. and Jurs, P.C. (1990) Development and Use of Charged Partial Surface Area Structural Descriptors in Computer-Assisted Quantitative Structure-Property Relationship Studies. Analytical Chemistry, 62(21), 2323–2329.

Sultan, P., Collins, I., Oystein, H., Federico, J.P. and Muhammad, U.I. (2010) Comparative study of different EOR method. Petroleum Engineering. Trondheim, Norway, Norwegian University of Science & Technology: 51.

Summerton, E., Zimbitas, G., Britton, M. and Bakalis, S. (2017) Low temperature stability of surfactant systems. Trends in Food Science & Technology, 60, 23-30.

Taber, J.J., Martin, F.D. and Seright, R.S. (1997) EOR Screening Criteria Revisited Part 1. SPE Reservoir Engineering, 12(03), 189-205.

Takeshi, H., Kiyoshi, M. and Kenjiro, M. (1970) The Properties of Aqueous Solutions of Sodium 2-Sulfoethyl Alkanoates and Sodium Alkyl β-Sulfopropionates. Bulletin of the Chemical Society of Japan, 43(12), 3913-3916.

Thakkar, K., Bharatiya, B., Ray, D., Aswal, V.K. and Bahadur, P. (2017) Cationic surfactants modulate aqueous micellization and wetting on PTFE by Triton X-100: Effect of alkyl chainlength, headgroup and counterion. Journal of Molecular Liquids, 241, 136-143.

Tiddy, G.J. and Khan, A. (1999) Formulation Science and Technology - Surfactants Needed! Current Opinion in Colloid & Interface Science, 4(6), 379-380.

Trawińska, A., Hallmann, E. and Mędrzycka, K. (2016) The effect of alkyl chain length on synergistic effects in micellization and surface tension reduction in nonionic gemini (S-10) and anionic surfactants mixtures. Colloids and Surfaces A: Physicochemical and Engineering Aspects, 506, 114-126.

Ueno, M., Yamamoto, S. and Meguro, K. (1974) Properties of aqueous solutions of several salts of α,ω-alkanediol disulfates. Journal of the American Oil Chemists Society, 51(8), 373-376.

Valint, P.L., J.Bock., M.W.Kim., M.L.Robbins., P.Steyn. and S.Zushma (1987) Krafft points and microemulsion phase behavior of some alkylarenesulfonates. Colloids and Surfaces, 26, 191-203.

van Speybroeck, V., Gani, R. and Meier, R.J. (2010) The calculation of thermodynamic properties of molecules. Chem Soc Rev, 39(5), 1764-1779.

Vautier-Giongo, C. and Bales, B.L. (2003) Estimate of the Ionization Degree of Ionic Micelles Based on Krafft Temperature. The journal of Physical Chemistry B, 107 (23), 5398-5403.

Wang, Z.W., Feng, J.L., Wang, Z.N., Li, G.Z. and Lou, A.J. (2006) Quantitative Structure-Property Relationship on Prediction of the Interaction Parameters δ 2 t of Organic Compounds. Journal of Dispersion Science and Technology, 27(1), 11-14.

Weil, J.K., Smith, F.D., Stirton, A.J. and Bistline, R.G. (1963) Long chain alkanesulfonates and 1-hydroxy-2-alkanesulfonates: Structure and property relations. Journal of the American Oil Chemists' Society, 40(10), 538-541.

Witthayapanyanon, A., Acosta, E.J., Harwell, J.H. and Sabatini, D.A. (2006) Formulation of ultralow interfacial tension systems using extended surfactants. Journal of Surfactants and Detergents, 9(4), 331-339.

Witthayapanyanon, A., Harwell, J.H. and Sabatini, D.A. (2008) Hydrophilic-lipophilic deviation (HLD) method for characterizing conventional and extended surfactants. J Colloid Interface Sci, 325(1), 259-266.

Wu, J., Xu, Y., Dabros, T. and Hamza, H. (2004) Development of a method for measurement of relative solubility of nonionic surfactants. Colloids and Surfaces A: Physicochemical and Engineering Aspects, 232(2-3), 229-237.

Xu, H., Li, P., Ma, K., Welbourn, R.J.L., Doutch, J., Penfold, J., Thomas, R.K., Roberts, D.W., Petkov, J.T., Choo, K.L. and Khoo, S.Y. (2018) Adsorption and self-assembly in methyl ester sulfonate surfactants, their eutectic mixtures and the role of electrolyte. Journal of Colloid and Interface Science, 516, 456-465.

Yuan, S., Cai, Z., Xu, G. and Jiang, Y. (2002) Quantitative structure-property relationships of surfactants: prediction of the critical micelle concentration of nonionic surfactants. Colloid & Polymer Science, 280(7), 630-636.

Zarate-Munoz, S., Boza Troncoso, A. and Acosta, E. (2015) The Cloud Point of Alkyl Ethoxylates and Its Prediction with the Hydrophilic-Lipophilic Difference (HLD) Framework. Langmuir, 31(44), 12000-12008.

Zarate-Muñoz, S., Texeira de Vasconcelos, F., Myint-Myat, K., Minchom, J. and Acosta, E. (2016) A Simplified Methodology to Measure the Characteristic

Curvature (Cc) of Alkyl Ethoxylate Nonionic Surfactants. <u>Journal of Surfactants and Detergents</u>, 19(2), 249-263.

Zhang, Q., Li, Y., Song, Y., Fu, H., Li, J. and Wang, Z. (2017) Properties of vesicles formation of single-chain branched carboxylate anionic surfactant in aqueous solutions. <u>Journal of Molecular Liquids</u>, 243, 431-438.

Zhang, T. and Blum, F.D. (2017) Cationic surfactant blocks radical-inhibiting sites on silica. <u>Journal of Colloid and Interface Science</u>, 504, 111-114.

APPENDICES

Appendix A   Chemical Properties and Mixing Ratio of Surfactant/Oil/Water System

The properties of surfactants that are used in the experiment are collected in this Appendix. In addition, the mixing ratio in single and mixed systems are also shown in the table.

Table A1 The properties of nonionic surfactant in the experiment

Name	Molecular formula	Average molecular weight	Cloud point (°C)
Dehydol LS 1 TH	C12-14EO1	244	No data
Dehydol LS 2 TH	C12-14EO2	288	No data
Dehydol LS 3 TH	C12-14EO3	332	51-53 (25%BDG/water)
Dehydol LS 5 TH	C12-14EO5	420	68-73 (25%BDG/water)
Dehydol LS 9 TH	C12-14EO9	596	72-82 (1% aq solution)
Dehydol LS 12 TH	C12-14EO12	728	79-83 (1% in 5% NaCl)
Marlox® RT42	C16-C18EO4PO2	548	No data
Marlox® RT64	C16-C18EO6PO4	752	No data

Table A2 The properties of oils used in the experiment

Name	Molecular formula	Flash point (°C)
Cyclohexane	C6H12	-18
n-Hexane	C6H14	-22
n-Heptane	C7H16	-4
Decahydronaphthalene	C10H18	57
n-Decane	C10H22	46
n-Dodecane	C12H26	84
n-Hexadecane	C16H34	135

Table A3 The mixing ratio of single surfactant system in each salinity

Salinity (g/100ml)	Salinity 30g/100ml (ml)	DI water (ml)	Surfactant solution 0.8 M (ml)	Oil (ml)	Total (ml)
0.0000	0.0000	1.7500	0.2500	2.0000	4.0000
0.5000	0.0333	1.7167	0.2500	2.0000	4.0000
1.0000	0.0667	1.6833	0.2500	2.0000	4.0000
1.5000	0.1000	1.6500	0.2500	2.0000	4.0000
2.0000	0.1333	1.6167	0.2500	2.0000	4.0000
2.5000	0.1667	1.5833	0.2500	2.0000	4.0000
3.0000	0.2000	1.5500	0.2500	2.0000	4.0000
3.5000	0.2333	1.5167	0.2500	2.0000	4.0000
4.0000	0.2667	1.4833	0.2500	2.0000	4.0000
4.5000	0.3000	1.4500	0.2500	2.0000	4.0000

Table A3 The mixing ratio of single surfactant system in each salinity (continued)

Salinity (g/100ml)	Salinity 30g/100ml (ml)	DI water (ml)	Surfactant solution 0.8 M (ml)	Oil (ml)	Total (ml)
5.0000	0.3333	1.4167	0.2500	2.0000	4.0000
5.5000	0.3667	1.3833	0.2500	2.0000	4.0000
6.0000	0.4000	1.3500	0.2500	2.0000	4.0000
6.5000	0.4333	1.3167	0.2500	2.0000	4.0000
7.0000	0.4667	1.2833	0.2500	2.0000	4.0000
7.5000	0.5000	1.2500	0.2500	2.0000	4.0000
8.0000	0.5333	1.2167	0.2500	2.0000	4.0000
8.5000	0.5667	1.1833	0.2500	2.0000	4.0000
9.0000	0.6000	1.1500	0.2500	2.0000	4.0000
9.5000	0.6333	1.1167	0.2500	2.0000	4.0000
10.0000	0.6667	1.0833	0.2500	2.0000	4.0000
10.5000	0.7000	1.0500	0.2500	2.0000	4.0000
11.0000	0.7333	1.0167	0.2500	2.0000	4.0000
11.5000	0.7667	0.9833	0.2500	2.0000	4.0000
12.0000	0.8000	0.9500	0.2500	2.0000	4.0000
12.5000	0.8333	0.9167	0.2500	2.0000	4.0000
13.0000	0.8667	0.8833	0.2500	2.0000	4.0000
13.5000	0.9000	0.8500	0.2500	2.0000	4.0000
14.0000	0.9333	0.8167	0.2500	2.0000	4.0000
14.5000	0.9667	0.7833	0.2500	2.0000	4.0000

Table A3 The mixing ratio of single surfactant system in each salinity (continued)

Salinity (g/100ml)	Salinity 30g/100ml (ml)	DI water (ml)	Surfactant solution 0.8 M (ml)	Oil (ml)	Total (ml)
15.0000	1.0000	0.7500	0.2500	2.0000	4.0000
15.5000	1.0333	0.7167	0.2500	2.0000	4.0000
16.0000	1.0667	0.6833	0.2500	2.0000	4.0000
16.5000	1.1000	0.6500	0.2500	2.0000	4.0000
17.0000	1.1333	0.6167	0.2500	2.0000	4.0000
17.5000	1.1667	0.5833	0.2500	2.0000	4.0000
18.0000	1.2000	0.5500	0.2500	2.0000	4.0000
18.5000	1.2333	0.5167	0.2500	2.0000	4.0000
19.0000	1.2667	0.4833	0.2500	2.0000	4.0000
19.5000	1.3000	0.4500	0.2500	2.0000	4.0000
20.0000	1.3333	0.4167	0.2500	2.0000	4.0000
20.5000	1.3667	0.3833	0.2500	2.0000	4.0000
21.0000	1.4000	0.3500	0.2500	2.0000	4.0000
21.5000	1.4333	0.3167	0.2500	2.0000	4.0000
22.0000	1.4667	0.2833	0.2500	2.0000	4.0000
22.2000	1.4800	0.2700	0.2500	2.0000	4.0000
22.5000	1.5000	0.2500	0.2500	2.0000	4.0000
23.0000	1.5333	0.2167	0.2500	2.0000	4.0000
23.5000	1.5667	0.1833	0.2500	2.0000	4.0000
24.0000	1.6000	0.1500	0.2500	2.0000	4.0000

Table A3 The mixing ratio of single surfactant system in each salinity (continued)

Salinity (g/100ml)	Salinity 30g/100ml (ml)	DI water (ml)	Surfactant solution 0.8 M (ml)	Oil (ml)	Total (ml)
24.5000	1.6333	0.1167	0.2500	2.0000	4.0000
25.0000	1.6667	0.0833	0.2500	2.0000	4.0000
25.5000	1.7000	0.0500	0.2500	2.0000	4.0000
26.0000	1.7333	0.0167	0.2500	2.0000	4.0000

Table A4 The mixing ratio of two-surfactant mixture

mole fraction of tested surfactant	Ref surfactant (ml)	Tested surfactant (ml)	salinity (ml)	oil (ml)	Total (ml)
0.100	0.225	0.025	1.750	2.000	4.000
0.200	0.200	0.050	1.750	2.000	4.000
0.300	0.175	0.075	1.750	2.000	4.000
0.400	0.150	0.100	1.750	2.000	4.000
0.500	0.125	0.125	1.750	2.000	4.000
0.600	0.100	0.150	1.750	2.000	4.000
0.700	0.075	0.175	1.750	2.000	4.000
0.800	0.050	0.200	1.750	2.000	4.000
0.900	0.025	0.225	1.750	2.000	4.000
1.000	0.000	0.250	1.750	2.000	4.000

Appendix B Salinity Scan of C12-14EO3 for Single Surfactant System

The figures that show phase of C12-14EO3/oil/water system are presented in this part. The salinity scan is carried out in a range 0 – 26%wt/vol.
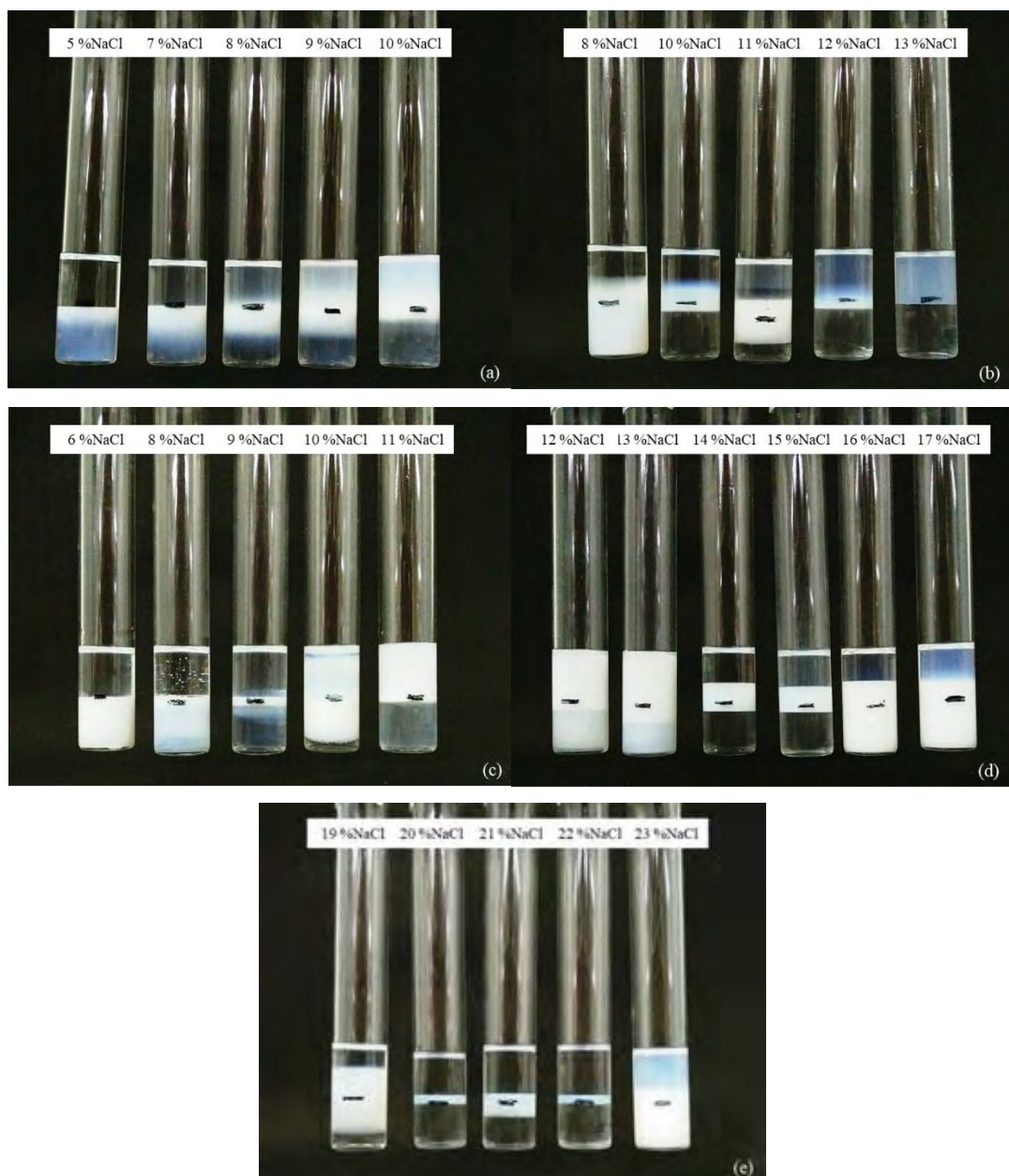
Figure B1 Salinity scan for 0.1 M C12-14EO3 with (a) Cyclohexane, (b) Heptane, (c) Decalin, (d) Dodecane and (e) Hexadecane at 25 °C.
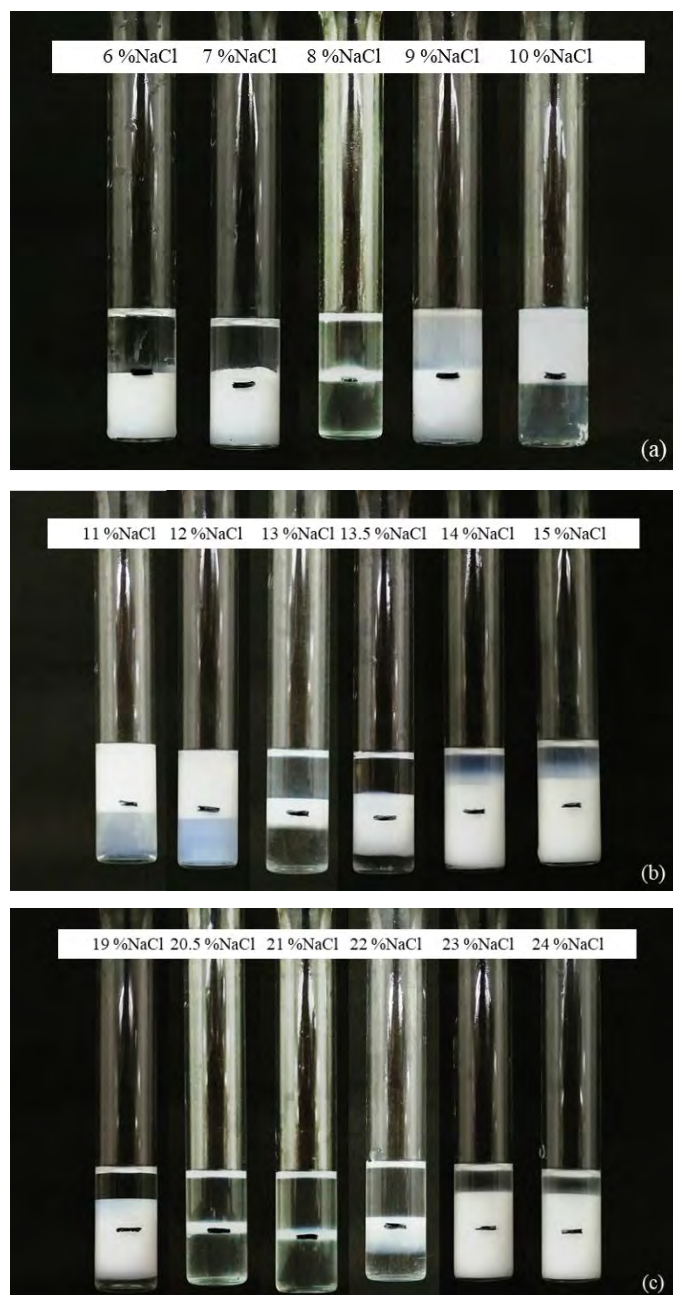
Figure B2 Salinity scan for 0.1 M C12-14EO3 with (a) Decalin, (b) Dodecane and (c) Hexadecane at 30 °C.
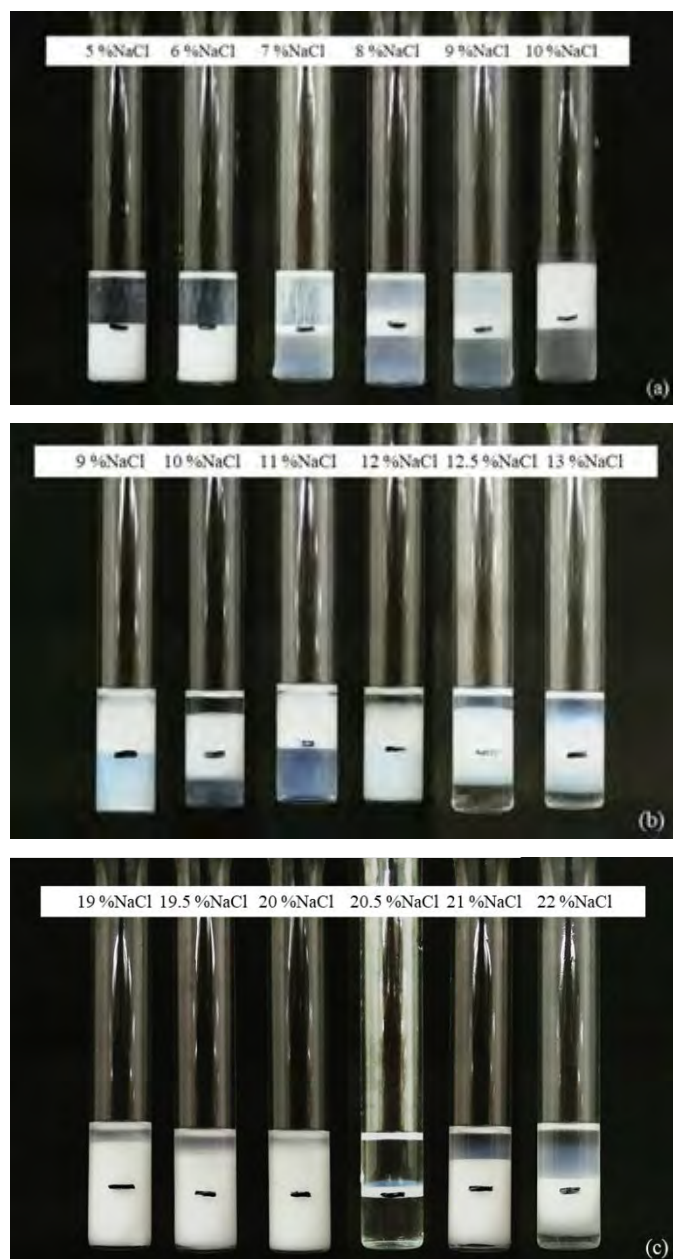
Figure B3 Salinity scan for 0.1 M C12-14EO3 with (a) Decalin, (b) Dodecane and (c) Hexadecane at 35 °C.
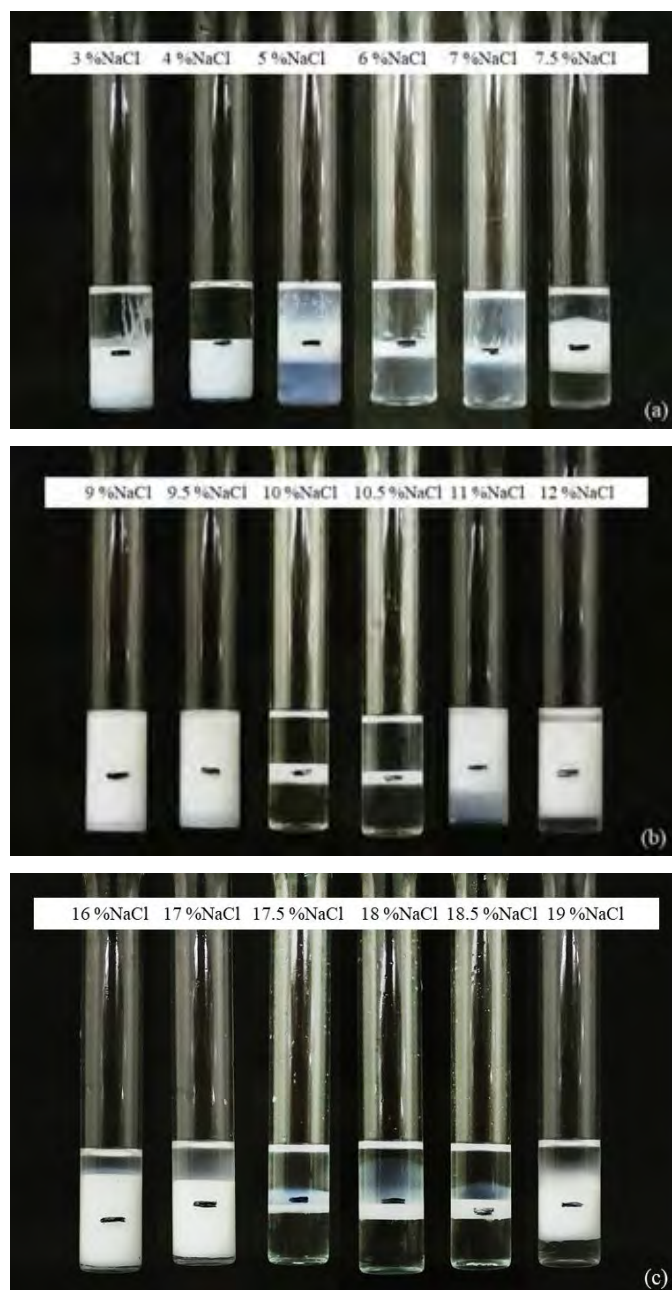
Figure B4 Salinity scan for 0.1 M C12-14EO3 with (a) Decalin, (b) Dodecane and (c) Hexadecane at 40 °C.
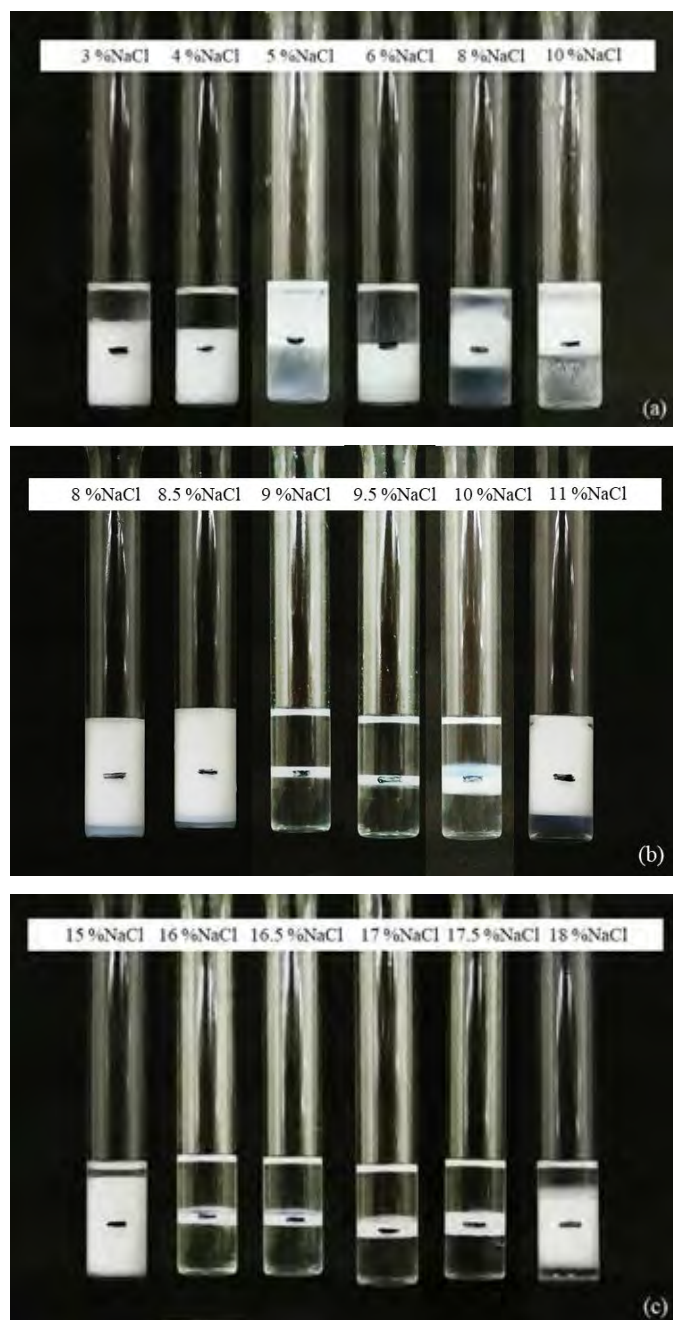
Figure B5 Salinity scan for 0.1 M C12-14EO3 with (a) Decalin, (b) Dodecane and (c) Hexadecane at 45 °C.
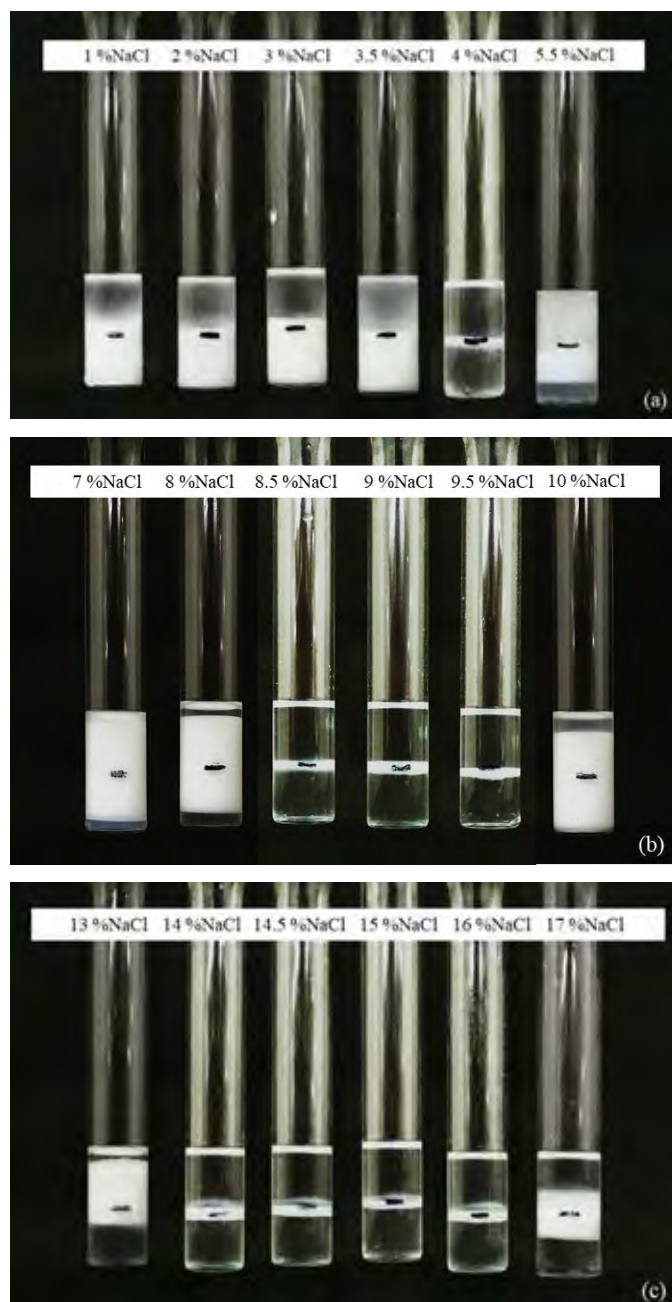
Figure B6 Salinity scan for 0.1 M C12-14EO3 with (a) Decalin, (b) Dodecane and (c) Hexadecane at 50 °C.
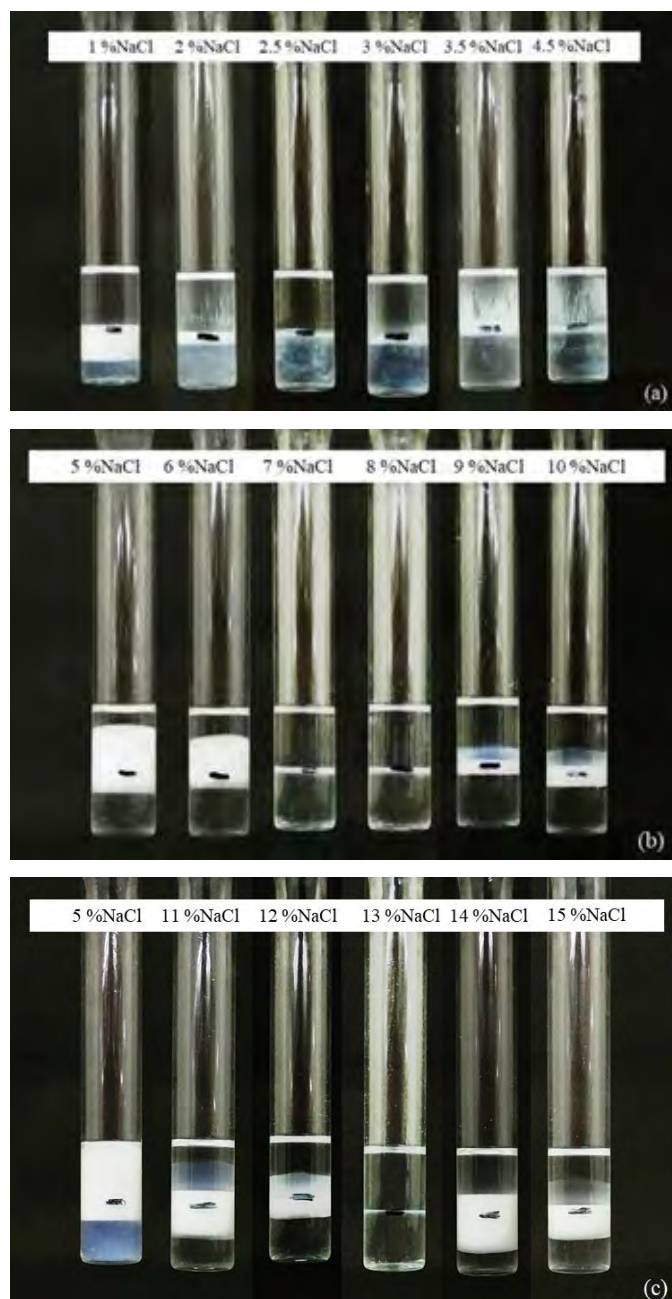
Figure B7 Salinity scan for 0.1 M C12-14EO3 with (a) Decalin, (b) Dodecane and (c) Hexadecane at 55 °C.

168
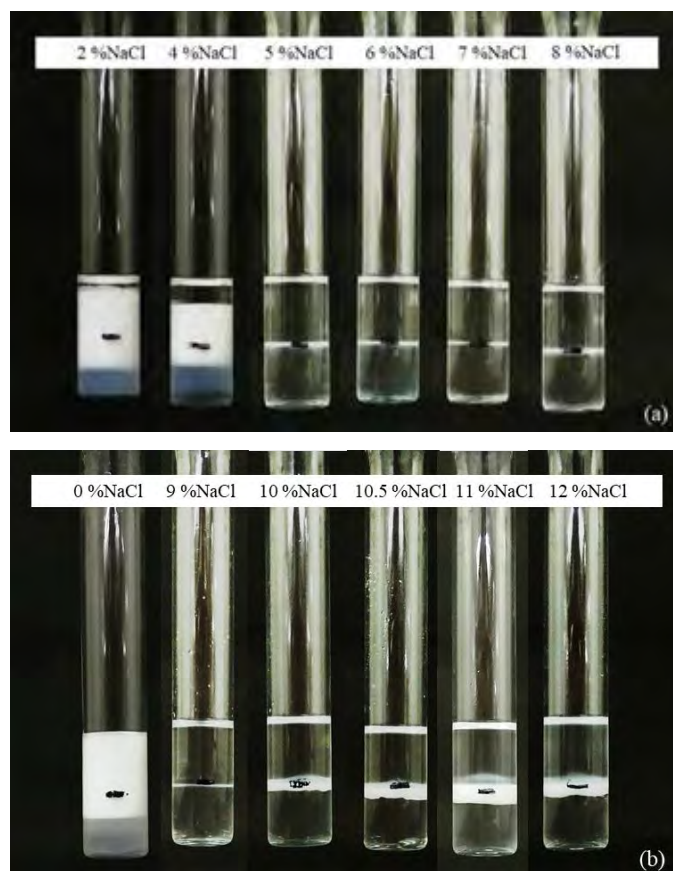
Figure B8 Salinity scan for 0.1 M C12-14EO3 with (a) Dodecane and (b) Hexadecane at 60 °C.
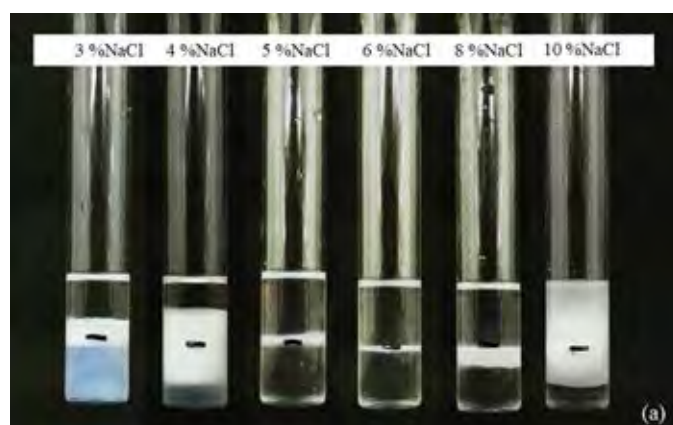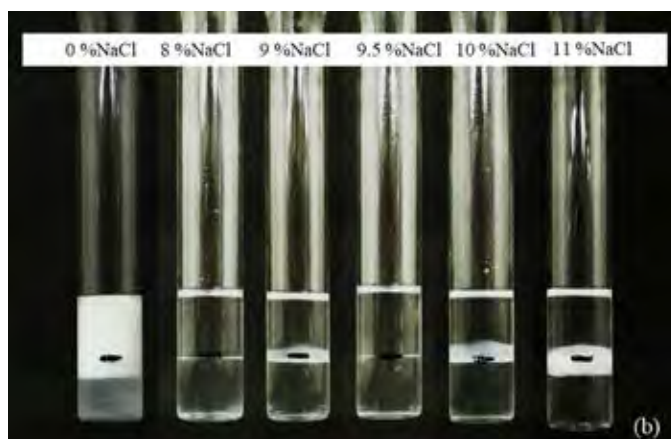
Figure B9 Salinity scan for 0.1 M C12-14EO3 with (a) Dodecane and (b) Hexadecane at 65 °C.
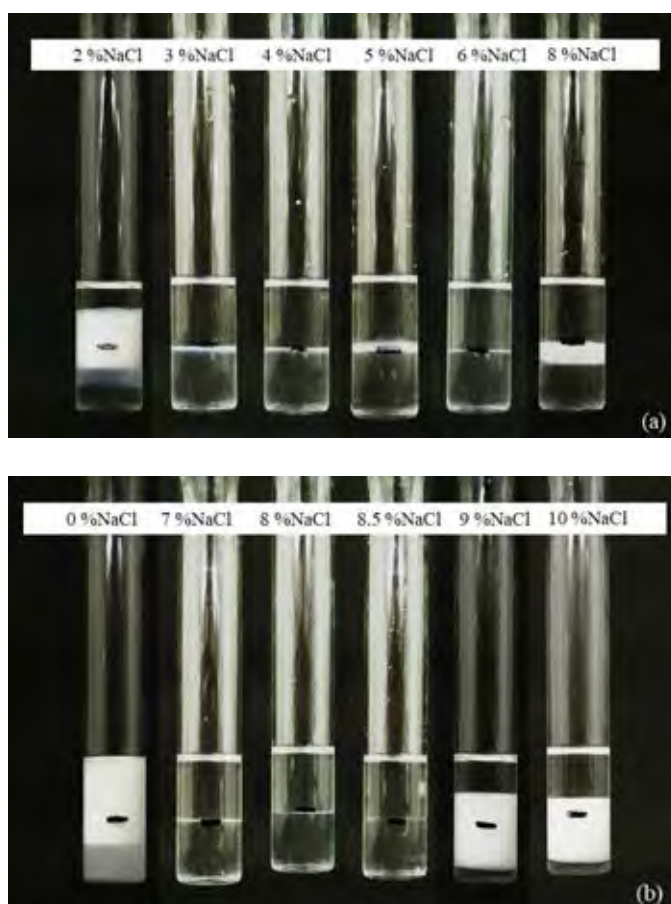
Figure B10 Salinity scan for 0.1 M C12-14EO3 with (a) Dodecane and (b) Hexadecane at 70 °C.
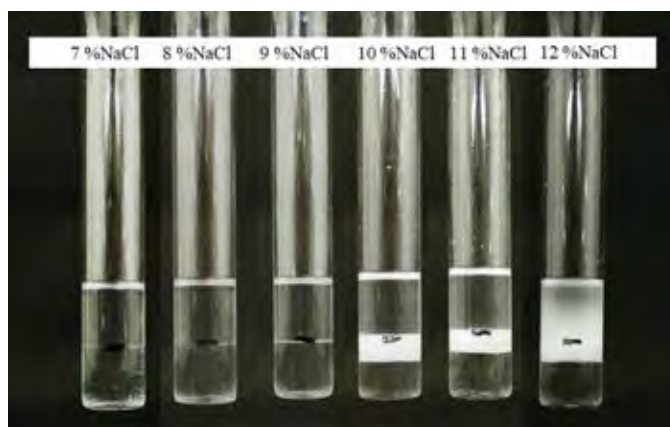
Figure B11 Salinity scan for 0.1 M C12-14EO3 with Hexadecane at 75 °C.
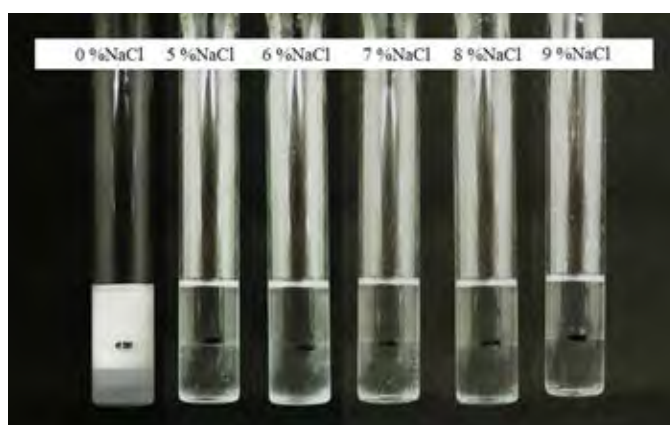
Figure B12 Salinity scan for 0.1 M C12-14EO3 with Hexadecane at 80 °C.
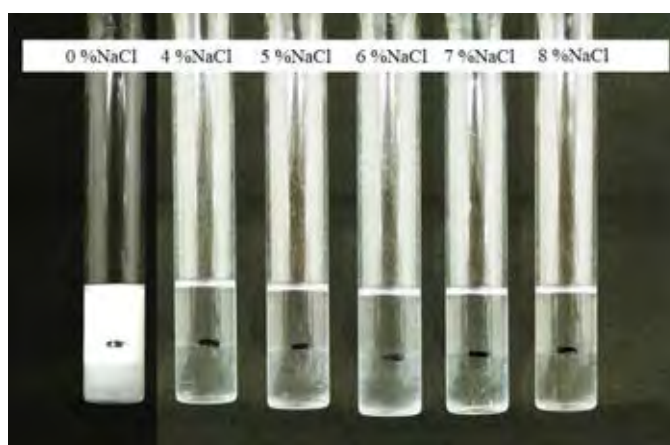
Figure B13 Salinity scan for 0.1 M C12-14EO3 with Hexadecane at 85 °C.
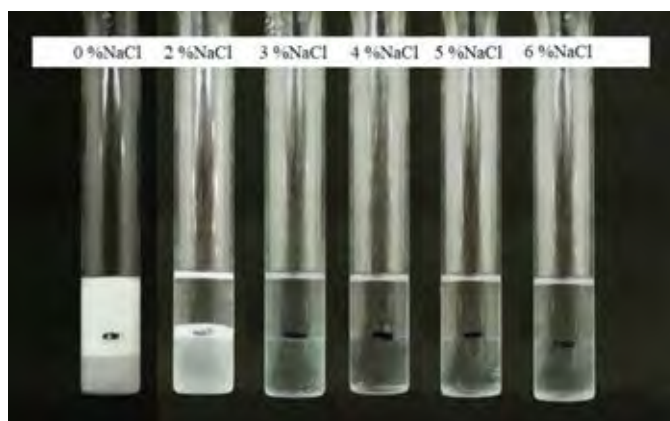
Figure B14 Salinity scan for 0.1 M C12-14EO3 with Hexadecane at 90 °C.
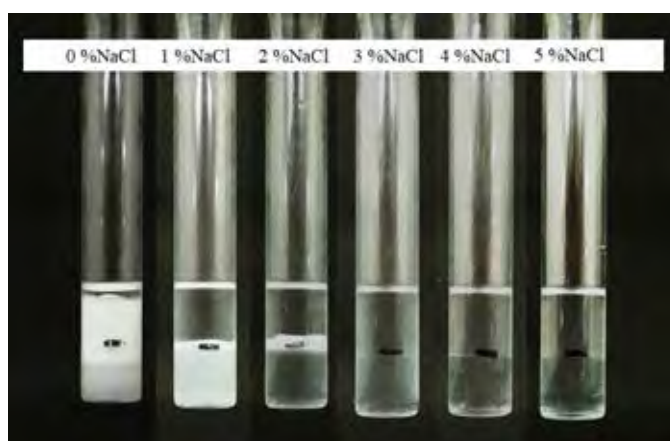
Figure B15 Salinity scan for 0.1 M C12-14EO3 with Hexadecane at 95 °C.

Appendix C Salinity Scan of C12-14EO5 for Single Surfactant System

The figures that show phase of C12-14EO5/oil/water system are presented in this part. The salinity scan is carried out in a range 0 – 26%wt/vol.
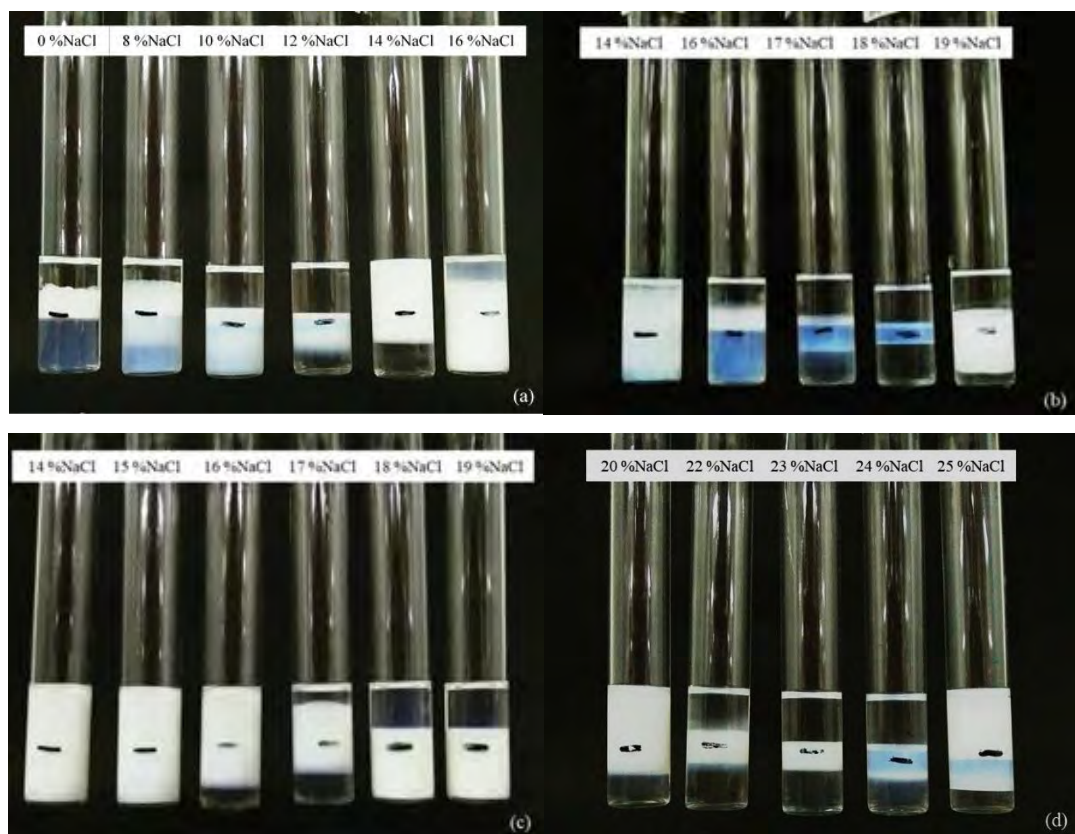
Figure C1 Salinity scan for 0.1 M C12-14EO5 with (a) Cyclohexane, (b) Heptane, (c) Decalin and (d) Dodecane at 25 °C.
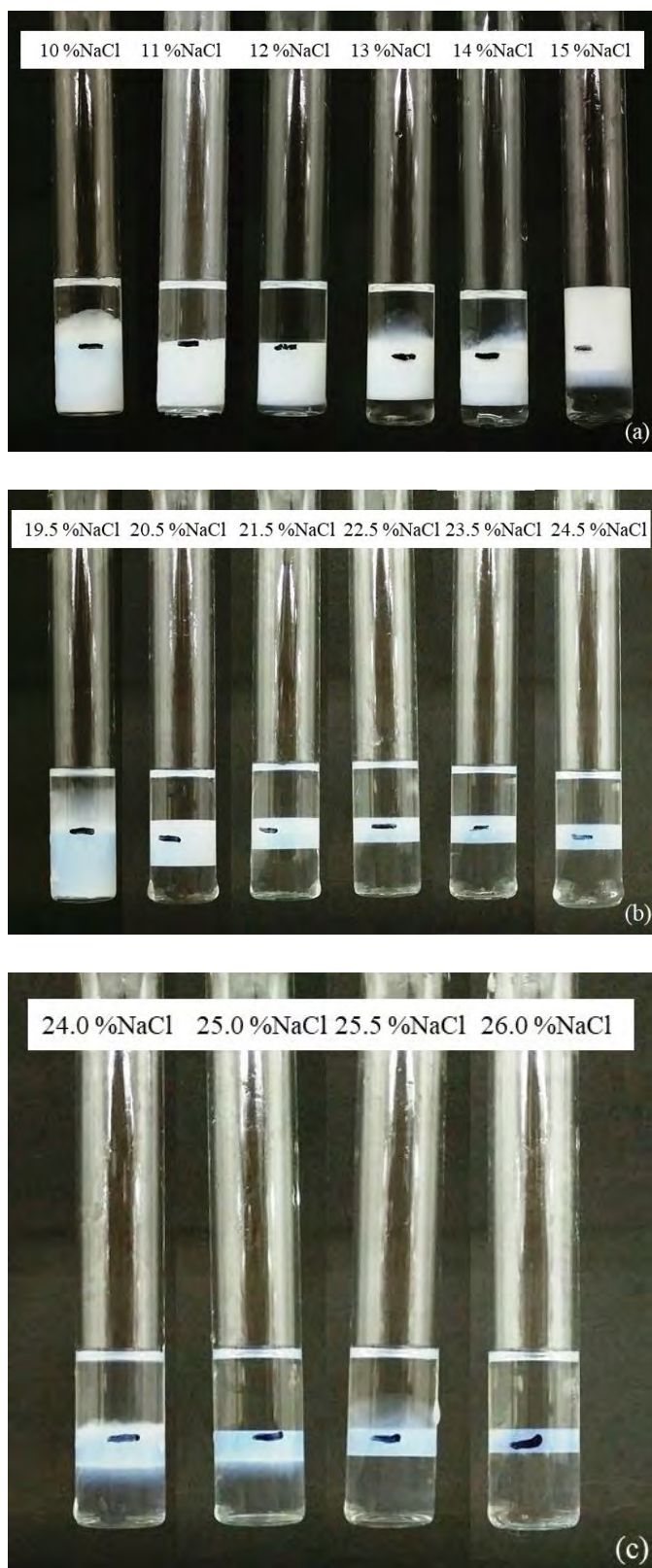
Figure C2 Salinity scan for 0.1 M C12-14EO5 with (a) Decalin, (b) Dodecane and (c) Hexadecane at 30 °C.
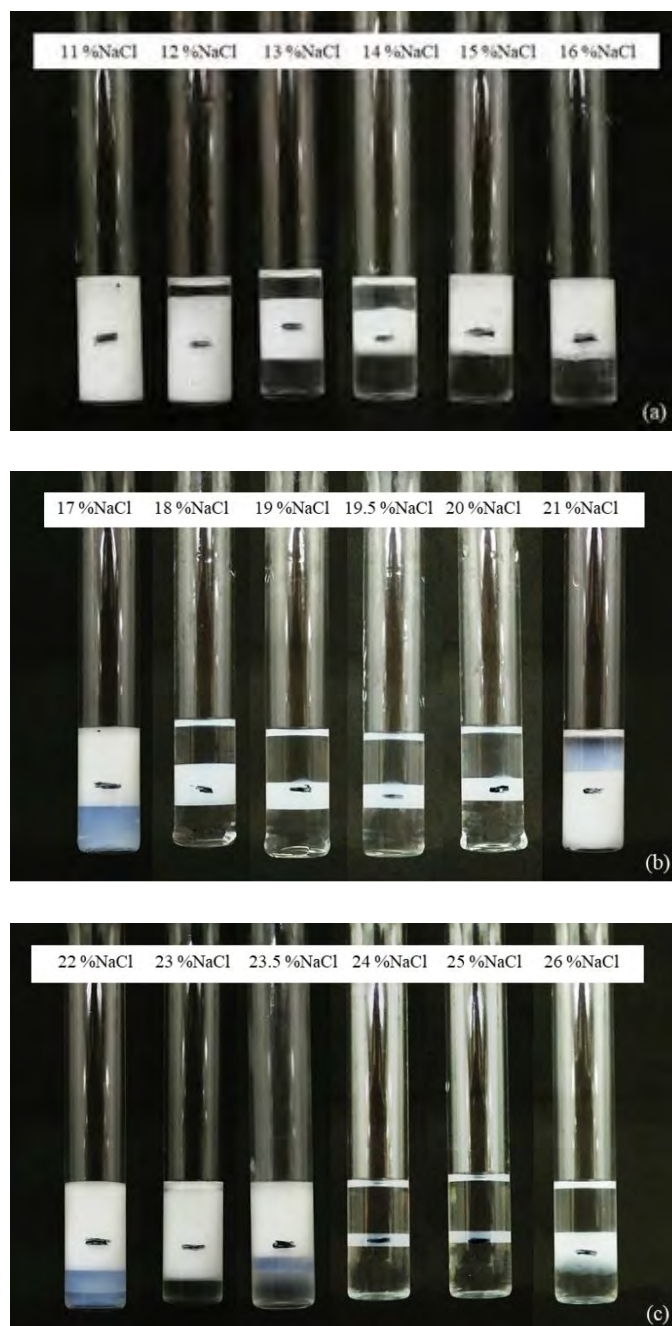
Figure C3 Salinity scan for 0.1 M C12-14EO5 with (a) Decalin, (b) Dodecane and (c) Hexadecane at 35 °C.
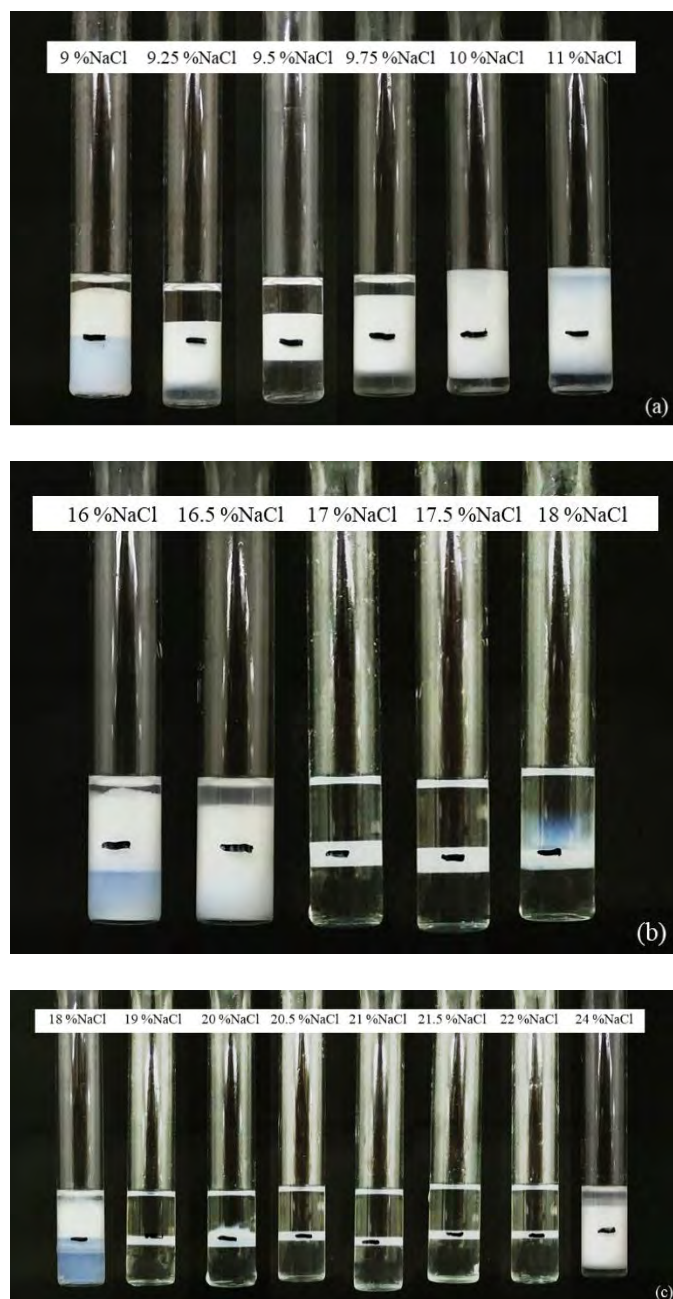
Figure C4 Salinity scan for 0.1 M C12-14EO5 with (a) Decalin, (b) Dodecane and (c) Hexadecane at 40 °C.
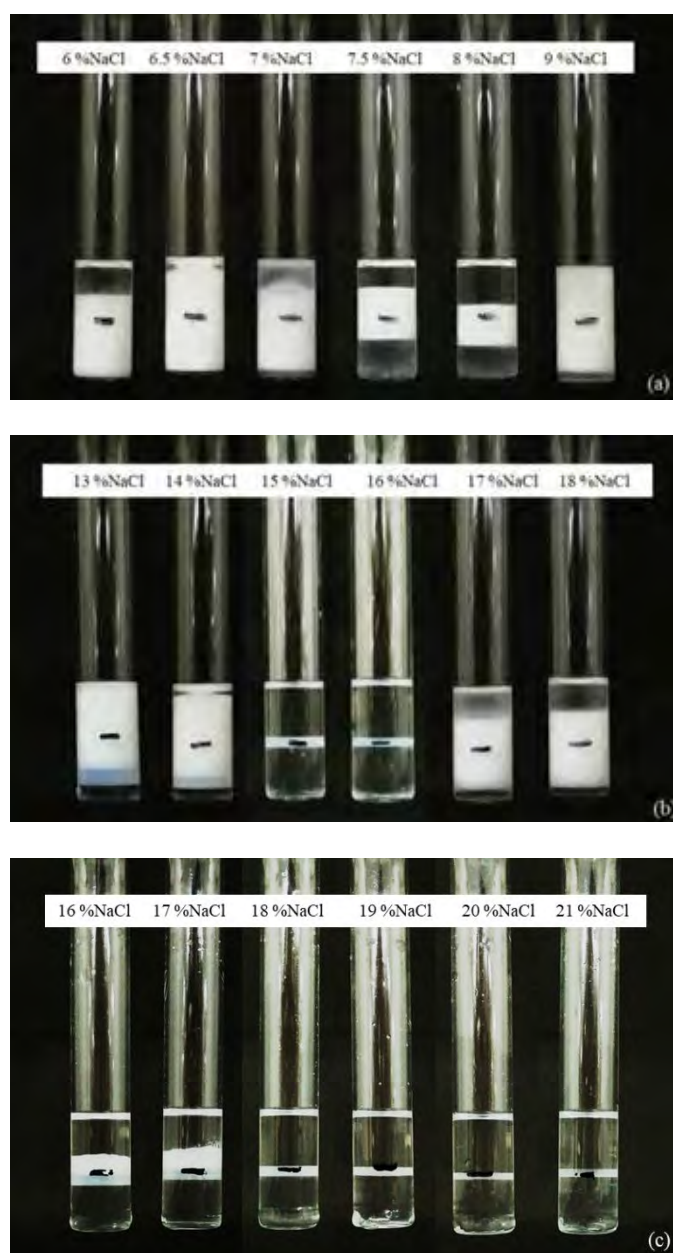
Figure C5 Salinity scan for 0.1 M C12-14EO5 with (a) Decalin, (b) Dodecane and (c) Hexadecane at 45 °C.
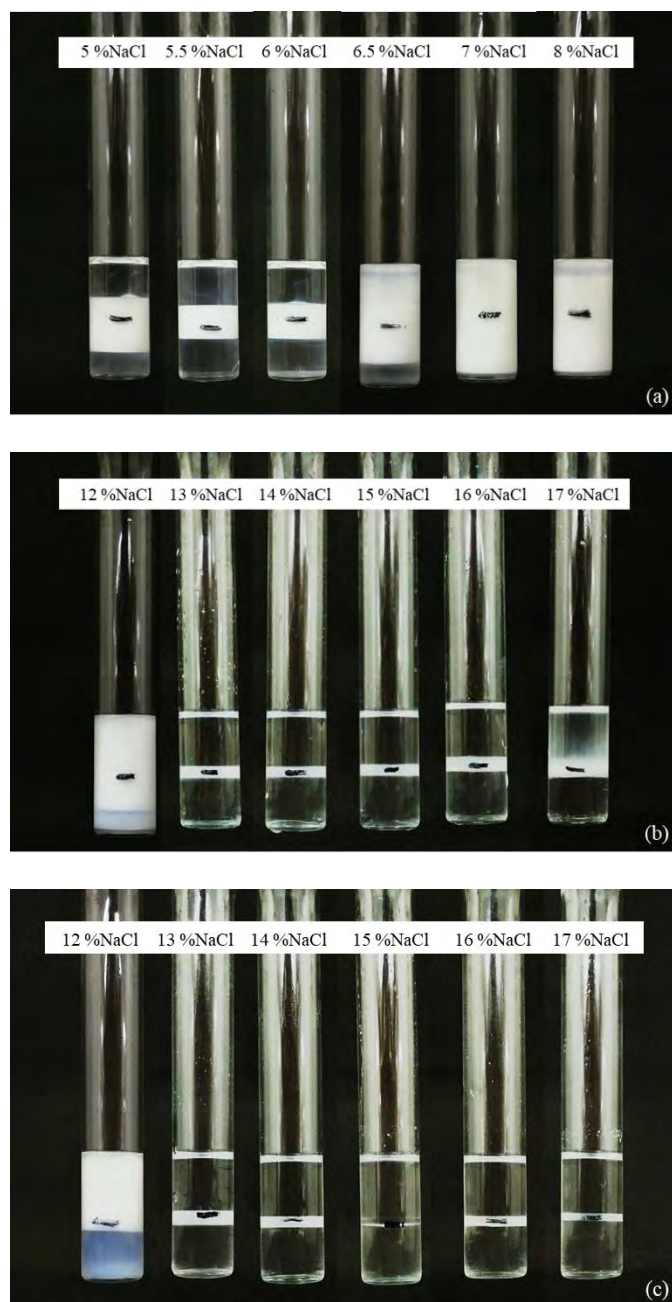
Figure C6 Salinity scan for 0.1 M C12-14EO5 with (a) Decalin, (b) Dodecane and (c) Hexadecane at 50 °C.
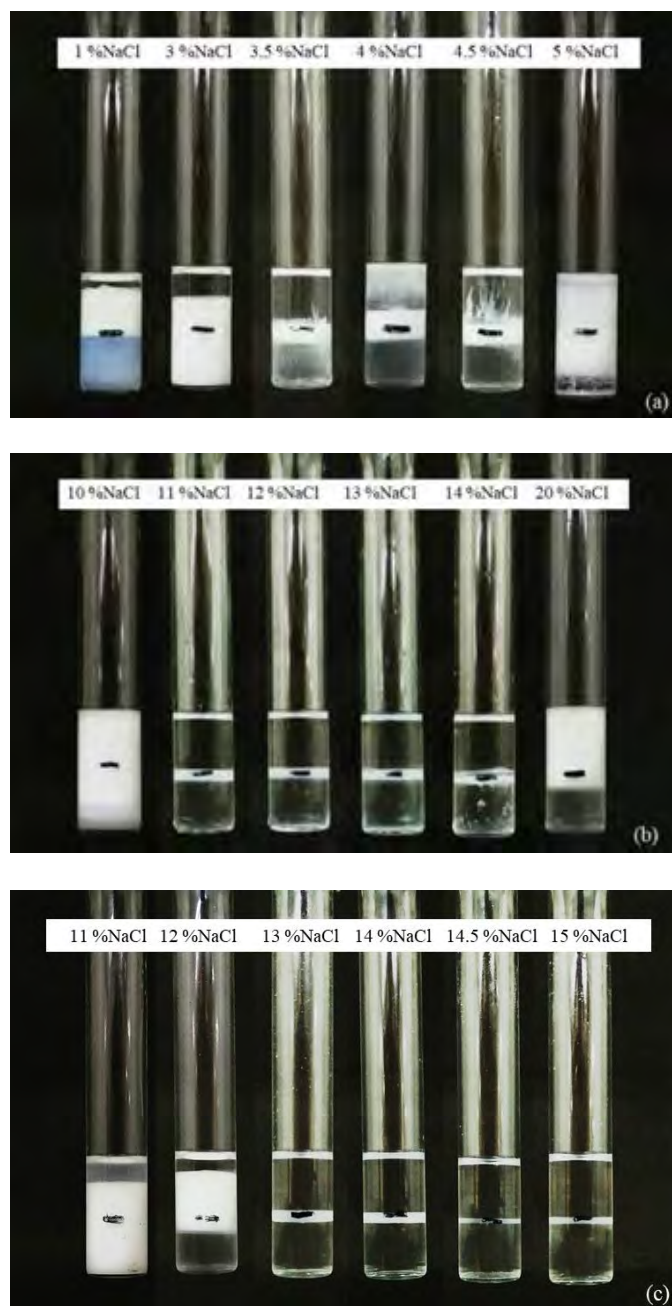
Figure C7 Salinity scan for 0.1 M C12-14EO5 with (a) Decalin, (b) Dodecane and (c) Hexadecane at 55 °C.
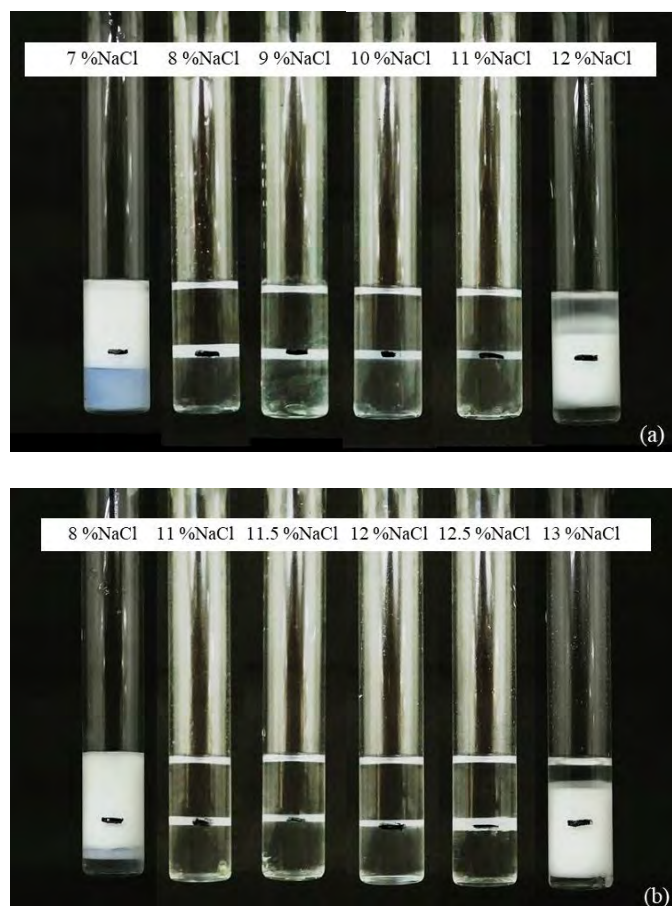
Figure C8 Salinity scan for 0.1 M C12-14EO5 with (a) Dodecane and (b) Hexadecane at 60 °C.
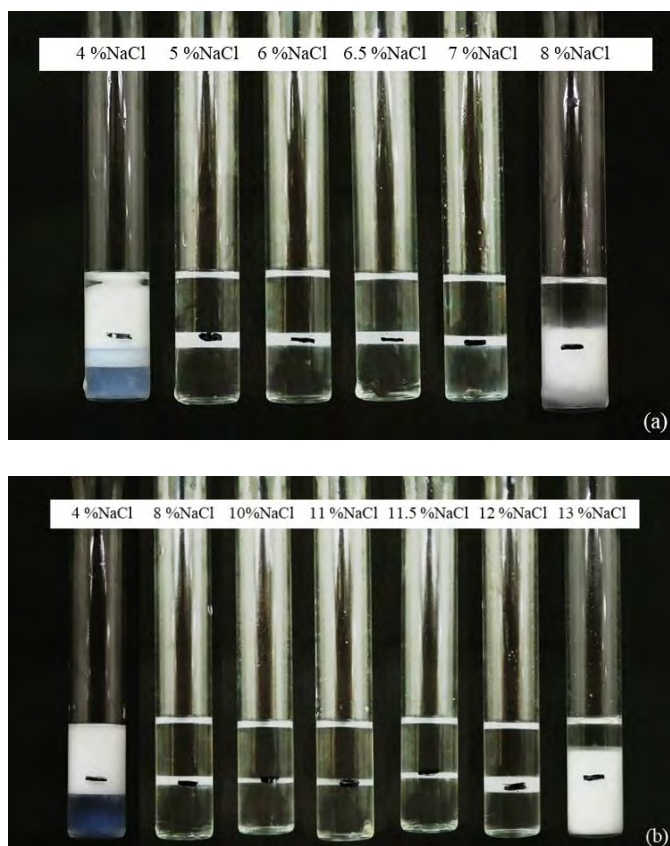
Figure C9 Salinity scan for 0.1 M C12-14EO5 with (a) Dodecane and (b) Hexadecane at 65 °C.
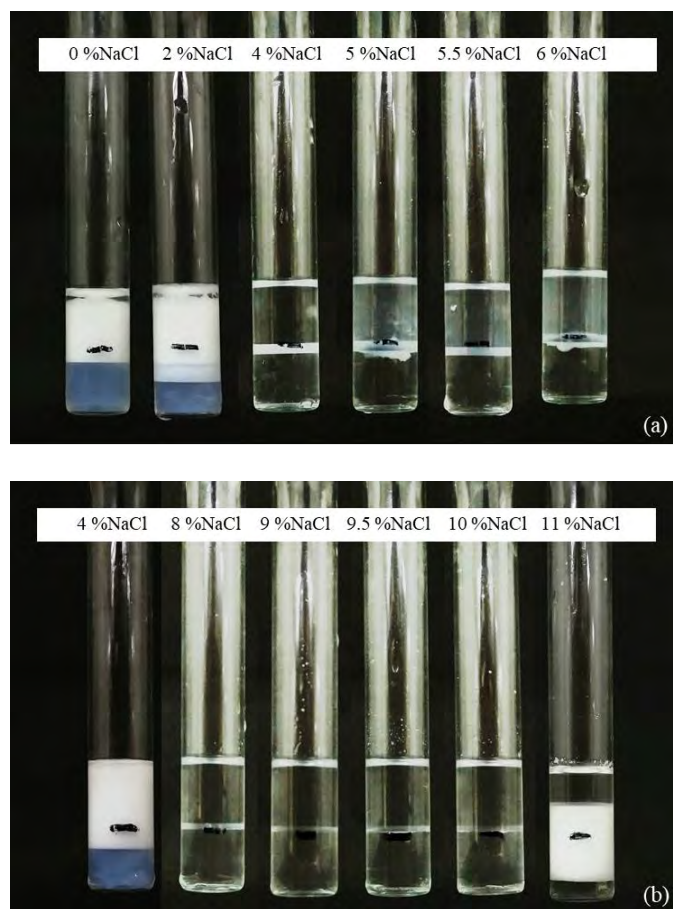
Figure C10 Salinity scan for 0.1 M C12-14EO5 with (a) Dodecane and (b) Hexadecane at 70 °C.
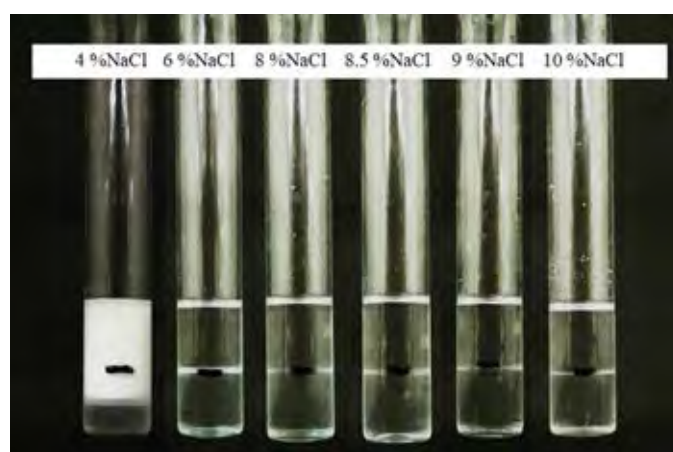
Figure C11 Salinity scan for 0.1 M C12-14EO5 with Hexadecane at 75 °C.
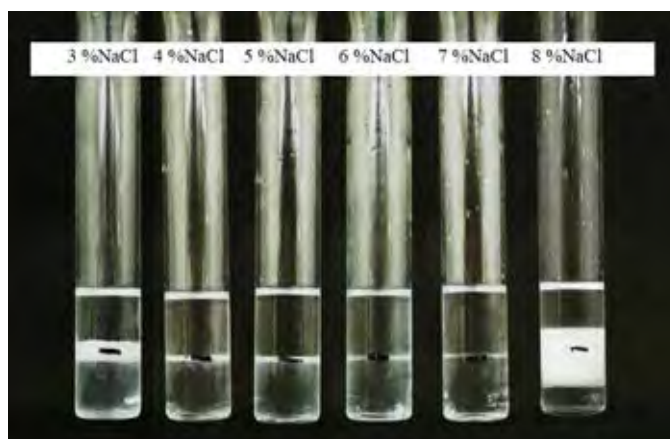
Figure C12 Salinity scan for 0.1 M C12-14EO5 with Hexadecane at 80 °C.
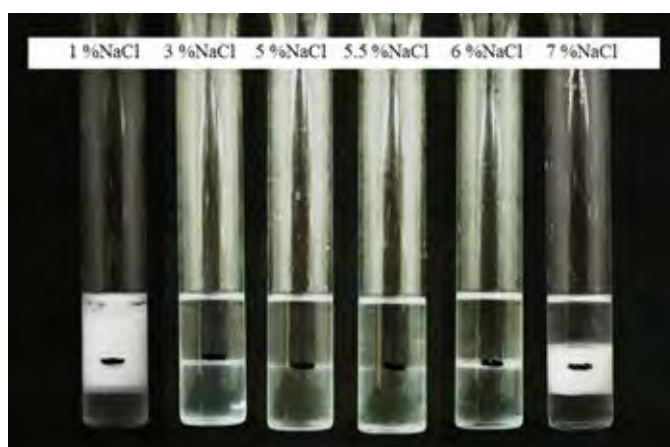
Figure C13 Salinity scan for 0.1 M C12-14EO5 with Hexadecane at 85 °C.
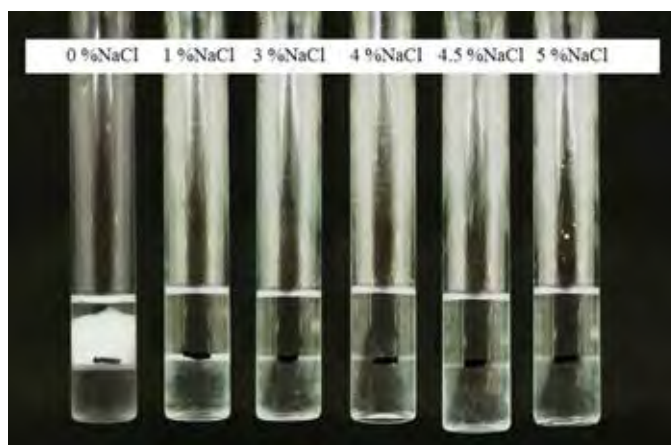
Figure C14 Salinity scan for 0.1 M C12-14EO5 with Hexadecane at 90 °C.

Figure C15 Salinity scan for 0.1 M C12-14EO5 with Hexadecane at 95 °C.

Appendix D Salinity Scan of C12-14EO9 for Single Surfactant System

The figures that show phase of C12-14EO9/oil/water system are presented in this part. The salinity scan is carried out in a range 0 – 26%wt/vol.
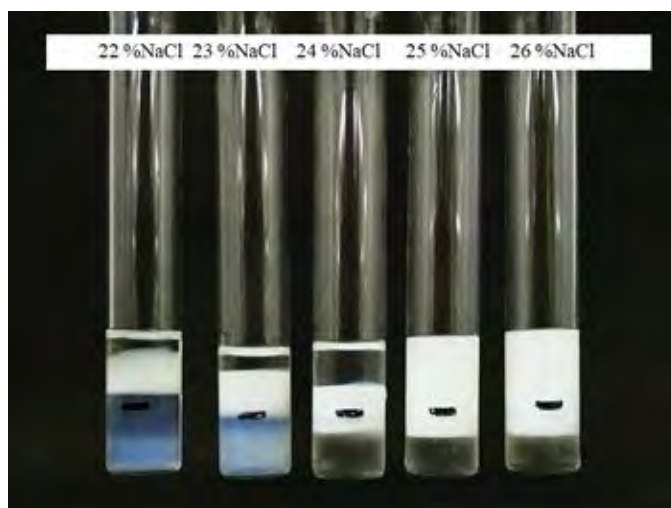
Figure D1 Salinity scan for 0.1 M C12-14EO9 with Cyclohexane at 25 °C.
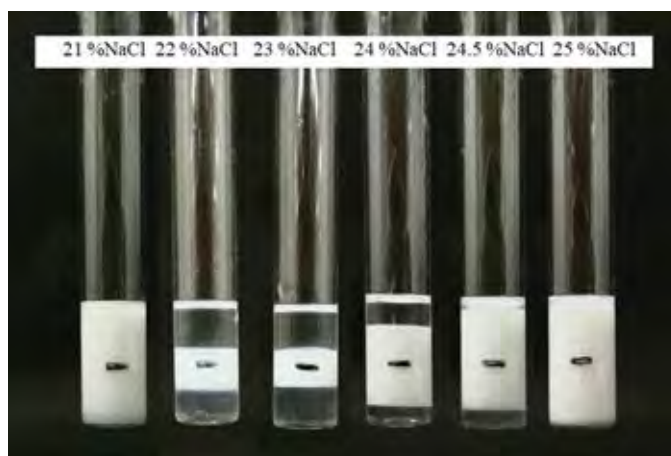
Figure D2 Salinity scan for 0.1 M C12-14EO9 with Decalin at 35 °C.
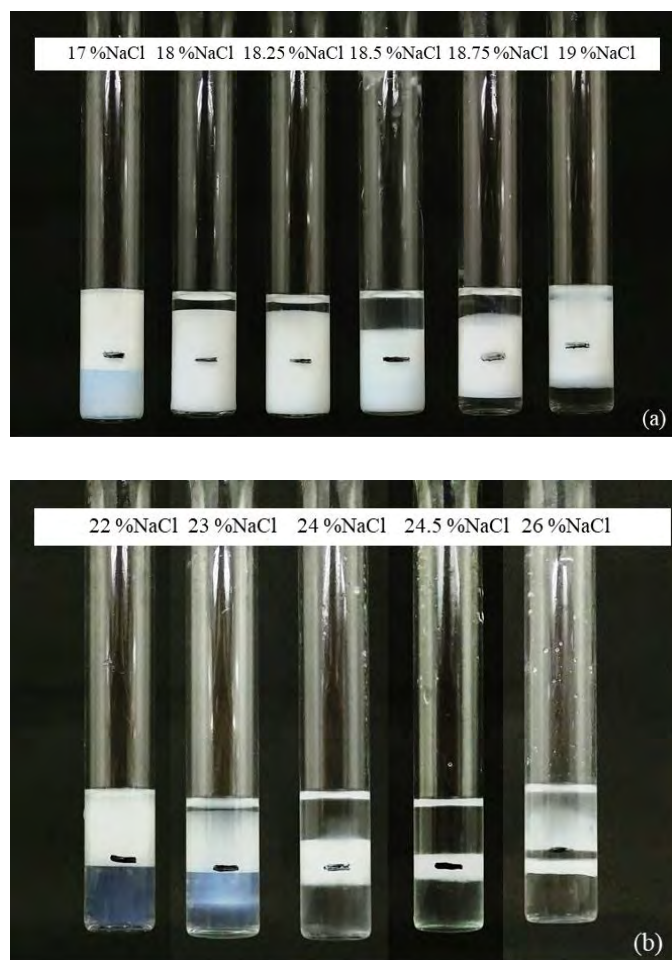
Figure D3 Salinity scan for 0.1 M C12-14EO9 with (a) Decalin and (b) Dodecane at 40 °C.
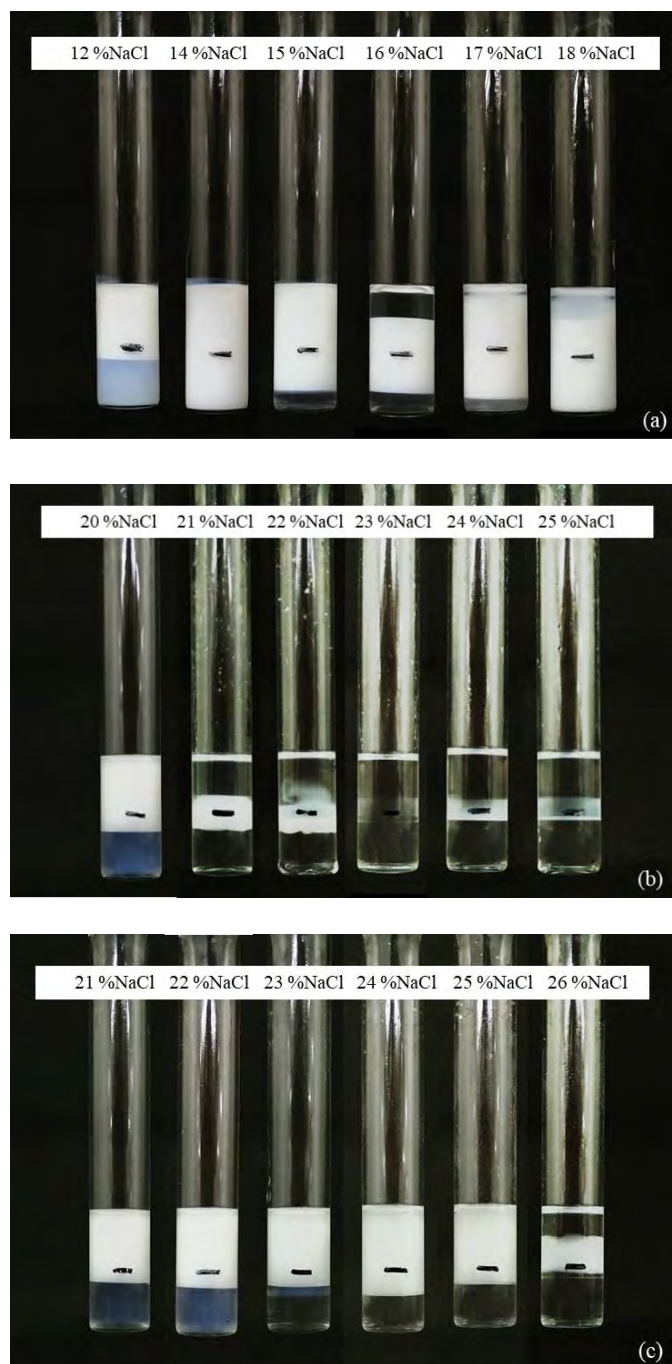
Figure D4 Salinity scan for 0.1 M C12-14EO9 with (a) Decalin, (b) Dodecane and (c) Hexadecane at 45 °C.
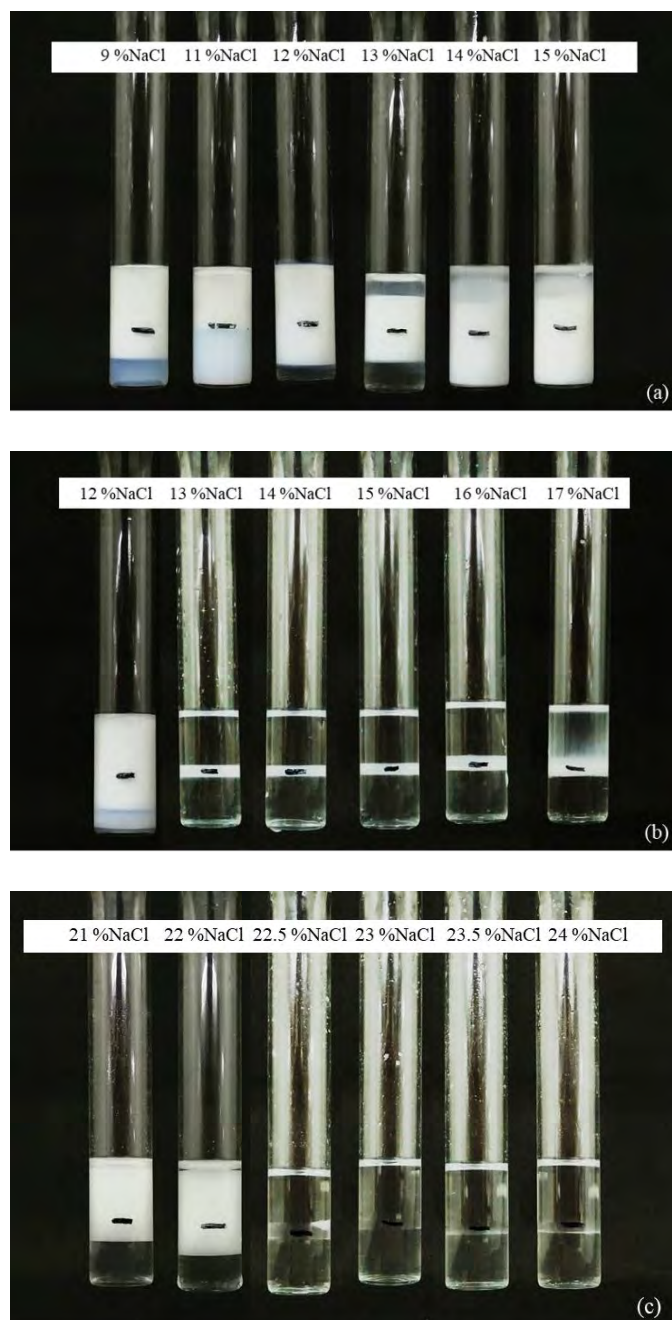
Figure D5 Salinity scan for 0.1 M C12-14EO9 with (a) Decalin, (b) Dodecane and (c) Hexadecane at 50 °C.
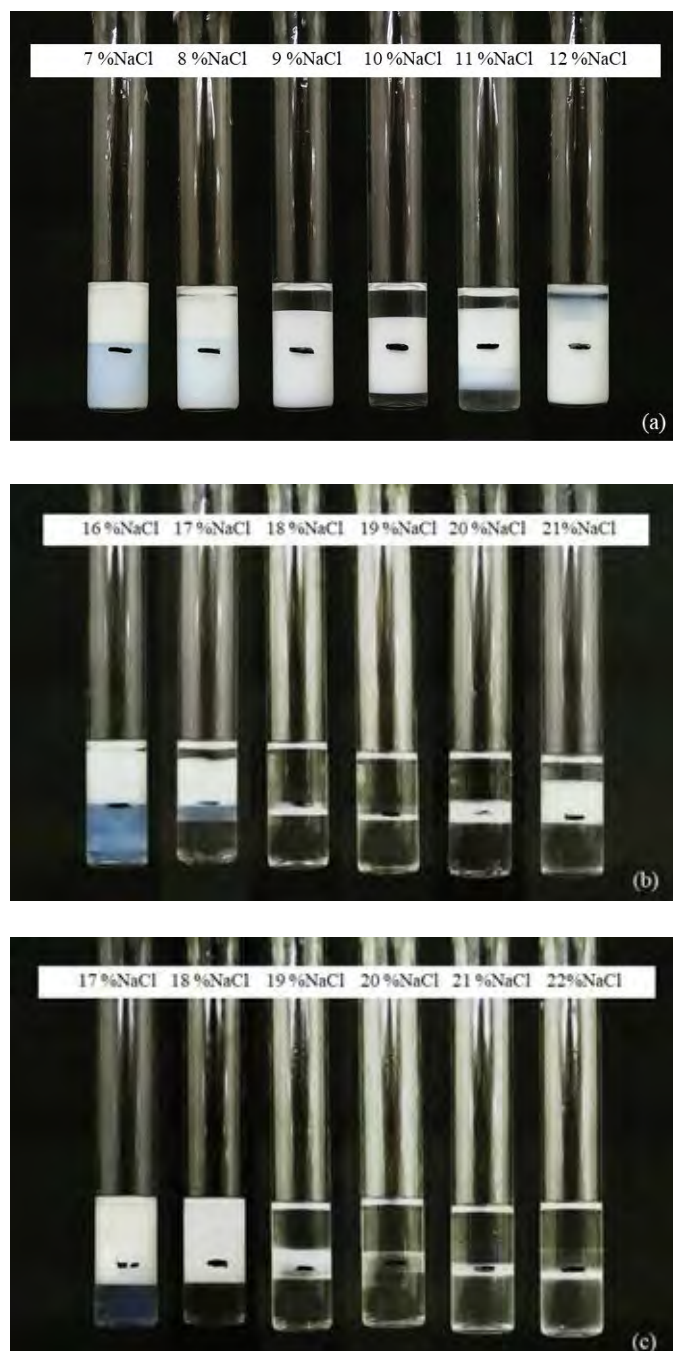
Figure D6 Salinity scan for 0.1 M C12-14EO9 with (a) Decalin, (b) Dodecane and (c) Hexadecane at 55 °C.
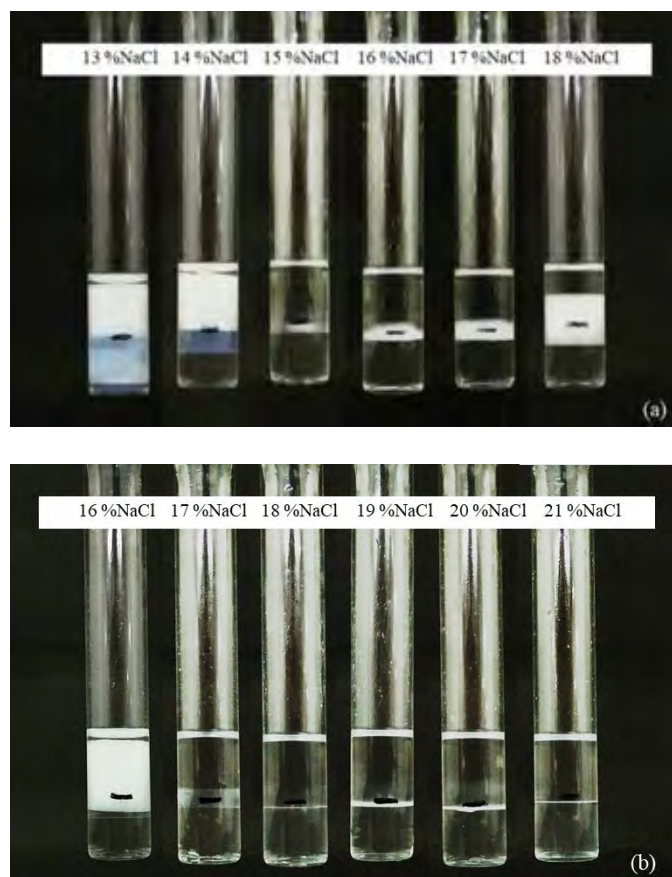
Figure D7 Salinity scan for 0.1 M C12-14EO9 with (a) Dodecane and (b) Hexadecane at 60 °C.
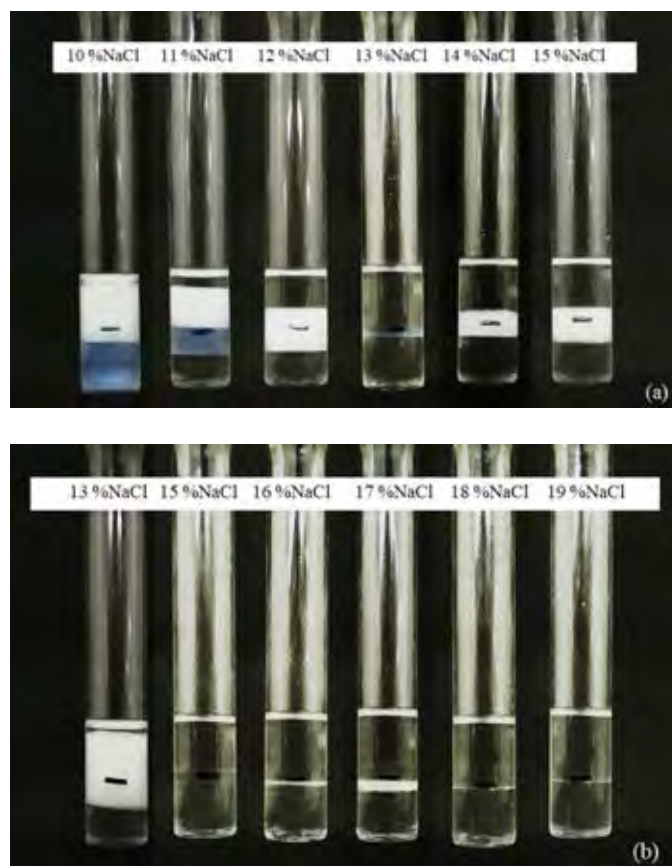
Figure D8 Salinity scan for 0.1 M C12-14EO9 with (a) Dodecane and (b) Hexadecane at 65 °C.
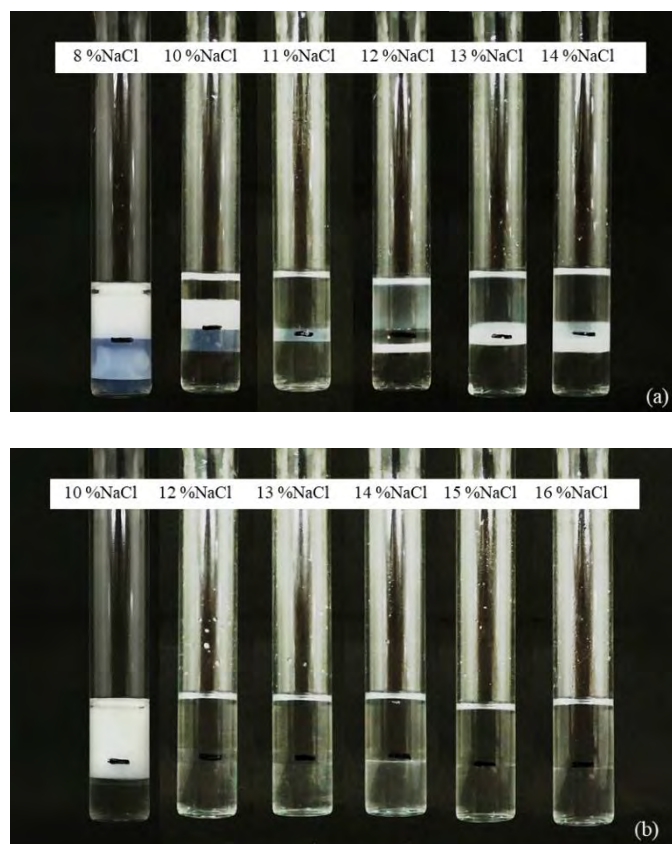
Figure D9 Salinity scan for 0.1 M C12-14EO9 with (a) Dodecane and (b) Hexadecane at 70 °C.

Figure D10 Salinity scan for 0.1 M C12-14EO9 with Hexadecane at 75 °C.

Figure D11 Salinity scan for 0.1 M C12-14EO9 with Hexadecane at 80 °C.
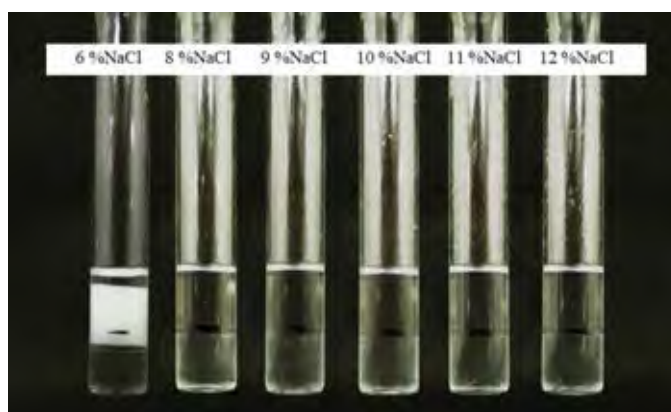
Figure D12 Salinity scan for 0.1 M C12-14EO9 with Hexadecane at 85 °C.
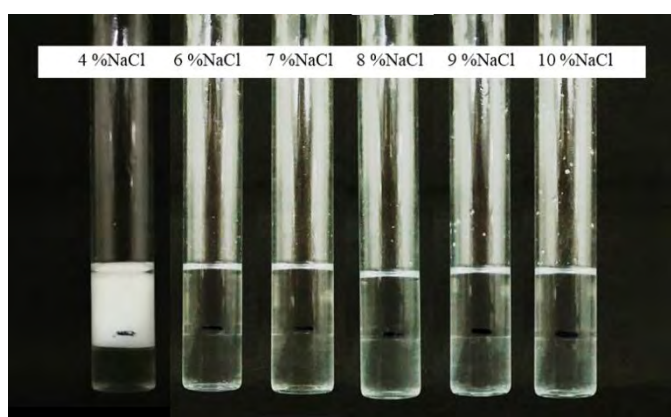
Figure D13 Salinity scan for 0.1 M C12-14EO9 with Hexadecane at 90 °C.
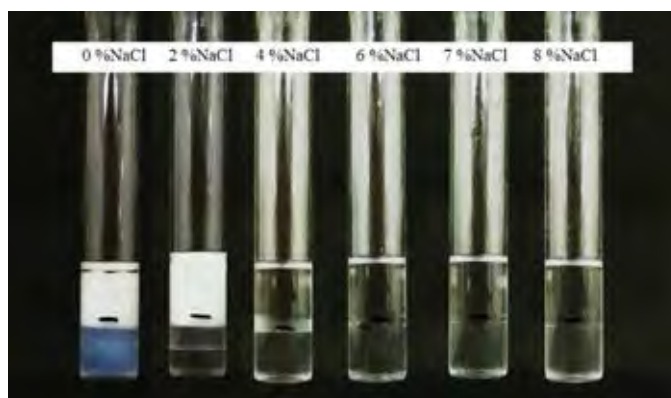
Figure D14 Salinity scan for 0.1 M C12-14EO9 with Hexadecane at 95 °C.

Appendix E Salinity Scan of Nonionic Surfactant for Mixed Surfactant System

The figures that show phase of mixed surfactant system are presented in this part. The salinity scan is carried out in a range 0 – 26%wt/vol and the mol fraction of test surfactant in mixed solution is carried out in a range 0.1-0.9. The reference surfactants are C12-14EO3, C12-14EO5 and C12-14EO9, mixed with test surfactants; C12-14EO1, C12-14EO2, C12-14EO12, C16-18PO2EO4 and C16-18PO4EO6 at room temperature.
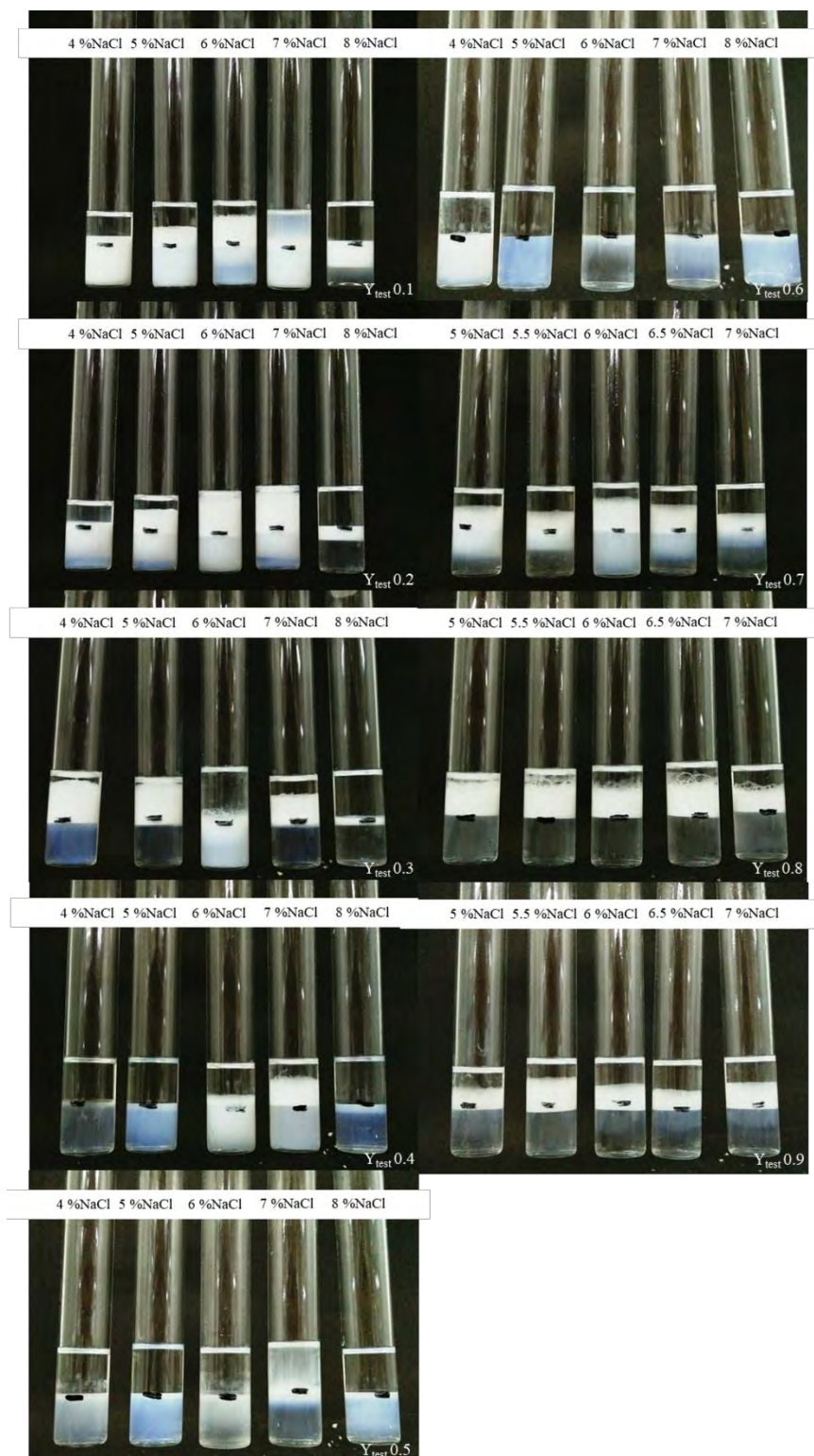
Figure E1 Salinity scan of mixed C12-14EO3 and C12-14EO1 with Cyclohexane.
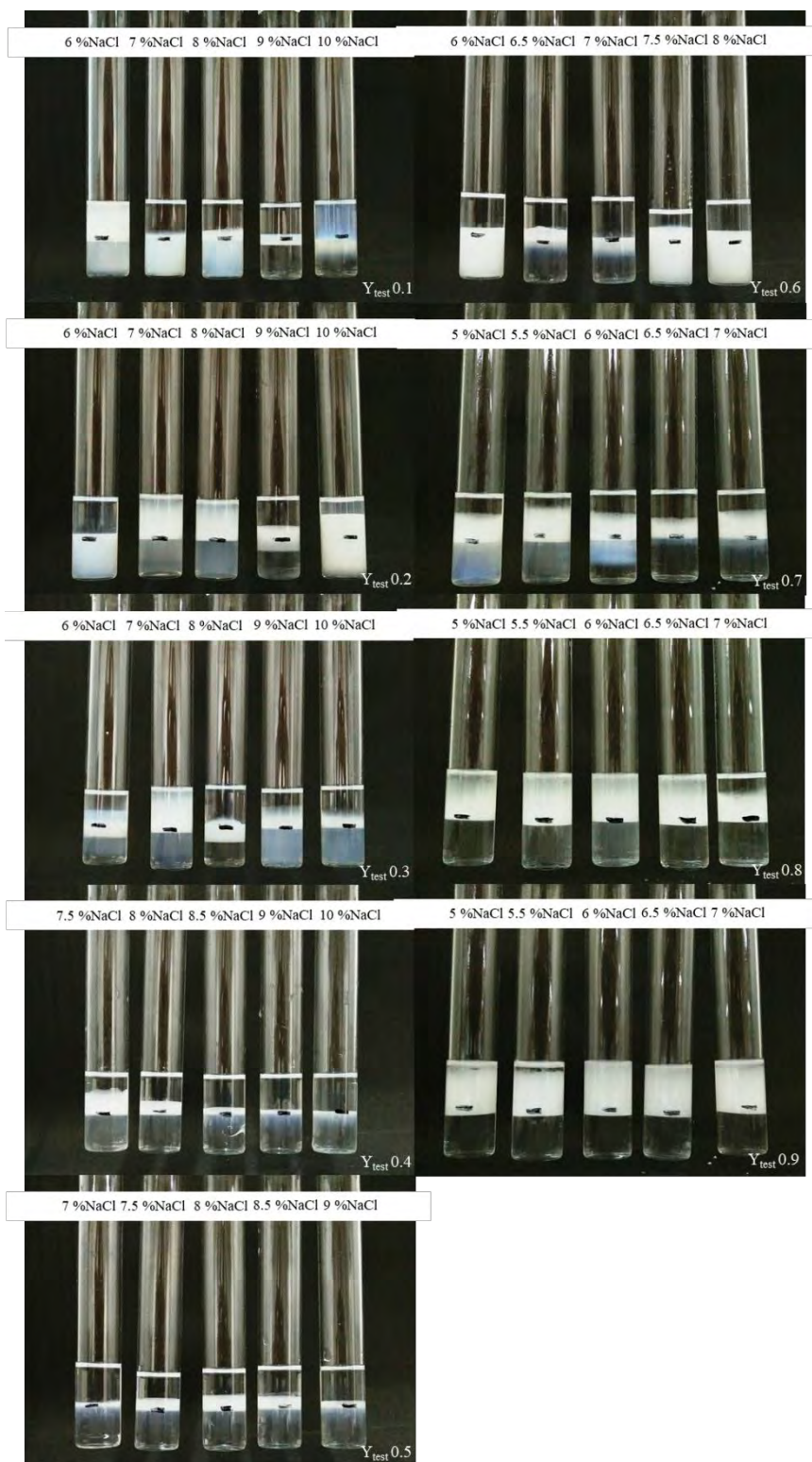
Figure E2 Salinity scan of mixed C12-14EO3 and C12-14EO1 with Heptane.

Figure E3 Salinity scan of mixed C12-14EO3 and C12-14EO1 with Decalin.

Figure E4 Salinity scan of mixed C12-14EO3 and C12-14EO2 with Cyclohexane.
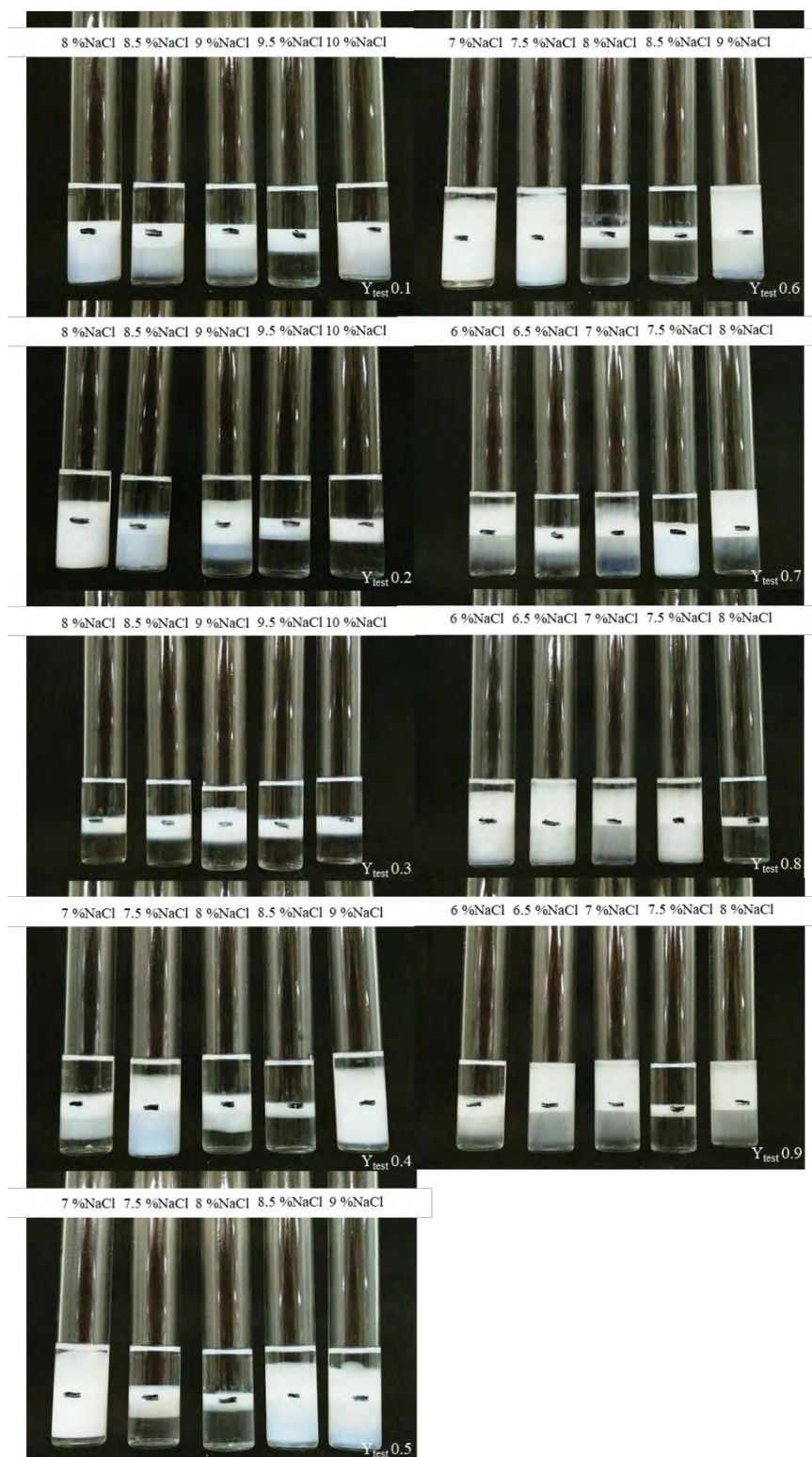
Figure E5 Salinity scan of mixed C12-14EO3 and C12-14EO2 with Heptane.
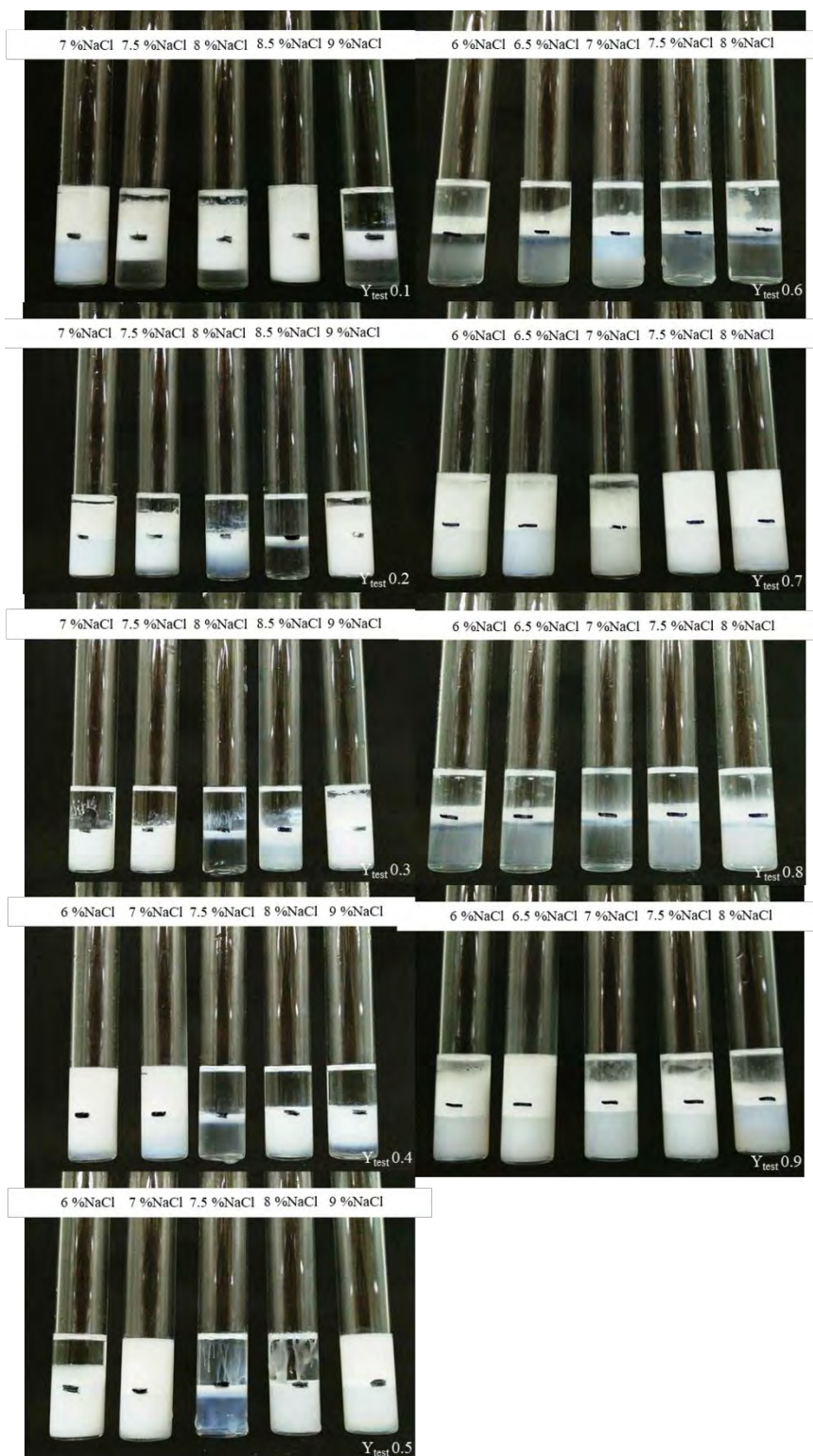
Figure E6 Salinity scan of mixed C12-14EO3 and C12-14EO2 with Decalin.
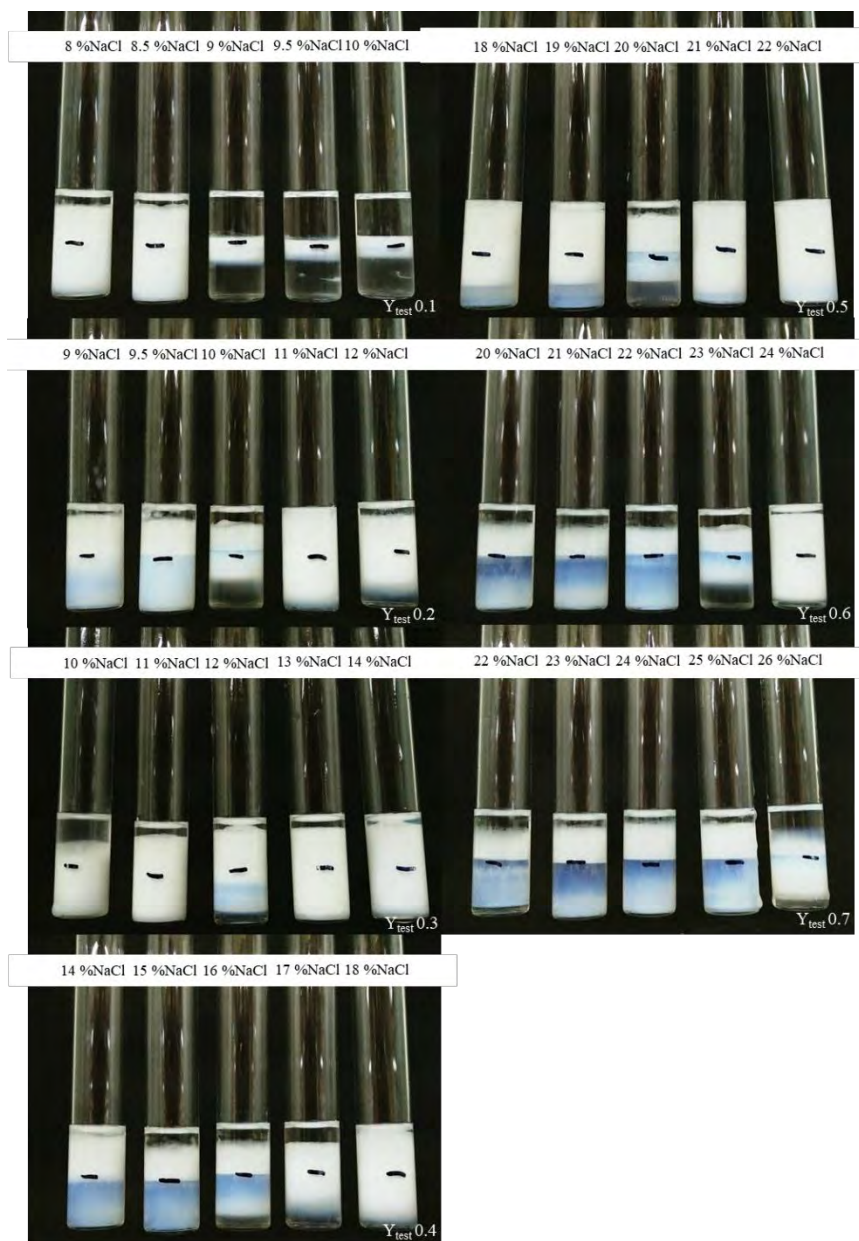
Figure E7 Salinity scan of mixed C12-14EO3 and C12-14EO12 with Cyclohexane.
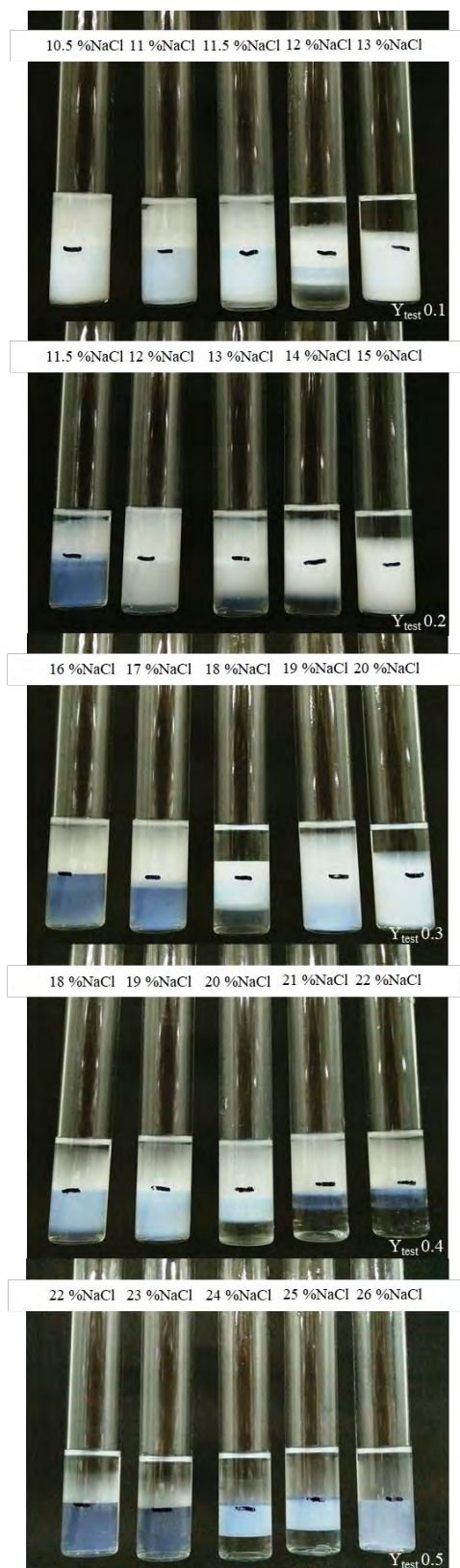
Figure E8 Salinity scan of mixed C12-14EO3 and C12-14EO12 with Heptane.
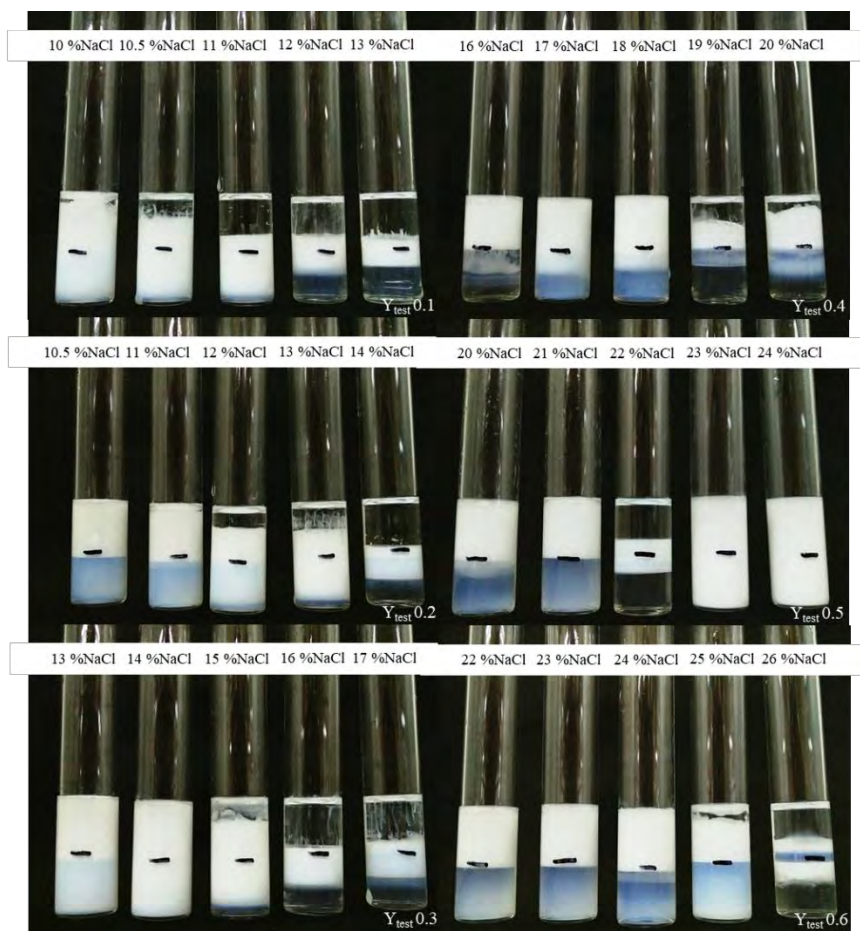
Figure E9 Salinity scan of mixed C12-14EO3 and C12-14EO12 with Decalin.
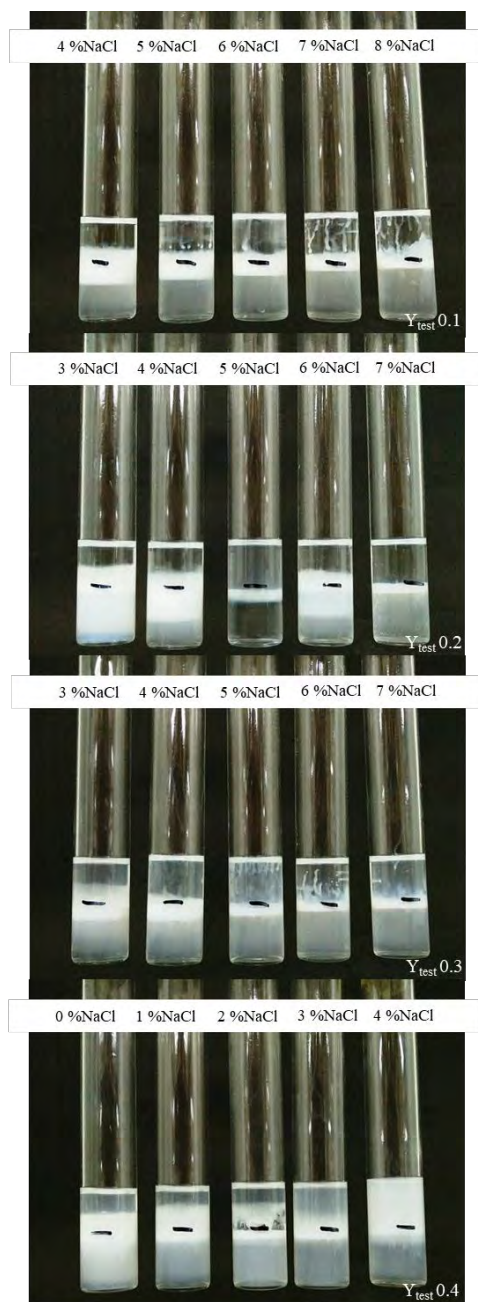
Figure E10 Salinity scan of mixed C12-14EO3 and C16-18PO2EO4 with Cyclohexane.
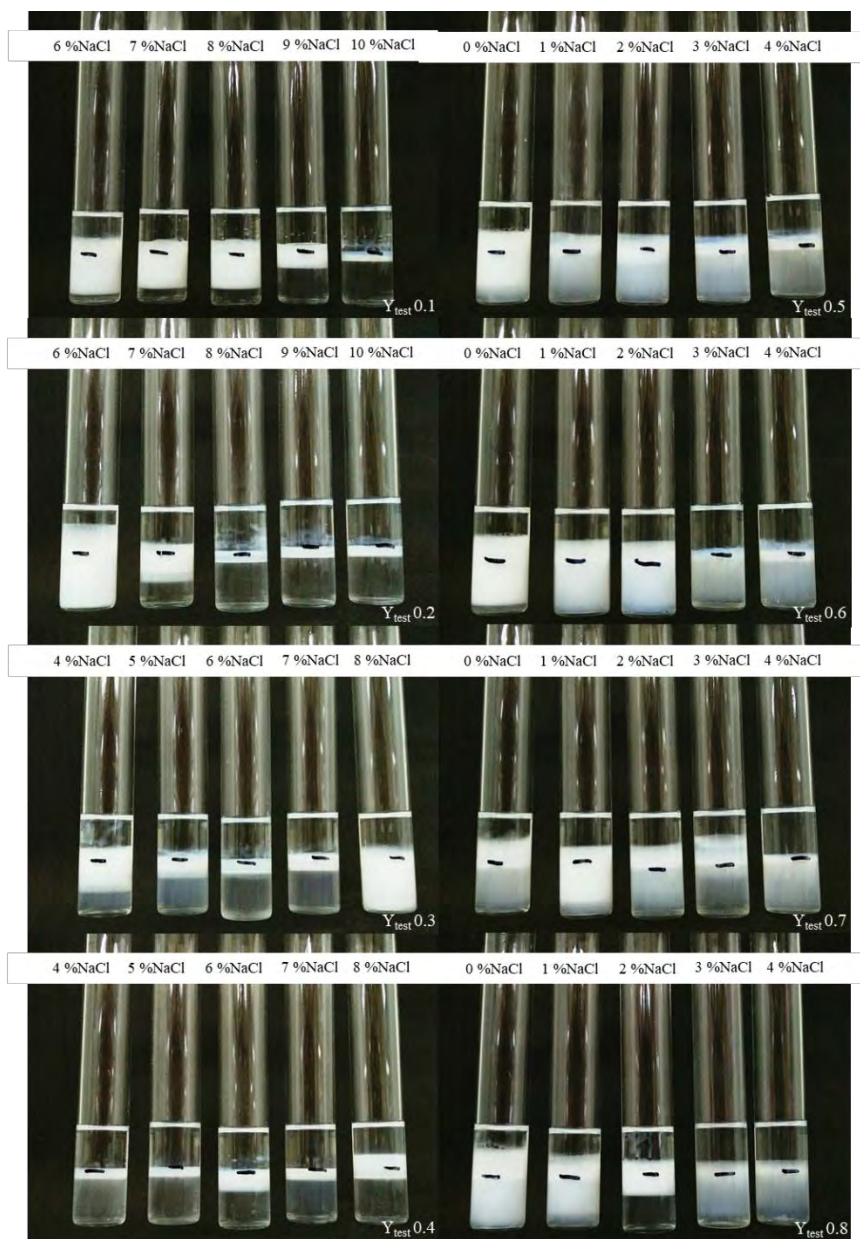
Figure E11 Salinity scan of mixed C12-14EO3 and C16-18PO2EO4 with Heptane.

Figure E12 Salinity scan of mixed C12-14EO3 and C16-18PO2EO4 with Decalin.
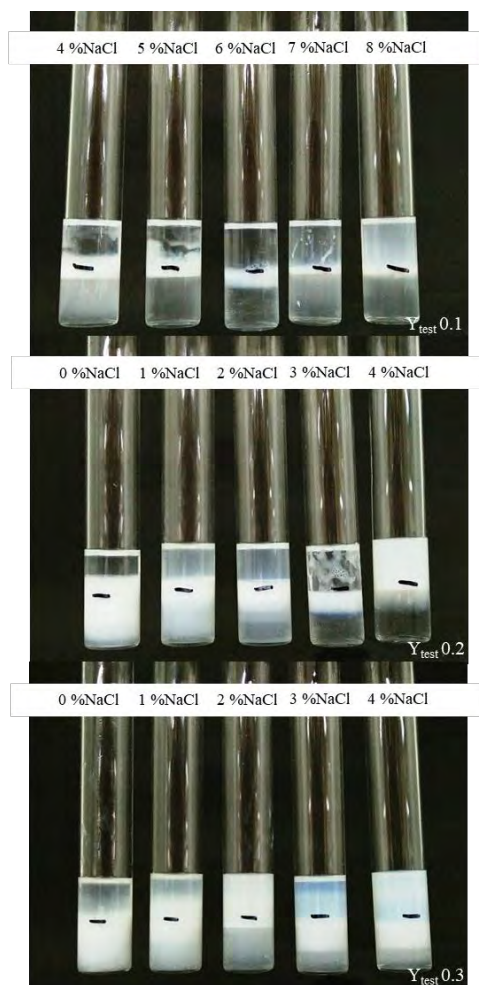
Figure E13   Salinity scan of mixed C12-14EO3 and C16-18PO4EO6 with Cyclohexane.
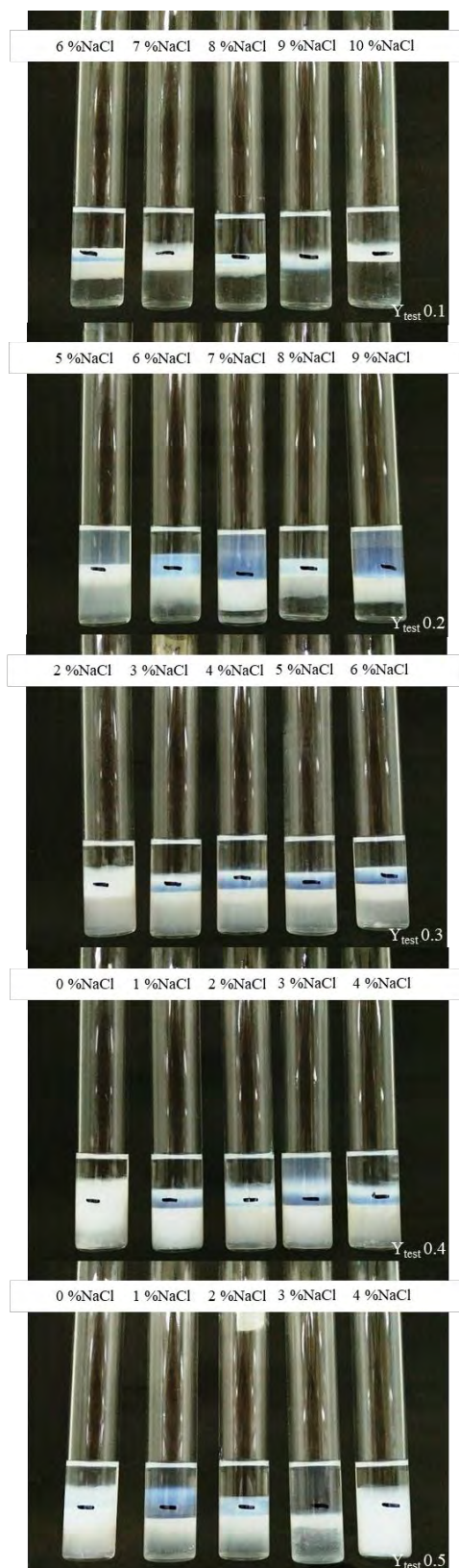
Figure E14 Salinity scan of mixed C12-14EO3 and C16-18PO4EO6 with Heptane.
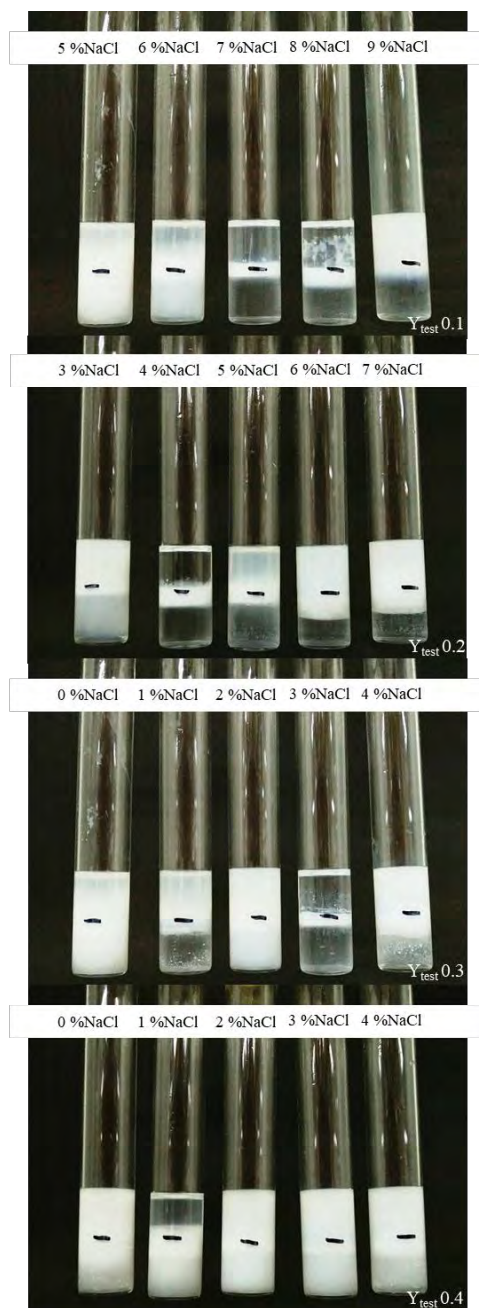
Figure E15 Salinity scan of mixed C12-14EO3 and C16-18PO4EO6 with Decalin.
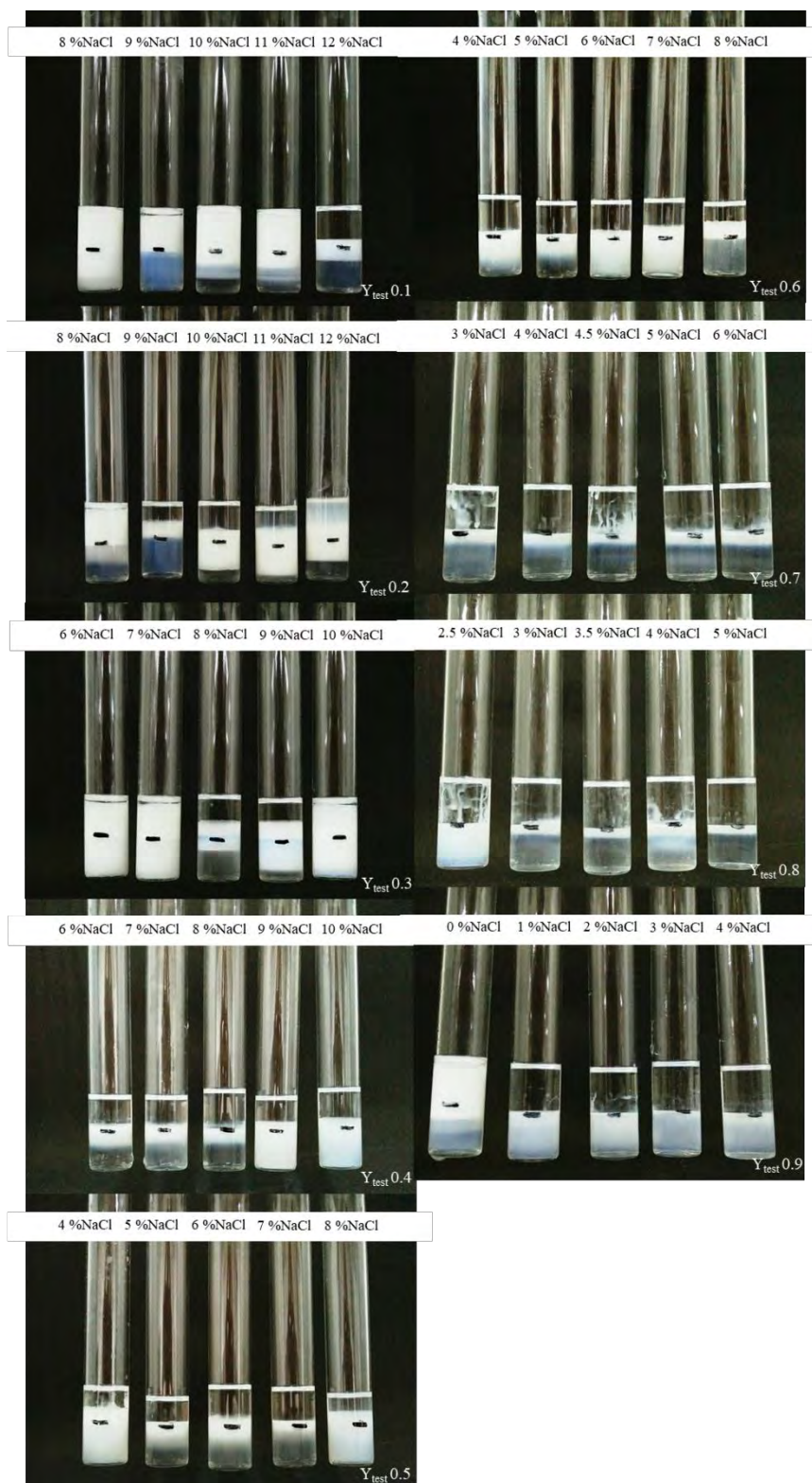
Figure E16 Salinity scan of mixed C12-14EO5 and C12-14EO1 with Cyclohexane.
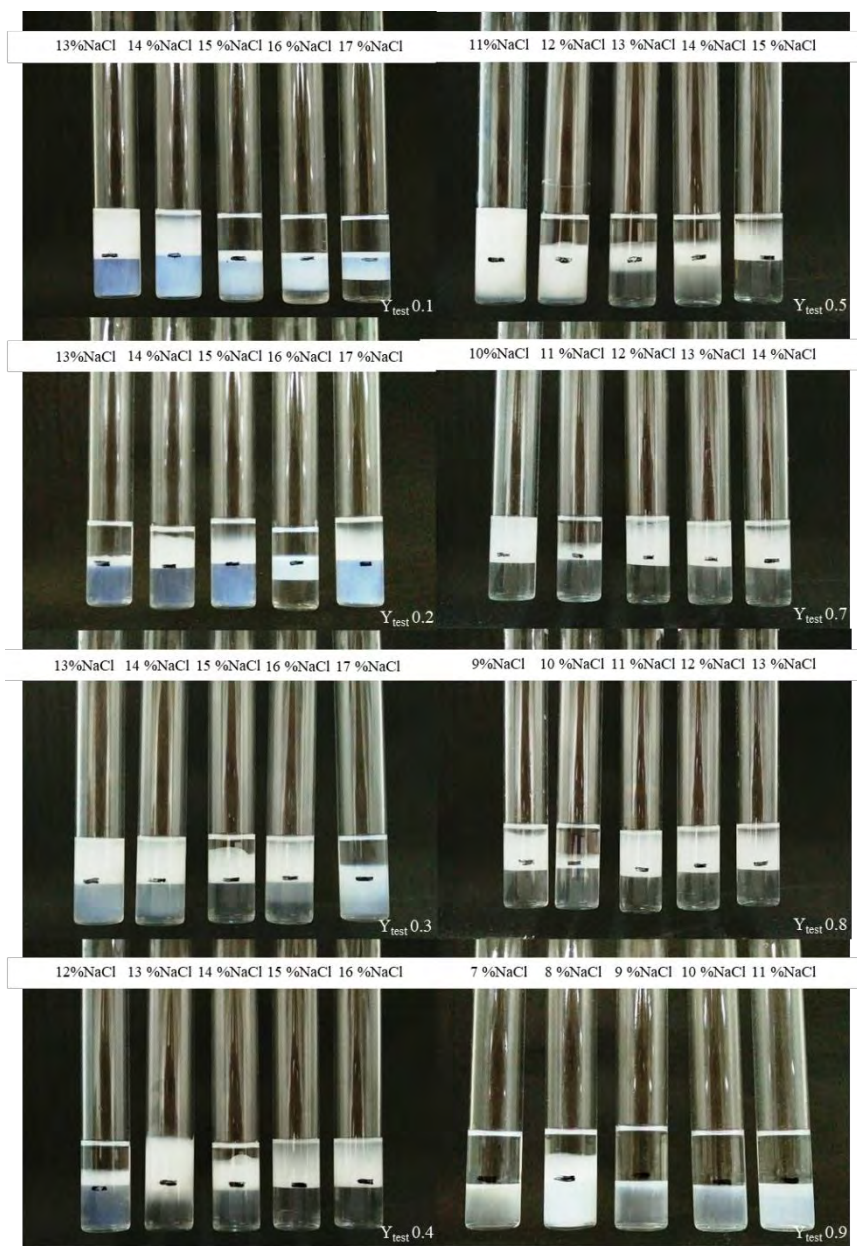
Figure E17 Salinity scan of mixed C12-14EO5 and C12-14EO1 with Heptane.
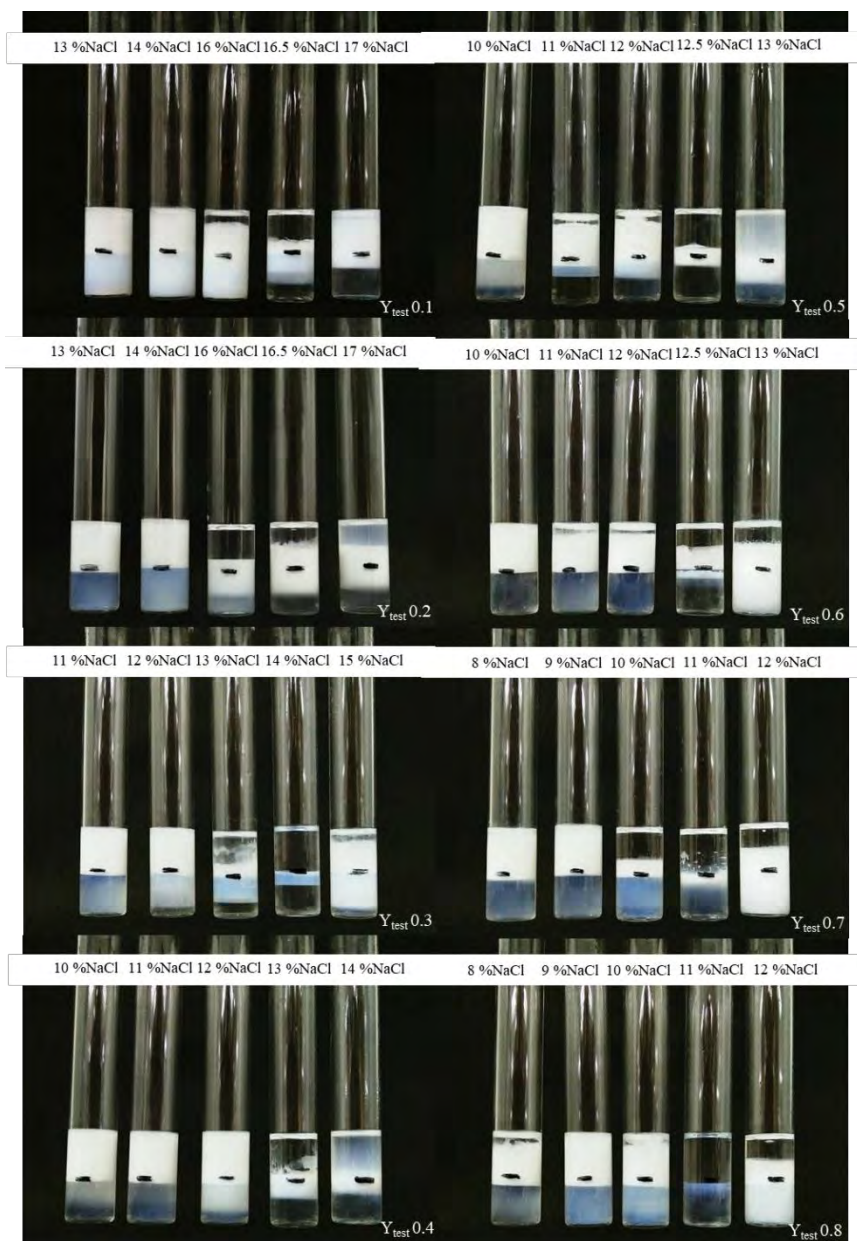
Figure E18 Salinity scan of mixed C12-14EO5 and C12-14EO1 with Decalin.

Figure E19 Salinity scan of mixed C12-14EO5 and C12-14EO2 with Cyclohexane.
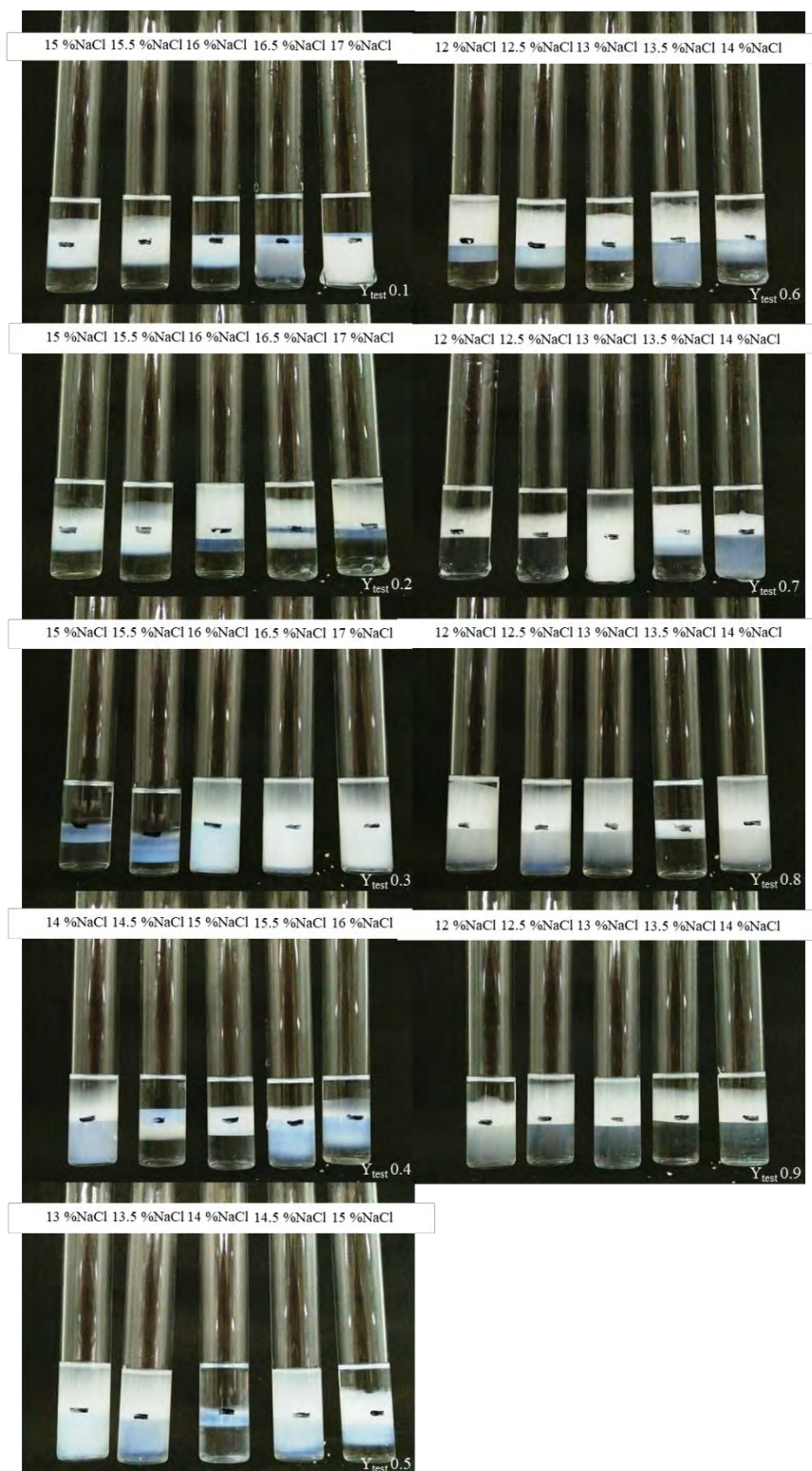
Figure E20 Salinity scan of mixed C12-14EO5 and C12-14EO2 with Heptane.

Figure E21 Salinity scan of mixed C12-14EO5 and C12-14EO2 with Decalin.
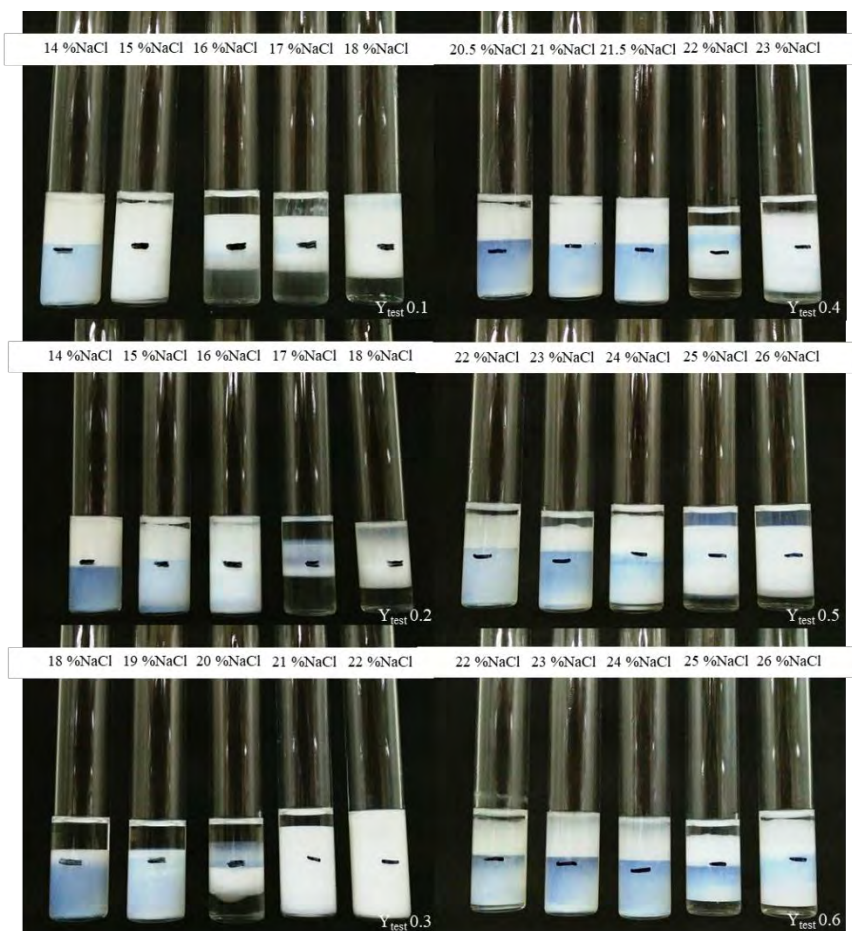
Figure E22 Salinity scan of mixed C12-14EO5 and C12-14EO12 with Cyclohexane.
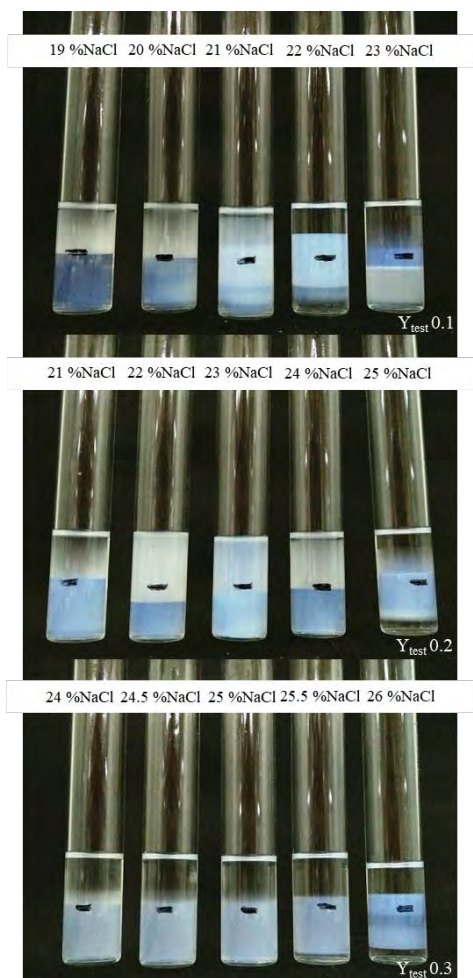
Figure E23 Salinity scan of mixed C12-14EO5 and C12-14EO12 with Heptane.
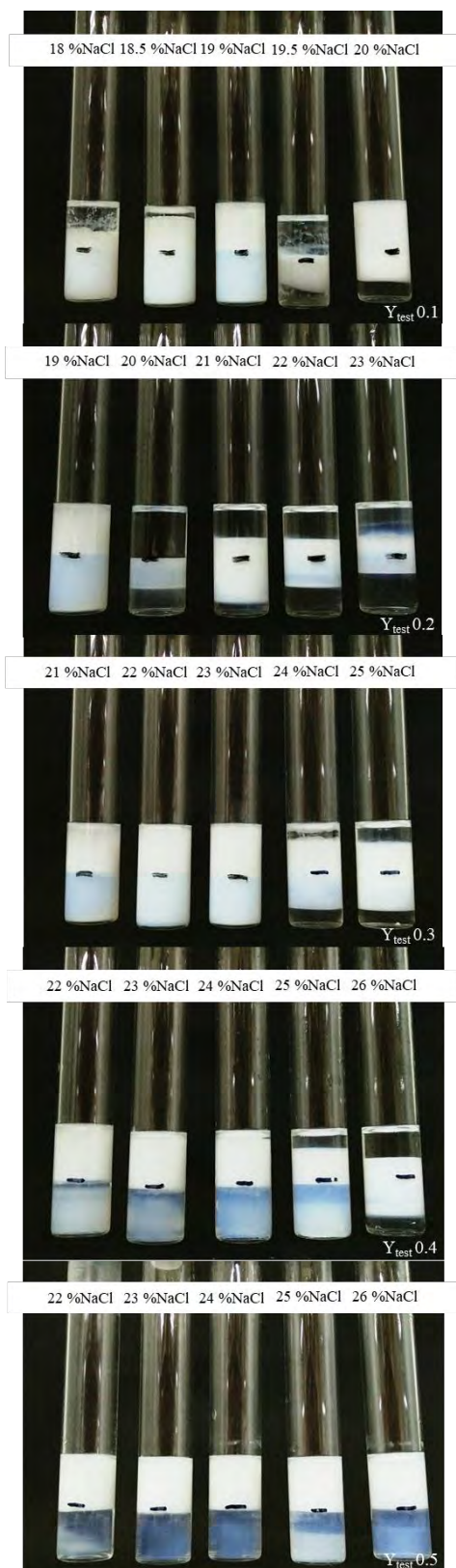
Figure E24 Salinity scan of mixed C12-14EO5 and C12-14EO12 with Decalin.
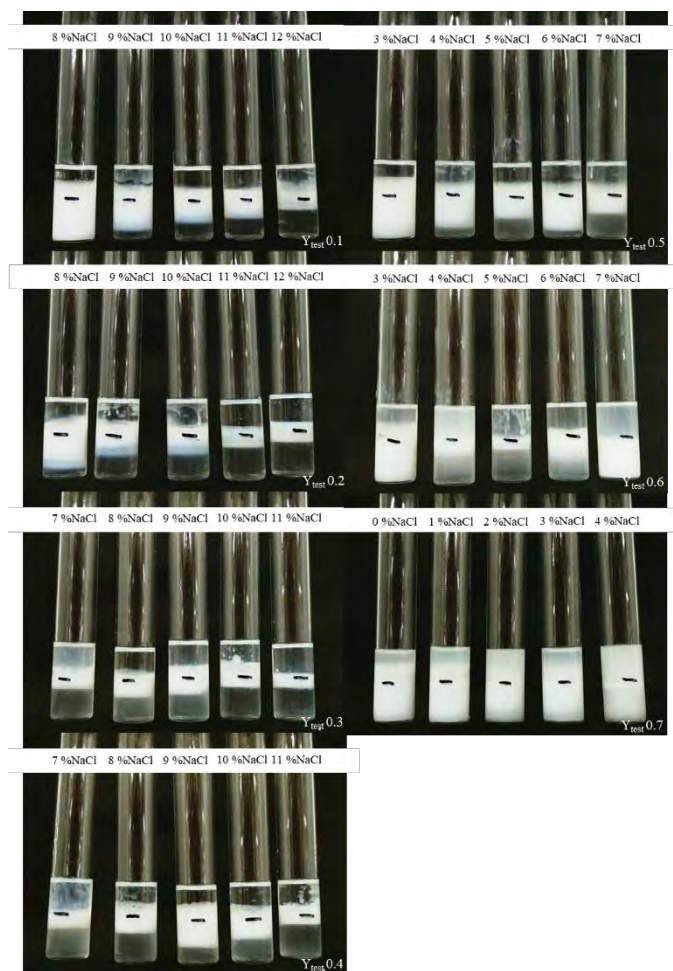
Figure E25 Salinity scan of mixed C12-14EO5 and C16-18PO2EO4 with Cyclohexane.

Figure E26 Salinity scan of mixed C12-14EO5 and C16-18PO2EO4 with Heptane.
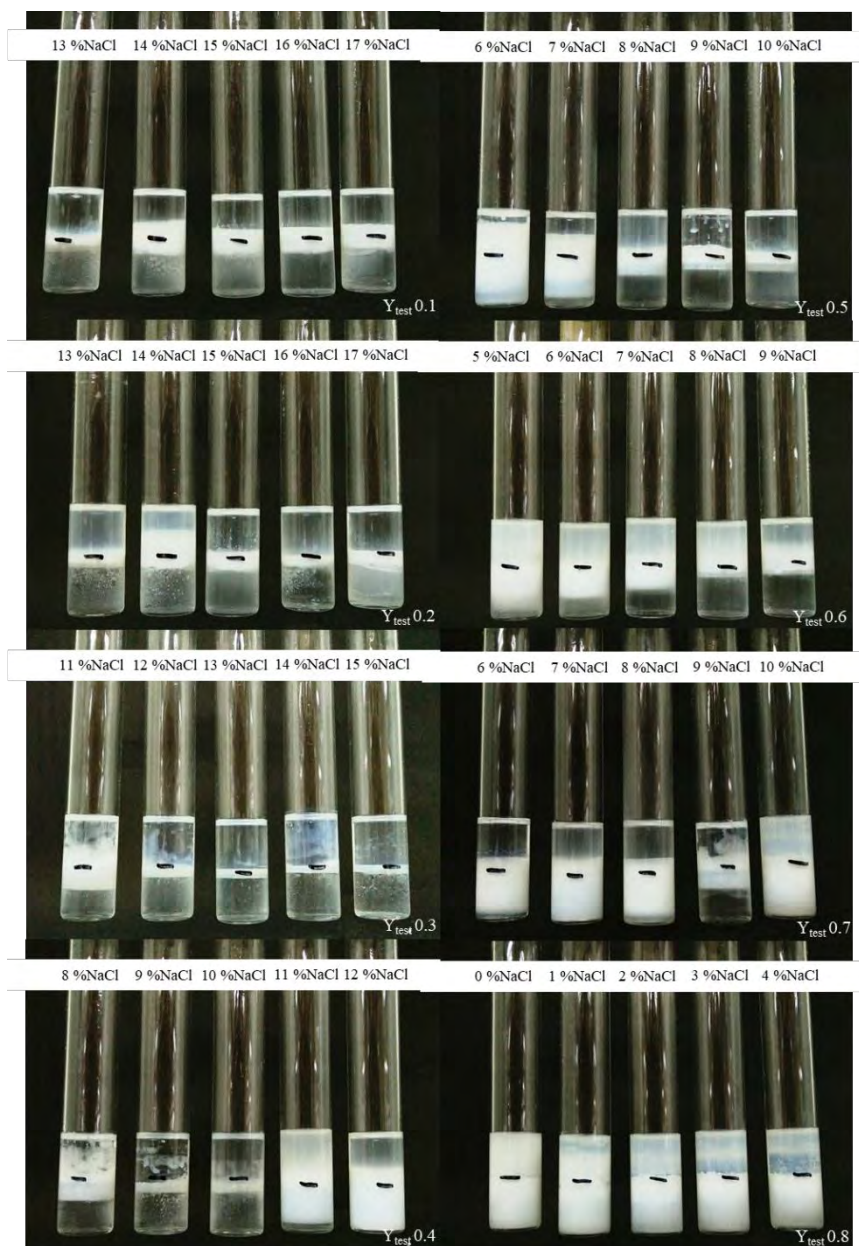
Figure E27 Salinity scan of mixed C12-14EO5 and C16-18PO2EO4 with Decalin.

Figure E28 Salinity scan of mixed C12-14EO5 and C16-18PO4EO6 with Cyclohexane.
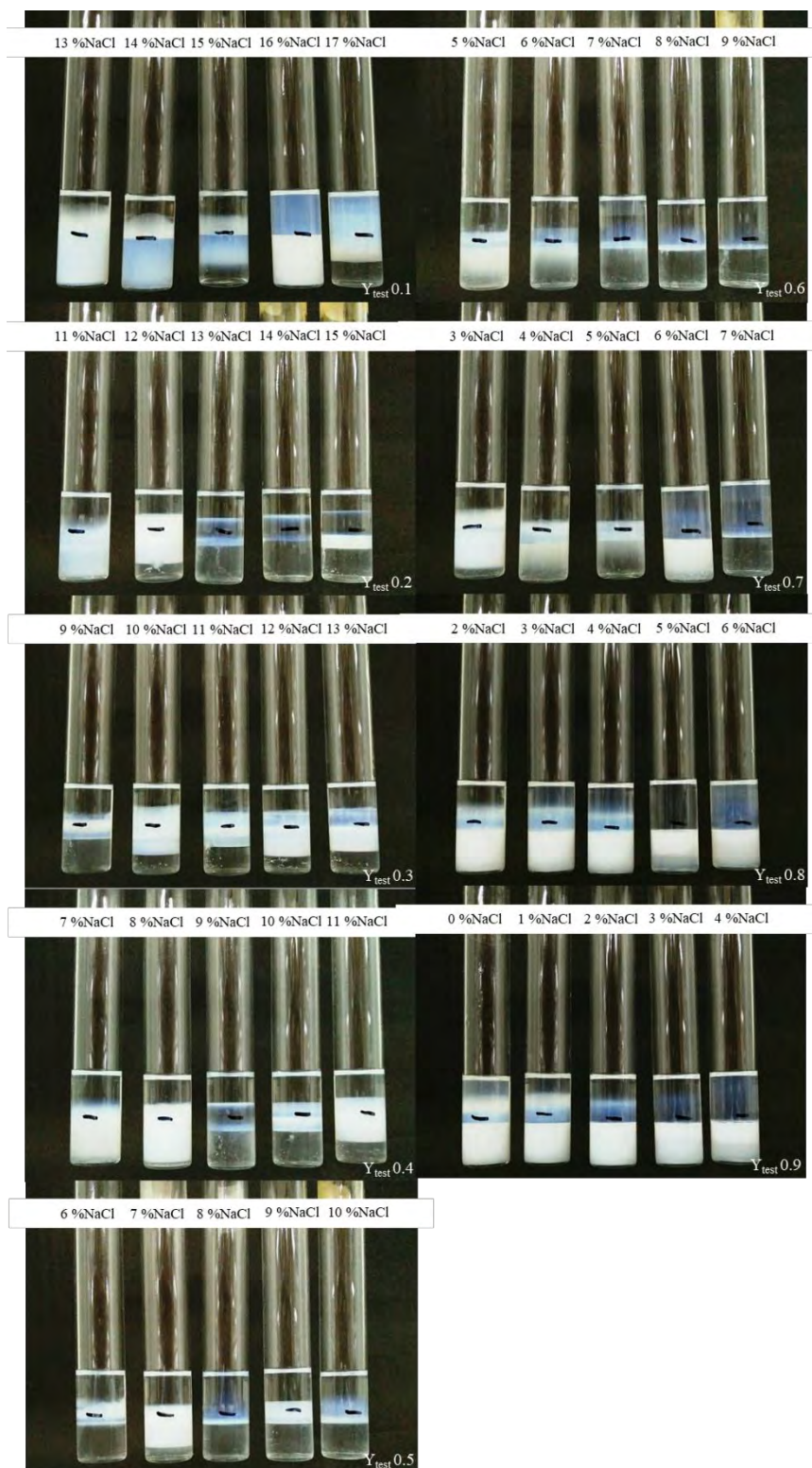
Figure E29 Salinity scan of mixed C12-14EO5 and C16-18PO4EO6 with Heptane.
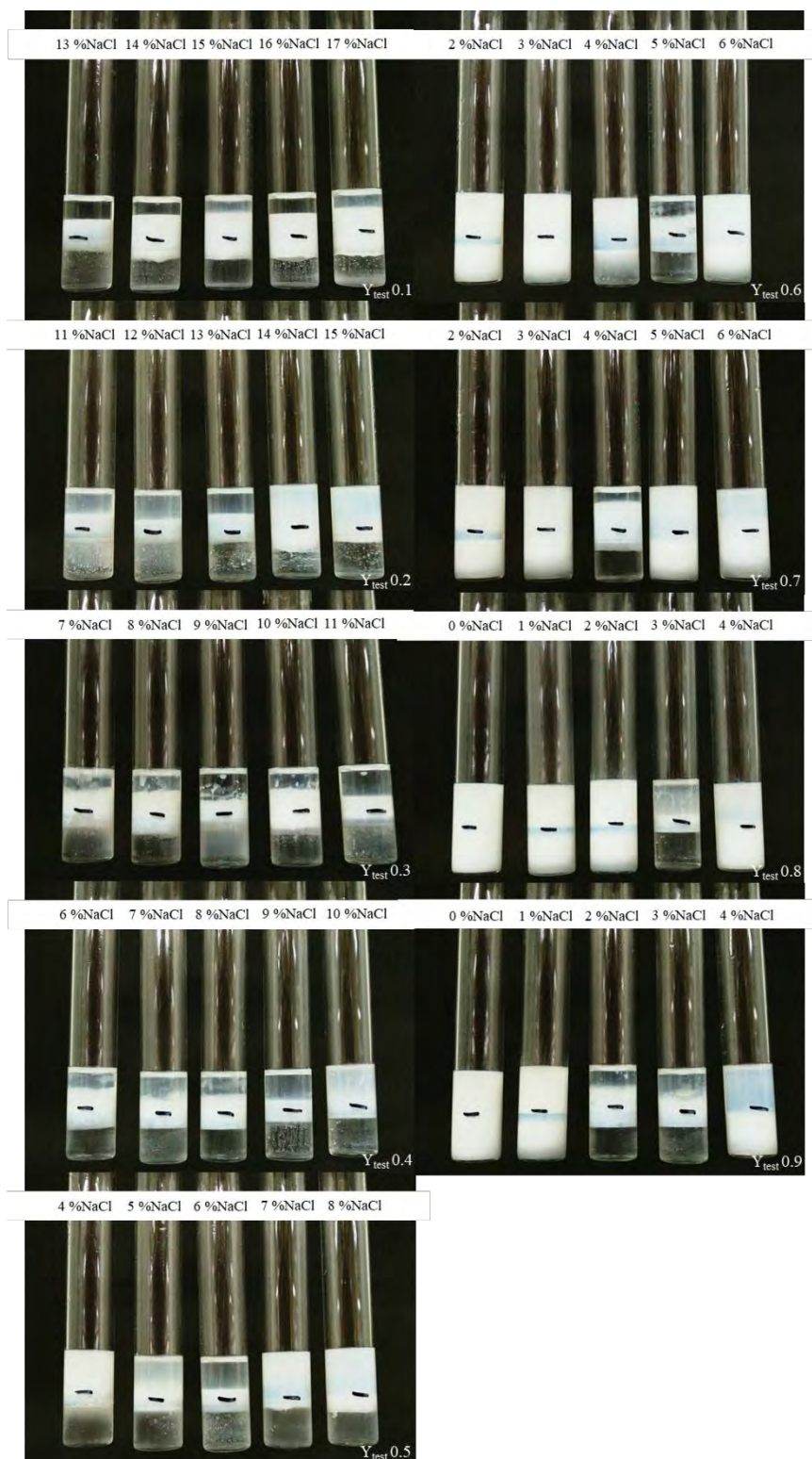
Figure E30 Salinity scan of mixed C12-14EO5 and C16-18PO4EO6 with Decalin.
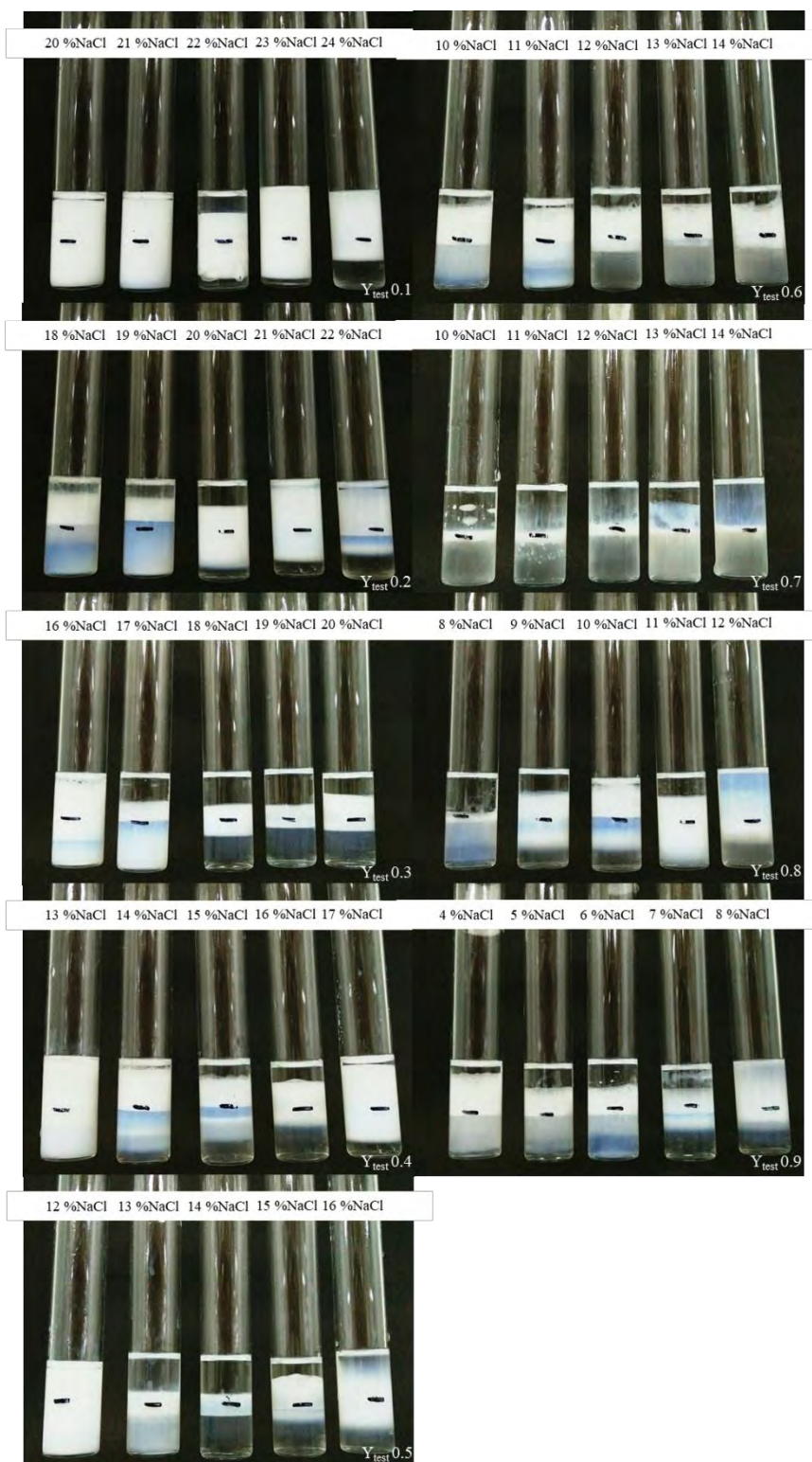
Figure E31 Salinity scan of mixed C12-14EO9 and C12-14EO1 with Cyclohexane.
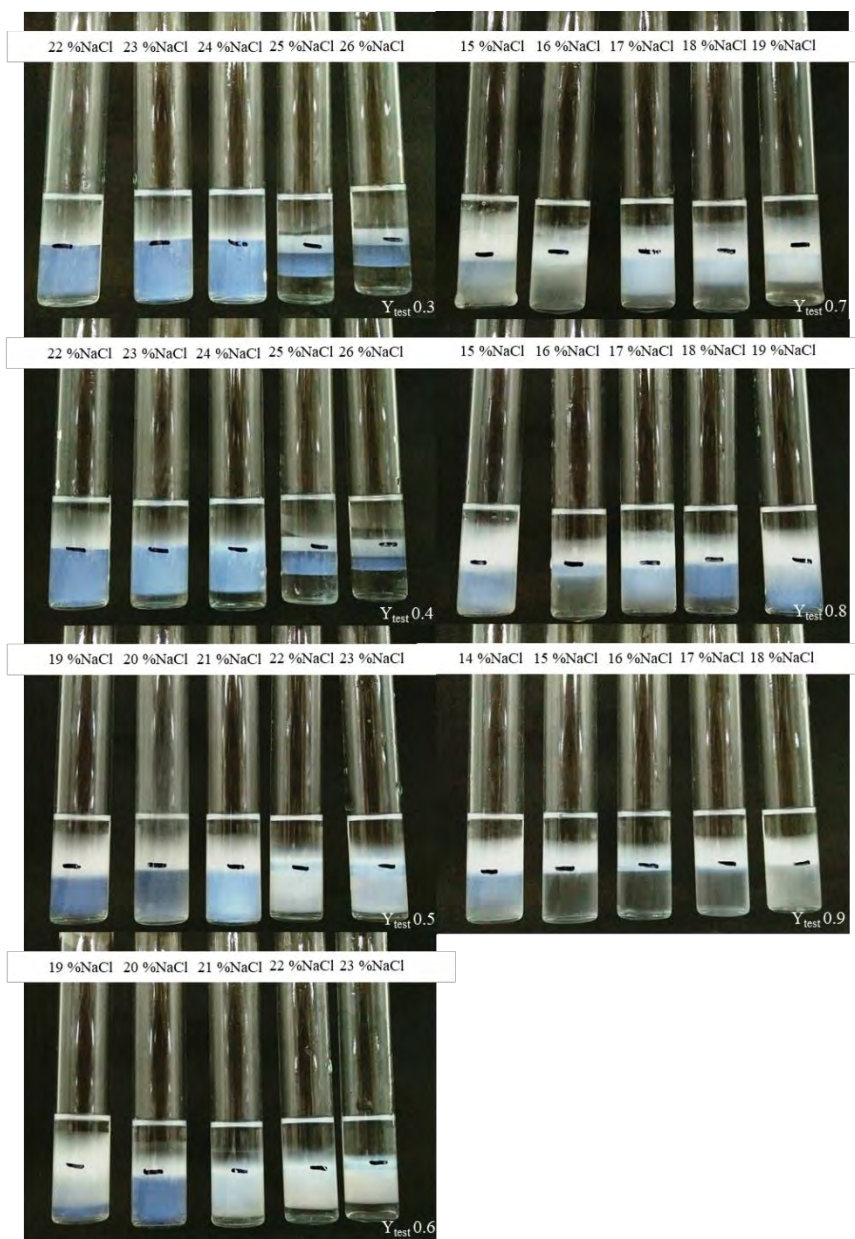
Figure E32 Salinity scan of mixed C12-14EO9 and C12-14EO1 with Heptane.
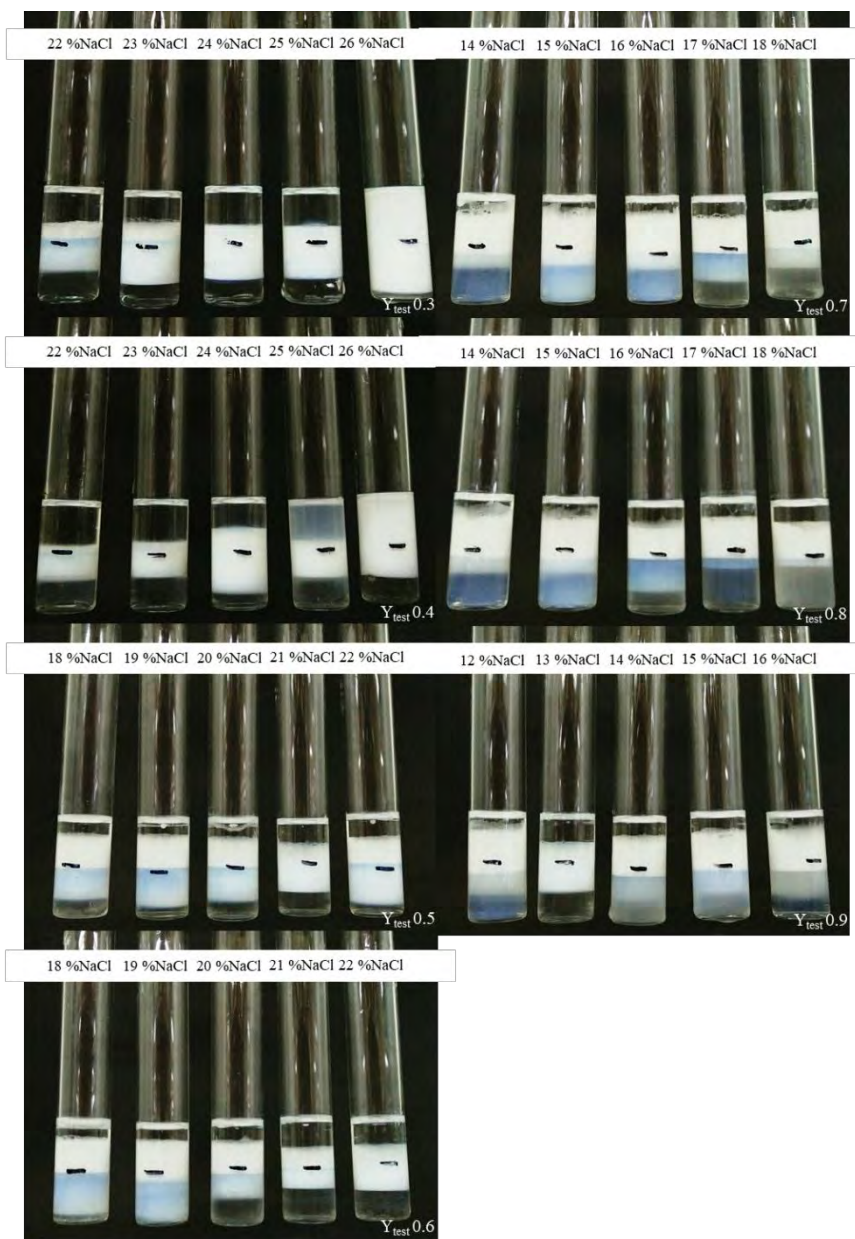
Figure E33 Salinity scan of mixed C12-14EO9 and C12-14EO1 with Decalin.
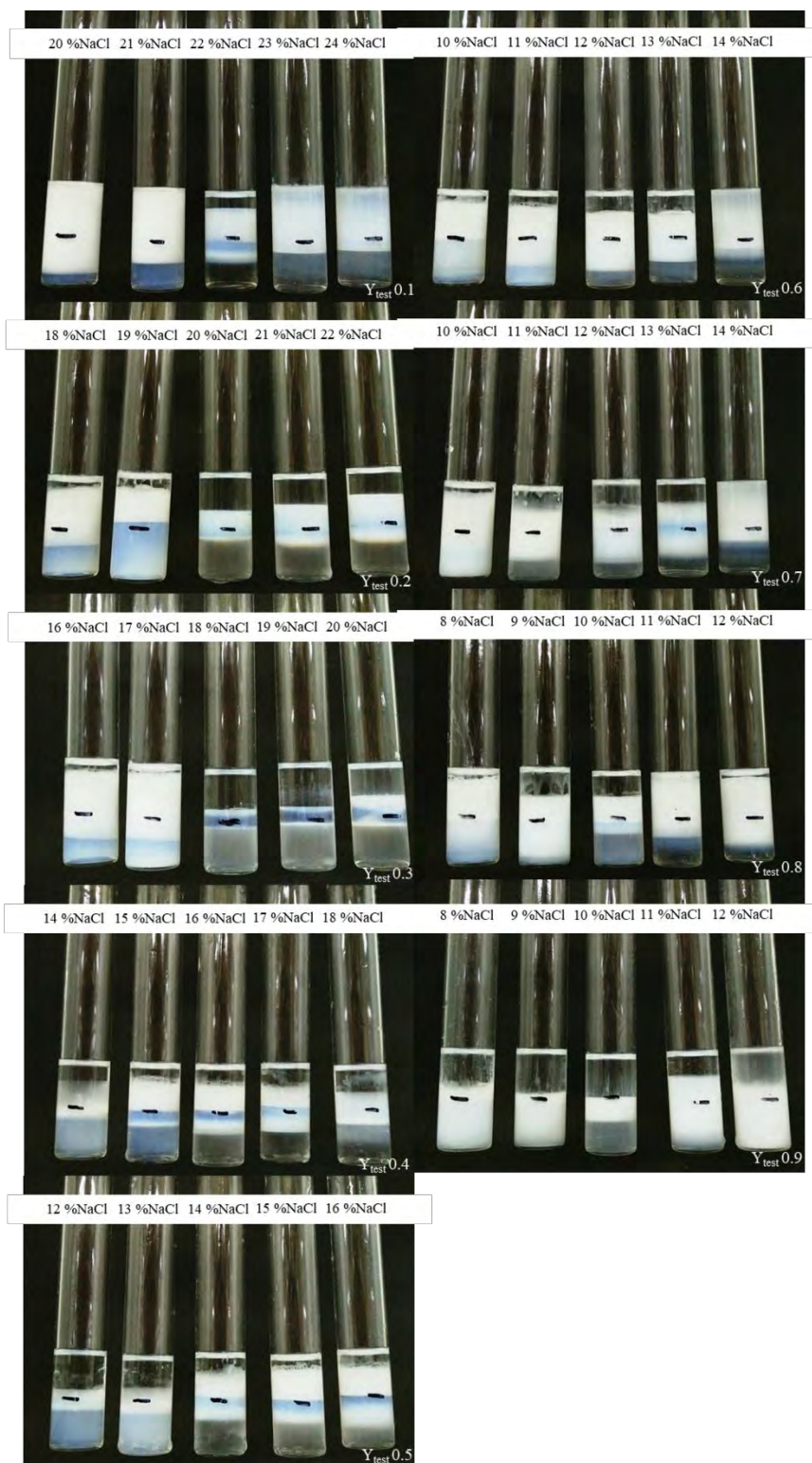
Figure E34 Salinity scan of mixed C12-14EO9 and C12-14EO2 with Cyclohexane.

Figure E35 Salinity scan of mixed C12-14EO9 and C12-14EO2 with Heptane.

230

Figure E36 Salinity scan of mixed C12-14EO9 and C12-14EO2 with Decalin.
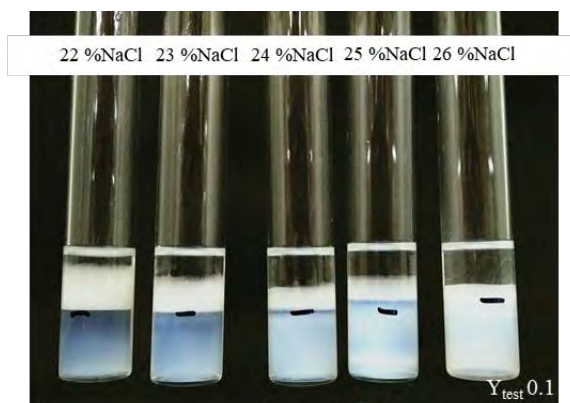
Figure E37 Salinity scan of mixed C12-14EO9 and C12-14EO12 with Cyclohexane.
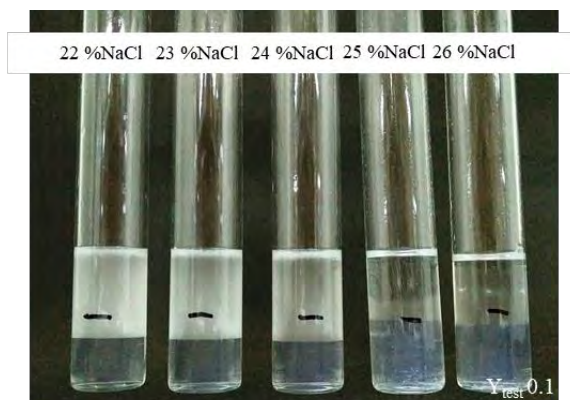
Figure E38 Salinity scan of mixed C12-14EO9 and C12-14EO12 with Heptane.
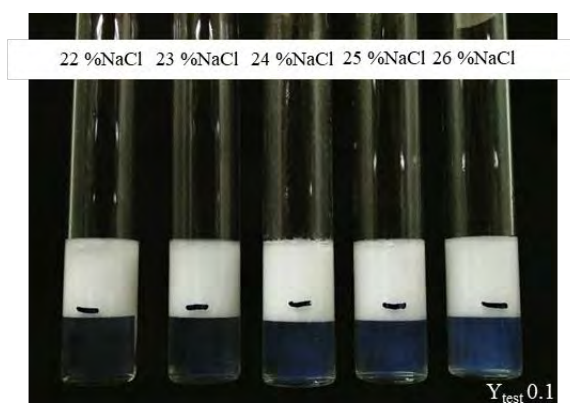
Figure E39 Salinity scan of mixed C12-14EO9 and C12-14EO12 with Decalin.
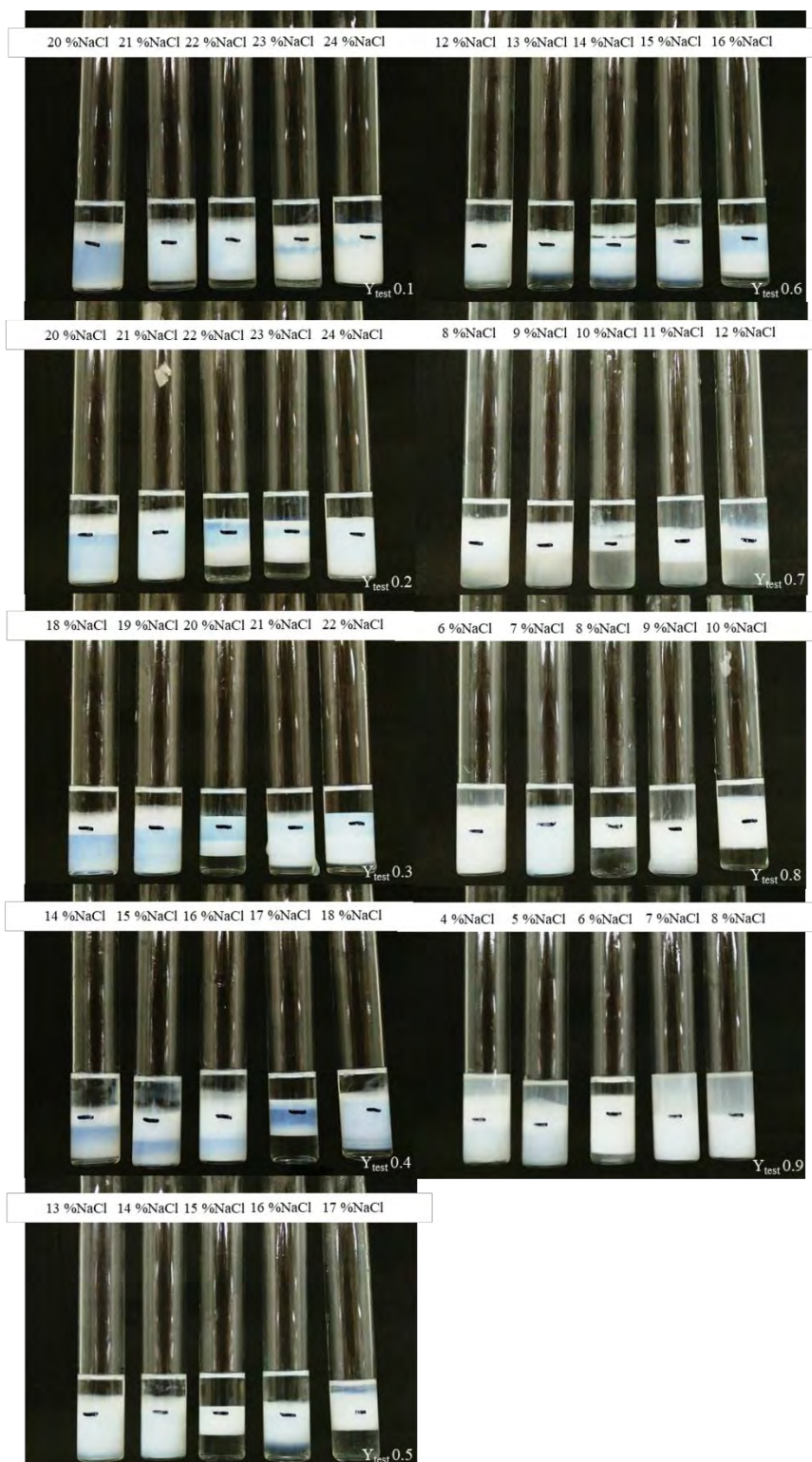
Figure E40   Salinity scan of mixed C12-14EO9 and C16-18PO2EO4 with Cyclohexane.
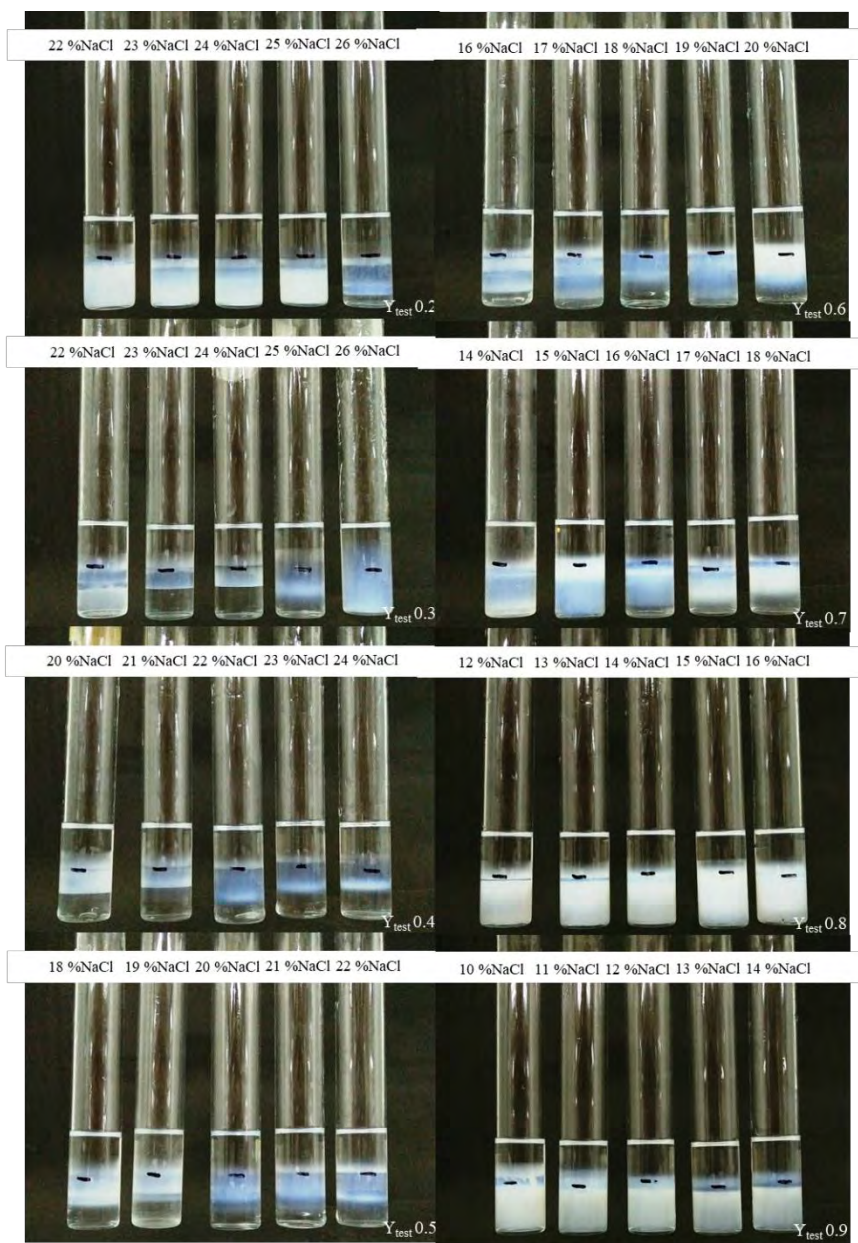
Figure E41 Salinity scan of mixed C12-14EO9 and C16-18PO2EO4 with Heptane.

Figure E42 Salinity scan of mixed C12-14EO9 and C16-18PO2EO4 with Decalin.

Figure E43 Salinity scan of mixed C12-14EO9 and C16-18PO4EO6 with Cyclohexane.
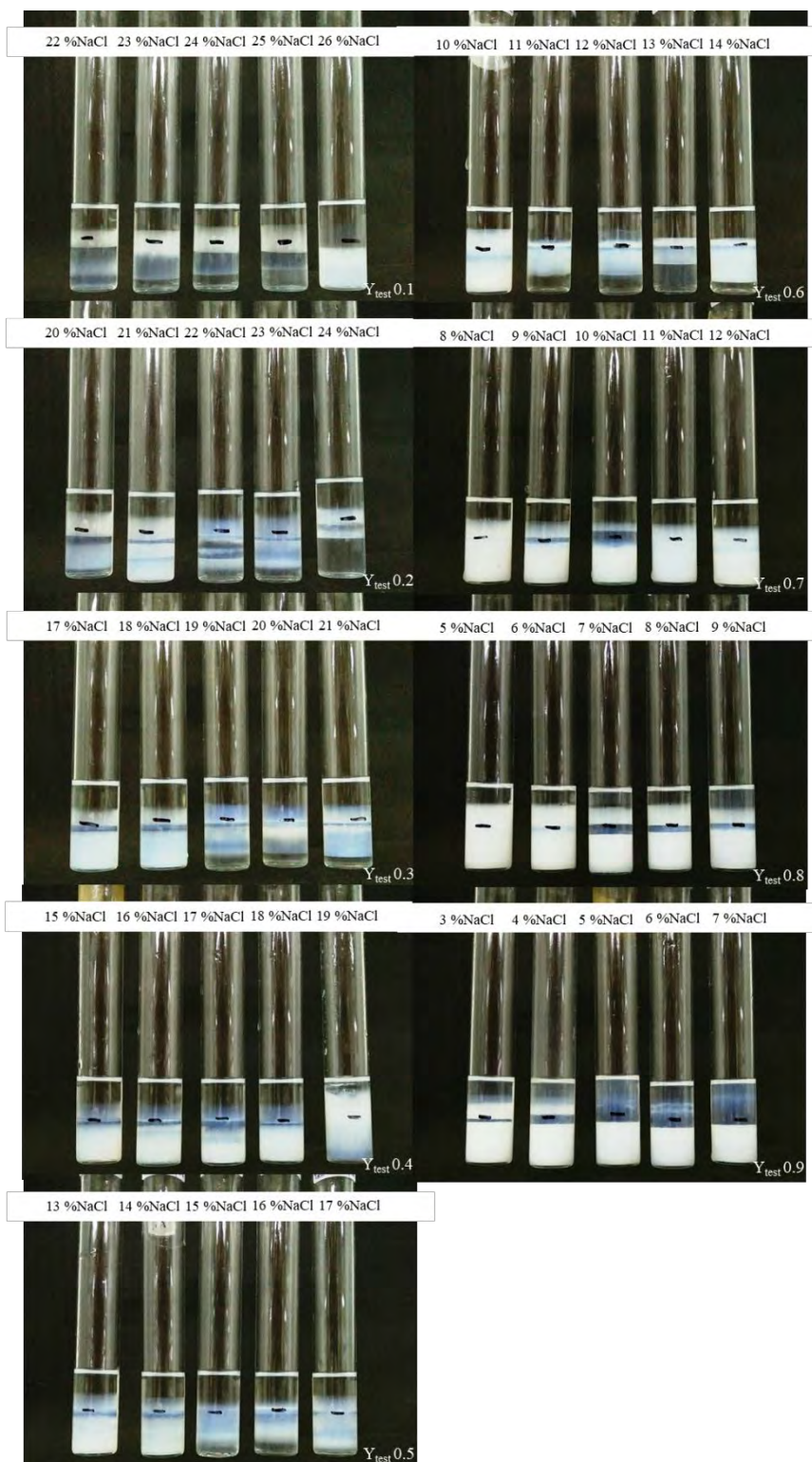
Figure E44 Salinity scan of mixed C12-14EO9 and C16-18PO4EO6 with Heptane.
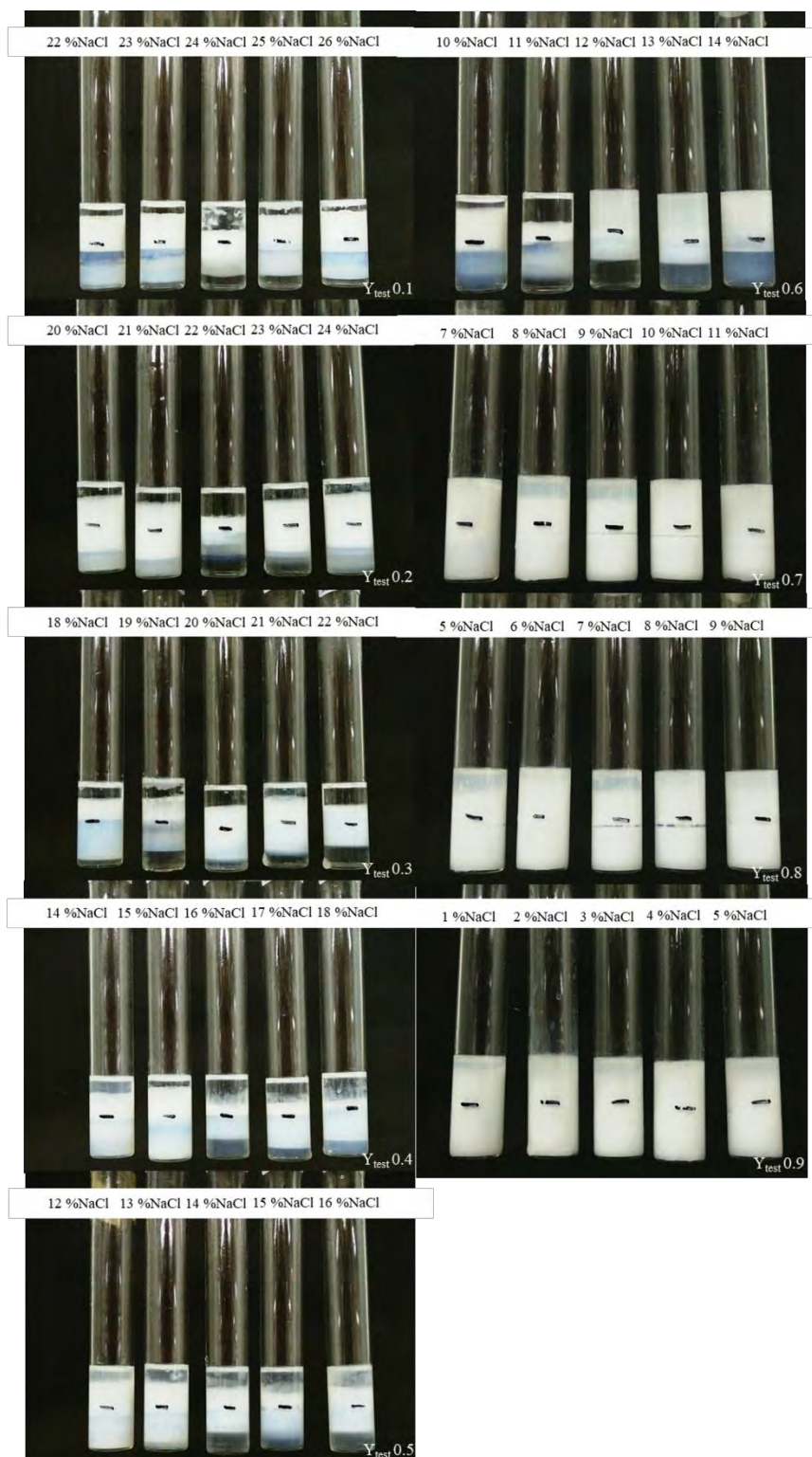
Figure E45 Salinity scan of mixed C12-14EO9 and C16-18PO4EO6 with Decalin.

Appendix F Coalescence Time of C12-14EO3 for Single Surfactant Systems

The results of coalescence time of C12-14EO3 from experiment are shown in figure F1-F15. The boundary of time is within 1,000 minutes and the boundary of salinity is in range of 0 – 26 %wt/vol.

Temp (°C)	Salinity (%wt/vol)	Time (min)
25	19	1000.00
	20	1000.00
	21	60.29
	22	27.44
	23	1000.00
	24	1000.00
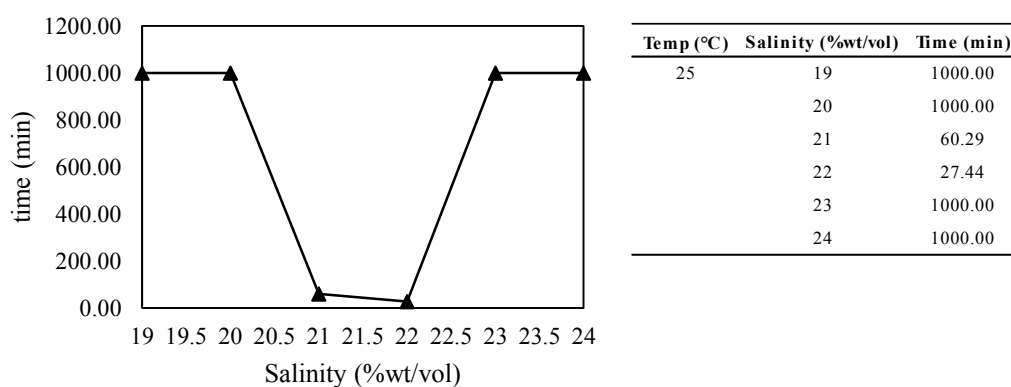
Figure F1 The coalescence time of C12-14EO3 with Hexadecane at 25 °C.

Temp (°C)	Salinity (%wt/vol)	Time (min)
30	0.0	1000
	11.0	1000
	12.0	1000
	13	239.24
	13.5	191.50
	14	1000
	15	1000
	16	1000

(a)

Temp (°C)	Salinity (%wt/vol)	Time (min)
30	18.0	1000.00
	19.0	1000.00
	20.5	199.27
	21.0	119.53
	22.0	141.03
	23.0	1000.00
	24.0	1000.00
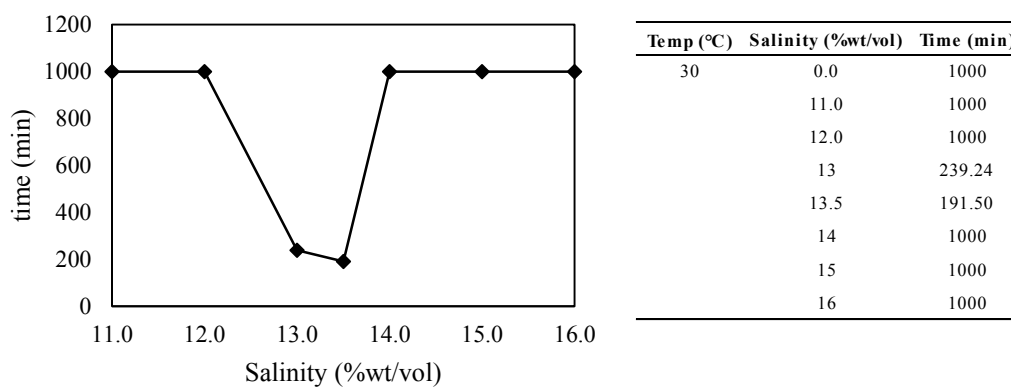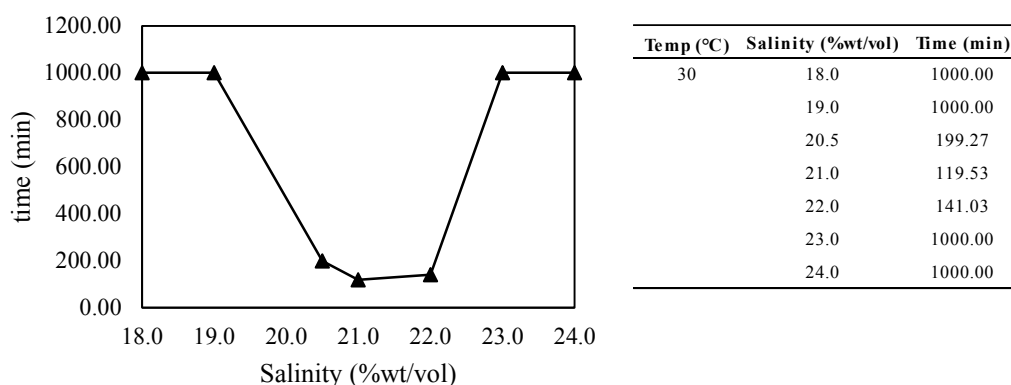
(b)

Figure F2 The coalescence time of C12-14EO3 with (a) Dodecane and (b) Hexadecane at 30 °C.

Temp (°C)	Salinity (%wt/vol)	Time (min)
35	4.0	1000.00
	5.0	1000.00
	6.0	1000.00
	7.0	146.20
	8.0	1000.00
	9.0	1000.00
	10.0	1000.00

(a)

Temp (°C)	Salinity (%wt/vol)	Time (min)
35	0.0	1000.00
	9.0	1000.00
	10.0	1000.00
	11.0	1000.00
	12.0	1000.00
	12.5	323.24
	13.0	1000.00
	14.0	1000.00

(b)
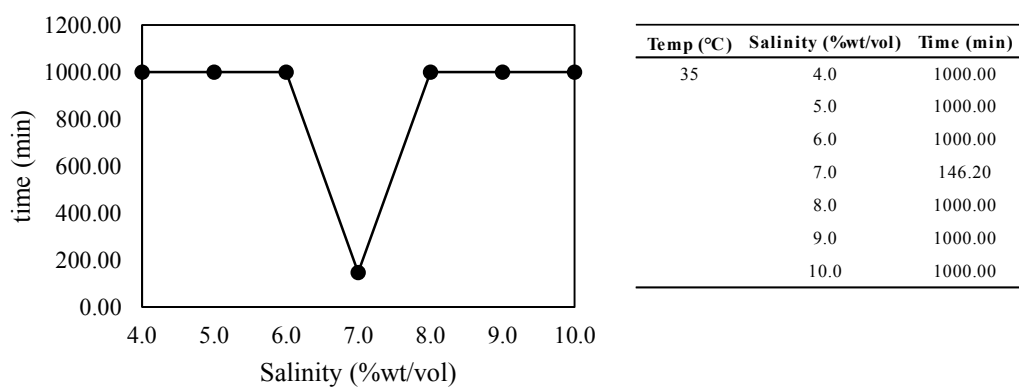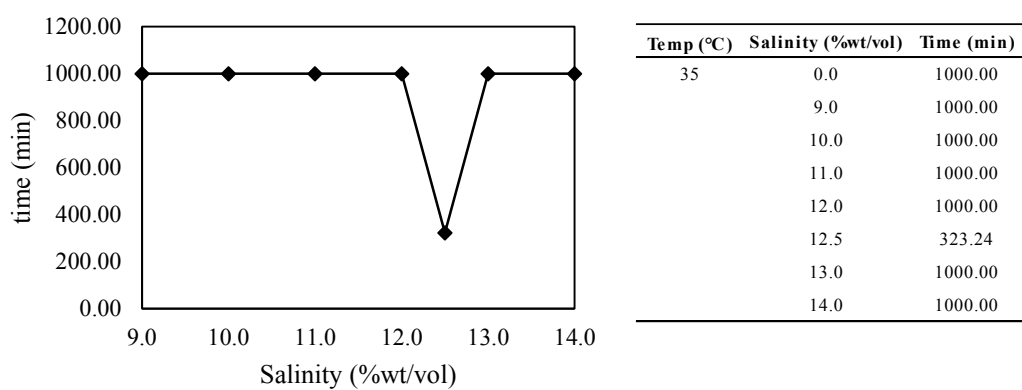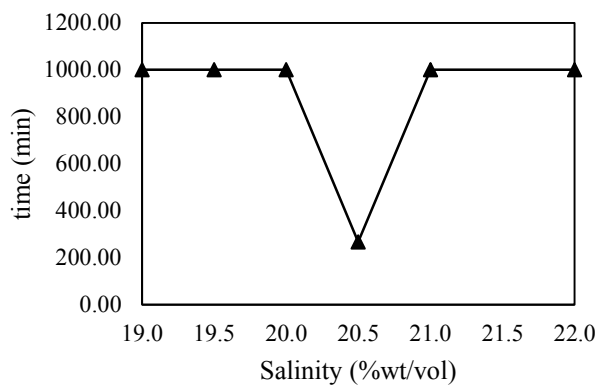
Temp (°C)	Salinity (%wt/vol)	Time (min)
35	0.0	1000.00
	19.0	1000.00
	19.5	1000.00
	20.0	1000.00
	20.5	268.07
	21.0	1000.00
	22.0	1000.00

(c)

Figure F3 The coalescence time of C12-14EO3 with (a) Decalin, (b) Dodecane and (c) Hexadecane at 35 °C.
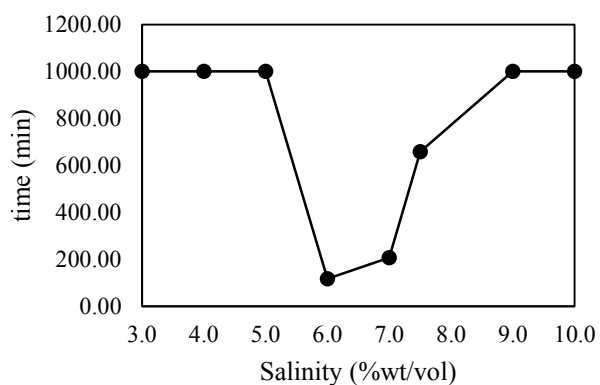
Temp (°C)	Salinity (%wt/vol)	Time (min)
40	3.0	1000.00
	4.0	1000.00
	5.0	1000.00
	6.0	117.46
	7.0	208.13
	7.5	658.55
	9.0	1000.00
	10.0	1000.00

(a)

Temp (°C)	Salinity (%wt/vol)	Time (min)
40	0.0	1000.00
	9.0	1000.00
	9.5	1000.00
	10.0	65.10
	10.5	39.51
	11.0	1000.00
	12.0	1000.00
	13.0	1000.00

(b)
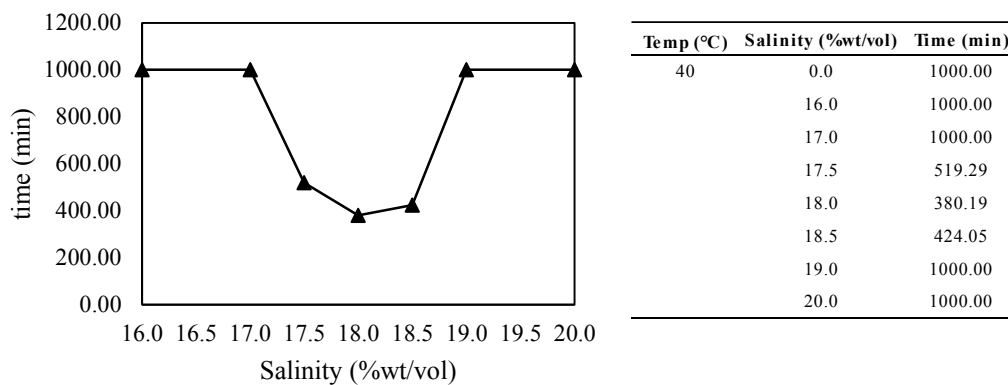
(c)

Figure F4 The coalescence time of C12-14EO3 with (a) Decalin, (b) Dodecane and (c) Hexadecane at 40 °C.

Temp (°C)	Salinity (%wt/vol)	Time (min)
40	0.0	1000.00
	16.0	1000.00
	17.0	1000.00
	17.5	519.29
	18.0	380.19
	18.5	424.05
	19.0	1000.00
	20.0	1000.00

(a)

Temp (°C)	Salinity (%wt/vol)	Time (min)
45	3.0	1000.00
	4.0	1000.00
	5.0	80.00
	6.0	1000.00
	8.0	1000.00
	10.0	1000.00

(b)

Temp (°C)	Salinity (%wt/vol)	Time (min)
45	0.0	1000.00
	7.0	1000.00
	8.0	1000.00
	8.5	1000.00
	9.0	60.12
	9.5	38.22
	10.0	126.09
	11.0	1000.00
	12.0	1000.00
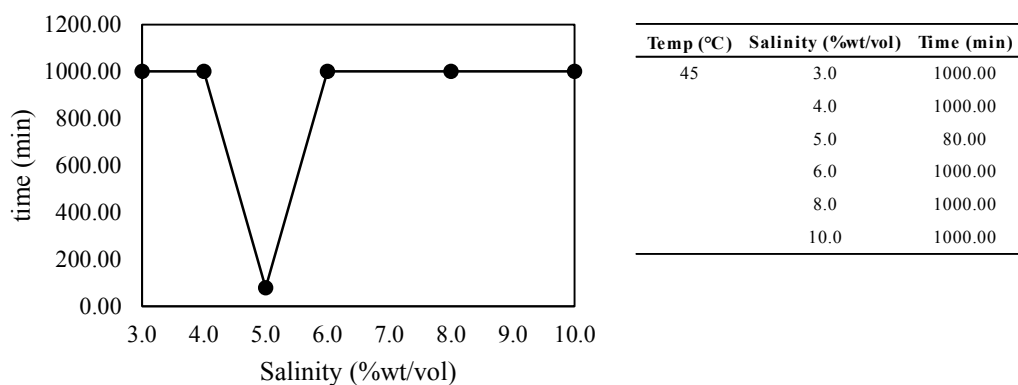
Temp (°C)	Salinity (%wt/vol)	Time (min)
45	0.0	1000.00
	14.0	1000.00
	15.0	1000.00
	15.5	208.37
	16.0	64.54
	16.5	179.37
	17.0	208.37
	17.5	269.03
	18.0	1000.00
	20.0	1000.00

(c)

Figure F5 The coalescence time of C12-14EO3 with (a) Decalin, (b) Dodecane and (c) Hexadecane at 45 °C.
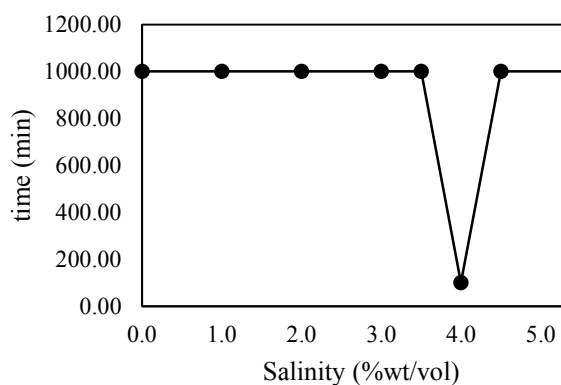
Temp (°C)	Salinity (%wt/vol)	Time (min)
50	0.0	1000.00
	1.0	1000.00
	2.0	1000.00
	3.0	1000.00
	3.5	1000.00
	4.0	101.51
	4.5	1000.00
	5.5	1000.00

(a)

Temp (°C)	Salinity (%wt/vol)	Time (min)
50	0.0	1000.00
	6.0	1000.00
	7.0	1000.00
	8.0	1000.00
	8.5	27.26
	9.0	162.16
	9.5	196.39
	10.0	1000.00
	11.0	1000.00

(b)

Temp (°C)	Salinity (%wt/vol)	Time (min)
50	0.0	1000.00
	12.0	1000.00
	13.0	1000.00
	13.5	100.29
	14.0	46.48
	14.5	197.10
	15.0	201.17
	16.0	234.47
	17.0	254.35
	18.0	1000.00
	20.0	1000.00
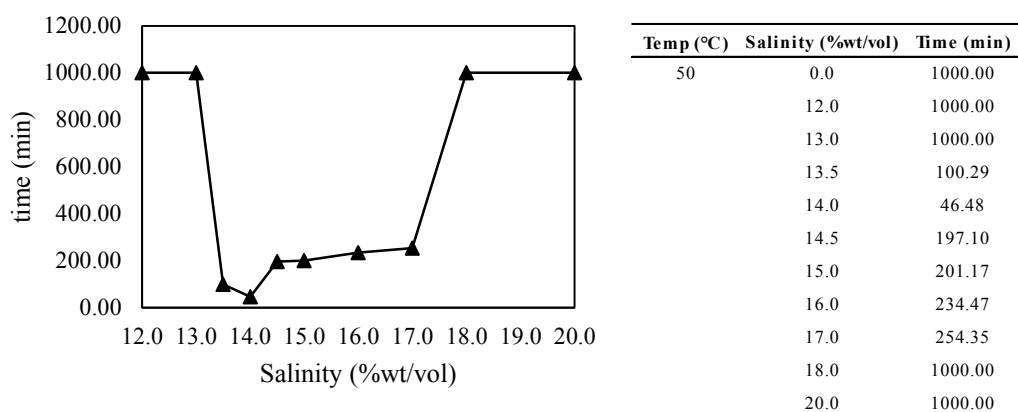
(c)

Figure F6 The coalescence time of C12-14EO3 with (a) Decalin, (b) Dodecane and (c) Hexadecane at 50 °C.

Temp (°C)	Salinity (%wt/vol)	Time (min)
55	0.0	1000.00
	1.0	1000.00
	1.5	1000.00
	2.0	1000.00
	2.5	80.18
	3.0	136.33
	3.5	1000.00
	4.5	1000.00
	5.5	1000.00

(a)

Temp (°C)	Salinity (%wt/vol)	Time (min)
55	0.0	1000.00
	4.0	1000.00
	5.0	234.36
	6.0	161.09
	7.0	47.13
	8.0	80.19
	9.0	101.00
	10.0	160.42
	11.0	1000.00
	12.0	1000.00

(b)

Temp (°C)	Salinity (%wt/vol)	Time (min)
55	0.0	1000.00
	5.0	1000.00
	8.0	234.52
	9.0	137.43
	10.0	98.00
	11.0	83.28
	12.0	73.52
	13.0	23.07
	14.0	94.20
	15.0	138.42
	18.0	1000.00
	20.0	1000.00
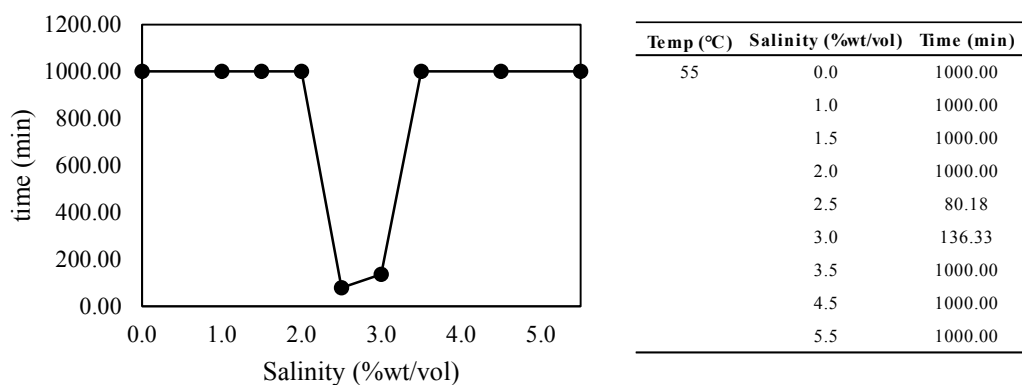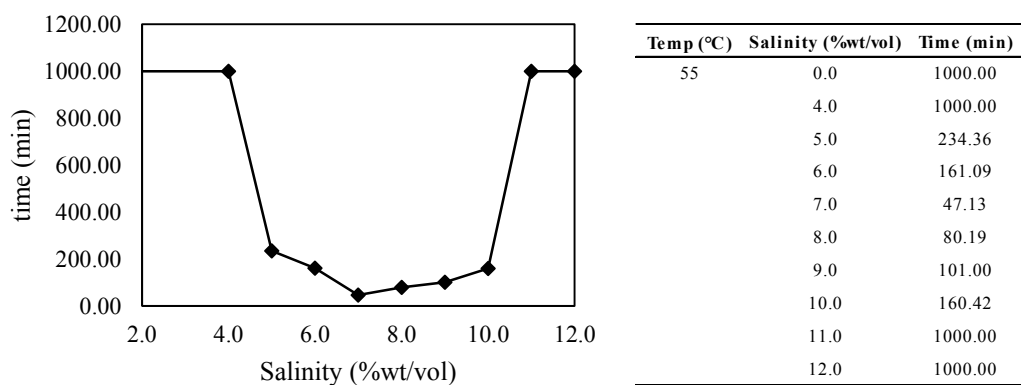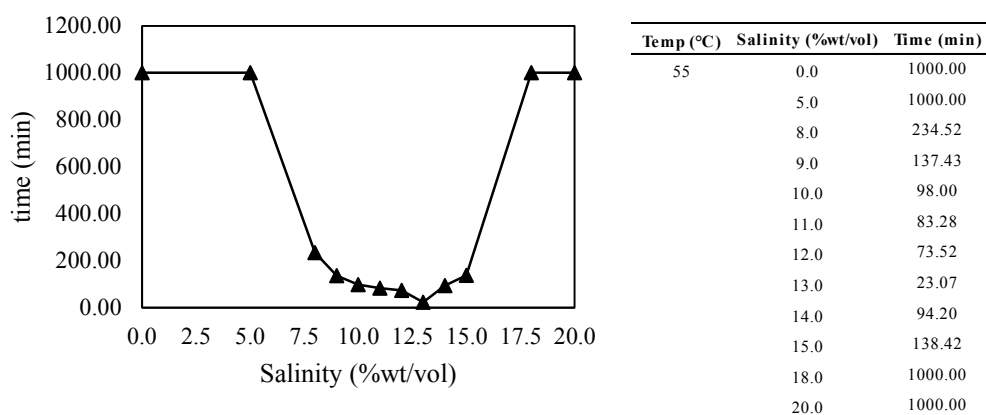
(c)

Figure F7 The coalescence time of C12-14EO3 with (a) Decalin, (b) Dodecane and (c) Hexadecane at 55 °C.

Temp (°C)	Salinity (%wt/vol)	Time (min)
60	0.0	1000.00
	2.0	1000.00
	4.0	1000.00
	5.0	183.04
	6.0	115.32
	7.0	138.53
	8.0	159.48
	9.0	1000.00
	10.0	1000.00

(a)

Temp (°C)	Salinity (%wt/vol)	Time (min)
60	0.0	1000.00
	5.0	1000.00
	8.0	191.18
	9.0	183.34
	9.5	138.04
	10.0	116.00
	10.5	91.49
	11.0	159.06
	12.0	184.13
	13.0	222.26
	15.0	1000.00
	18.0	1000.00
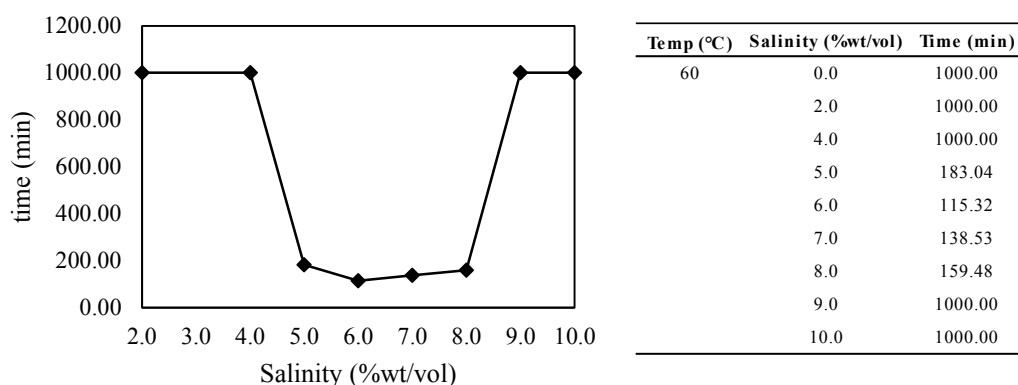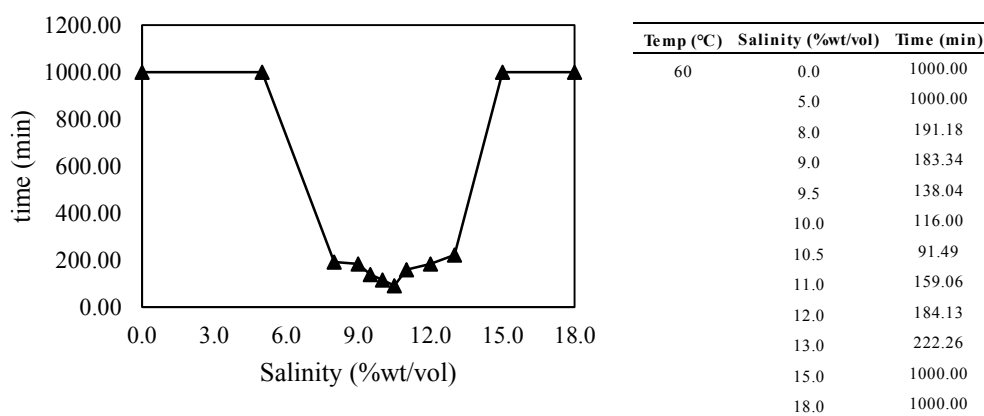
(b)

Figure F8 The coalescence time of C12-14EO3 with (a) Dodecane and (b) Hexadecane at 60 °C.

Temp (°C)	Salinity (%wt/vol)	Time (min)
65	2.0	1000.00
	3.0	1000.00
	4.0	1000.00
	5.0	58.40
	6.0	71.54
	8.0	144.44
	10.0	1000.00
	11.0	1000.00

(a)

Temp (°C)	Salinity (%wt/vol)	Time (min)
65	0.0	1000
	5.0	1000
	8.0	170.37
	8.5	86.15
	9.0	80.30
	9.5	69.00
	10.0	97.55
	11.0	127.40
	12.0	238.00
	14.0	1000
	15.0	1000
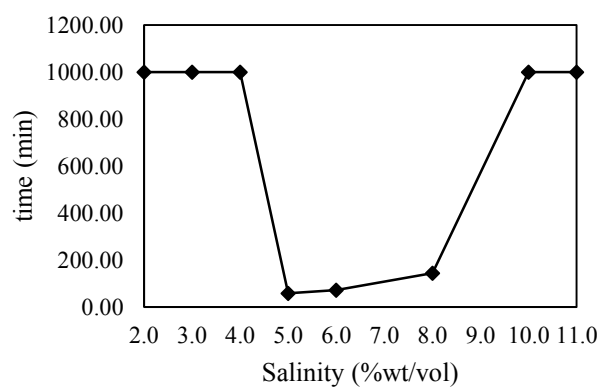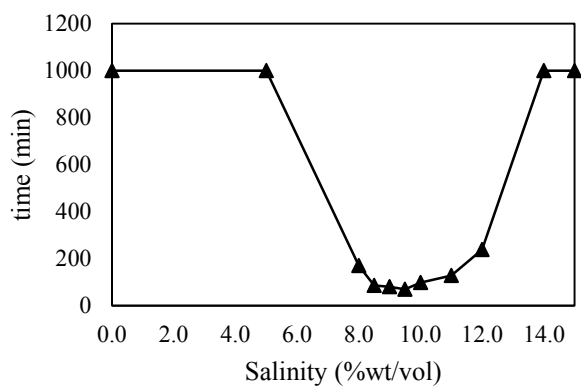
(b)

Figure F9 The coalescence time of C12-14EO3 with (a) Dodecane and (b) Hexadecane at 65 °C.
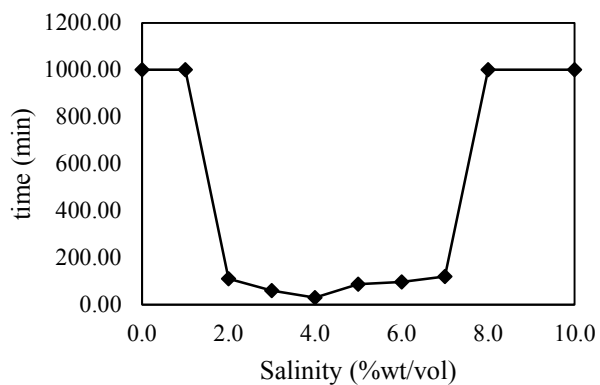
Temp (°C)	Salinity (%wt/vol)	Time (min)
70	0.0	1000.00
	1.0	1000.00
	2.0	111.23
	3.0	60.11
	4.0	30.30
	5.0	87.21
	6.0	97.44
	7.0	120.57
	8.0	1000.00
	10.0	1000.00

(a)
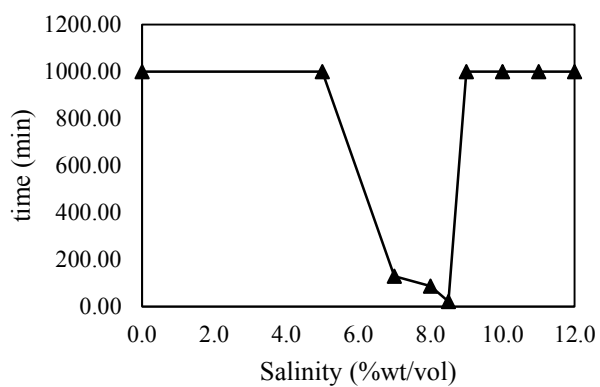
Temp (°C)	Salinity (%wt/vol)	Time (min)
70	0.0	1000.00
	5.0	1000.00
	7.0	129.22
	8.0	86.23
	8.5	21.21
	9.0	1000.00
	10.0	1000.00
	11.0	1000.00
	12.0	1000.00

(b)

Figure F10 The coalescence time of C12-14EO3 with (a) Dodecane and (b) Hexadecane at 70 °C.
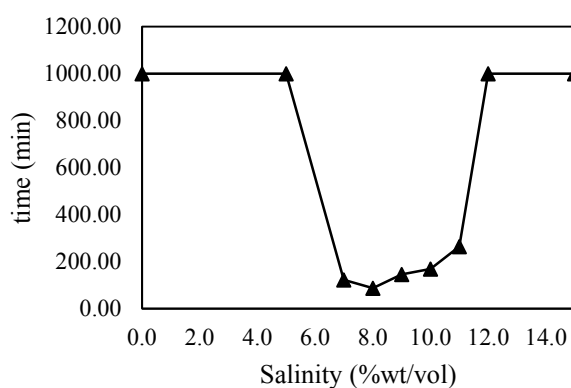
Temp (°C)	Salinity (%wt/vol)	Time (min)
75	0.0	1000.00
	5.0	1000.00
	7.0	123.12
	8.0	87.18
	9.0	145.32
	10.0	169.14
	11.0	264.17
	12.0	1000.00
	15.0	1000.00

Figure F11 The coalescence time of C12-14EO3 with Hexadecane at 75 °C.

Temp (°C)	Salinity (%wt/vol)	Time (min)
80	0.0	1000.00
	2.0	1000.00
	5.0	118.25
	6.0	81.30
	7.0	60.43
	8.0	118.14
	9.0	138.41
	10.0	163.42
	12.0	1000.00
	14.0	1000.00
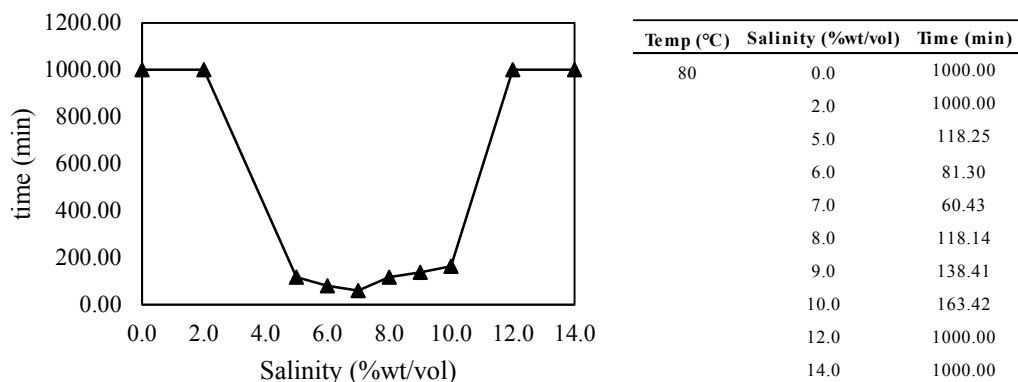
Figure F12 The coalescence time of C12-14EO3 with Hexadecane at 80 °C.

Temp (°C)	Salinity (%wt/vol)	Time (min)
85	0.0	1000.00
	2.0	1000.00
	4.0	59.09
	5.0	28.42
	6.0	79.47
	7.0	82.33
	8.0	142.38
	9.0	151.25
	10.0	186.58
	11.0	1000.00
	12.0	1000.00
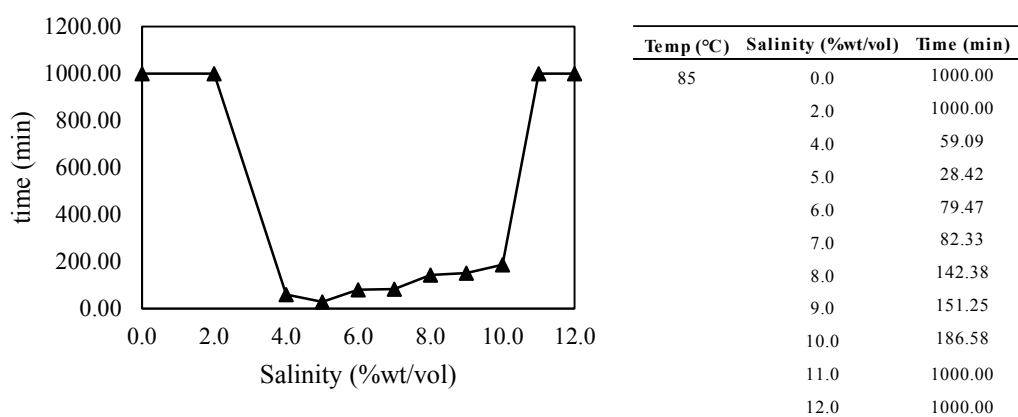
Figure F13 The coalescence time of C12-14EO3 with Hexadecane at 85 °C.

Temp (°C)	Salinity (%wt/vol)	Time (min)
90	0.0	1000.00
	2.0	1000.00
	3.0	105.00
	4.0	59.12
	5.0	80.24
	6.0	104.34
	7.0	128.44
	8.0	208.52
	10.0	1000.00
	12.0	1000.00
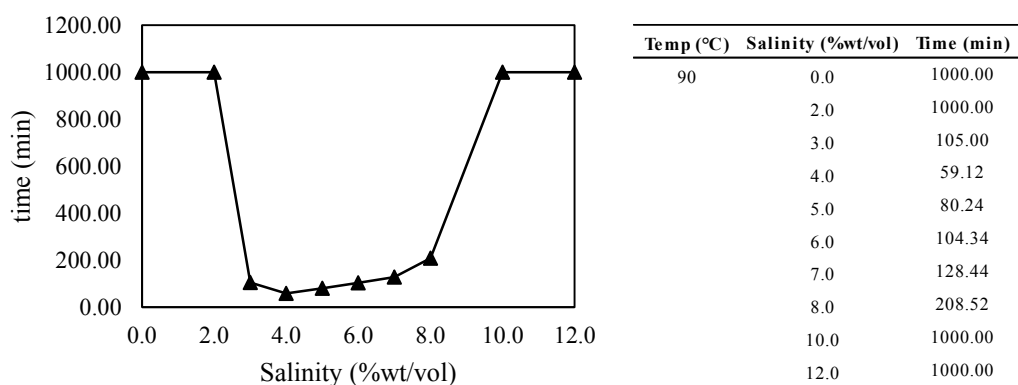
Figure F14 The coalescence time of C12-14EO3 with Hexadecane at 90 °C.

Temp (℃)	Salinity (%wt/vol)	Time (min)
95	0.0	1000.00
	1.0	1000.00
	2.0	102.57
	3.0	50.36
	4.0	122.00
	5.0	136.53
	6.0	156.20
	8.0	1000.00
	10.0	1000.00
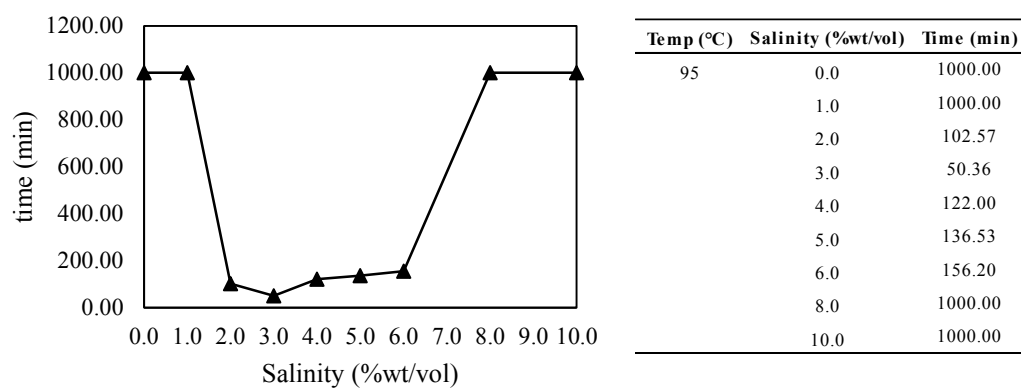
Figure F15 The coalescence time of C12-14EO3 with Hexadecane at 95 °C.

Appendix G Coalescence Time of C12-14EO5 for Single Surfactant Systems

The results of coalescence time of C12-14EO5 from experiment are shown in figure G1-G14. The boundary of time is within 1,000 minutes and the boundary of salinity is in range of 0 – 26 %wt/vol.

Temp (°C)	Salinity (%wt/vol)	time (min)
30	0.0	1000.00
	13.0	1000.00
	13.5	1000.00
	14.0	567.26
	14.5	240.12
	15.0	1000.00
	15.5	1000.00
	16.0	1000.00
	17.0	1000.00

(a)

Temp (°C)	Salinity (%wt/vol)	Time (min)
30	0.0	1000.00
	17.0	1000.00
	18.0	1000.00
	19.0	1000.00
	20.0	1000.00
	21.0	196.11
	22.0	1000.00
	23.0	1000.00
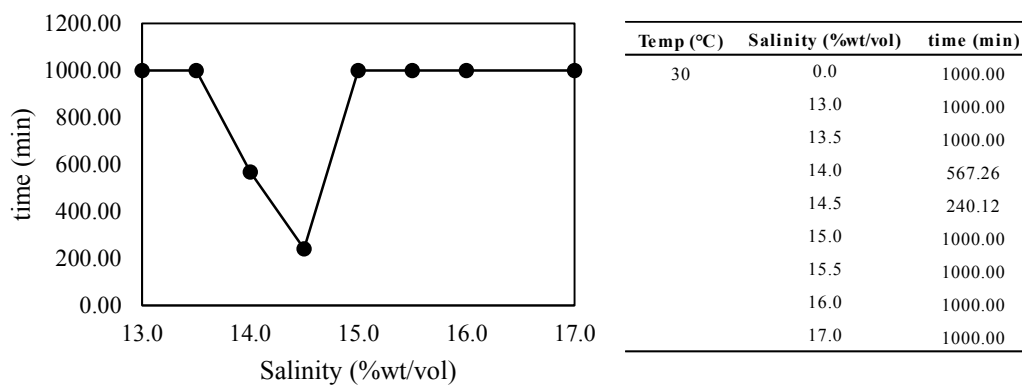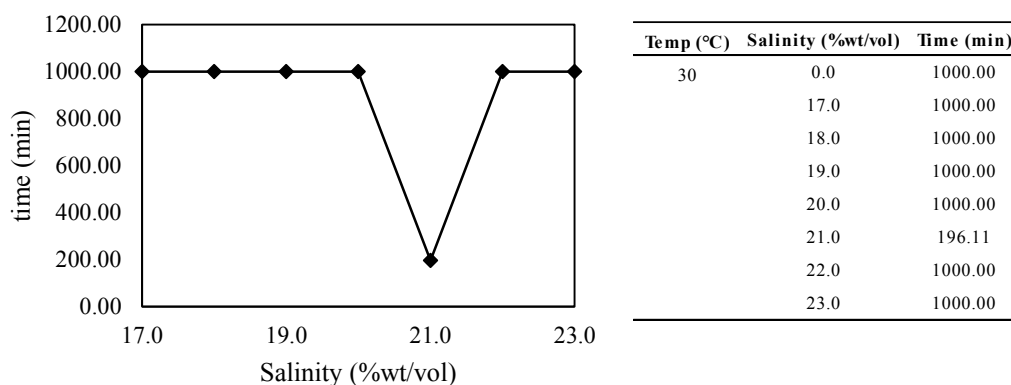
(b)

Figure G1 The coalescence time of C12-14EO5 with (a) Decalin and (b) Dodecane at 30 °C.

(a)
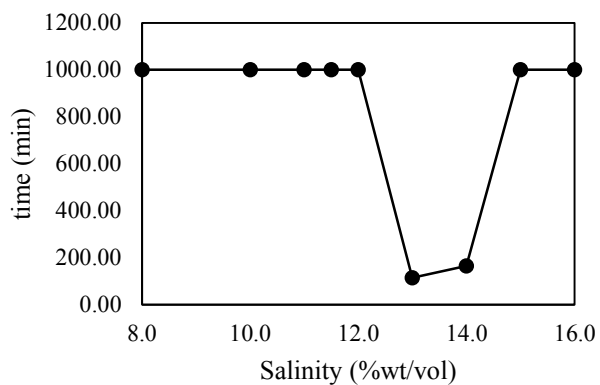
Temp (°C)	Salinity (%wt/vol)	time (min)
35	0.0	1000.00
	8.0	1000.00
	10.0	1000.00
	11.0	1000.00
	11.5	1000.00
	12.0	1000.00
	13.0	115.21
	14.0	165.42
	15.0	1000.00
	16.0	1000.00

(b)

Temp (°C)	Salinity (%wt/vol)	time (min)
35	0.0	1000.00
	15.0	1000.00
	16.0	1000.00
	17.0	1000.00
	18.0	73.33
	19.0	72.53
	19.5	47.38
	20.0	143.57
	21.0	1000.00
	22.5	1000.00

(c)

Temp (°C)	Salinity (%wt/vol)	time (min)
35	0.0	1000.00
	16.0	1000.00
	20.0	1000.00
	21.0	1000.00
	22.0	1000.00
	23.0	1000.00
	23.5	1000.00
	24.0	40.28
	25.0	114.12
	26.0	240.01

Figure G2 The coalescence time of C12-14EO5 with (a) Decalin, (b) Dodecane and (c) Hexadecane at 35 °C.
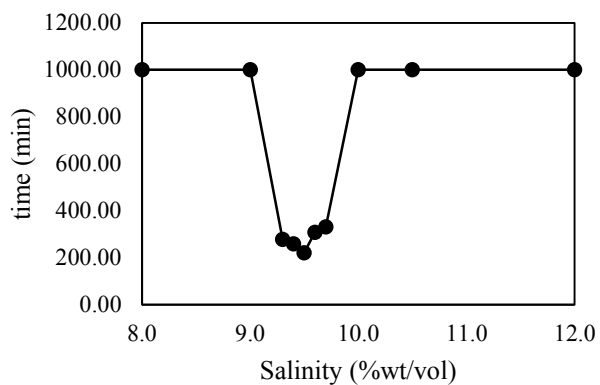
Temp (°C)	Salinity (%wt/vol)	time (min)
40	0.0	1000.00
	8.0	1000.00
	9.0	1000.00
	9.3	279.15
	9.4	259.25
	9.5	221.17
	9.6	308.22
	9.7	331.08
	10.0	1000.00
	10.5	1000.00
	12.0	1000.00

(a)
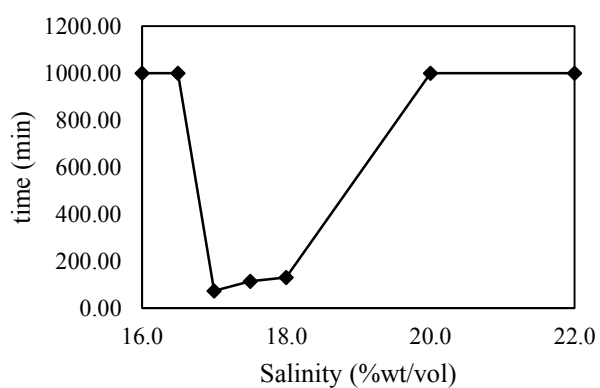
Temp (°C)	Salinity (%wt/vol)	time (min)
40	0.0	1000.00
	16.0	1000.00
	16.5	1000.00
	17.0	73.01
	17.5	114.48
	18.0	130.36
	20.0	1000.00
	22.0	1000.00

(b)
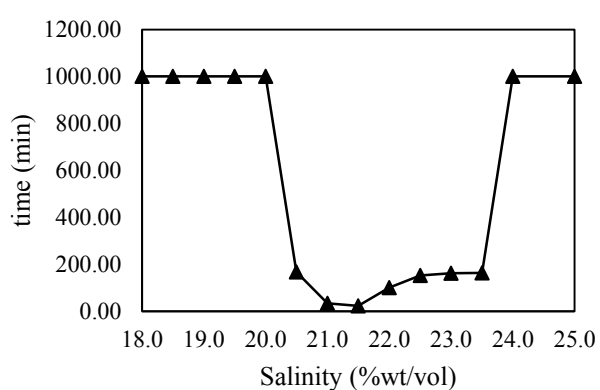
Temp (°C)	Salinity (%wt/vol)	time (min)
40	18.0	1000.00
	18.5	1000.00
	19.0	1000.00
	19.5	1000.00
	20.0	1000.00
	20.5	167.52
	21.0	34.46
	21.5	24.18
	22.0	101.26
	22.5	153.45
	23.0	163.19
	23.5	164.06
	24.0	1000.00
	25.0	1000.00

(c)

Figure G3 The coalescence time of C12-14EO5 with (a) Decalin, (b) Dodecane and (c) Hexadecane at 40 °C.
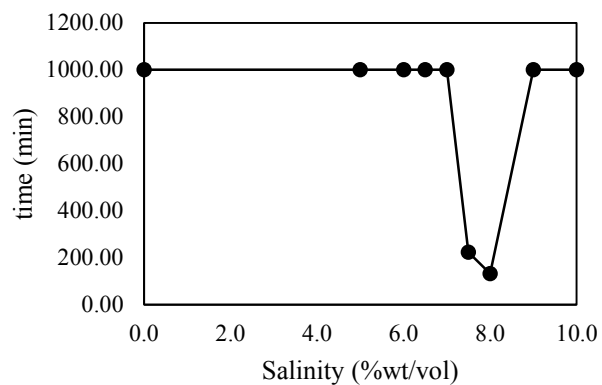
Temp (°C)	Salinity (%wt/vol)	time (min)
45	0.0	1000.00
	5.0	1000.00
	6.0	1000.00
	6.5	1000.00
	7.0	1000.00
	7.5	223.34
	8.0	133.25
	9.0	1000.00
	10.0	1000.00

(a)
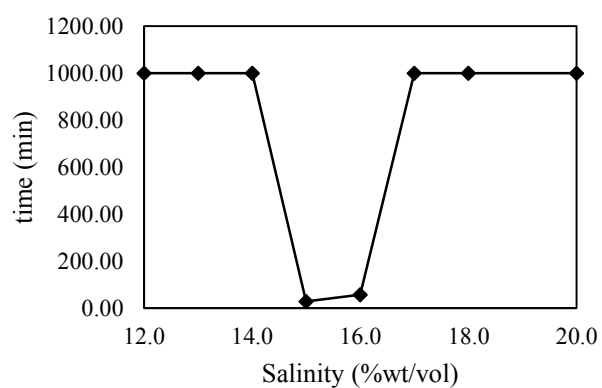
Temp (°C)	Salinity (%wt/vol)	Time (min)
45	0.0	1000.00
	12.0	1000.00
	13.0	1000.00
	14.0	1000.00
	15.0	28.09
	16.0	57.11
	17.0	1000.00
	18.0	1000.00
	20.0	1000.00

(b)
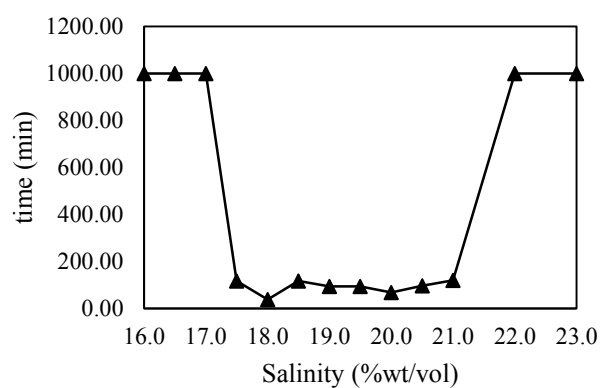
Temp (°C)	Salinity (%wt/vol)	time (min)
45	0.0	1000.00
	16.0	1000.00
	16.5	1000.00
	17.0	1000.00
	17.5	116.32
	18.0	38.27
	18.5	116.32
	19.0	93.51
	19.5	93.51
	20.0	68.28
	20.5	96.16
	21.0	119.52
	22.0	1000.00
	23.0	1000.00

(c)

Figure G4 The coalescence time of C12-14EO5 with (a) Decalin, (b) Dodecane and (c) Hexadecane at 45 °C.

(a)
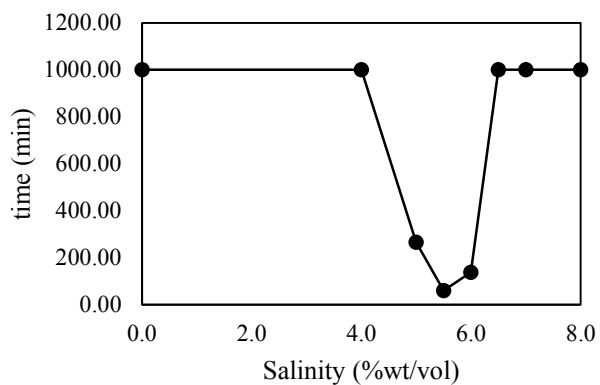
Temp (°C)	Salinity (%wt/vol)	time (min)
50	0.0	1000.00
	4.0	1000.00
	5.0	266.54
	5.5	61.03
	6.0	138.26
	6.5	1000.00
	7.0	1000.00
	8.0	1000.00

(b)
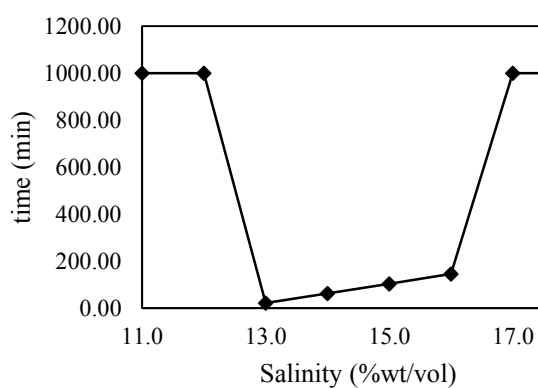
Temp (°C)	Salinity (%wt/vol)	Time (min)
50	0.0	1000.00
	8.0	1000.00
	11.0	1000.00
	12.0	1000.00
	13.0	21.01
	14.0	62.58
	15.0	103.37
	16.0	146.08
	17.0	1000.00
	18.0	1000.00

(c)
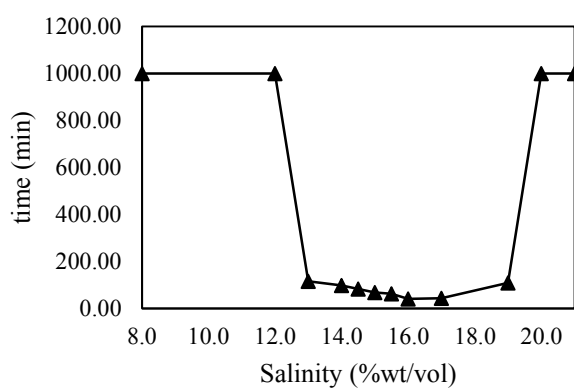
Temp (°C)	Salinity (%wt/vol)	time (min)
50	0.0	1000.00
	4.0	1000.00
	8.0	1000.00
	12.0	1000.00
	13.0	116.04
	14.0	98.08
	14.5	82.48
	15.0	68.04
	15.5	62.26
	16.0	41.05
	17.0	43.48
	19.0	109.13
	20.0	1000.00
	21.0	1000.00

Figure G5 The coalescence time of C12-14EO5 with (a) Decalin, (b) Dodecane and (c) Hexadecane at 50 °C.

(a)

Temp (°C)	Salinity (%wt/vol)	time (min)
55	0.0	1000.00
	1.0	1000.00
	2.0	1000.00
	3.0	1000.00
	3.5	227.57
	4.0	177.43
	4.5	195.49
	5.0	1000.00
	10.0	1000.00

(b)

Temp (°C)	Salinity (%wt/vol)	Time (min)
55	0.0	1000.00
	2.0	1000.00
	6.0	1000.00
	8.0	1000.00
	9.0	1000.00
	10.0	1000.00
	11.0	19.10
	12.0	39.37
	13.0	52.38
	14.0	68.30
	15.0	1000.00
	20.0	1000.00

(c)

Temp (°C)	Salinity (%wt/vol)	time (min)
55	0.0	1000.00
	4.0	1000.00
	8.0	1000.00
	10.0	1000.00
	11.0	1000.00
	11.5	1000.00
	12.0	1000.00
	12.5	115.19
	13.0	102.34
	14.0	95.05
	14.5	51.57
	15.0	73.27
	15.5	78.23
	16.0	250.02
	17.0	1000.00
	18.0	1000.00

Figure G6 The coalescence time of C12-14EO5 with (a) Decalin, (b) Dodecane and (c) Hexadecane at 55 °C.
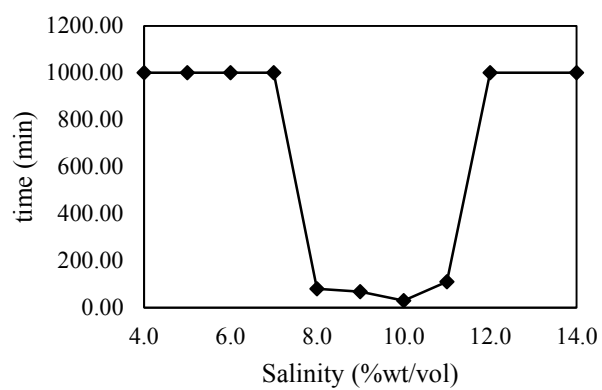
Temp (°C)	Salinity (%wt/vol)	Time (min)
60	0.0	1000.00
	2.0	1000.00
	4.0	1000.00
	5.0	1000.00
	6.0	1000.00
	7.0	1000.00
	8.0	81.44
	9.0	68.58
	10.0	31.03
	11.0	111.43
	12.0	1000.00
	14.0	1000.00

(a)
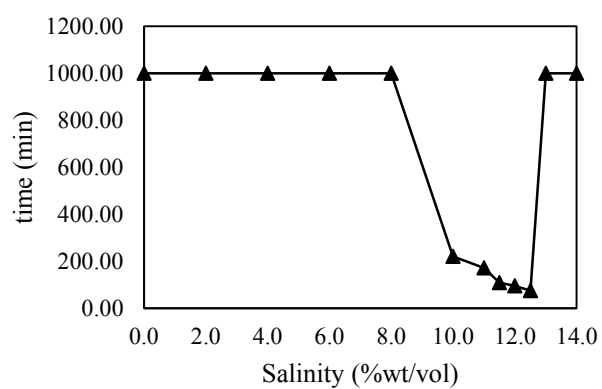
Temp (°C)	Salinity (%wt/vol)	time (min)
60	0.0	1000.00
	2.0	1000.00
	4.0	1000.00
	6.0	1000.00
	8.0	1000.00
	10.0	220.55
	11.0	171.18
	11.5	109.45
	12.0	96.10
	12.5	75.24
	13.0	1000.00
	14.0	1000.00

(b)

Figure G7 The coalescence time of C12-14EO5 with (a) Dodecane and (b) Hexadecane at 60 °C.
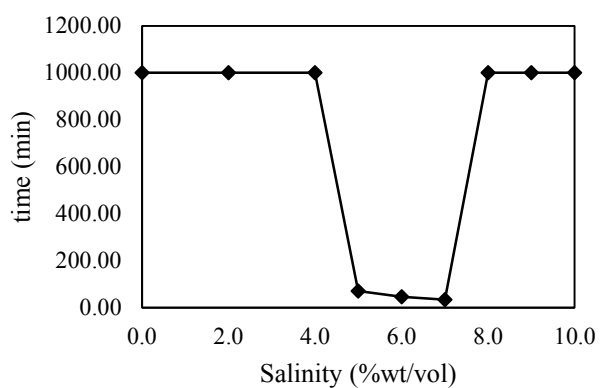
Temp (°C)	Salinity (%wt/vol)	Time (min)
65	0.0	1000.00
	2.0	1000.00
	4.0	1000.00
	5.0	71.41
	6.0	47.32
	7.0	34.01
	8.0	1000.00
	9.0	1000.00
	10.0	1000.00

(a)
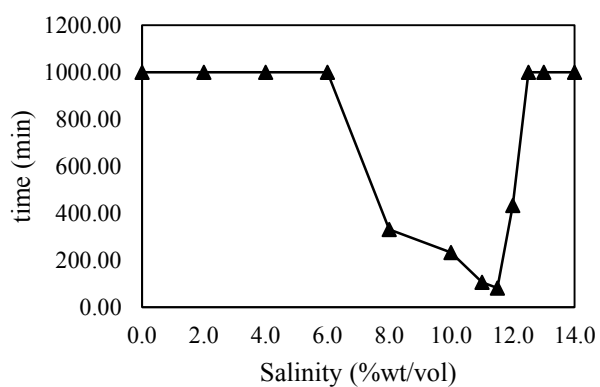
Temp (°C)	Salinity (%wt/vol)	time (min)
65	0.0	1000.00
	2.0	1000.00
	4.0	1000.00
	6.0	1000.00
	8.0	330.43
	10.0	232.41
	11.0	105.04
	11.5	80.57
	12.0	433.19
	12.5	1000.00
	13.0	1000.00
	14.0	1000.00

(b)

Figure G8 The coalescence time of C12-14EO5 with (a) Dodecane and (b) Hexadecane at 65 °C.
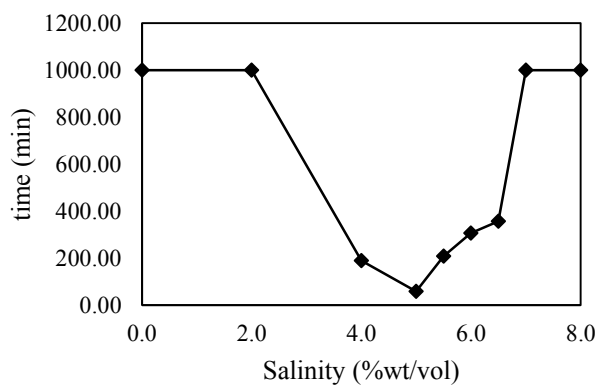
Temp (°C)	Salinity (%wt/vol)	Time (min)
70	0.0	1000.00
	2.0	1000.00
	4.0	189.10
	5.0	58.35
	5.5	208.10
	6.0	307.14
	6.5	357.04
	7.0	1000.00
	8.0	1000.00

(a)

Temp (°C)	Salinity (%wt/vol)	time (min)
70	0.0	1000.00
	2.0	1000.00
	4.0	1000.00
	6.0	230.47
	8.0	194.38
	9.0	154.20
	9.5	120.17
	10.0	65.09
	10.5	101.00
	11.0	1000.00
	12.0	1000.00

(b)
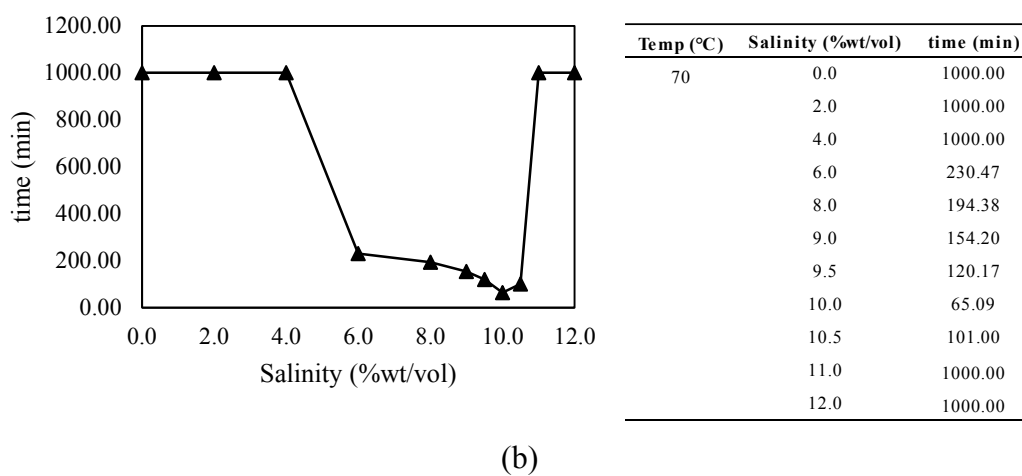
Figure G9 The coalescence time of C12-14EO5 with (a) Dodecane and (b) Hexadecane at 70 °C.

Temp (°C)	Salinity (%wt/vol)	time (min)
75	0.0	1000.00
	2.0	1000.00
	4.0	1000.00
	6.0	236.31
	7.0	179.34
	7.5	140.04
	8.0	115.07
	8.5	73.32
	9.0	92.35
	10.0	140.22
	12.0	1000.00
	13.0	1000.00
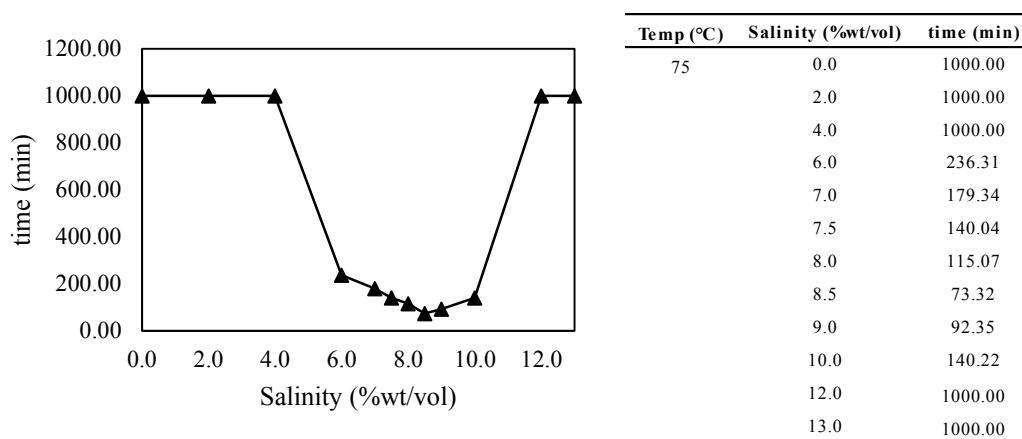
Figure G10 The coalescence time of C12-14EO5 with Hexadecane at 75 °C.

Temp (°C)	Salinity (%wt/vol)	time (min)
80	0.0	1000.00
	1.0	1000.00
	2.0	1000.00
	3.0	1000.00
	4.0	180.24
	5.0	160.34
	6.0	95.27
	6.5	67.32
	7.0	35.19
	7.5	239.41
	8.0	1000.00
	9.0	1000.00
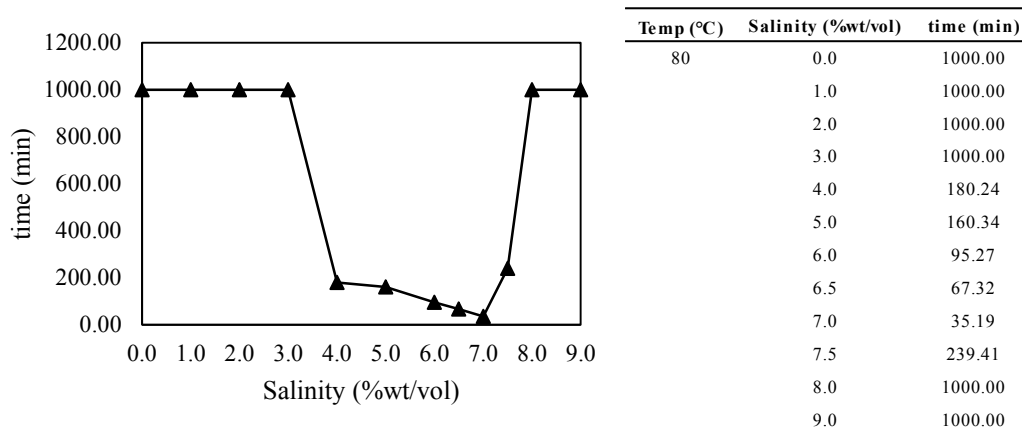
Figure G11 The coalescence time of C12-14EO5 with Hexadecane at 80 °C.

Temp (°C)	Salinity (%wt/vol)	time (min)
85	0.0	1000.00
	1.0	1000.00
	2.0	175.52
	3.0	156.37
	4.0	123.07
	5.0	87.35
	5.5	54.58
	6.0	244.41
	6.5	311.07
	7.0	1000.00
	8.0	1000.00
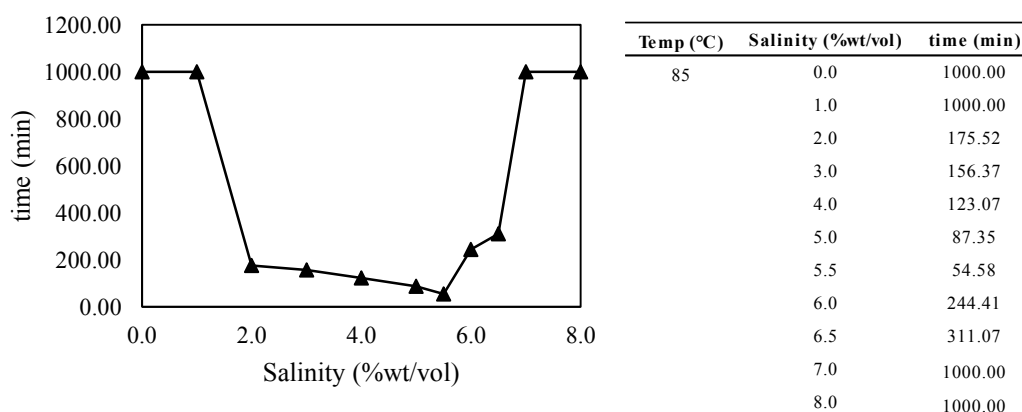
Figure G12 The coalescence time of C12-14EO5 with Hexadecane at 85 °C.

Temp (ºC)	Salinity (%wt/vol)	time (min)
90	0.0	1000.00
	1.5	282.08
	2.0	255.51
	2.5	234.48
	3.0	193.51
	3.5	142.32
	4.0	120.26
	4.5	87.55
	5.0	112.20
	6.0	1000.00
	7.0	1000.00
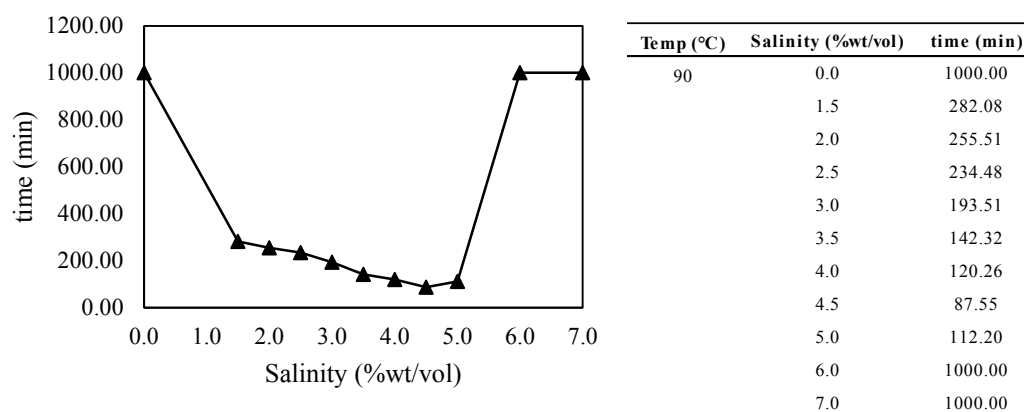
Figure G13 The coalescence time of C12-14EO5 with Hexadecane at 90 °C.

Temp (ºC)	Salinity (%wt/vol)	time (min)
95	0.0	1000.00
	0.5	216.13
	1.0	200.47
	1.5	172.39
	2.0	154.25
	2.5	91.51
	3.0	180.14
	5.0	1000.00
	6.0	1000.00
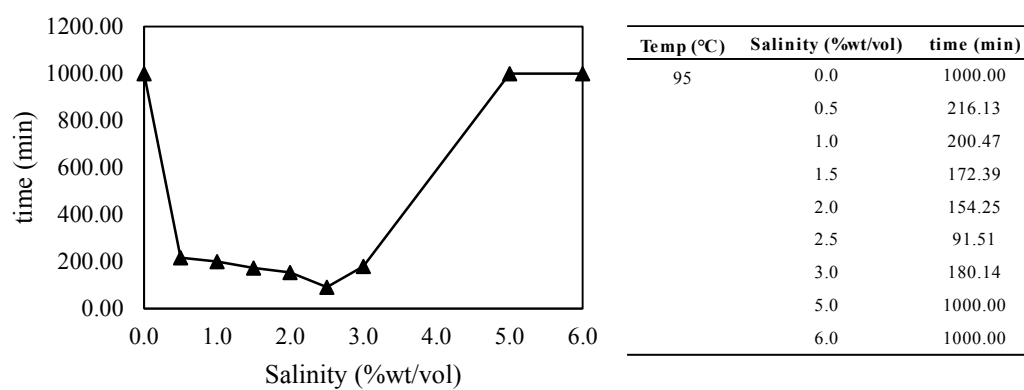
Figure G14 The coalescence time of C12-14EO5 with Hexadecane at 95 °C.

Appendix H Coalescence Time of C12-14EO9 for Single Surfactant Systems

The results of coalescence time of C12-14EO9 from experiment are shown in figure H1-H13. The boundary of time is within 1,000 minutes and the boundary of salinity is in range of 0 – 26 %wt/vol.

Temp (°C)	Salinity (%wt/vol)	Time (min)
35	21.0	1000.00
	21.5	1000.00
	22.0	248.35
	23.0	634.13
	24.0	1000.00
	24.5	1000.00
	25.0	1000.00
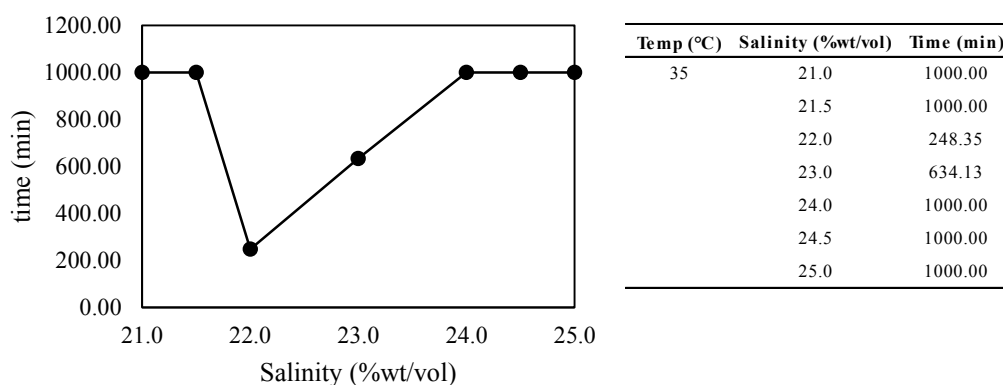
Figure H1 The coalescence time of C12-14EO9 with Decalin at 35 °C.

Temp (°C)	Salinity (%wt/vol)	Time (min)
40	0.00	1000.00
	15.00	1000.00
	16.00	1000.00
	17.00	1000.00
	18.00	1000.00
	18.25	1000.00
	18.50	1000.00
	18.75	585.00
	19.00	1000.00
	20.00	1000.00
	20.50	1000.00
	21.00	1000.00

(a)

Temp (°C)	Salinity (%wt/vol)	Time (min)
40	22.0	1000.00
	23.0	1000.00
	24.0	83.52
	24.5	149.24
	25.5	420.00
	26.0	1000.00
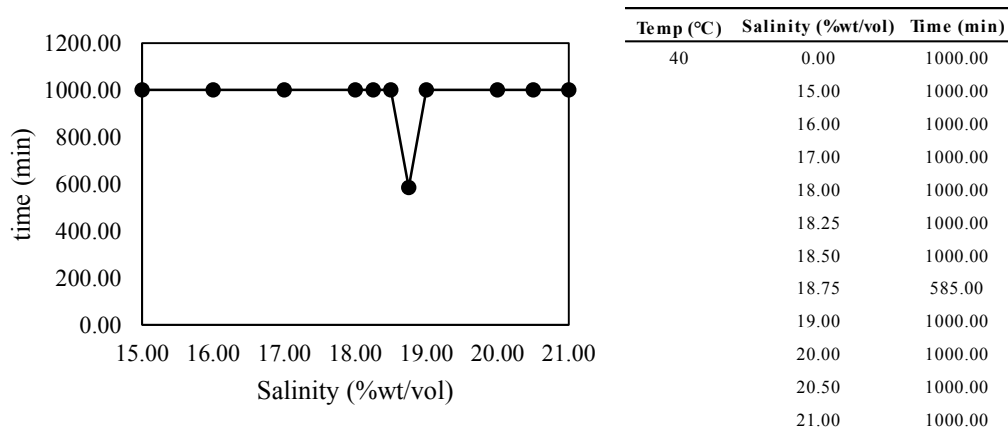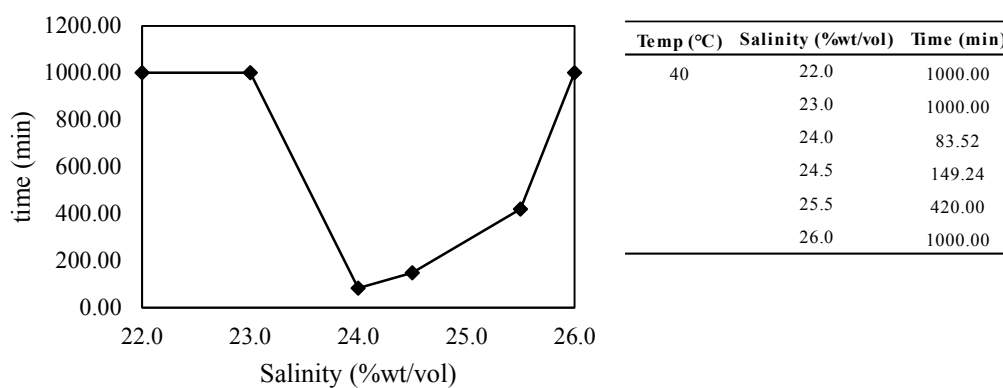
(b)

Figure H2 The coalescence time of C12-14EO9 with (a) Decalin and (b) Dodecane at 40 °C.

Temp (°C)	Salinity (%wt/vol)	Time (min)
45	0.0	1000.00
	10.0	1000.00
	11.0	1000.00
	12.0	1000.00
	13.0	1000.00
	14.0	1000.00
	15.0	1000.00
	16.0	294.02
	17.0	1000.00
	18.0	1000.00

(a)

Temp (°C)	Salinity (%wt/vol)	Time (min)
45	0.0	1000.00
	18.0	1000.00
	19.0	1000.00
	20.0	1000.00
	21.0	184.60
	22.0	98.23
	23.0	152.51
	24.0	192.13
	25.0	198.10
	26.0	1000.00

(b)

Temp (°C)	Salinity (%wt/vol)	Time (min)
45	0.0	1000.00
	20.0	1000.00
	21.0	1000.00
	22.0	1000.00
	23.0	1000.00
	23.5	1000.00
	24.0	1000.00
	24.5	1000.00
	25.0	1000.00
	26.0	205.46
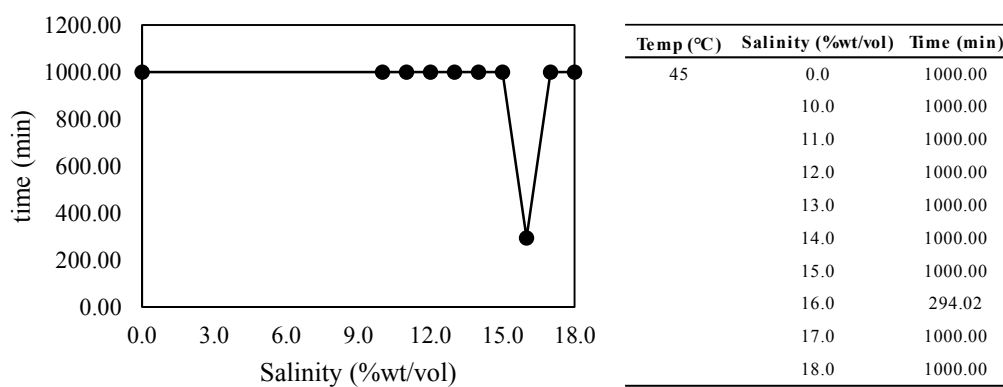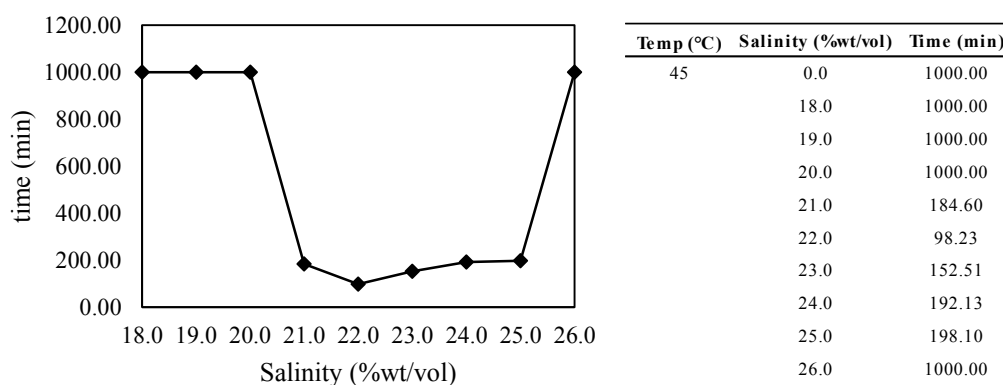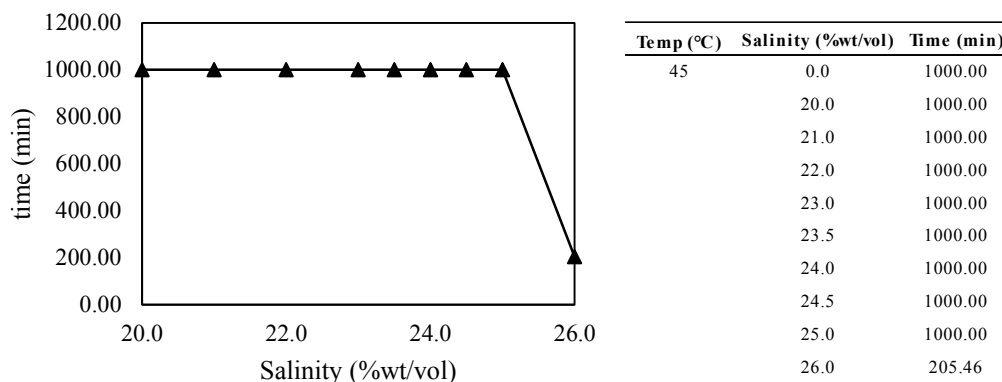
(c)

Figure H3 The coalescence time of C12-14EO9 with (a) Decalin, (b) Dodecane and (c) Hexadecane at 45 °C.

Temp (°C)	Salinity (%wt/vol)	Time (min)
50	0.0	1000.00
	6.0	1000.00
	8.0	1000.00
	9.0	1000.00
	10.0	1000.00
	11.0	1000.00
	12.0	1000.00
	13.0	162.30
	14.0	1000.00
	15.0	1000.00

(a)

Temp (°C)	Salinity (%wt/vol)	Time (min)
50	0.0	1000.00
	15.0	1000.00
	18.0	1000.00
	19.0	33.17
	20.0	78.38
	20.5	110.02
	21.0	161.59
	21.5	180.00
	22.0	202.09
	23.0	1000.00
	24.0	1000.00

(b)
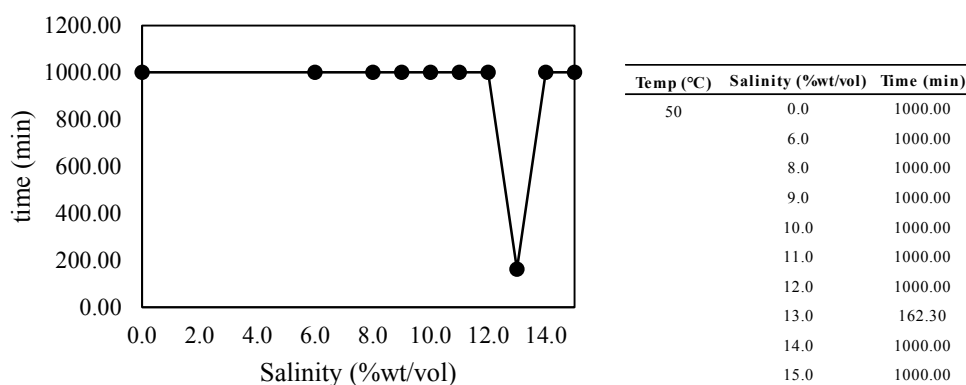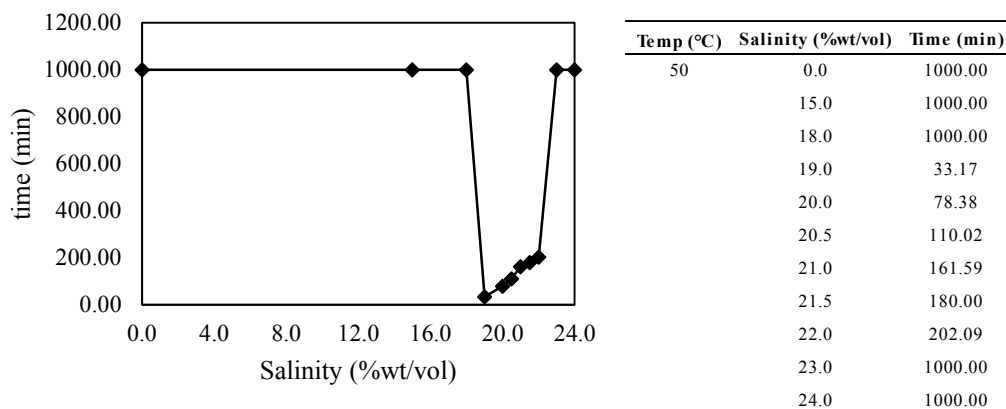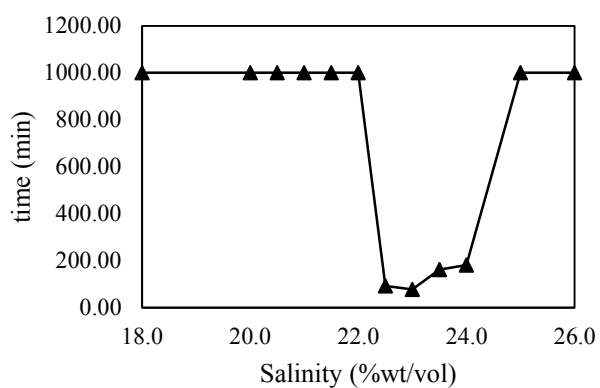
Temp (°C)	Salinity (%wt/vol)	Time (min)
50	0.0	1000.00
	18.0	1000.00
	20.0	1000.00
	20.5	1000.00
	21.0	1000.00
	21.5	1000.00
	22.0	1000.00
	22.5	93.35
	23.0	77.58
	23.5	163.12
	24.0	182.00
	25.0	1000.00
	26.0	1000.00

(c)

Figure H4 The coalescence time of C12-14EO9 with (a) Decalin, (b) Dodecane and (c) Hexadecane at 50 °C.
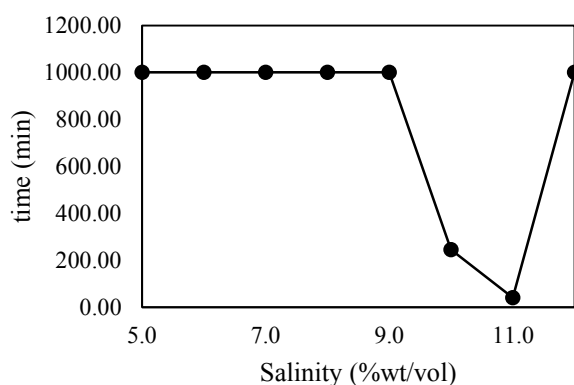
Temp (°C)	Salinity (%wt/vol)	Time (min)
55	5.0	1000.00
	6.0	1000.00
	7.0	1000.00
	8.0	1000.00
	9.0	1000.00
	10.0	245.48
	11.0	42.00
	12.0	1000.00
	13.0	1000.00

(a)
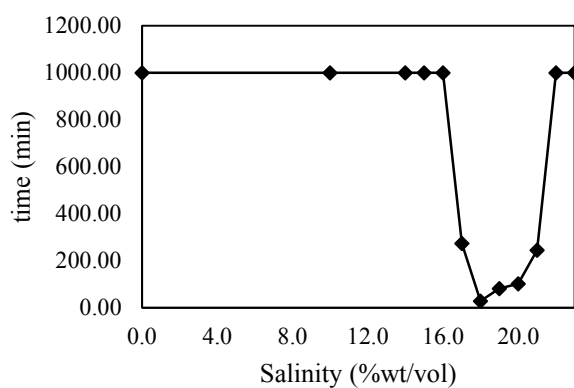
Temp (°C)	Salinity (%wt/vol)	Time (min)
55	0.0	1000.00
	10.0	1000.00
	14.0	1000.00
	15.0	1000.00
	16.0	1000.00
	17.0	274.17
	18.0	28.21
	19.0	81.20
	20.0	102.51
	21.0	245.22
	22.0	1000.00
	23.0	1000.00

(b)

Temp (°C)	Salinity (%wt/vol)	Time (min)
55	0.0	1000.00
	15.0	1000.00
	17.0	1000.00
	18.0	1000.00
	19.0	127.23
	20.0	22.55
	20.5	66.50
	21.0	79.38
	21.5	93.20
	22.0	109.41
	24.0	1000.00
	25.0	1000.00

(c)
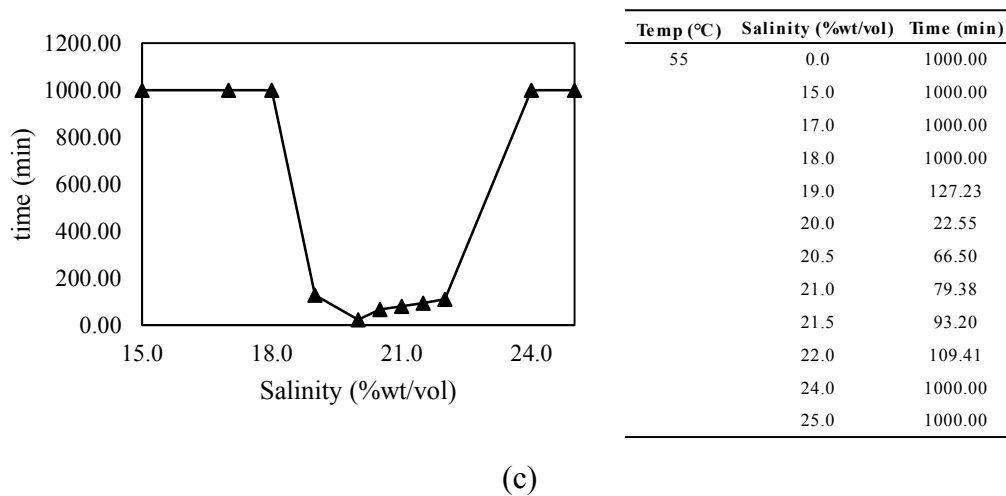
Figure H5 The coalescence time of C12-14EO9 with (a) Decalin, (b) Dodecane and (c) Hexadecane at 55 °C.

Temp (°C)	Salinity (%wt/vol)	Time (min)
60	0.0	1000.00
	4.0	1000.00
	8.0	1000.00
	10.0	1000.00
	11.0	1000.00
	13.0	1000.00
	14.0	1000.00
	15.0	32.01
	16.0	68.32
	17.0	106.36
	18.0	202.14
	19.0	1000.00
	20.0	1000.00

(a)
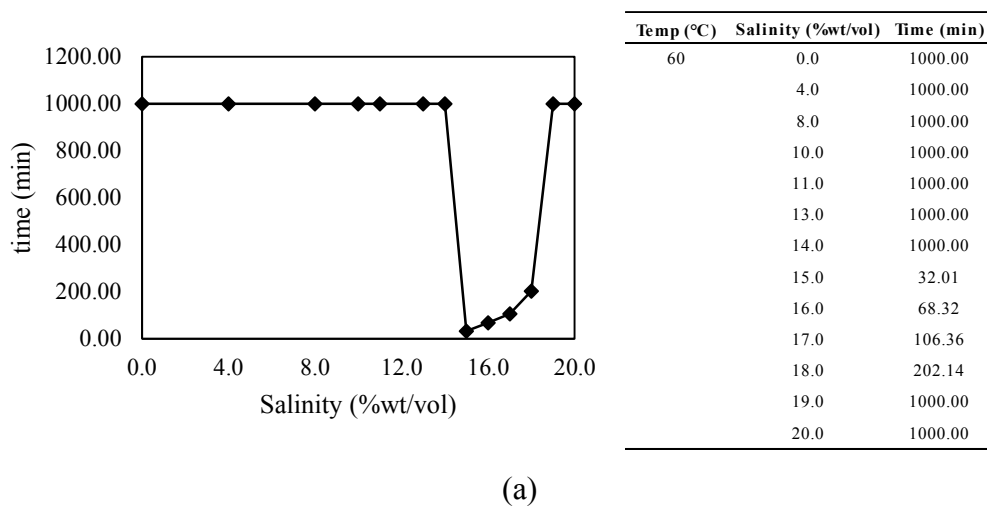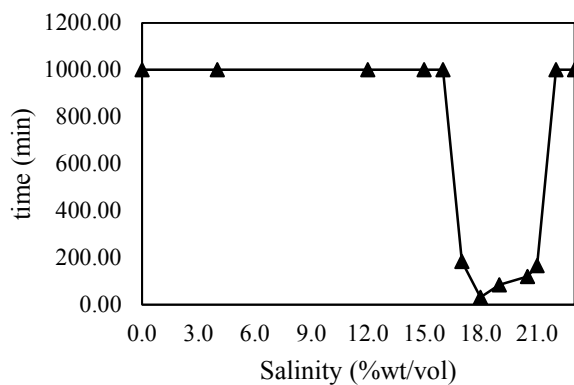
Temp (°C)	Salinity (%wt/vol)	Time (min)
60	0.0	1000.00
	4.0	1000.00
	12.0	1000.00
	15.0	1000.00
	16.0	1000.00
	17.0	184.05
	18.0	31.29
	19.0	85.06
	20.5	120.01
	21.0	167.41
	22.0	1000.00
	23.0	1000.00

(b)

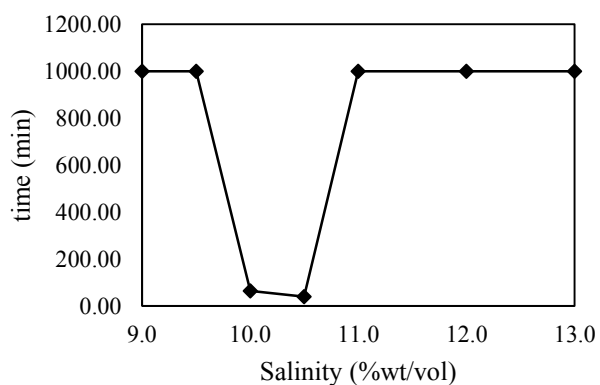**Figure H6** The coalescence time of C12-14EO9 with (a) Dodecane and (b) Hexadecane at 60 °C.
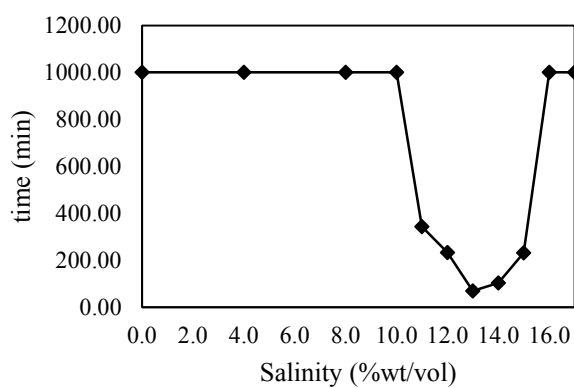
Temp (°C)	Salinity (%wt/vol)	Time (min)
65	0.0	1000.00
	4.0	1000.00
	8.0	1000.00
	10.0	1000.00
	11.0	343.53
	12.0	233.40
	13.0	70.34
	14.0	104.45
	15.0	232.30
	16.0	1000.00
	17.0	1000.00

(a)

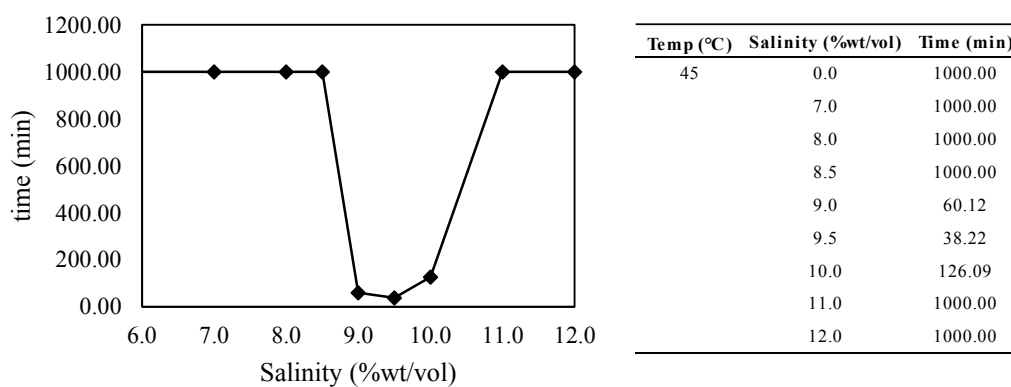| Temp (°C)	Salinity (%wt/vol)	Time (min)
65	0.0	1000.00
	4.0	1000.00
	8.0	1000.00
	12.0	1000.00
	13.0	1000.00
	14.0	154.32
	15.0	89.03
	16.0	54.50
	17.0	155.05
	18.0	173.40
	19.0	233.40
	20.0	293.25
	22.0	1000.00
	23.0	1000.00

(b)
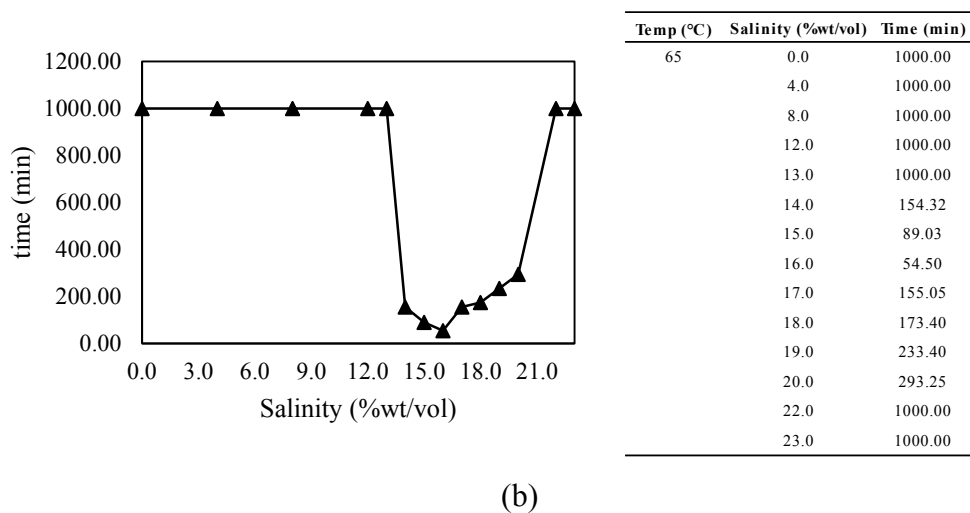
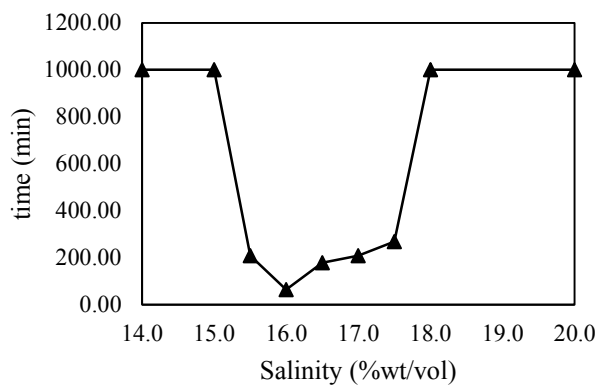**Figure H7** The coalescence time of C12-14EO9 with (a) Dodecane and (b) Hexadecane at 65 °C.

Temp (°C)	Salinity (%wt/vol)	Time (min)
70	0.0	1000.00
	4.0	1000.00
	8.0	1000.00
	10.0	60.34
	11.0	42.41
	12.0	126.31
	13.0	154.22
	14.0	182.47
	15.0	1000.00
	16.0	1000.00

(a)

(b)
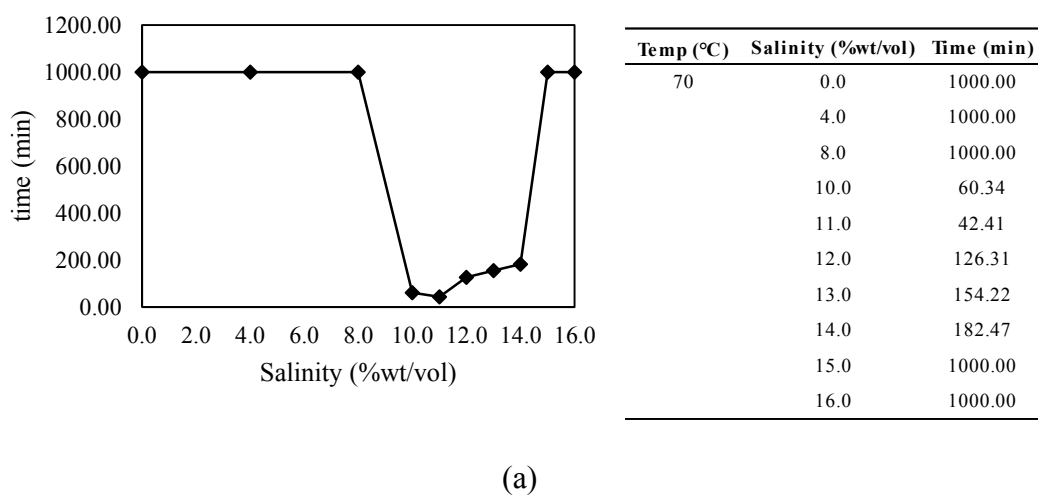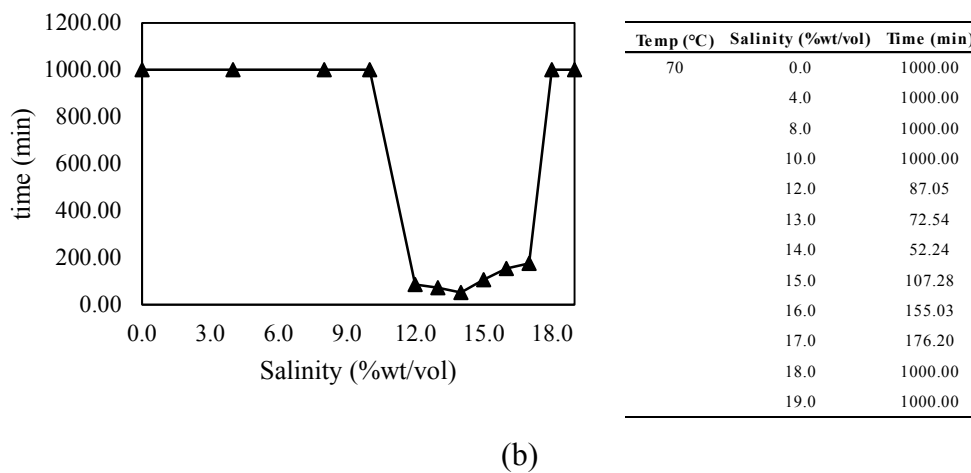
Figure H8 The coalescence time of C12-14EO9 with (a) Dodecane and (b) Hexadecane at 70 °C.

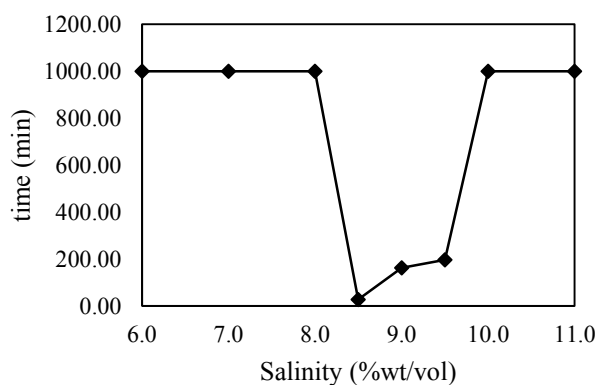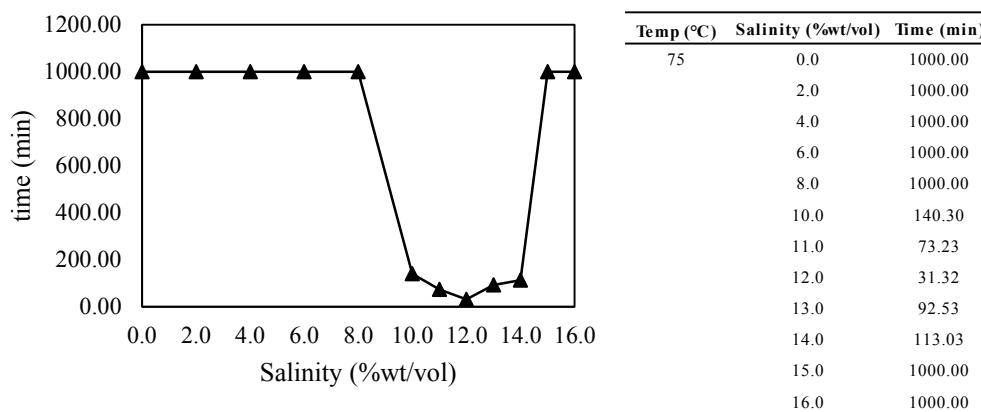**Figure H9** The coalescence time of C12-14EO9 with Hexadecane at 75 °C.

Temp (°C)	Salinity (%wt/vol)	Time (min)
80	0.0	1000.00
	2.0	1000.00
	4.0	1000.00
	6.0	1000.00
	8.0	153.04
	10.0	82.50
	11.0	46.49
	12.0	92.43
	13.0	112.55
	14.0	128.05
	16.0	1000.00
	17.0	1000.00
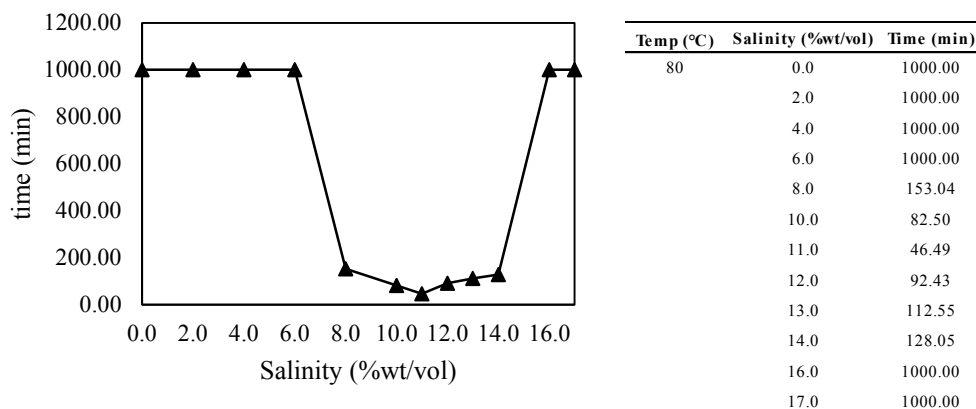
Figure H10 The coalescence time of C12-14EO9 with Hexadecane at 80 °C.

Temp (°C)	Salinity (%wt/vol)	Time (min)
85	0.0	1000.00
	2.0	1000.00
	4.0	1000.00
	6.0	1000.00
	8.0	80.55
	9.0	21.51
	10.0	63.34
	11.0	81.28
	12.0	100.35
	13.0	103.27
	14.0	154.11
	16.0	1000.00
	17.0	1000.00
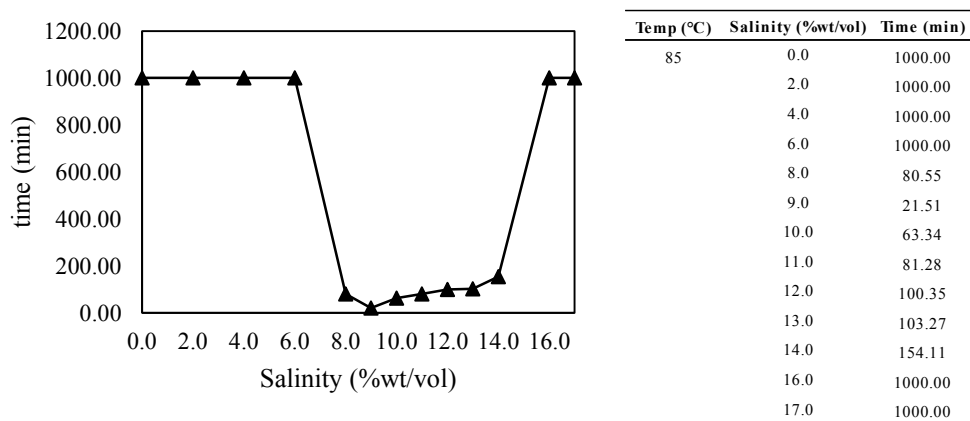
Figure H11 The coalescence time of C12-14EO9 with Hexadecane at 85 °C.

Temp (°C)	Salinity (%wt/vol)	Time (min)
90	0.0	1000.00
	2.0	1000.00
	4.0	1000.00
	6.0	65.55
	7.0	35.24
	8.0	15.07
	9.0	82.19
	10.0	144.03
	12.0	1000.00
	13.0	1000.00
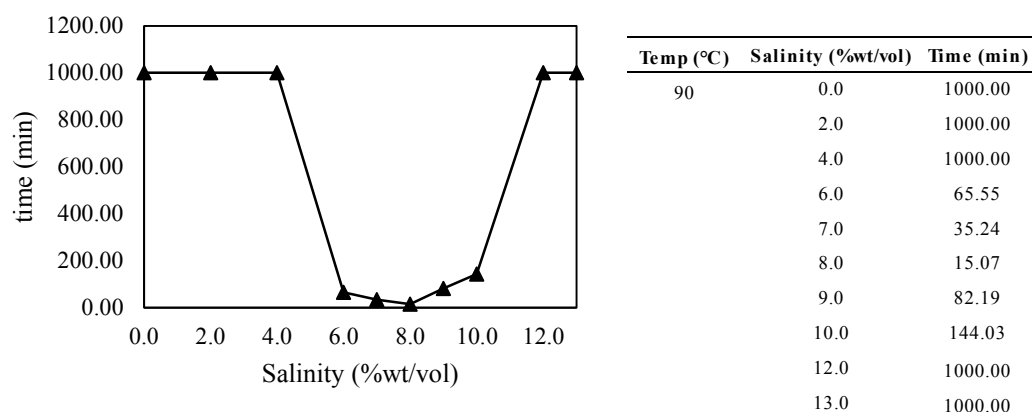
Figure H12 The coalescence time of C12-14EO9 with Hexadecane at 90 °C.

Temp (°C)	Salinity (%wt/vol)	Time (min)
95	0.0	1000.00
	2.0	1000.00
	4.0	186.44
	6.0	11.54
	7.0	53.57
	8.0	94.20
	9.0	116.17
	10.0	147.28
	12.0	1000.00
	13.0	1000.00
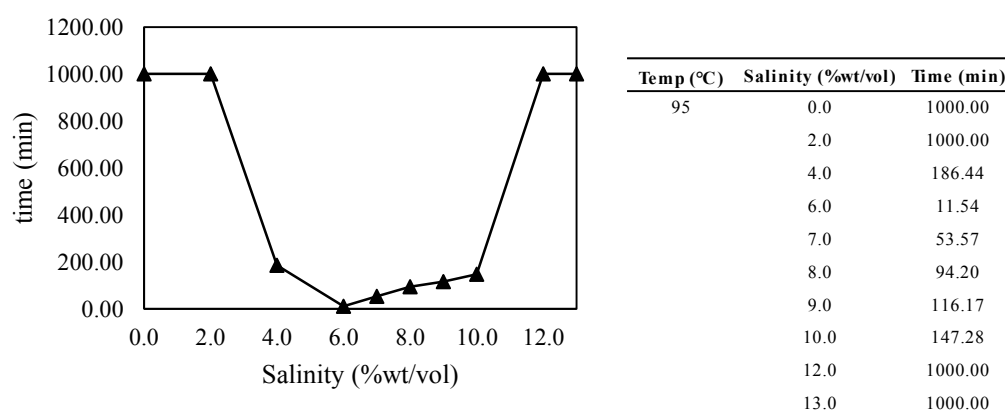
Figure H13 The coalescence time of C12-14EO9 with Hexadecane at 95 °C.

Appendix I   Measurement of Dynamic Interfacial Tension for EACN Calculation

The results of interfacial tension are shown in Figure I1-I7 for all oil (cyclohexane, hexane, heptane, decalin, decane, dodecane and hexadecane) included in this work. The salinity at the minimum interfacial tension are used to calculate the EACN value of each oil.
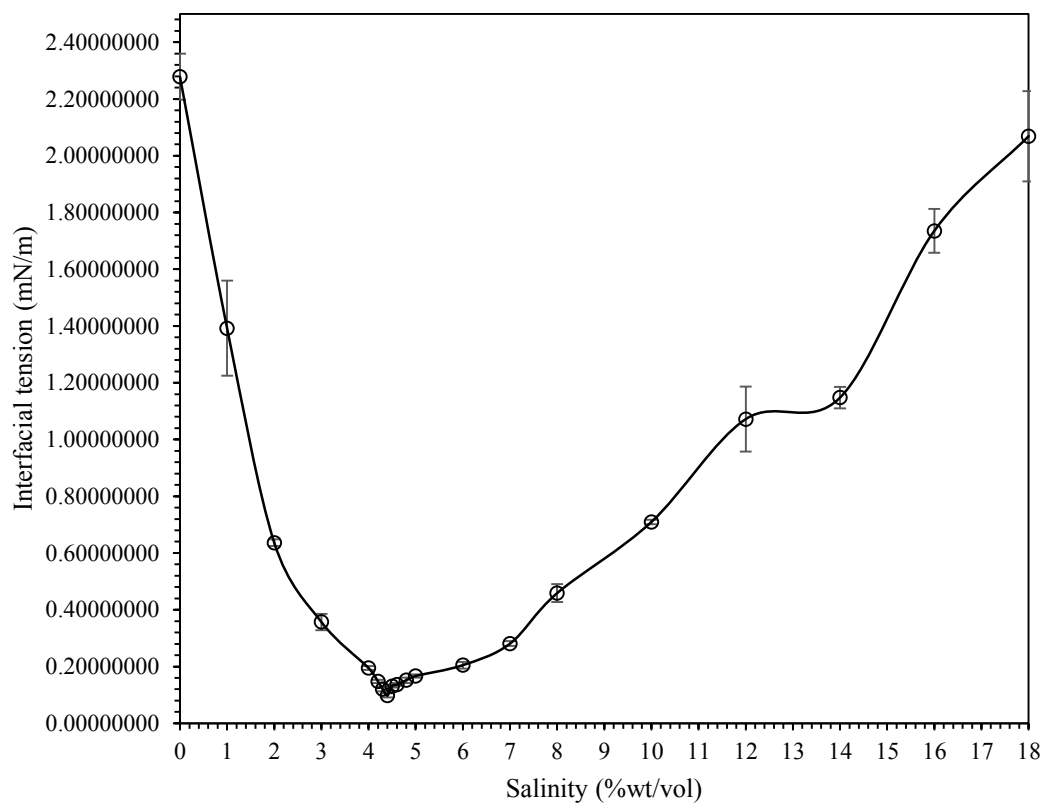
Salinity (%wt/vol)	IFT (mN/m)	Salinity (%wt/vol)	IFT (mN/m)
0.0	2.27840897	4.8	0.15173012
1.0	1.39218667	5.0	0.16679236
2.0	0.63633430	6.0	0.20489987
3.0	0.35686921	7.0	0.28081169
4.0	0.19481515	8.0	0.45861810
4.2	0.14776669	10.0	0.70966218
4.3	0.12013747	12.0	1.07188310
4.4	0.09841349	14.0	1.14773427
4.5	0.13097446	16.0	1.73527610
4.6	0.13649113	18.0	2.06891227

Figure I1 The interfacial tension of SDHS system with cyclohexane.
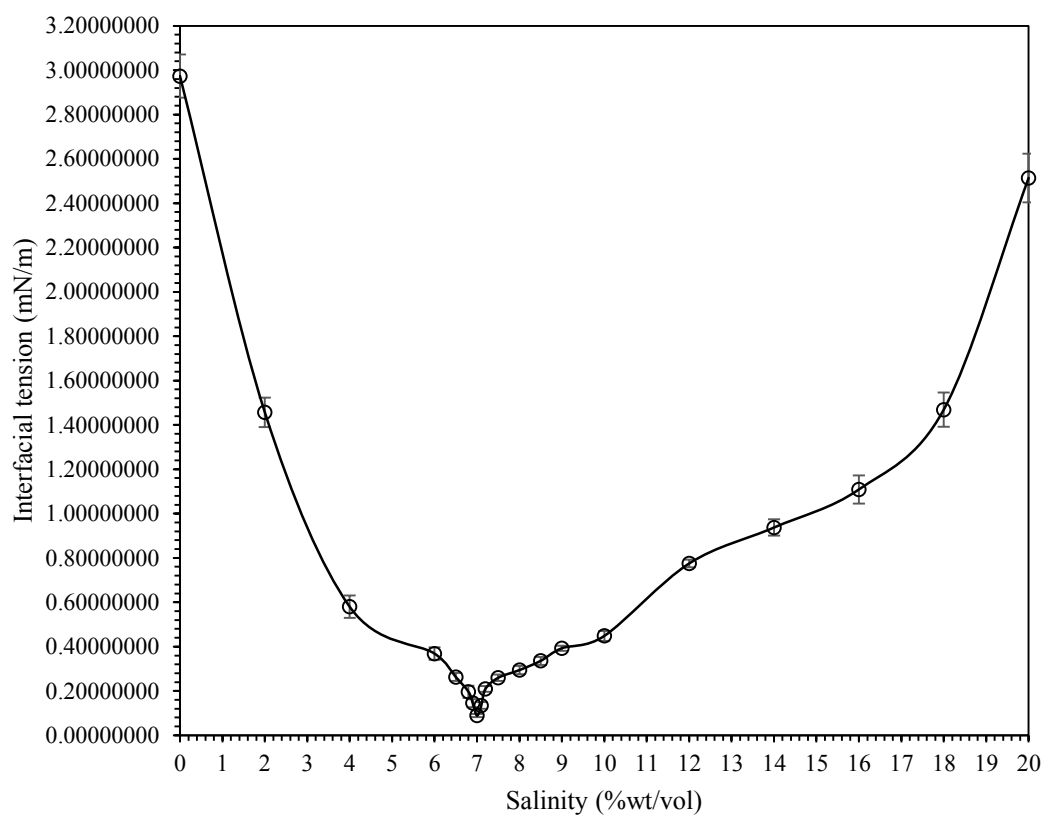
Salinity (%wt/vol)	IFT (mN/m)	Salinity (%wt/vol)	IFT (mN/m)
0.0	2.97348860	7.5	0.25956228
2.0	1.45705917	8.0	0.29408068
4.0	0.57986076	8.5	0.33570911
6.0	0.36840604	9.0	0.39273717
6.5	0.26305014	10.0	0.44815396
6.8	0.19640464	12.0	0.77502153
6.9	0.14508115	14.0	0.93719981
7.0	0.08891920	16.0	1.10888147
7.1	0.13468241	18.0	1.46888500
7.2	0.20956706	20.0	2.51363733

Figure I2 The interfacial tension of SDHS system with hexane.
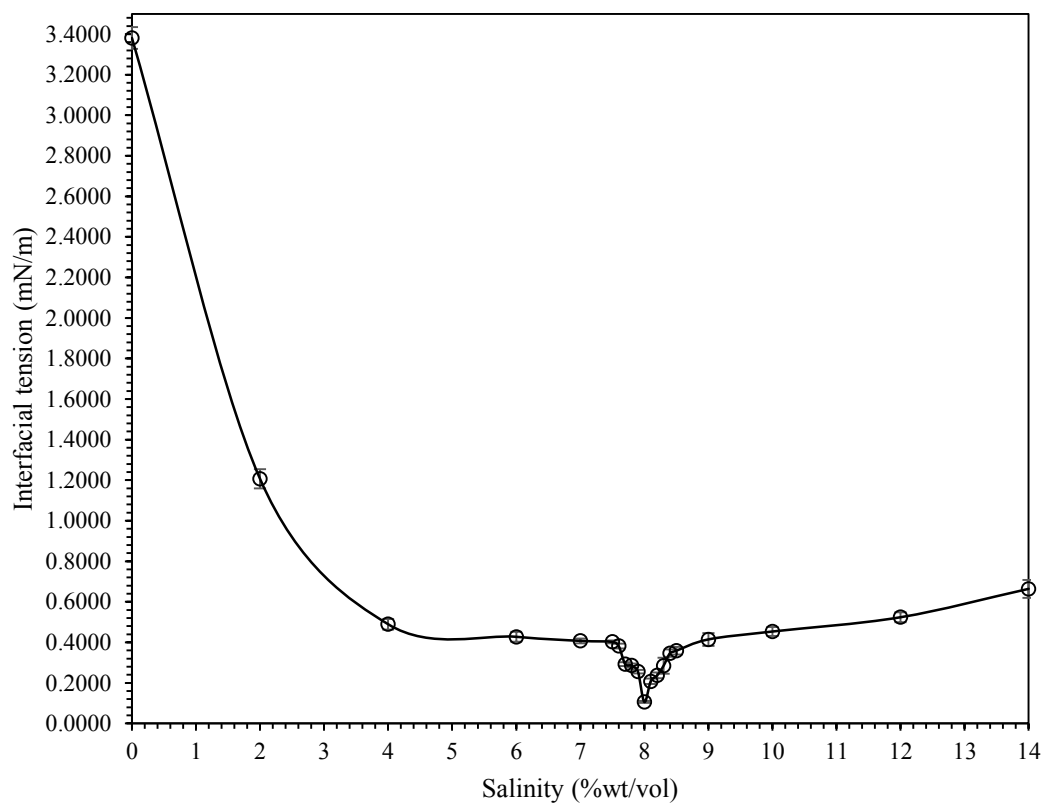
Salinity (%wt/vol)	IFT (mN/m)	Salinity (%wt/vol)	IFT (mN/m)
0.0	3.38084467	8.0	0.10594291
2.0	1.20621893	8.1	0.20771702
4.0	0.48933993	8.2	0.23687234
6.0	0.42732698	8.3	0.28416586
7.0	0.40736458	8.4	0.34640391
7.5	0.40224564	8.5	0.35865817
7.6	0.38171118	9.0	0.41451999
7.7	0.29294442	10.0	0.45348242
7.8	0.28539816	12.0	0.52382720
7.9	0.25593743	14.0	0.66387464

Figure I3 The interfacial tension of SDHS system with heptane.
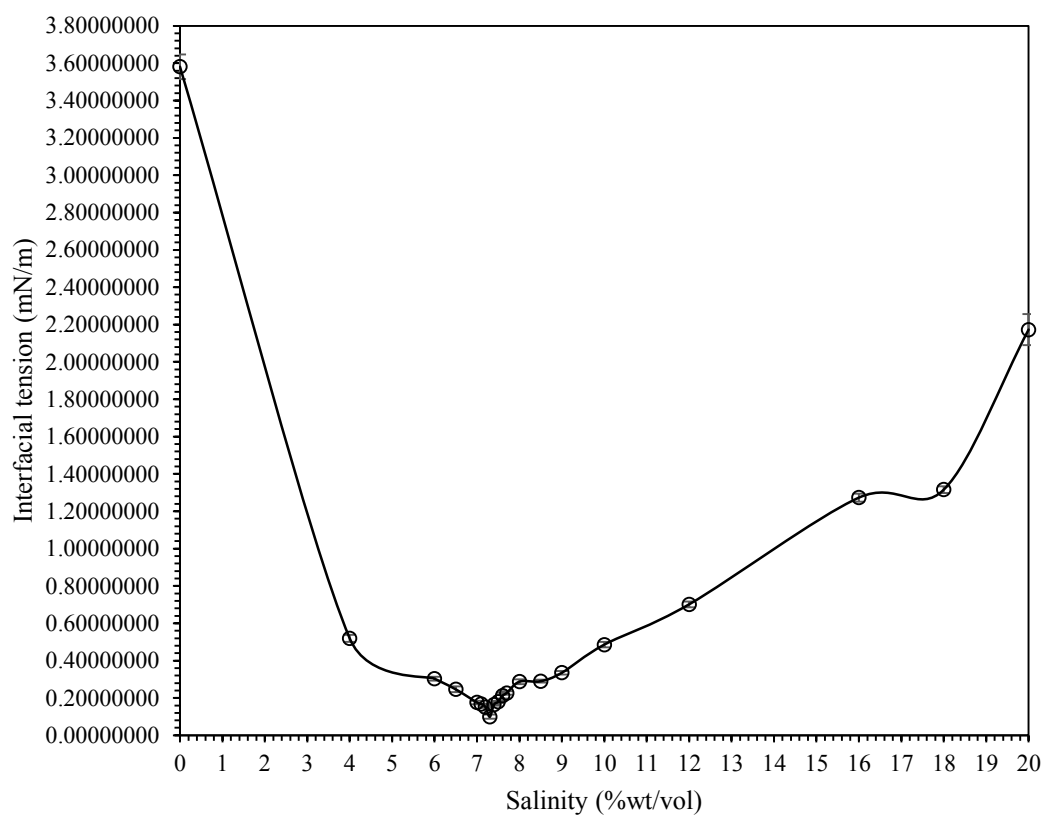
Salinity (%wt/vol)	IFT (mN/m)	Salinity (%wt/vol)	IFT (mN/m)
0.0	3.58087837	7.6	0.21219242
4.0	0.51940546	7.7	0.22684125
6.0	0.30319377	8.0	0.28710282
6.5	0.24613631	8.5	0.28972663
7.0	0.17591089	9.0	0.33492061
7.1	0.16799809	10.0	0.48559721
7.2	0.15114001	12.0	0.70155977
7.3	0.09941871	16.0	1.27296143
7.4	0.16420237	18.0	1.31584427
7.5	0.17970319	20.0	2.17291710

Figure I4 The interfacial tension of SDHS system with decalin.
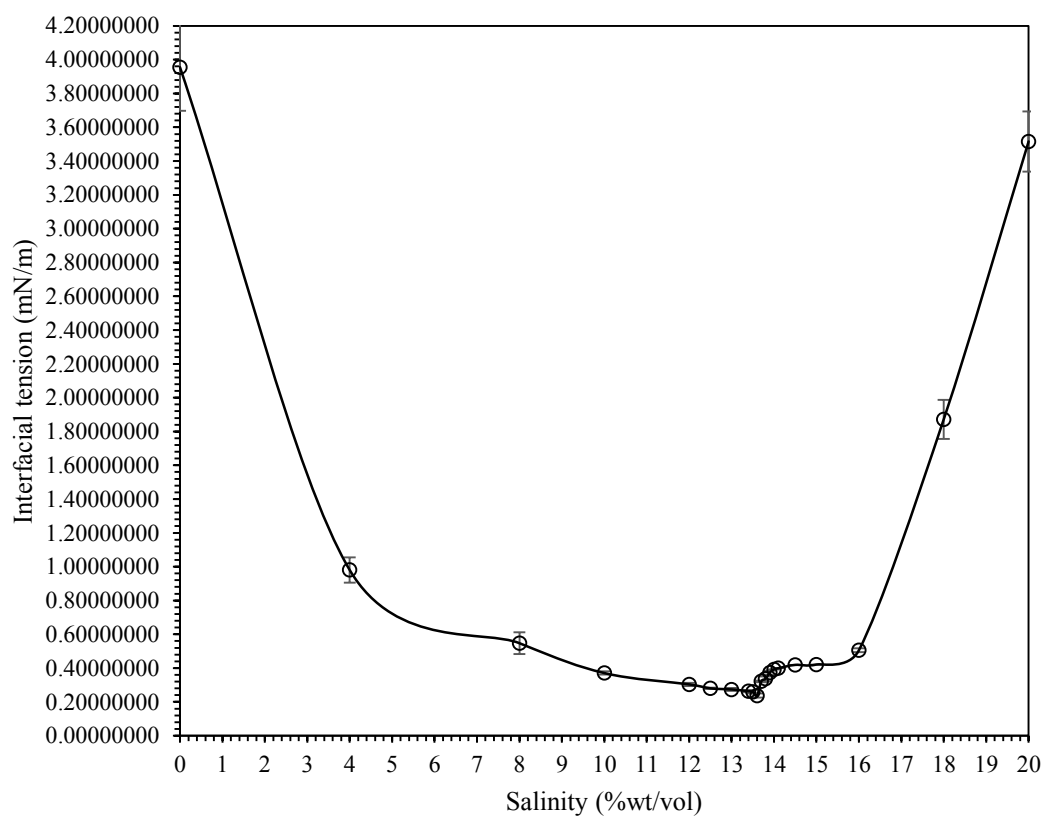
Salinity (%wt/vol)	IFT (mN/m)	Salinity (%wt/vol)	IFT (mN/m)
0.0	3.95528627	13.7	0.32163549
4.0	0.98048500	13.8	0.33671087
8.0	0.54738050	13.9	0.37304825
10.0	0.37072485	14.0	0.39257215
12.0	0.30368188	14.1	0.39945560
12.5	0.28027563	14.5	0.41899637
13.0	0.27373499	15.0	0.42133241
13.4	0.26333462	16.0	0.50524440
13.5	0.25971256	18.0	1.87229267
13.6	0.23714530	20.0	3.51577457

Figure I5 The interfacial tension of SDHS system with decane.
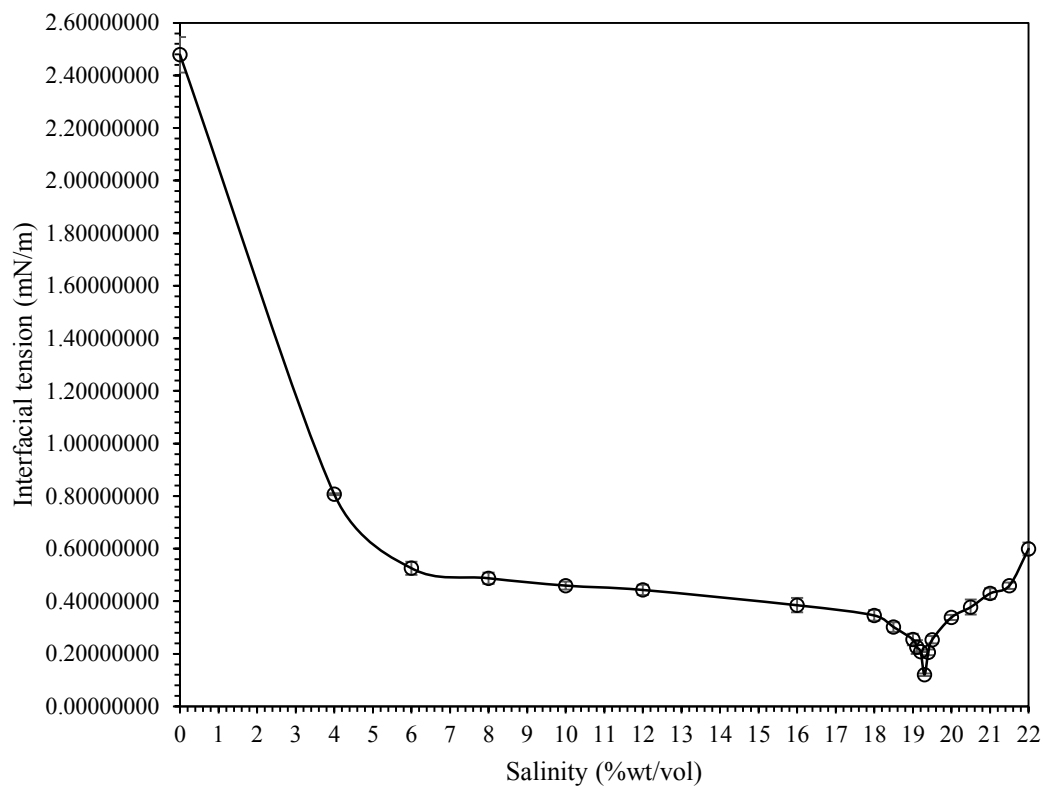
Salinity (%wt/vol)	IFT (mN/m)	Salinity (%wt/vol)	IFT (mN/m)
0.0	2.47882933	19.1	0.22556460
4.0	0.80677613	19.2	0.20862245
6.0	0.52576198	19.3	0.12084748
8.0	0.48757682	19.4	0.20589281
10.0	0.45956650	19.5	0.25363123
12.0	0.44296687	20	0.33844931
16.0	0.38485196	20.5	0.37776422
18.0	0.34590112	21	0.42950637
18.5	0.30195362	21.5	0.45953648
19.0	0.25456592	22	0.59902948

Figure I6 The interfacial tension of SDHS system with dodecane.
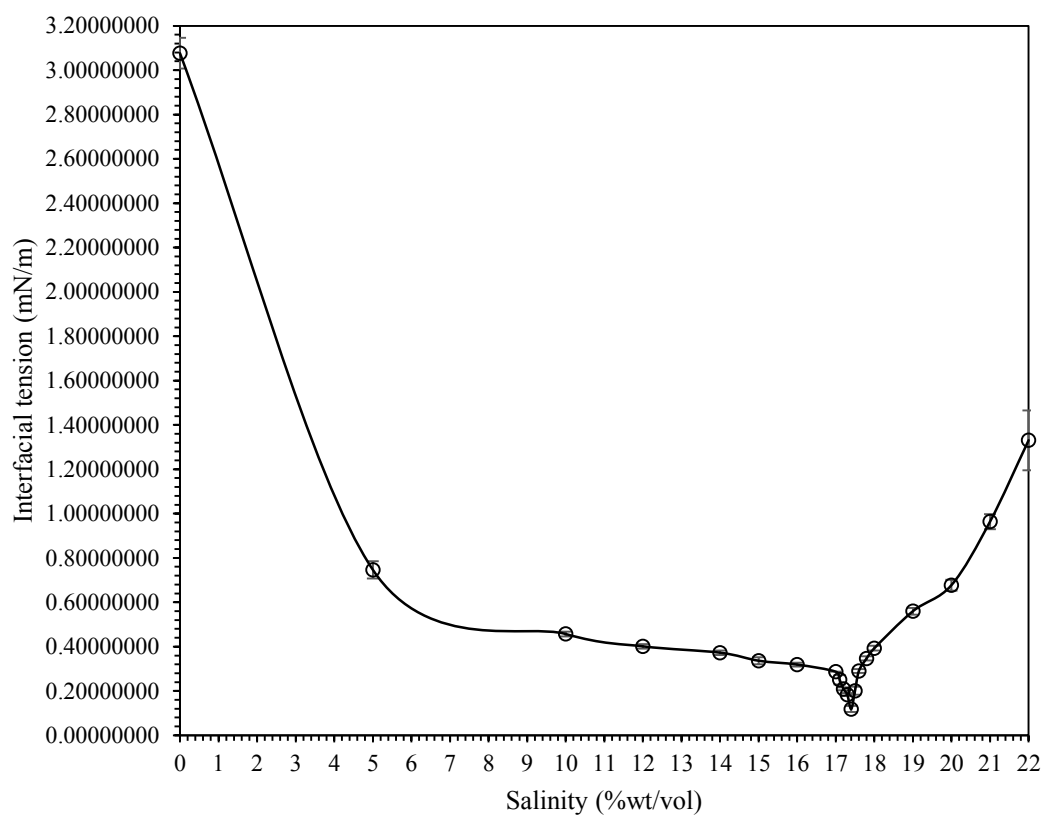
Salinity (%wt/vol)	IFT (mN/m)	Salinity (%wt/vol)	IFT (mN/m)
0.0	3.07637807	17.3	0.18323923
5.0	0.74669589	17.4	0.11866102
10.0	0.45681205	17.5	0.20086895
12.0	0.40123347	17.6	0.29001360
14.0	0.37269895	17.8	0.34668080
15.0	0.33642714	18.0	0.39276904
16.0	0.31906995	19.0	0.55969241
17.0	0.28700418	20.0	0.67750344
17.1	0.25076365	21.0	0.96390749
17.2	0.20932239	22.0	1.33069833

Figure I7 The interfacial tension of SDHS system with hexadecane mixed with heptane (ratio 1:1).

Appendix J Group Occurrences for Characteristic Curvature Model for Anionic Surfactant

The group structures for GC model that occur in the database of C_c model are shown in this appendix. The structure of anionic surfactants is divided into small molecules as Marrero *et al.* (2001) concept. The number of occurrence groups are counted and shown in the table. The data are used for regression analysis to find the contributions for the GC model.

Table J1 First-order group occurrence for Characteristic curvature model of anionic surfactant

		Group Occurrences									
First-order		**CH$_3$**	**CH$_2$**	**CH**	**CH=CH**	**CH$_2$-O**	**CH$_2$COO**	**CHCOO**	**CONH**	**SO$_3^-$**	**OSO$_3^-$**
Coefficient		0.6325	0.2088	-0.2082	-0.5123	-0.1555	-1.0115	0.2491	-4.8786	0.0297	-2.1970
Name	**C$_{ca}$**										
SDHS Na Dihexylsulfosuccinate	-0.920	2	10	0	0	0	1	1	0	1	0
SDBS Na Dodecyl Benzene sulfonate	-0.900	1	10	0	0	0	0	0	0	0	0
SDS/SLS Na Dodecyl Sulfate	-2.500	1	11	0	0	0	0	0	0	0	1
Sodium Octanoate	-3.000	1	5	0	0	0	1	0	0	0	0
Sodium Decanoate	-2.550	1	7	0	0	0	1	0	0	0	0
Sodium Dodecanoate	-2.100	1	9	0	0	0	1	0	0	0	0
Sodium stearate	-0.750	1	15	0	0	0	1	0	0	0	0
Sodium Oleate	-1.700	1	13	0	1	0	1	0	0	0	0
Sodium Dimethylnaphthalene sulfonate	-3.500	0	0	0	0	0	0	0	0	0	0
Sodium Strearoyl glutamate	-5.000	1	17	0	0	0	1	1	1	0	0
Lecithin	4.000	4	30	1	1	0	2	0	0	0	0
NaC12PO4Sulfate	-1.900	5	11	4	0	4	0	0	0	0	1
NaC12PO6Sulfate	-1.600	7	11	6	0	6	0	0	0	0	1
NaC12PO10sulfate	-1.000	11	11	10	0	10	0	0	0	0	1
NaBrancedC12PO4Sulfate	-1.400	6	9	5	0	4	0	0	0	0	1
NaBrancedC12PO6Sulfate	-1.100	8	9	7	0	6	0	0	0	0	1

Table J1 First-order group occurrence for Characteristic curvature model of anionic surfactant (Continued)

Name	C_{ca}	PO$_4^-$	aC fused aro	aCH	aC-CH$_3$	aC-CH$_2$	aC-SO$_3^-$	CH$_3$N$^+$	CH$_{2,cyc}$	CH$_{cyc}$
First-order		group								
Coefficient		1.5828	0.0444	-0.0335	0.0300	0.0047	0.0197	-0.0551	0.3260	-0.0212
SDHS Na Dihexylsulfosuccinate	-0.920	0	0	0	0	0	0	0	0	0
SDBS Na Dodecyl Benzene sulfonate	-0.900	0	0	4	0	1	1	0	0	0
SDS/SLS Na Dodecyl Sulfate	-2.500	0	0	0	0	0	0	0	0	0
Sodium Octanoate	-3.000	0	0	0	0	0	0	0	0	0
Sodium Decanoate	-2.550	0	0	0	0	0	0	0	0	0
Sodium Dodecanoate	-2.100	0	0	0	0	0	0	0	0	0
Sodium stearate	-0.750	0	0	0	0	0	0	0	0	0
Sodium Oleate	-1.700	0	0	0	0	0	0	0	0	0
Sodium Dimethylnaphthalene sulfonate	-3.500	0	2	5	2	0	1	0	0	0
Sodium Strearoyl glutamate	-5.000	0	0	0	0	0	0	0	0	0
Lecithin	4.000	1	0	0	0	0	0	1	0	0
NaC12PO4Sulfate	-1.900	0	0	0	0	0	0	0	0	0
NaC12PO6Sulfate	-1.600	0	0	0	0	0	0	0	0	0
NaC12PO10sulfate	-1.000	0	0	0	0	0	0	0	0	0
NaBrancedC12PO4Sulfate	-1.400	0	0	0	0	0	0	0	0	0
NaBrancedC12PO6Sulfate	-1.100	0	0	0	0	0	0	0	0	0

Table J1 First-order group occurrence for Characteristic curvature model of anionic surfactant (Continued)

Name	C_{ca}	CH₃	CH₂	CH	CH=CH	CH₂-O	CH₂COO	CHCOO	CONH	SO₃⁻	OSO₃⁻
First-order		CH₃	CH₂	CH	CH=CH	CH₂-O	CH₂COO	CHCOO	CONH	SO₃⁻	OSO₃⁻
Coefficient		0.6325	0.2088	-0.2082	-0.5123	-0.1555	-1.0115	0.2491	-4.8786	0.0297	-2.1970
NaBrancedC12PO8Sulfate	-0.800	10	9	9	0	8	0	0	0	0	1
NaBrancedC12PO10Sulfate	-0.500	12	9	11	0	10	0	0	0	0	1
NaBrancedC14PO8Sulfate	-0.600	10	11	9	0	8	0	0	0	0	1
NaC12PO14EO2sulfate	0.740	15	13	14	0	16	0	0	0	0	1
NaC10PO18EO2Sulfate	1.990	19	11	18	0	20	0	0	0	0	1
NaC8PO4EOSulfate	-2.470	5	8	4	0	5	0	0	0	0	1
NaC8PO4Sulfate	-2.480	5	7	4	0	4	0	0	0	0	1
NaC10PO4EOSulfate	-2.220	5	10	4	0	5	0	0	0	0	1
NaC10PO4Sulfate	-2.150	5	9	4	0	4	0	0	0	0	1
NaC12EO3Sulfate	-2.890	1	14	0	0	3	0	0	0	0	1
Sodium naphthenate	-2.400	1	2	0	0	0	1	0	0	0	0
NaC12-15EO2Sulfate	-2.970	1	12.5	0	0	2	0	0	0	0	1
NaC12-13PO8Sulfate	-0.784	9	11.5	8	0	8	0	0	0	0	1
NaC12-13PO3Sulfate	-1.770	4	11.5	3	0	3	0	0	0	0	1
Br-Oxo 123	-1.550	6	9.5	5	0	4	0	0	0	0	1
TDA	-1.610	8	6	7	0	4	0	0	0	0	1
L-Oxol123	-1.950	5	11.5	4	0	4	0	0	0	0	1

Table J1 First-order group occurrence for Characteristic curvature model of anionic surfactant (Continued)

Name	C_{ca}	PO$_4^-$	aC fused aro	aCH	aC-CH$_3$	aC-CH$_2$	aC-SO$_3^-$	CH$_3$N$^+$	CH$_{2,cyc}$	CH$_{cyc}$
		1.5828	0.0444	-0.0335	0.0300	0.0047	0.0197	-0.0551	0.3260	-0.0212
NaBrancedC12PO8Sulfate	-0.800	0	0	0	0	0	0	0	0	0
NaBrancedC12PO10Sulfate	-0.500	0	0	0	0	0	0	0	0	0
NaBrancedC14PO8Sulfate	-0.600	0	0	0	0	0	0	0	0	0
NaC12PO14EO2sulfate	0.740	0	0	0	0	0	0	0	0	0
NaC10PO18EO2Sulfate	1.990	0	0	0	0	0	0	0	0	0
NaC8PO4EOSulfate	-2.470	0	0	0	0	0	0	0	0	0
NaC8PO4Sulfate	-2.480	0	0	0	0	0	0	0	0	0
NaC10PO4EOSulfate	-2.220	0	0	0	0	0	0	0	0	0
NaC10PO4Sulfate	-2.150	0	0	0	0	0	0	0	0	0
NaC12EO3Sulfate	-2.890	0	0	0	0	0	0	0	0	0
Sodium naphthenate	-2.400	0	0	0	0	0	0	0	3	2
NaC12-15EO2Sulfate	-2.970	0	0	0	0	0	0	0	0	0
NaC12-13PO8Sulfate	-0.784	0	0	0	0	0	0	0	0	0
NaC12-13PO3Sulfate	-1.770	0	0	0	0	0	0	0	0	0
Br-Oxo 123	-1.550	0	0	0	0	0	0	0	0	0
TDA	-1.610	0	0	0	0	0	0	0	0	0
L-Oxol123	-1.950	0	0	0	0	0	0	0	0	0

Table J2 Higher-order group occurrence for Characteristic curvature model of anionic surfactant

Name	Higher-order	AROMRINGs^{1}s^4	-EO-	-PO-	CH$_{cyc}$-CH$_2$	OOC-(CH$_n$)$_m$-COO	COO-(CH$_n$)$_m$-OOC	AROMFUSED[2]s^{1}s^2
	Coefficient	0.0122	0.0475	-0.0310	0.0747	-0.0170	-0.0551	0.0225
Name	C_{ca}							
SDHS Na Dihexylsulfosuccinate	-0.920	0	0	0	0	1	0	0
SDBS Na Dodecyl Benzene sulfonate	-0.900	1	0	0	0	0	0	0
SDS/SLS Na Dodecyl Sulfate	-2.500	0	0	0	0	0	0	0
Sodium Octanoate	-3.000	0	0	0	0	0	0	0
Sodium Decanoate	-2.550	0	0	0	0	0	0	0
Sodium Dodecanoate	-2.100	0	0	0	0	0	0	0
Sodium stearate	-0.750	0	0	0	0	0	0	0
Sodium Oleate	-1.700	0	0	0	0	0	0	0
Sodium Dimethylnaphthalene sulfonate	-3.500	0	0	0	0	0	0	1
Sodium Strearoyl glutamate	-5.000	0	0	0	0	1	0	0
Lecithin	4.000	0	0	0	0	0	1	0
NaC12PO4Sulfate	-1.900	0	0	4	0	0	0	0
NaC12PO6Sulfate	-1.600	0	0	6	0	0	0	0
NaC12PO10sulfate	-1.000	0	0	10	0	0	0	0
NaBrancedC12PO4Sulfate	-1.400	0	0	4	0	0	0	0
NaBrancedC12PO6Sulfate	-1.100	0	0	6	0	0	0	0

Table J2 Higher-order group occurrence for Characteristic curvature model of anionic surfactant (Continued)

Name	Higher-order Coefficient	Group Occurrences						
		AROMRINGs[1]s[4]	-EO-	-PO-	$CH_{cyc}-CH_2$	$OOC-(CH_n)_m-COO$	$COO-(CH_n)_m-OOC$	AROMFUSED[2]s[1]s[2]
	Coefficient	0.0122	0.0475	-0.0310	0.0747	-0.0170	-0.0551	0.0225
Name	C_{ca}							
NaBrancedC12PO8Sulfate	-0.800	0	0	8	0	0	0	0
NaBrancedC12PO10Sulfate	-0.500	0	0	10	0	0	0	0
NaBrancedC14PO8Sulfate	-0.600	0	0	8	0	0	0	0
NaC12PO14EO2sulfate	0.740	0	2	14	0	0	0	0
NaC10PO18EO2Sulfate	1.990	0	2	18	0	0	0	0
NaC8PO4EOSulfate	-2.470	0	1	0	0	0	0	0
NaC8PO4Sulfate	-2.480	0	0	0	0	0	0	0
NaC10PO4EOSulfate	-2.220	0	1	4	0	0	0	0
NaC10PO4Sulfate	-2.150	0	0	4	0	0	0	0
NaC12EO3Sulfate	-2.890	0	3	0	0	0	0	0
Sodium naphthenate	-2.400	0	0	0	2	0	0	0
NaC12-15EO2Sulfate	-2.970	0	2	0	0	0	0	0
NaC12-13PO8Sulfate	-0.784	0	0	8	0	0	0	0
NaC12-13PO3Sulfate	-1.770	0	0	3	0	0	0	0
Br-Oxo 123	-1.550	0	0	4	0	0	0	0
TDA	-1.610	0	0	4	0	0	0	0
L-Oxol123	-1.950	0	0	4	0	0	0	0

Appendix K Example Calculation of Characteristic Curvature Model for Anionic Surfactant

This appendix shows the example calculation when the characteristic curvature GC model is applied to the anionic surfactant. The represents from various structure are chosen for calculation the characteristic curvature, as compared to the experimental value.

Table K1 Example calculation of Characteristic curvature of Sodium Dihexyl sulfosuccinate (SDHS)

Sodium Dihexyl sulfosuccinate		
Molecular structure: First-order group:		
Groups	Occurrences	Coefficients
CH_3	2	0.6325
CH_2	10	0.2088
CH_2COO	1	-1.0115
$CHCOO$	1	0.2491
SO_3^-	1	0.0297
Second-order group:		
Groups	Occurrences	Coefficients
No Second-order group		
Third-order group:		
Groups	Occurrences	Coefficients
OOC-$(CH_n)_m$-COO	1	-0.0170
C_{ca} calculation		
$C_{ca} = \Sigma_i N_i C_i + \Sigma_j M_j D_j + \Sigma_k O_k E_k + Constant = (2 \times 0.6325) + (10 \times 0.2088) + (1 \times -1.0115) + (1 \times 0.2491) + (1 \times 0.0297) + (1 \times -0.0170) + -3.5236 = -0.92$		
Experimental value = -0.92 %Absolute deviation from experimental value = 0.00%		

Table K2 Example calculation of Characteristic curvature of Sodium Decanoate
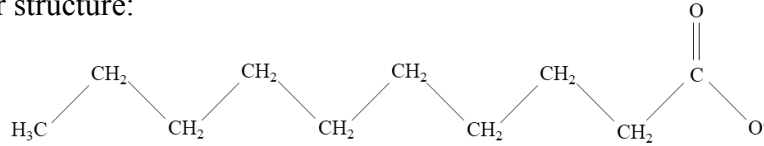
Sodium Decanoate		
Molecular structure:		
First-order group:		
Groups	Occurrences	Coefficients
CH_3	1	0.6325
CH_2	7	0.2088
CH_2COO	1	-1.0115
Second-order group:		
Groups	Occurrences	Coefficients
No Second-order group		
Third-order group:		
Groups	Occurrences	Coefficients
No Third-order group		
C_{ca} calculation		
$C_{ca} = \Sigma_i N_i C_i + \Sigma_j M_j D_j + \Sigma_k O_k E_k + Constant = (1 \times 0.6325) + (7 \times 0.2088) + (1 \times -1.0115) + -3.5236 = -2.44$		
Experimental value = -2.55 %Absolute deviation from experimental value = 4.28%		

Table K3 Example calculation of Characteristic curvature of NaC12PO6Sulfate
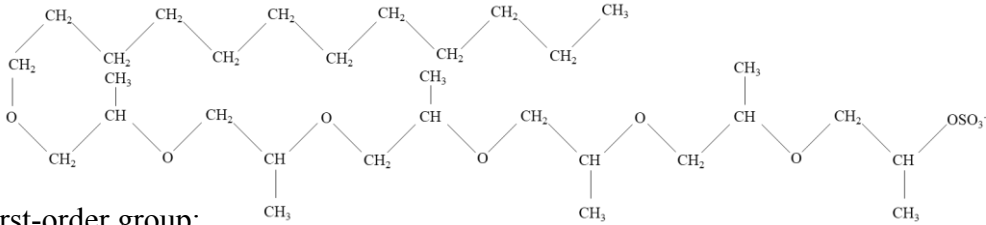
NaC12PO6Sulfate

Molecular structure:

First-order group:

Groups	Occurrences	Coefficients
CH_3	7	0.6325
CH_2	11	0.2088
CH	6	-0.2082
CH_2O	6	-0.1555
OSO_3^-	1	-2.1970

Second-order group:

Groups	Occurrences	Coefficients
-PO-	6	-0.0310

Third-order group:

Groups	Occurrences	Coefficients
No Third-order group		

C_{ca} calculation

$C_{ca} = \Sigma_i N_i C_i + \Sigma_j M_j D_j + \Sigma_k O_k E_k + Constant = (7 \times 0.6325) + (11 \times 0.2088) + (6 \times -0.2082) + (6 \times -0.1555) + (1 \times -2.1970) + (6 \times -0.0310) + -3.5236 = -1.36$

Experimental value = -1.60

%Absolute deviation from experimental value = 13.75%

Table K4 Example calculation of Characteristic curvature of Sodium Branced dodecyl-PO8Sulfate

NaBrancedC12PO8Sulfate		
Molecular structure: First-order group:		

Groups	Occurrences	Coefficients
CH_3	10	0.6325
CH_2	9	0.2088
CH	9	-0.2082
CH_2O	8	-0.1555
OSO_3^-	1	-2.1970

Second-order group:

Groups	Occurrences	Coefficients
-PO-	8	-0.0310

Third-order group:

Groups	Occurrences	Coefficients
No Third-order group		

C_{ca} calculation

$C_{ca} = \Sigma_i N_i C_i + \Sigma_j M_j D_j + \Sigma_k O_k E_k + Constant = (10 \times 0.6325) + (9 \times 0.2088) + (9 \times -0.2082) + (8 \times -0.1555) + (1 \times -2.1970) + (8 \times -0.0310) + -3.5236 = -0.88$

Experimental value = -0.80

%Absolute deviation from experimental value = 10.22%

Table K5 Example calculation of Characteristic curvature of NaC12EO3Sulfate

NaC12EO3Sulfate

Molecular structure:

First-order group:

Groups	Occurrences	Coefficients
CH_3	1	0.6325
CH_2	14	0.2088
CH_2O	3	-0.1555
OSO_3^-	1	-2.1970

Second-order group:

Groups	Occurrences	Coefficients
-EO-	3	0.0475

Third-order group:

Groups	Occurrences	Coefficients
No Third-order group		

C_{ca} calculation

$C_{ca} = \Sigma_i N_i C_i + \Sigma_j M_j D_j + \Sigma_k O_k E_k + Constant = (1 \times 0.6325) + (14 \times 0.2088) + (3 \times -0.1555) + (1 \times -2.1970) + (1 \times 0.0475) + -3.5236 = -2.49$

Experimental value = -2.89

%Absolute deviation from experimental value = 13.90%

Table K6 Example calculation of Characteristic curvature of Sodium naphthenate

Sodium naphthenate		
Molecular structure: First-order group:		
Groups	Occurrences	Coefficients
CH_3	1	0.6325
CH_2	2	0.2088
CH_2COO	1	-1.0115
$CH_{2,cyc}$	3	0.3260
CH_{cyc}	2	-0.0212
Second-order group:		
Groups	Occurrences	Coefficients
CH_{cyc}-CH_2	1	0.0747
Third-order group:		
Groups	Occurrences	Coefficients
No Third-order group		
C_{ca} calculation		
$C_{ca} = \Sigma_i N_i C_i + \Sigma_j M_j D_j + \Sigma_k O_k E_k + Constant = (1x0.6325) + (2x0.2088) + (1x-1.0115) + (3x0.3260) x (2x-0.0212) x (1x0.0747) + -3.5236 = -2.40$		
Experimental value = -2.40 %Absolute deviation from experimental value = 0.00%		

Table K7 Example calculation of Characteristic curvature of Sodium Hexadecanoate that is not included in the database

Sodium Hexadecanoate		
Molecular structure:		
First-order group:		
Groups	Occurrences	Coefficients
CH_3	1	0.6325
CH_2	13	0.2088
CH_2COO	1	-1.0115
Second-order group:		
Groups	Occurrences	Coefficients
No Second-order group		
Third-order group:		
Groups	Occurrences	Coefficients
No Third-order group		
C_{ca} calculation		
$C_{ca} = \Sigma_i N_i C_i + \Sigma_j M_j D_j + \Sigma_k O_k E_k + Constant = (1 \times 0.6325) + (13 \times 0.2088) + (1 \times -1.0115) + -3.5236 = -1.19$		
Experimental value = -1.20 %Absolute deviation from experimental value = 1.02%		

Appendix L   Group Occurrences for Characteristic Curvature Model for Nonionic Surfactant

The group structures for GC-model that occur in the database of C_c model are shown in this appendix. The structure of nonionic surfactants is divided into small molecules as Marrero *et al.* (2001) concept. The number of occurrence groups are counted and shown in the table. The data are used for regression analysis to find the contributions for the GC-model.

Table L1 First-order group occurrence for Characteristic curvature model of nonionic surfactant

Name	C_{cn}	Group Occurrences							
First-order		CH₃	CH₂	CH	-C-	CH=CH	CH₂-O	HOCH₂CH₂O	aC-CH₂
Coefficient		3.8748	-0.1414	-2.4252	4.0524	1.6764	-0.1672	-2.9765	1.2456
C6EO3	0.100	1	7	0	0	0	2	1	0
C6EO4	-1.600	1	8	0	0	0	3	1	0
C8EO4	0.300	1	10	0	0	0	3	1	0
C8EO5	-1.000	1	11	0	0	0	4	1	0
C9EO4.5	-0.960	1	11.5	0	0	0	3.5	1	0
C9EO5	-0.450	1	12	0	0	0	4	1	0
C10EO4	1.300	1	12	0	0	0	3	1	0
C10EO6	-0.900	1	14	0	0	0	5	1	0
C11.5EO5	-1.005	1	14.5	0	0	0	4	1	0
iC13EO8	-1.200	2	17	1	0	0	7	1	0
C14EO7	-0.700	1	19	0	0	0	6	1	0
C9PhEO2	1.000	1	9	0	0	0	0	1	1
C9PhEO5	0.120	1	12	0	0	0	3	1	1
C9PhEO9	-1.600	1	16	0	0	0	7	1	1
$C_{18}H_{34}O_6$	3.500	1	10	1	0	0	0	0	0
$C_{28}H_{52}O_{12}$	-0.800	1	16	0	0	0	0	0	0

Table L1 First-order group occurrence for Characteristic curvature model of nonionic surfactant (Continued)

Name	C_{cn}	Group Occurrences							
First-order		**aCH**	**aC-O**	**OH**	**O$_{cyc}$**	**CH$_{cyc}$**	**CH$_{2,cyc}$**	**CH$_2$COO**	**-O-**
Coefficient		0.0282	0.0071	-3.0494	16.1778	-1.5918	0.0789	0.2786	-0.3101
C6EO3	0.100	0	0	0	0	0	0	0	0
C6EO4	-1.600	0	0	0	0	0	0	0	0
C8EO4	0.300	0	0	0	0	0	0	0	0
C8EO5	-1.000	0	0	0	0	0	0	0	0
C9EO4.5	-0.960	0	0	0	0	0	0	0	0
C9EO5	-0.450	0	0	0	0	0	0	0	0
C10EO4	1.300	0	0	0	0	0	0	0	0
C10EO6	-0.900	0	0	0	0	0	0	0	0
C11.5EO5	-1.005	0	0	0	0	0	0	0	0
iC13EO8	-1.200	0	0	0	0	0	0	0	0
C14EO7	-0.700	0	0	0	0	0	0	0	0
C9PhEO2	1.000	4	1	0	0	0	0	0	0
C9PhEO5	0.120	4	1	0	0	0	0	0	0
C9PhEO9	-1.600	4	1	0	0	0	0	0	0
C$_{18}$H$_{34}$O$_6$	3.500	0	0	3	1	3	1	1	0
C$_{28}$H$_{52}$O$_{12}$	-0.800	0	0	7	2	9	0	1	1

Table L1 First-order group occurrence for Characteristic curvature model of nonionic surfactant (Continued)

Name	C_{cn}	Group Occurrences							
	First-order	CH_3	CH_2	CH	-C-	CH=CH	CH_2-O	$HOCH_2CH_2O$	aC-CH_2
	Coefficient	3.8748	-0.1414	-2.4252	4.0524	1.6764	-0.1672	-2.9765	1.2456
$C_{48}H_{90}O_{13}$	4.000	2	33	0	0	0	0	0	0
C16EO14	-2.900	1	28	0	0	0	13	1	0
C10Glucoside	-1.700	1	9	0	0	0	1	0	0
C12Glucoside	-1.000	1	11	0	0	0	1	0	0
Marlox RT42	0.550	3	18	2	0	0	5	1	0
Marlox RT64	1.140	5	23	4	0	0	9	1	0
Dehydol EO1	0.320	1	12	0	0	0	0	1	0
Dehydol EO2	-0.090	1	13	0	0	0	1	1	0
Dehydol EO3	-0.410	1	14	0	0	0	2	1	0
Dehydol EO5	-0.910	1	16	0	0	0	4	1	0
Dehydol EO9	-2.210	1	20	0	0	0	8	1	0
Dehydol EO12	-3.660	1	23	0	0	0	11	1	0
C9GEO6	-3.300	1	13	0	1	0	3	3	0
iC13EO6	0.070	2	15	1	0	0	5	1	0
C12EO6.5	-1.200	1	16.5	0	0	0	5.5	1	0
C58H114O26	-4.400	1	26	1	0	0	17	3	0
C64H124O26	-3.000	1	29	1	0	1	17	3	0

Table L1 First-order group occurrence for Characteristic curvature model of nonionic surfactant (Continued)

Name	C_{cn}	aCH	aC-O	OH	O_{cyc}	CH_{cyc}	$CH_{2,cyc}$	CH_2COO	-O-
		Group Occurrences							
First-order Coefficient		0.0282	0.0071	-3.0494	16.1778	-1.5918	0.0789	0.2786	-0.3101
$C_{48}H_{90}O_{13}$	4.000	0	0	6	2	9	0	2	1
C16EO14	-2.900	0	0	0	0	0	0	0	0
C10Glucoside	-1.700	0	0	4	1	5	0	0	0
C12Glucoside	-1.000	0	0	4	1	5	0	0	0
Marlox RT42	0.550	0	0	0	0	0	0	0	0
Marlox RT64	1.140	0	0	0	0	0	0	0	0
Dehydol EO1	0.320	0	0	0	0	0	0	0	0
Dehydol EO2	-0.090	0	0	0	0	0	0	0	0
Dehydol EO3	-0.410	0	0	0	0	0	0	0	0
Dehydol EO5	-0.910	0	0	0	0	0	0	0	0
Dehydol EO9	-2.210	0	0	0	0	0	0	0	0
Dehydol EO12	-3.660	0	0	0	0	0	0	0	0
C9GEO6	-3.300	0	0	0	0	0	0	0	0
iC13EO6	0.070	0	0	0	0	0	0	0	0
C12EO6.5	-1.200	0	0	0	0	0	0	0	0
$C_{58}H_{114}O_{26}$	-4.400	0	0	0	1	3	1	1	0
$C_{64}H_{124}O_{26}$	-3.000	0	0	0	1	3	1	1	0

Table L2 Second-order group occurrence for Characteristic curvature model of nonionic surfactant

Name	C_{cn}	Group Occurrences						
	Second-order	AROMRINGs[1]s[4]	CH_{cyc}-OH	CH_{cyc}-CH_2	CH_{cyc}-CH	CH_{cyc}-O	C_{cyc}-CH_2	$(CH_3)_2CH$
	Coefficient	0.0071	0.3676	-0.0833	0.0789	-0.2332	-0.3101	0.6385
C6EO3	0.100	0	0	0	0	0	0	0
C6EO4	-1.600	0	0	0	0	0	0	0
C8EO4	0.300	0	0	0	0	0	0	0
C8EO5	-1.000	0	0	0	0	0	0	0
C9EO4.5	-0.960	0	0	0	0	0	0	0
C9EO5	-0.450	0	0	0	0	0	0	0
C10EO4	1.300	0	0	0	0	0	0	0
C10EO6	-0.900	0	0	0	0	0	0	0
C11.5EO5	-1.005	0	0	0	0	0	0	0
iC13EO8	-1.200	0	0	0	0	0	0	1
C14EO7	-0.700	0	0	0	0	0	0	0
C9PhEO2	1.000	1	0	0	0	0	0	0
C9PhEO5	0.120	1	0	0	0	0	0	0
C9PhEO9	-1.600	1	0	0	0	0	0	0
$C_{18}H_{34}O_6$	3.500	0	2	0	1	0	0	0
$C_{28}H_{52}O_{12}$	-0.800	0	5	2	0	2	1	0

Table L2 Second-order group occurrence for Characteristic curvature model of nonionic surfactant (Continued)

Name	Second-order	Group Occurrences						
	Coefficient	AROMRINGs[1]s[4]	CH_{cyc}-OH	CH_{cyc}-CH_2	CH_{cyc}-CH	CH_{cyc}-O	C_{cyc}-CH_2	$(CH_3)_2CH$
		0.0071	0.3676	-0.0833	0.0789	-0.2332	-0.3101	0.6385
Name	C_{cn}							
$C_{48}H_{90}O_{13}$	4.000	0	5	2	0	2	1	0
C16EO14	-2.900	0	0	0	0	0	0	0
C10Glucoside	-1.700	0	3	1	0	1	0	0
C12Glucoside	-1.000	0	3	1	0	1	0	0
Marlox RT42	0.550	0	0	0	0	0	0	0
Marlox RT64	1.140	0	0	0	0	0	0	0
Dehydol EO1	0.320	0	0	0	0	0	0	0
Dehydol EO2	-0.090	0	0	0	0	0	0	0
Dehydol EO3	-0.410	0	0	0	0	0	0	0
Dehydol EO5	-0.910	0	0	0	0	0	0	0
Dehydol EO9	-2.210	0	0	0	0	0	0	0
Dehydol EO12	-3.660	0	0	0	0	0	0	0
C9GEO6	-3.300	0	0	0	0	0	0	0
iC13EO6	0.070	0	0	0	0	0	0	1
C12EO6.5	-1.200	0	0	0	0	0	0	0
C58H114O26	-4.400	0	0	0	1	2	0	0
C64H124O26	-3.000	0	0	0	1	2	0	0

Table L3 Third-order group occurrence for Characteristic curvature model of nonionic surfactant

Name	C_{cn}	Group Occurrences			
	Third-order	$(CH)_n$-C_6H_4-$(OCH_2CH_2)_m$	$(CH)_n$-$(OCH_2CH_2)_m$, m = 3, n < 8 and m > 3, n ≥ 8	$(CH)_n$-$(OCH_2CH_2)_m$, n ≥ 12	$(CH)_n$-$(OCH_2CH_2)_m$, n = 5
	Coefficient	0.0071	0.9765	2.0510	-0.4909
C6EO3	0.100	0	1	0	1
C6EO4	-1.600	0	0	0	1
C8EO4	0.300	0	1	0	0
C8EO5	-1.000	0	1	0	0
C9EO4.5	-0.960	0	1	0	0
C9EO5	-0.450	0	1	0	0
C10EO4	1.300	0	1	0	0
C10EO6	-0.900	0	1	0	0
C11.5EO5	-1.005	0	1	0	0
iC13EO8	-1.200	0	0	0	0
C14EO7	-0.700	0	0	1	0
C9PhEO2	1.000	1	0	0	0
C9PhEO5	0.120	1	0	0	0
C9PhEO9	-1.600	1	0	0	0
$C_{18}H_{34}O_6$	3.500	0	0	0	0
$C_{28}H_{52}O_{12}$	-0.800	0	0	0	0

Table L3 Third-order group occurrence for Characteristic curvature model of nonionic surfactant (Continued)

Name	Third-order	Group Occurrences			
		$(CH)_n\text{-}C_6H_4\text{-}(OCH_2CH_2)_m$	$(CH)_n\text{-}(OCH_2CH_2)_m$, m = 3, n < 8 and m > 3, n ≥ 8	$(CH)_n\text{-}(OCH_2CH_2)_m$, n ≥ 12	$(CH)_n\text{-}(OCH_2CH_2)_m$, n = 5
	Coefficient	0.0071	0.9765	2.0510	-0.4909
Name	C_{cn}				
$C_{48}H_{90}O_{13}$	4.000	0	0	0	0
C16EO14	-2.900	0	0	1	0
C10Glucoside	-1.700	0	0	0	0
C12Glucoside	-1.000	0	0	0	0
Marlox RT42	0.550	0	0	0	0
Marlox RT64	1.140	0	0	0	0
Dehydol EO1	0.320	0	1	0	0
Dehydol EO2	-0.090	0	1	0	0
Dehydol EO3	-0.410	0	1	0	0
Dehydol EO5	-0.910	0	1	0	0
Dehydol EO9	-2.210	0	1	0	0
Dehydol EO12	-3.660	0	1	0	0
C9GEO6	-3.300	0	0	0	0
iC13EO6	0.070	0	0	0	0
C12EO6.5	-1.200	0	1	0	0
C58H114O26	-4.400	0	0	0	0
C64H124O26	-3.000	0	0	0	0

Appendix M   Example Calculation of Characteristic Curvature Model for Nonionic Surfactant

This appendix shows the example calculation when the characteristic curvature GC-model is applied to the nonionic surfactant. The represents from various structure are chosen for calculation the characteristic curvature, as compared to the experimental value.

Table M1 Example calculation of Characteristic curvature of Alcohol polyethylene oxide C9EO5

Alcohol polyethylene oxide C9EO5		
Molecular structure: First-order group:		
Groups	Occurrences	Coefficients
CH_3	1	3.8748
CH_2	12	-0.1414
CH_2-O	4	-0.1672
$HOCH_2CH_2O$	1	-2.9765
Second-order group:		
Groups	Occurrences	Coefficients
No Second-order group		
Third-order group:		
Groups	Occurrences	Coefficients
$(CH)_n\text{-}(OCH_2CH_2)_m$, $m = 3$, $n < 8$ and $m > 3$, $n \geq 8$	1	0.9765
C_{ca} calculation		
$C_{ca} = \Sigma_i N_i C_i + \Sigma_j M_j D_j + \Sigma_k O_k E_k + Constant = (1 \times 3.8748) + (12 \times -0.1414) +$ $(4 \times -0.1672) + (1 \times -2.9765) + (1 \times 0.7846) + 0.0402 = -0.45$		
Experimental value = -0.45 %Absolute deviation from experimental value = 0.06%		

Table M2 Example calculation of Characteristic curvature of Marlox® RT42

<table>
<tr><td colspan="3" align="center">Marlox® RT42</td></tr>
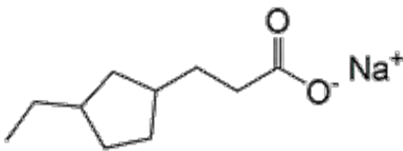<tr><td colspan="3">Molecular structure:

First-order group:</td></tr>
<tr><td align="center">Groups</td><td align="center">Occurrences</td><td align="center">Coefficients</td></tr>
<tr><td align="center">CH_3</td><td align="center">3</td><td align="center">3.8748</td></tr>
<tr><td align="center">CH_2</td><td align="center">18</td><td align="center">-0.1414</td></tr>
<tr><td align="center">CH_2-O</td><td align="center">5</td><td align="center">-0.1672</td></tr>
<tr><td align="center">CH</td><td align="center">2</td><td align="center">-2.4252</td></tr>
<tr><td align="center">$HOCH_2CH_2O$</td><td align="center">1</td><td align="center">-2.9765</td></tr>
<tr><td colspan="3">Second-order group:</td></tr>
<tr><td align="center">Groups</td><td align="center">Occurrences</td><td align="center">Coefficients</td></tr>
<tr><td colspan="3" align="center">No Second-order group</td></tr>
<tr><td colspan="3">Third-order group:</td></tr>
<tr><td align="center">Groups</td><td align="center">Occurrences</td><td align="center">Coefficients</td></tr>
<tr><td colspan="3" align="center">No Third-order group</td></tr>
<tr><td colspan="3">**C_{ca} calculation**</td></tr>
<tr><td colspan="3">$C_{ca} = \Sigma_i N_i C_i + \Sigma_j M_j D_j + \Sigma_k O_k E_k + Constant = (1 \times 3.8748) + (18 \times -0.1414) + (5 \times -0.1672) + (2 \times -2.4252) + (1 \times -2.9765) + 0.0402 = 0.46$</td></tr>
<tr><td colspan="3">Experimental value = 0.55

%Absolute deviation from experimental value = 16.92%</td></tr>
</table>

Table M3 Example calculation of Characteristic curvature of sucrose palimitate ($C_{28}H_{52}O_{12}$)
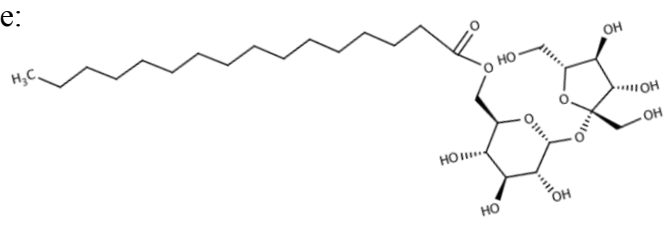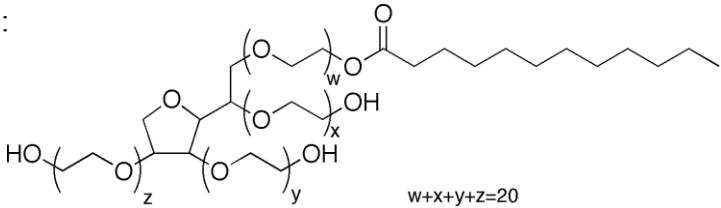
Sucrose palimitate ($C_{28}H_{52}O_{12}$)		
Molecular structure: First-order group:		
Groups	Occurrences	Coefficients
CH_3	1	3.8748
CH_2	16	-0.1414
OH	7	-3.0494
O_{cyc}	2	16.1778
CH_{cyc}	9	-1.5918
CH_2COO	1	0.2786
-O-	1	-0.3101
Second-order group:		
Groups	Occurrences	Coefficients
CH_{cyc}-OH	5	0.3676
CH_{cyc}-CH_2	2	-0.0833
CH_{cyc}-O	2	-0.2332
C_{cyc}-CH_2	1	-0.3101
Third-order group:		
Groups	Occurrences	Coefficients
No Third-order group		
C_{ca} calculation		
$C_{ca} = \Sigma_i N_i C_i + \Sigma_j M_j D_j + \Sigma_k O_k E_k + Constant = -0.80$		
Experimental value = -0.80		
%Absolute deviation from experimental value = 0.00%		

Table M4 Example calculation of Characteristic curvature of Polysorbate 20

Polysorbate 20		
Molecular structure: **First-order group:**		
Groups	Occurrences	Coefficients
CH_3	1	3.8748
CH_2	26	-0.1414
CH	1	-2.4252
CH_2-O	17	-0.1672
$HOCH_2CH_2O$	3	-2.9765
O_{cyc}	1	16.1778
CH_{cyc}	3	-1.5918
$CH_{2,cyc}$	1	0.0789
CH_2COO	1	0.2786
Second-order group:		
Groups	Occurrences	Coefficients
CH_{cyc}-CH	1	0.0789
CH_{cyc}-O	2	-0.2332
Third-order group:		
Groups	Occurrences	Coefficients
No Third-order group		
C_{ca} calculation		
$C_{ca} = \Sigma_i N_i C_i + \Sigma_j M_j D_j + \Sigma_k O_k E_k + Constant = -2.58$		
Experimental value = -4.40 %Absolute deviation from experimental value = 41.23%		

Appendix N Group Occurrences for Krafft Point Model of Anionic Surfactant

The group structures for GC-model that occur in the database of T_k model are shown in this appendix. The structure of anionic surfactants is divided into small molecules as Marrero *et al.* (2001) concept. The number of occurrence groups are counted and shown in the table. The data are used for regression analysis to find the contributions for the GC-model.

Table N1 First-order group occurrence for Krafft point model of anionic surfactant

Name	$T_{k,exp}$ (°C)	Group Occurrences							
	First-order	CH$_3$	CH$_2$	CH	CH$_2$O	CH$_2$COO	SO$_3^-$	OSO$_3^-$	aC-O
	Coefficients	45.9329	6.1141	-54.1220	-15.5808	1.2907	26.5247	32.6298	65.8270
C10SO3	22.5	1	9	0	0	0	1	0	0
C12SO3	38.0	1	11	0	0	0	1	0	0
C14SO3	48.0	1	13	0	0	0	1	0	0
C17SO3	62.0	1	16	0	0	0	1	0	0
C18SO3	70.0	1	17	0	0	0	1	0	0
C10OSO3	8.0	1	9	0	0	0	0	1	0
C12OSO3	19.0	1	11	0	0	0	0	1	0
C13OSO3	20.8	1	12	0	0	0	0	1	0
C14OSO3	30.0	1	13	0	0	0	0	1	0
C15OSO3	31.5	1	14	0	0	0	0	1	0
C16OSO3	45.0	1	15	0	0	0	0	1	0
C18OSO3	56.0	1	17	0	0	0	0	1	0
C7PhSO3	9.0	1	5	0	0	0	0	0	0
C8PhSO3	18.5	1	6	0	0	0	0	0	0
2C10PhSO3	22.0	2	7	0	0	0	0	0	0
2C12PhSO3	31.5	2	9	0	0	0	0	0	0
2C16PhSO3	54.2	2	13	0	0	0	0	0	0
2C18PhSO3	60.8	2	15	0	0	0	0	0	0
2C13COSO3	11.0	2	11	1	0	0	0	1	0
2C15COSO3	25.0	2	13	1	0	0	0	1	0

Table N1 First-order group occurrence for Krafft point model of anionic surfactant (Continue)

Name	$T_{k,exp}$ (°C)	Group Occurrences							
First-order		**aCH**	**aC-CH₂**	**aC-CH**	**aC-SO₃⁻**	**aC fused aro**	**CF₃**	**CF₂**	**COO⁻**
Coefficients		-2.7166	69.9810	22.0837	0.0060	-0.2730	38.7274	16.0812	0.0137
C10SO3	22.5	0	0	0	0	0	0	0	0
C12SO3	38.0	0	0	0	0	0	0	0	0
C14SO3	48.0	0	0	0	0	0	0	0	0
C17SO3	62.0	0	0	0	0	0	0	0	0
C18SO3	70.0	0	0	0	0	0	0	0	0
C10OSO3	8.0	0	0	0	0	0	0	0	0
C12OSO3	19.0	0	0	0	0	0	0	0	0
C13OSO3	20.8	0	0	0	0	0	0	0	0
C14OSO3	30.0	0	0	0	0	0	0	0	0
C15OSO3	31.5	0	0	0	0	0	0	0	0
C16OSO3	45.0	0	0	0	0	0	0	0	0
C18OSO3	56.0	0	0	0	0	0	0	0	0
C7PhSO3	9.0	4	1	0	1	0	0	0	0
C8PhSO3	18.5	4	1	0	1	0	0	0	0
2C10PhSO3	22.0	4	0	1	1	0	0	0	0
2C12PhSO3	31.5	4	0	1	1	0	0	0	0
2C16PhSO3	54.2	4	0	1	1	0	0	0	0
2C18PhSO3	60.8	4	0	1	1	0	0	0	0
2C13COSO3	11.0	0	0	0	0	0	0	0	0
2C15COSO3	25.0	0	0	0	0	0	0	0	0

Table N1 First-order group occurrence for Krafft point model of anionic surfactant (Continue)

Name	First-order	Group Occurrences							
		CH$_3$	CH$_2$	CH	CH$_2$O	CH$_2$COO	SO$_3^-$	OSO$_3^-$	aC-O
	Coefficients	45.9329	6.1141	-54.1220	-15.5808	1.2907	26.5247	32.6298	65.8270
Name	T$_{k,exp}$ (°C)								
2C17COSO3	30.0	2	15	1	0	0	0	1	0
C16E1OSO3	36.0	1	16	0	1	0	0	1	0
C16E2OSO3	24.0	1	17	0	2	0	0	1	0
C16E3OSO3	19.0	1	18	0	3	0	0	1	0
C18E3OSO3	32.0	1	20	0	3	0	0	1	0
C18E4OSO3	18.0	1	21	0	4	0	0	1	0
C10AESO3	8.1	1	10	0	0	1	1	0	0
C12AESO3	24.2	1	12	0	0	1	1	0	0
C14AESO3	36.2	1	14	0	0	1	1	0	0
C10RSO3	12.5	1	10	0	0	1	0	1	0
C12RSO3	26.5	1	12	0	0	1	0	1	0
C14RSO3	39.0	1	14	0	0	1	0	1	0
O3SOC12OSO3	12.0	0	12	0	0	0	0	2	0
O3SOC14OSO3	24.8	0	14	0	0	0	0	2	0
O3SOC16OSO3	39.1	0	16	0	0	0	0	2	0
O3SOC18OSO3	44.9	0	18	0	0	0	0	2	0
O3SPhOC6OPhSO3	20.0	0	6	0	0	0	0	0	2
O3SPhOC8OPhSO3	28.0	0	8	0	0	0	0	0	2
O3SPhOC10OPhSO3	59.0	0	10	0	0	0	0	0	2
O3SPhOC12OPhSO3	70.0	0	12	0	0	0	0	0	2

Table N1 First-order group occurrence for Krafft point model of anionic surfactant (Continue)

Name	First-order $T_{k,exp}$ (°C)	Group Occurrences							
	Coefficients	aCH	aC-CH$_2$	aC-CH	aC-SO$_3^-$	aC fused aro	CF$_3$	CF$_2$	COO$^-$
		-2.7166	69.9810	22.0837	0.0060	-0.2730	38.7274	16.0812	0.0137
2C17COSO3	30.0	0	0	0	0	0	0	0	0
C16E1OSO3	36.0	0	0	0	0	0	0	0	0
C16E2OSO3	24.0	0	0	0	0	0	0	0	0
C16E3OSO3	19.0	0	0	0	0	0	0	0	0
C18E3OSO3	32.0	0	0	0	0	0	0	0	0
C18E4OSO3	18.0	0	0	0	0	0	0	0	0
C10AESO3	8.1	0	0	0	0	0	0	0	0
C12AESO3	24.2	0	0	0	0	0	0	0	0
C14AESO3	36.2	0	0	0	0	0	0	0	0
C10RSO3	12.5	0	0	0	0	0	0	0	0
C12RSO3	26.5	0	0	0	0	0	0	0	0
C14RSO3	39.0	0	0	0	0	0	0	0	0
O3SOC12OSO3	12.0	0	0	0	0	0	0	0	0
O3SOC14OSO3	24.8	0	0	0	0	0	0	0	0
O3SOC16OSO3	39.1	0	0	0	0	0	0	0	0
O3SOC18OSO3	44.9	0	0	0	0	0	0	0	0
O3SPhOC6OPhSO3	20.0	8	0	0	2	0	0	0	0
O3SPhOC8OPhSO3	28.0	8	0	0	2	0	0	0	0
O3SPhOC10OPhSO3	59.0	8	0	0	2	0	0	0	0
O3SPhOC12OPhSO3	70.0	8	0	0	2	0	0	0	0

Table N1 First-order group occurrence for Krafft point model of anionic surfactant (Continue)

		Group Occurrences							
First-order		**CH$_3$**	**CH$_2$**	**CH**	**CH$_2$O**	**CH$_2$COO**	**SO$_3^-$**	**OSO$_3^-$**	**aC-O**
Coefficients		45.9329	6.1141	-54.1220	-15.5808	1.2907	26.5247	32.6298	65.8270
Name	**T$_{k,exp}$ (°C)**								
O3SCRC12RCSO3	23.5	0	16	0	0	2	2	0	0
O3SCRC14RCSO3	31.0	0	18	0	0	2	2	0	0
O3SCRC16RCSO3	38.5	0	20	0	0	2	2	0	0
1,4 NS-8	9.0	1	6	0	0	0	0	0	0
1,4 NS-10	21.0	1	8	0	0	0	0	0	0
1,4 NS-14	50.0	1	12	0	0	0	0	0	0
1,4 NS-16	64.0	1	14	0	0	0	0	0	0
C7F15COONa	8.6	0	0	0	0	0	0	0	0
C8F17COONa	24.6	0	0	0	0	0	0	0	0
C7F15SO3Na	56.5	0	0	0	0	0	1	0	0
C10F21COONa	58.3	0	0	0	0	0	0	0	0
C12F25COONa	89.0	0	0	0	0	0	0	0	0
C8F17SO3Na	75.0	0	0	0	0	0	1	0	0

Table N1 First-order group occurrence for Krafft point model of anionic surfactant (Continue)

Name	$T_{k,exp}$ (°C)	aCH	aC-CH$_2$	aC-CH	aC-SO$_3^-$	aC fused aro	CF$_3$	CF$_2$	COO$^-$
	First-order Coefficients	-2.7166	69.9810	22.0837	0.0060	-0.2730	38.7274	16.0812	0.0137
O3SCRC12RCSO3	23.5	0	0	0	0	0	0	0	0
O3SCRC14RCSO3	31.0	0	0	0	0	0	0	0	0
O3SCRC16RCSO3	38.5	0	0	0	0	0	0	0	0
1,4 NS-8	9.0	6	1	0	1	2	0	0	0
1,4 NS-10	21.0	6	1	0	1	2	0	0	0
1,4 NS-14	50.0	6	1	0	1	2	0	0	0
1,4 NS-16	64.0	6	1	0	1	2	0	0	0
C7F15COONa	8.6	0	0	0	0	0	1	6	1
C8F17COONa	24.6	0	0	0	0	0	1	7	1
C7F15SO3Na	56.5	0	0	0	0	0	1	6	0
C10F21COONa	58.3	0	0	0	0	0	1	9	1
C12F25COONa	89.0	0	0	0	0	0	1	11	1
C8F17SO3Na	75.0	0	0	0	0	0	1	7	0

Table N2 Higher-order group occurrence for Krafft point model of anionic surfactant

Name	$T_{k,exp}$ (°C)	AROMRINGs[1]s[4]	$^-O_3$S-aromatic-O	OOC-(CH$_2$)$_n$-COO	^-O_xS-(CH$_2$)$_n$-OCO	aC-O-(CH$_2$)$_n$-O-aC	AROFUSEDs[1]s[4]	$^-O_3$S-alkyl tail
		Higher-order			Group Occurrences			
	Coefficients	0.0060	-0.0005	-7.6915	-0.1607	-0.0003	-0.1365	21.6530
C10SO3	22.5	0	0	0	0	0	0	1
C12SO3	38.0	0	0	0	0	0	0	1
C14SO3	48.0	0	0	0	0	0	0	1
C17SO3	62.0	0	0	0	0	0	0	1
C18SO3	70.0	0	0	0	0	0	0	1
C10OSO3	8.0	0	0	0	0	0	0	0
C12OSO3	19.0	0	0	0	0	0	0	0
C13OSO3	20.8	0	0	0	0	0	0	0
C14OSO3	30.0	0	0	0	0	0	0	0
C15OSO3	31.5	0	0	0	0	0	0	0
C16OSO3	45.0	0	0	0	0	0	0	0
C18OSO3	56.0	0	0	0	0	0	0	0
C7PhSO3	9.0	1	0	0	0	0	0	0
C8PhSO3	18.5	1	0	0	0	0	0	0
2C10PhSO3	22.0	1	0	0	0	0	0	0
2C12PhSO3	31.5	1	0	0	0	0	0	0
2C16PhSO3	54.2	1	0	0	0	0	0	0
2C18PhSO3	60.8	1	0	0	0	0	0	0
2C13COSO3	11.0	0	0	0	0	0	0	0
2C15COSO3	25.0	0	0	0	0	0	0	0

Table N2 Higher-order group occurrence for Krafft point model of anionic surfactant (Continue)

Name	Tk,exp	Group Occurrences						
		AROMRINGs[1]s[4]	^-O_3S-aromatic-O	OOC-$(CH_2)_n$-COO	^-O_xS-$(CH_2)_n$-OCO	aC-O-$(CH_2)_n$-O-aC	AROFUSEDs[1]s[4]	^-O_3S-alkyl tail
	Higher-order Coefficients	0.0060	-0.0005	-7.6915	-0.1607	-0.0003	-0.1365	21.6530
2C17COSO3	30.0	0	0	0	0	0	0	0
C16E1OSO3	36.0	0	0	0	0	0	0	0
C16E2OSO3	24.0	0	0	0	0	0	0	0
C16E3OSO3	19.0	0	0	0	0	0	0	0
C18E3OSO3	32.0	0	0	0	0	0	0	0
C18E4OSO3	18.0	0	0	0	0	0	0	0
C10AESO3	8.1	0	0	0	1	0	0	0
C12AESO3	24.2	0	0	0	1	0	0	0
C14AESO3	36.2	0	0	0	1	0	0	0
C10RSO3	12.5	0	0	0	1	0	0	0
C12RSO3	26.5	0	0	0	1	0	0	0
C14RSO3	39.0	0	0	0	1	0	0	0
O3SOC12OSO3	12.0	0	0	0	0	0	0	0
O3SOC14OSO3	24.8	0	0	0	0	0	0	0
O3SOC16OSO3	39.1	0	0	0	0	0	0	0
O3SOC18OSO3	44.9	0	0	0	0	0	0	0
O3SPhOC6OPhSO3	20.0	2	2	0	0	1	0	0
O3SPhOC8OPhSO3	28.0	2	2	0	0	1	0	0
O3SPhOC10OPhSO3	59.0	2	2	0	0	1	0	0
O3SPhOC12OPhSO3	70.0	2	2	0	0	1	0	0

Table N2 Higher-order group occurrence for Krafft point model of anionic surfactant (Continue)

Name	Tk,exp	AROMRINGs[1]s[4]	^-O_3S-aromatic-O	OOC-(CH$_2$)$_n$-COO	^-O_xS-(CH$_2$)$_n$-OCO	aC-O-(CH$_2$)$_n$-O-aC	AROFUSEDs[1]s[4]	^-O_3S-alkyl tail
		Group Occurrences						
Higher-order								
Coefficients		0.0060	-0.0005	-7.6915	-0.1607	-0.0003	-0.1365	21.6530
O3SCRC12RCSO3	23.5	0	0	1	2	0	0	0
O3SCRC14RCSO3	31.0	0	0	1	2	0	0	0
O3SCRC16RCSO3	38.5	0	0	1	2	0	0	0
1,4 NS-8	9.0	1	0	0	0	0	1	0
1,4 NS-10	21.0	1	0	0	0	0	1	0
1,4 NS-14	50.0	1	0	0	0	0	1	0
1,4 NS-16	64.0	1	0	0	0	0	1	0
C7F15COONa	8.6	0	0	0	0	0	0	0
C8F17COONa	24.6	0	0	0	0	0	0	0
C7F15SO3Na	56.5	0	0	0	0	0	0	1
C10F21COONa	58.3	0	0	0	0	0	0	0
C12F25COONa	89.0	0	0	0	0	0	0	0
C8F17SO3Na	75.0	0	0	0	0	0	0	1

Appendix O Example calculation of the Krafft point GC-model of anionic surfactant

The Krafft point GC-model of anionic surfactant applies to each anionic group: Linear-Alkyl Sulfonate, Linear-Alkyl Sulfate, Linear-Alkyl Phenyl Sulfonate, Branched-Alkyl Phenyl Sulfonate, Branched-Alkyl Sulfate, Linear-Alkyl Ethoxylate Sulfate, Linear-Acyl ethoxylate Sulfonate, Linear-Acyl ethoxylate Sulfate, Linear-Alkyl Disulfate, 1,n-Di(p-Sulfonicphenoxy)-Alkane, 1,n-Di(Sulfoalkanoate)-Alkane, Alkyl Naphthalene Sulfonate and Linear-Fluorocarbon Surfactants. The example calculation are shown in the Table O1-O13.

Table O1 Example calculation of Krafft point of C14SO3 (Tetradecyl sulfonate) for linear-alkyl sulfonate surfactant

C14SO3

Molecular structure:

First-order group:

Groups	Occurrences	Coefficients (°C)
CH_3	1	45.9329
CH_2	13	6.1141
SO_3^-	1	26.5247

Second-order group:

Groups	Occurrences	Coefficients (°C)
No Second-order group		

Third-order group:

Groups	Occurrences	Coefficients (°C)
^-O_3S-alkyl tail	1	21.6530

T_k calculation

$T_{k,calc}$ (°C) $= \Sigma_i N_i C_i + \Sigma_j M_j D_j + \Sigma_k O_k E_k + $ Constant $= (1 \times 45.9329) + (13 \times 6.1141) + (1 \times 26.5247) + (1 \times 21.6530) + (-126.6285) = 49.96$ °C

Experimental value $= 48.00$ °C

%Absolute deviation from experimental value $= 2.16\%$

Table O2 Example calculation of Krafft point of C14OSO3 (Tetradecyl sulfate) for linear-alkyl sulfate surfactant

C14OSO3		
Molecular structure:		
First-order group:		
Groups	Occurrences	Coefficients (°C)
CH_3	1	45.9329
CH_2	13	6.1141
OSO_3^-	1	32.6928
Second-order group:		
Groups	Occurrences	Coefficients (°C)
No Second-order group		
Third-order group:		
Groups	Occurrences	Coefficients (°C)
No Third-order group		
T_k calculation		
$T_{k,calc}$ (°C) $= \Sigma_i N_i C_i + \Sigma_j M_j D_j + \Sigma_k O_k E_k +$ Constant $= (1 \times 45.9329) + (13 \times 6.1141) + (1 \times 32.6928) + (-126.6285) = 31.42$ °C		
Experimental value $= 30.00$ °C %Absolute deviation from experimental value $= 4.72\%$		

Table O3 Example calculation of Krafft point of C7PhSO3 (Heptaphenyl sulfonate) for linear-alkyl phenyl sulfonate surfactant
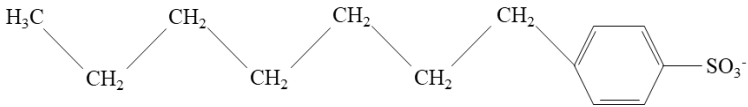
<table>
<tr><td colspan="3" align="center">C7PhSO3</td></tr>
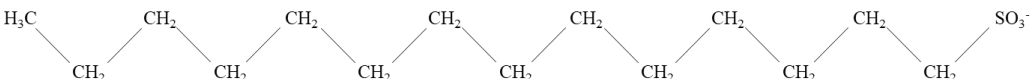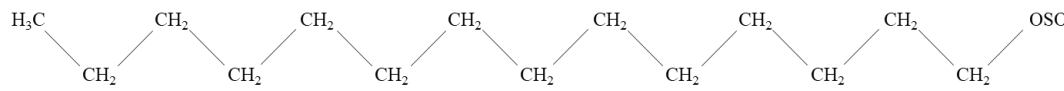<tr><td colspan="3">Molecular structure:</td></tr>
<tr><td colspan="3"></td></tr>
<tr><td colspan="3">First-order group:</td></tr>
<tr><td align="center">Groups</td><td align="center">Occurrences</td><td align="center">Coefficients (°C)</td></tr>
<tr><td align="center">CH_3</td><td align="center">1</td><td align="center">45.9329</td></tr>
<tr><td align="center">CH_2</td><td align="center">5</td><td align="center">6.1141</td></tr>
<tr><td align="center">aCH</td><td align="center">4</td><td align="center">-2.7166</td></tr>
<tr><td align="center">$aC-CH_2$</td><td align="center">1</td><td align="center">69.9810</td></tr>
<tr><td align="center">$aC-SO_3^-$</td><td align="center">1</td><td align="center">0.0060</td></tr>
<tr><td colspan="3">Second-order group:</td></tr>
<tr><td align="center">Groups</td><td align="center">Occurrences</td><td align="center">Coefficients (°C)</td></tr>
<tr><td align="center">$AROMRINGs^1s^4$</td><td align="center">1</td><td align="center">0.0060</td></tr>
<tr><td colspan="3">Third-order group:</td></tr>
<tr><td align="center">Groups</td><td align="center">Occurrences</td><td align="center">Coefficients (°C)</td></tr>
<tr><td colspan="3" align="center">No Third-order group</td></tr>
<tr><td colspan="3">T_k calculation</td></tr>
<tr><td colspan="3">$T_{k,calc}$ (°C) = $\Sigma_i N_i C_i + \Sigma_j M_j D_j + \Sigma_k O_k E_k$ + Constant = (1x45.9329) + (5x6.1141) + (4x-2.7166) + (1x69.9810) + (1x0.0060) + (1x0.0060) + (-126.6285)
= 9.00 °C</td></tr>
<tr><td colspan="3">Experimental value = 9.00 °C

%Absolute deviation from experimental value = 0.02%</td></tr>
</table>

Table O4 Example calculation of Krafft point of 2C12PhSO3 for branched-alkyl phenyl sulfonate surfactant

2C12PhSO3

Molecular structure:

First-order group:

Groups	Occurrences	Coefficients (°C)
CH$_3$	2	45.9329
CH$_2$	9	6.1141
aCH	4	-2.7166
aC-CH	1	22.0837
aC-SO$_3^-$	1	0.0060

Second-order group:

Groups	Occurrences	Coefficients (°C)
AROMRINGs^{1}s^4	1	0.0060

Third-order group:

Groups	Occurrences	Coefficients (°C)
No Third-order group		

T$_k$ calculation

$T_{k,calc}$ (°C) = $\Sigma_i N_i C_i + \Sigma_j M_j D_j + \Sigma_k O_k E_k$ + Constant = (2x45.9329) + (9x6.1141) + (4x-2.7166) + (1x22.0837) + (1x0.0060) + (1x0.0060) + (-126.6285)

= 31.49 °C

Experimental value = 31.50 °C

%Absolute deviation from experimental value = 0.02%

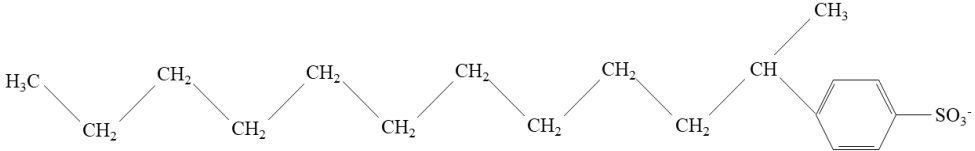**Table O5** Example calculation of Krafft point of 2C15COSO3 for branched-alkyl sulfate surfactant

2C15COSO3
Molecular structure:

First-order group:

Groups	Occurrences	Coefficients (°C)
CH_3	2	45.9329
CH_2	13	6.1141
CH	1	-54.1220
OSO_3^-	1	32.6928

Second-order group:

Groups	Occurrences	Coefficients (°C)
No Second-order group		

Third-order group:

Groups	Occurrences	Coefficients (°C)
No Third-order group		

T_k calculation

$T_{k,calc}$ (°C) = $\Sigma_i N_i C_i + \Sigma_j M_j D_j + \Sigma_k O_k E_k$ + Constant = (2x45.9329) + (13x6.1141) + (1x-54.1220) + (1x32.6928) + (-126.6285) = 23.23 °C

Experimental value = 25.00 °C

%Absolute deviation from experimental value = 7.09%

Table O6 Example calculation of Krafft point of C16E2OSO3 for linear-alkyl ethoxylate sulfate surfactant

C16E2OSO3		
Molecular structure:		
First-order group:		
Groups	Occurrences	Coefficients (°C)
CH_3	1	45.9329
CH_2	17	6.1141
CH_2-O	2	-15.5808
OSO_3^-	1	32.6928
Second-order group:		
Groups	Occurrences	Coefficients (°C)
No Second-order group		
Third-order group:		
Groups	Occurrences	Coefficients (°C)
No Third-order group		
T_k calculation		
$T_{k,calc}$ (°C) $= \Sigma_i N_i C_i + \Sigma_j M_j D_j + \Sigma_k O_k E_k$ + Constant = (1x45.9329) + (17x6.1141) + (2x-15.5808) + (1x32.6928) + (-126.6285) = 24.71 °C		
Experimental value = 24.00 °C %Absolute deviation from experimental value = 2.97%		

Table O7 Example calculation of Krafft point of C12AESO3 for linear-acyl ethoxylate sulfonate surfactant

C12AESO3
Molecular structure:

First-order group:

Groups	Occurrences	Coefficients (°C)
CH_3	1	45.9329
CH_2	12	6.1141
CH_2COO	1	1.2907
SO_3^-	1	26.5247

Second-order group:

Groups	Occurrences	Coefficients (°C)
No Second-order group		

Third-order group:

Groups	Occurrences	Coefficients (°C)
$-O_xS-(CH_2)_n-OCO$	1	-0.1607

T_k calculation

$T_{k,calc}$ (°C) = $\Sigma_i N_i C_i + \Sigma_j M_j D_j + \Sigma_k O_k E_k$ + Constant = (1x45.9329) + (12x6.1141) + (1x1.2907) + (1x26.5247) + (1x-0.1607) + (-126.6285) = 20.33 °C

Experimental value = 24.20 °C

%Absolute deviation from experimental value = 16.0%

Table O8 Example calculation of Krafft point of C12AEOSO3 for linear-acyl ethoxylate sulfate surfactant
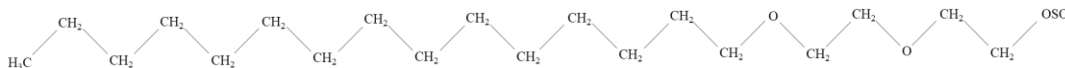
C12AEOSO3		
Molecular structure:		
First-order group:		
Groups	Occurrences	Coefficients (°C)
CH_3	1	45.9329
CH_2	12	6.1141
CH_2COO	1	1.2907
OSO_3^-	1	32.6928
Second-order group:		
Groups	Occurrences	Coefficients (°C)
No Second-order group		
Third-order group:		
Groups	Occurrences	Coefficients (°C)
$-O_xS-(CH_2)_n-OCO$	1	-0.1607
T_k calculation		
$T_{k,calc}$ (°C) = $\Sigma_i N_i C_i + \Sigma_j M_j D_j + \Sigma_k O_k E_k$ + Constant = (1x45.9329) + (12x6.1141) + (1x1.2907) + (1x32.6928) + (1x-0.1607) + (-126.6285) = 26.43 °C		
Experimental value = 26.50 °C %Absolute deviation from experimental value = 0.25%		

Table O9 Example calculation of Krafft point of O3SOC16OSO3 for linear-alkyl disulfate surfactant

<table>
<tr><td colspan="3" align="center">O3SOC16OSO3</td></tr>
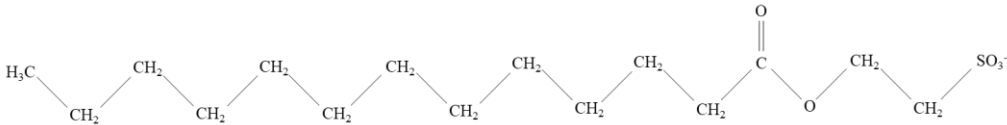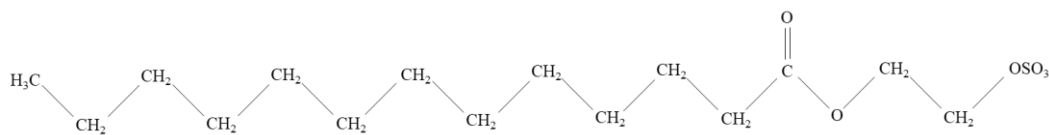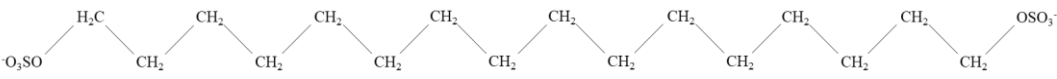<tr><td colspan="3">Molecular structure:
</td></tr>
<tr><td colspan="3">First-order group:</td></tr>
<tr><td align="center">Groups</td><td align="center">Occurrences</td><td align="center">Coefficients (°C)</td></tr>
<tr><td align="center">CH_2</td><td align="center">16</td><td align="center">6.1141</td></tr>
<tr><td align="center">OSO_3^-</td><td align="center">2</td><td align="center">32.6928</td></tr>
<tr><td colspan="3">Second-order group:</td></tr>
<tr><td align="center">Groups</td><td align="center">Occurrences</td><td align="center">Coefficients (°C)</td></tr>
<tr><td colspan="3" align="center">No Second-order group</td></tr>
<tr><td colspan="3">Third-order group:</td></tr>
<tr><td align="center">Groups</td><td align="center">Occurrences</td><td align="center">Coefficients (°C)</td></tr>
<tr><td colspan="3" align="center">No Third-order group</td></tr>
<tr><td colspan="3">T_k calculation</td></tr>
<tr><td colspan="3">$T_{k,calc}$ (°C) = $\Sigma_i N_i C_i + \Sigma_j M_j D_j + \Sigma_k O_k E_k$ + Constant = (16x6.1141) + (2x32.6928) + (-126.6285) = 36.46 °C</td></tr>
<tr><td colspan="3">Experimental value = 39.10 °C

%Absolute deviation from experimental value = 6.76%</td></tr>
</table>

Table O10 Example calculation of Krafft point of O3SPhOC8OPhSO3 for 1,n-di(p-sulfonicphenoxy)-alkane surfactant
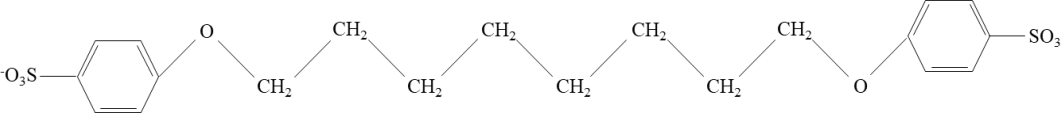
O3SPhOC8OPhSO3		
Molecular structure:		
First-order group:		
Groups	Occurrences	Coefficients (°C)
CH_2	8	6.1141
aC-O	2	65.8270
aCH	8	-2.7166
aC-SO$_3^-$	2	0.0060
Second-order group:		
Groups	Occurrences	Coefficients (°C)
AROMRINGs^{1}s^4	2	0.0060
$^-O_3$S-aromatic-O	2	-0.0005
Third-order group:		
Groups	Occurrences	Coefficients (°C)
aC-O-(CH$_2$)$_n$-O-aC	1	-0.0003
T$_k$ calculation		
$T_{k,calc}$ (°C) = $\Sigma_i N_i C_i + \Sigma_j M_j D_j + \Sigma_k O_k E_k$ + Constant = (8x6.1141) + (2x65.8270) + (8x-2.7166) + (2x0.0060) + (2x0.0060) + (2x-0.0005) + (1x-0.0003) + (-126.6285) = 32.23 °C		
Experimental value = 28.00 °C %Absolute deviation from experimental value = 15.10%		

Table O11 Example calculation of Krafft point of O3SCEAC14AECSO3 for 1,n-di(sulfoalkanoate)-alkane surfactant

O3SCEAC14AECSO3
Molecular structure:

First-order group:		
Groups	Occurrences	Coefficients (°C)
CH_2	18	6.1141
CH_2COO	2	1.2907
SO_3^-	2	26.5247

Second-order group:		
Groups	Occurrences	Coefficients (°C)
No Second-order group		

Third-order group:		
Groups	Occurrences	Coefficients (°C)
$OOC\text{-}(CH_2)_n\text{-}COO$	1	-7.6915
$^-O_xS\text{-}(CH_2)_n\text{-}OCO$	2	-0.1607

T_k calculation

$T_{k,calc}$ (°C) = $\Sigma_i N_i C_i + \Sigma_j M_j D_j + \Sigma_k O_k E_k$ + Constant = (18x6.1141) + (2x1.2907) + (2x26.5247) + (1x-7.6915) + (2x-0.1607) + (-126.6285) = 31.04 °C

Experimental value = 31.00 °C

%Absolute deviation from experimental value = 0.14%

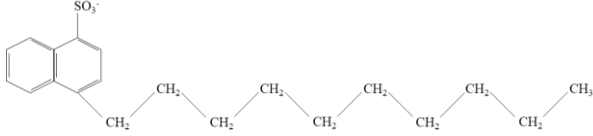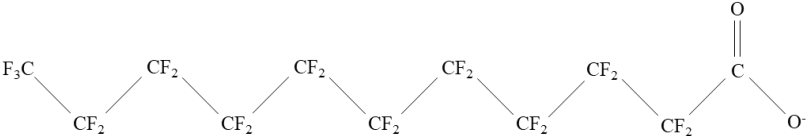**Table O12** Example calculation of Krafft point of 1,4 NS-10 for alkyl naphthalene sulfonate surfactant

1,4 NS-10		
Molecular structure: First-order group:		
Groups	Occurrences	Coefficients (°C)
CH$_3$	1	45.9329
CH$_2$	8	6.1141
aCH	6	-2.7166
aC-CH$_2$	1	69.9810
aC-SO$_3^-$	1	0.0060
aC fused aromatic ring	2	-0.2730
Second-order group:		
Groups	Occurrences	Coefficients (°C)
AROMRINGs^{1}s^4	1	0.0060
Third-order group:		
Groups	Occurrences	Coefficients (°C)
AROFUSEDs^{1}s^4	1	-0.1365
T$_k$ calculation		
T$_{k,calc}$ (°C) = $\Sigma_i N_i C_i + \Sigma_j M_j D_j + \Sigma_k O_k E_k$ + Constant = (1x45.9329) + (8x6.1141) + (6x-2.7166) + (1x69.9810) + (1x0.0060) + (2x-0.2730) + (1x0.0060) + (1x-0.1365) + (-126.6285) = 21.23 °C		
Experimental value = 21.00 °C %Absolute deviation from experimental value = 1.09%		

Table O13 Example calculation of Krafft point of C10F21COONa for linear-fluorocarbon surfactant

C10F21COONa

Molecular structure:

First-order group:

Groups	Occurrences	Coefficients (°C)
CH$_3$	1	45.9329
CH$_2$	9	6.1141
COO$^-$	1	0.0137

Second-order group:

Groups	Occurrences	Coefficients (°C)
No Second-order group		

Third-order group:

Groups	Occurrences	Coefficients (°C)
No Third-order group		

T$_k$ calculation

$T_{k,calc}$ (°C) = $\Sigma_i N_i C_i + \Sigma_j M_j D_j + \Sigma_k O_k E_k$ + Constant = (1x45.9329) + (9x6.1141) + (1x0.0137) + (-126.6285) = 56.84 °C

Experimental value = 58.30 °C

%Absolute deviation from experimental value = 2.50%

CURRICULUM VITAE

Name: Mr. Woramet Chanachichalermwong

Date of Birth: October 20, 1993

Nationality: Thai

University Education:

  2016-2018   Master Degree of Petroleum Technology, The Petroleum and Petrochemical College, Chulalongkorn University, Bangkok, Thailand

  2012-2015   Bachelor Degree of Chemical Technology, Faculty of Science, Chulalongkorn University, Bangkok, Thailand

Work Experience:

  2014   Position: Trainee process engineer

       Company name: PTT Global Chemical Public Company Limited

Proceedings:

1. Chanachichalermwong, W., Charoensaeng, A., and Suriyapraphadilok, U., (2018, June 5) Development of Group-Contribution Model for the Characteristic Curvature of Nonionic Surfactant (C_{cn}) by Using Available Database and Measured C_{cn}. Proceedings of The 24th PPC Symposium on Petroleum, Petrochemicals, and Polymers and The 9th Research Symposium on Petrochemicals and Materials Technology, Bangkok, Thailand.

2. Chanachichalermwong, W., Charoensaeng, A., and Suriyapraphadilok, U., (2017, Oct 18-20) Krafft Point Estimation for Anionic Surfactant based on Group Contribution Method. Proceedings of The 7th International Thai Institute of Chemical Engineering and Applied Chemistry Conference 2017 (ITChE 2017), Bangkok, Thailand.